Role of Rab20 in phagosome maturation and mycobacterial killing

Von der Fakultät für Lebenswissenschaften

der Technischen Universität Carolo-Wilhelmina zu Braunschweig

zur Erlangung des Grades

eines Doktors der Naturwissenschaften

(Dr. rer. nat.)

genehmigte

D i s s e r t a t i o n

von Gang Pei
aus Henan, China

1. Referent: Prof. Dr. Michael Steinert
2. Referent: apl. Professor Dr. Manfred Rohde
eingereicht am: 27.05.2013
mündliche Prüfung (Disputation) am: 16.09.2013

Druckjahr 2013

Acknowledgements

First and foremost, I would like to express my deepest gratitude to my supervisor, Dr. Maximiliano Gutierrez, for giving me the opportunity to join the lab and the excellent supervision. I am grateful for his understanding, patience, encouragement, support and input throughout these years. I really enjoy the time in his lab.

I would like to thank all the past and present members in Maxi's lab for creating a friendly and stimulating atmosphere. Specifically, I would like to thank Ianina for generating plasmids related to this thesis, Achim for the help with experiments, Cristina for the helpful discussion and advice, Bahram for the interesting discussion and the generous help, Marc for the collaboration and support and Cristiane for the laughter. I also would like to thank all for critical reading of this thesis and the feedback.

I would like to thank Prof. Dr. Gareth Griffiths and Dr. Urska Repnik for their collaboration in electron microscopy. I also would like to thank the members of my thesis committee, Prof. Dr. Beate Sodeik and Prof. Dr. Lothar Jänsch, for their helpful and stimulating discussions.

I would like to thank Prof. Dr. Lixin Zhang who helped me greatly at the beginning of the road to research. His continuous encouragement and advice is very much appreciated.

I would like to thank my friends, Lichun, Lisha, Puwei, Jie, Wufeng, Hao, Hani Kaba and Thomas Marandu for their great support and company. Special thanks are given to Wenfang for standing beside me through many hard times.

Last but not least, I would like to thank my family for their never-ending love, support and belief on me. Without them I would not be able to finish this thesis. I would especially like to thank my grandfather who always loved me. This thesis is dedicated to the memory of him.

Role of Rab20 in phagosome maturation and mycobacterial killing

Abstract

Phagosome maturation is a progressive process, in which nascent phagosomes sequentially interact with early endosomes, late endosomes and lysosomes, leading to the formation of phagolysosomes. It is a critical part for innate immunity to eliminate intracellular pathogens and for adaptive immunity to process antigens. There is compelling evidence that IFN-γ is able to regulate phagosome trafficking and consequently the immune function of this process. However, the molecular link by which IFN-γ modulates phagosome trafficking and function is not known. Rab is a family of small GTPases, which function as central membrane organizers coordinating extracellular immune mediators and the intracellular trafficking. In this thesis, the role of Rab20 in phagosome maturation and its modulation by IFN-γ was investigated. IFN-γ enhanced Rab20 expression and Rab20 association to phagosomes in macrophages. Moreover, Rab20 association to phagosomes induced an early delay in phagosome maturation with the prolonged duration of Rab5 and PI3P association. Conversely, the expression of the dominant negative mutant of Rab20 and knockdown of Rab20 accelerated phagosome maturation decreasing the time that Rab5 and PI3P retained to phagosomes. Particularly, the killing of mycobacteria was not affected by the expression of Rab20 wild type. This work further demonstrated that Rab20 was required for the delay in phagosome maturation induced by IFN-γ. Rabex-5, as an effector of Rab20, was recruited to phagosomes by Rab20 in an IFN-γ dependent manner. Higher level of Rabex5 in phagosome results in a transient increase of active Rab5 in phagosomes. Altogether, this work uncovers Rab20 as a key player in the mechanism by which IFN-γ induces a delay in phagosome maturation in macrophages.

Die Rolle von Rab20 in der phagosomalen Reifung und der Einfluss von Rab20 in der Abtötung von Mykobakterien

Zusammenfassung

Die Reifung von Phagosomen ist ein progressiver Prozess in dem ein Phagosom nach und nach mit frühen Endosomen, späten Endosomen und letztendlich mit Lysosomen interagiert. Es entsteht ein Phagolysosom. Dieser Prozess spielt sowohl für das angeborene Immunsystem eine entscheidende Rolle indem es intrazellulare Pathogene eliminiert, als auch für das adaptive Immunsystem. Es konnte gezeigt werden, dass Interferon-γ (IFN- γ) generell regulierend auf den Reifungsprozess und dadurch verknüpfte Immunfunktionen wirken kann. Durch welche Akteure IFN-γ die Phagosomenreifung moduliert ist jedoch weitestgehend unbekannt.

Rab Proteine gehören zu der Familie der kleinen GTPasen. Als Membranproteine, die auf Vesikeln lokalisiert sind, koordinieren sie die intrazellulare Antwort auf extrazellulare Reize. IFN-γ steigert nicht nur die Proteinexpression von Rab20 in der Zelle, sondern auch die Assoziation von Rab20 am Phagosom in Makrophagen. Befindet sich Rab20 am Phagosom so induziert es, in einem frühen Stadium, eine verlängerte Assoziation von Rab5 und PI3P mit dem Selbigen. Ein gegenteiliger Effekt ist zu erkennen, exprimiert man eine dominant negative Mutante von Rab20 oder generiert einen Rab20 knock-down in Makrophagen. In diesem Fall verkürzt sich der Zeitraum in dem Rab5 und PI3P mit dem Phagosom assoziiert sind. Auf das Überleben von Mykobakterien in Makrophagen hatte die Überexpression von Rab20 keinen Einfluss.

Weiterhin wird gezeigt, dass Rabex5 ein Effektor von Rab20 ist und als solcher durch Rab20 zum Phagosom rekrutiert wird. Dieser Prozess ist IFN-γ abhängig. In Folge dessen führt eine erhöhte Konzentration von Rabex5 am Phagosom zu einer vorrübergehend erhöhten Konzentration von aktivem Rab5 am Phagosom. Zusammenfassend kann gesagt werden, dass diese Dissertation Rab20 als einen der molekularen Hauptakteure beschreibt, der für die IFN-γ induzierte Verzögerung der Phagosomenreifung in Makrophagen verantwortlich ist.

Abbreviations

Abp140	Actin binding protein 140
AP1	Adaptor protein 1
AP2	Adaptor protein 2
Arf1	ADP-ribosylation factor 1
Arp2/3	Actin-related protein 2/3
ATCC	American Type Culture Collection
BDNF	Brain-derived neurotrophic factor
BFA	Brefeldin A
BHK	Baby hamster kidney
BMM	Bone marrow macrophage
BSA	Bovine serium albumin
CCVs	Clathrin-coated vesicles
Ccz1	Calcium Caffeine Zinc sensitivity
Cdc42	Cell division control protein 42 homolog
CD-MPR	Cation-dependent mannose 6-phosphate receptor
CFU	Colony forming units
CGN	*cis*-Golgi network
CHO cells	Chinese hamster ovary cells
CI-MPR	Cation-independent mannose 6-phosphate receptor
CYP27b1	25-Hydroxyvitamin D_3 1-alpha-hydroxylase
COP	Coat protein complex
DEFB4	Defensin beta 4
D-MEM	Dulbecco's modified eagles medium
EBP50	Ezrin/radixin/moesin (ERM)-binding phosphoprotein 50
ECVs	Endosomal carrier vesicles
EEs	Early endosomes
EEA1	Early endosome antigen 1
EET domain	Early endosome targeting domain
EGF	Epidermal growth factor
EGFR	Epidermal growth factor receptor
ER	Endoplasmic reticulum
ERK	Extracellular-signal regulated kinase
FBS	Fetal bovin serum
FcγR	Fcγ receptors
FYVE	Named after Fab 1, YOTB, Vac 1 and EEA1
GalT	β1, 4-galactosyltransferase 1
GAPs	GTPase-activating proteins
GDFs	GDI displacement factors
GDIs	GDP dissociation inhibitors

GEFs	Guanine exchange factors
GGAs	Golgi-localized, γ-ear-containing, ADP-ribosylation factor-binding proteins
GGTs	Geranylgeranyl transferases
GLUT4	Glucose transporter type 4
GPI	Glycosylphosphatidylinositol
HIV	Human immunodeficiency virus
H2M	A non-classical MHC II in mouse
HOPS	Homotypic fusion and vacuole protein sorting
hRME-6	Mammalian ortholog of receptor-mediated endocytosis protein 6
HyD	Hybrid detector
iNOS	Inducible nitric oxide synthase
INPP5E	72-kDa inositol polyphosphate 5-phosphatase
IP	Immunoprecipitation
ITAM	Immunoreceptor tyrosine-based activation motif
LAMP-1	Lysosomal-associated membrane protein 1
LAMP-2	Lysosomal-associated membrane protein 2
LDL	Low-density lipoprotein
LEs	Late endosomes
Ii	Invariant chain
LmpA	Lysosomal integral membrane protein
LPS	Lipopolysaccharide
***M.bovis* BCG**	*M.bovis* bacillus Calmette–Guérin
M-CSF	Macrophage colony stimulating factor
MEK1/2	Mitogen-activated protein kinase
MHC II	Major histocompatibility complex class II
MIU	Motif interacting with ubiquitin
Mon1	MONensin sensitivity
MPRs	Mannose 6-phosphate receptors
mVPS39	Mammalian Vps39
NK cells	Natural killer cells
NSF	N-ethylmaleimide-sensitive factor
ORP1L	Oxysterol-binding protein homologue
PBS	Dulbecco's phosphate buffered saline
PCR	Polymerase chain reaction
PI-3 kinases	Phosphatidylinositide 3-kinases
PIKfyve	FYVE finger-containing phosphoinositide kinase
PIM	Phosphatidylinositol mannoside
PI3P	Phosphatidylinositol 3-phosphate
PI(3,4)P_2	Phosphatidylinositol (3,4)-bisphosphate
PI(4,5)P_2	Phosphatidylinositol (4,5)-bisphosphate
PI(3,4,5)P_3	Phosphatidylinositol (3,4,5)-triphosphate

PKC	Protein kinase C
PMT	Photomultipliers
PR	Proline-rich region
PTEN	Phosphatase and tensin homolog
RabCDR	Rab complementarity-determining region
RabF	Rab family motifs
Rab11-FIP2	Rab11 family interacting protein 2
RabSFs	Rab subfamily motifs
Ras	Rat sarcoma
REPs	Rab escort proteins
RILP	Rab-interacting lysosomal protein
Rubicon	Run domain protein as Beclin 1 interacting and cysteine-rich containing
SCVs	*S. typhimurium*-containing vacuoles
SNAREs	Soluble N-ethylmaleimide-sensitive fusion attachment protein receptor
SNX	Sortin nexin
SopB	Secreted effector protein B
Src	Rous sarcoma oncogene cellular homolog
SRP	Signal recognition particle
SV40	Simian virus 40
Syk	Spleen tyrosine kinase
TB	Tuberculosis
TGN	*trans*-Golgi network
TLR2	Toll-like receptor 2
t-SNAREs	Target- membrane SNAREs
T3SS	Type 3 secretion system
UVRAG	UV radiation resistance-associated gene protein
VAMP	Vesicle-associated membrane protein
v-ATPase	Vacuolar-type H^+-ATPase
VHS	Named after VPS27, Hrs and STAM
v-SNAREs	Vesicle-membrane SNAREs
VPS-C complex	Class C vacuole protein sorting
Vps34	Vacuolar protein sorting 34
WASP	Wiskott-Aldrich syndrome protein
ZnF	Zinc-finger

Table of contents

1. Introduction

Membrane trafficking

Eukaryotic cells differ fundamentally from prokaryotes by possessing internal membranous compartments. These compartments, also called organelles, are separated from the cytosol by phospholipid bilayers to maintain their distinct compositions and functions (Tokarev AA *et al*. 2009, Alberts B *et al*. 2010). Although the organelles are segregated spatially, they are connected functionally by transporting different cargos from one compartment to another. On the other hand, cells need to communicate with the environment through internalizing nutrients and secreting signaling molecules. In most of the cases, these transport steps are directed through membrane trafficking (Tokarev AA *et al*. 2009, Alberts B *et al*. 2010).

Depending on the transport direction in relation to cell membrane, membrane trafficking is divided into three major routes: the biosynthetic secretory pathway, the endocytic pathway and the retrieval pathway (**Fig. 1.1**). The biosynthetic secretory pathways were originally described in pancreatic exocrine cells (Palade G. 1975). Proteins targeted to specific compartments are first recognized by a cytosolic ribonucleoprotein complex, the signal recognition particle (SRP), via amino-terminal signal sequences (Rapoport TA. 2007). Then the nascent polypeptides are quickly targeted to the membrane of the endoplasmic reticulum (ER) by the SRP complex. Once on the ER membrane, the SRP complex is dissociated. Afterwards, the polypeptides are co-translationally inserted into the ER lumen by the translocon-Sec61 complex (Swanton E and Bulleid NJ. 2003). In the ER lumen, the newly synthesized proteins are properly folded in the presence of many chaperones. If proteins are not correctly folded, they are retained in the ER lumen and degraded. The newly synthesized proteins are modified with glycosylations or proline hydroxylations in the ER lumen for correct folding (Braakman I and Bulleid NJ. 2011). The properly folded proteins are transported from the ER to the Golgi complex via coat protein complex II (COP II)-coated vesicles. By directly or indirectly binding COP II through the exit signal, membrane or soluble cargo proteins are concentrated into vesicles derived from the ER. Then the COP II vesicles go through a series of Golgi sub-compartments; *cis*-Golgi network (CGN), *cis*-cisterna, medial-cisterna, *trans*-cisterna and finally *trans*-Golgi network (TGN) (Tokarev AA *et al*. 2009). During this process, the cargo proteins are further glycosylated in a successive sequence when they move from the CGN to the TGN. The TGN is the final Golgi complex area where cargo proteins are sorted into different transport vesicles and delivered to their destinations such as the plasma membrane, endosomes or

lysosomes (Harter C and Wieland F. 1996). To achieve the specificity of sorting, cargo proteins or cargo receptors are recognized by coat proteins through specific sorting signals (Alberts B *et al*. 2010). The best known sorting mechanism is the one associated to the cation-dependent and cation-independent mannose 6-phosphate receptors (MPRs). The tyrosine motif YXXΦ (where X is any amino acid, Φ is an amino acid with bulky hydrophobic residue) of MPRs is recognized by the μ subunit of all adaptins. This sorting motif guides the cargos to endosomes or lysosomes and the internalization from the plasma membrane. Similarly, the dileucine motif [DE]XXX[LI] (where X is any amino acid) probably binds μ or β–subunits of adaptor protein 1 (AP1) and AP2. This motif is also involved in the endosomal and lysosomal targeting (Bonifacino JS and Traub LM. 2003). Other than adaptins, the Golgi-localized, γ-ear-containing, ADP-ribosylation factor-binding proteins (GGAs) are also involved in the TGN sorting by functioning as adaptors (Bonifacino JS and Traub LM. 2003). GGAs bind the DXXLL motifs of MPRs through the VHS (named after VPS27, Hrs and STAM) domain and mutations in these motifs induce defective lysosomal enzyme sorting (Zhu Y *et al*. 2001, Puertollano R *et al*. 2001). Sortilin is also implicated in directing some lysosomal enzymes from the TGN to lysosomes (Lefrancois S *et al*. 2003, Ni X and Morales CR. 2006). Moreover, sortilin is also involved in delivery of some lysosomal proteins directly to phagosomes (Wähe A *et al*. 2010). The sortilin-mediated sorting from the TGN to lysosomes may be guided by interacting with GGAs through the DXXLL motif of cytosolic tail of sortilin.

There is an intricate balance between the biosynthetic secretory pathways and the retrieval pathways. In this way, proteins can be transported back to the donor compartments. Many endocytosed molecules are recycled back from early endosomes or sorting endosomes to the plasma membrane. Rab4 and Rab11, as the central organizers, regulate recycling pathways to the plasma membrane (Maxfield FR and McGraw TE. 2004). Some molecules are returned from early or late endosomes to the Golgi complex and some ER-resident proteins can be transported back from the Golgi complex to the ER. It has been shown that Rab9 regulates the recycling from late endosomes to the TGN (Lombardi D *et al*. 1993, Riederer MA *et al*. 1994). The coat protein COP I is required for the retrograde transport from the Golgi complex to the ER. On one hand, COP I facilitates the formation of the transport vesicles. On the other hand, COP I is also involved in cargo selection (Kirchhausen T. 2000). COP I recognizes proteins with dilysine motifs (KKXX or KXKXX, where X is any amino acid) in the cytoplasmic carboxy-terminal domain of cargo proteins (Kirchhausen T. 2000).

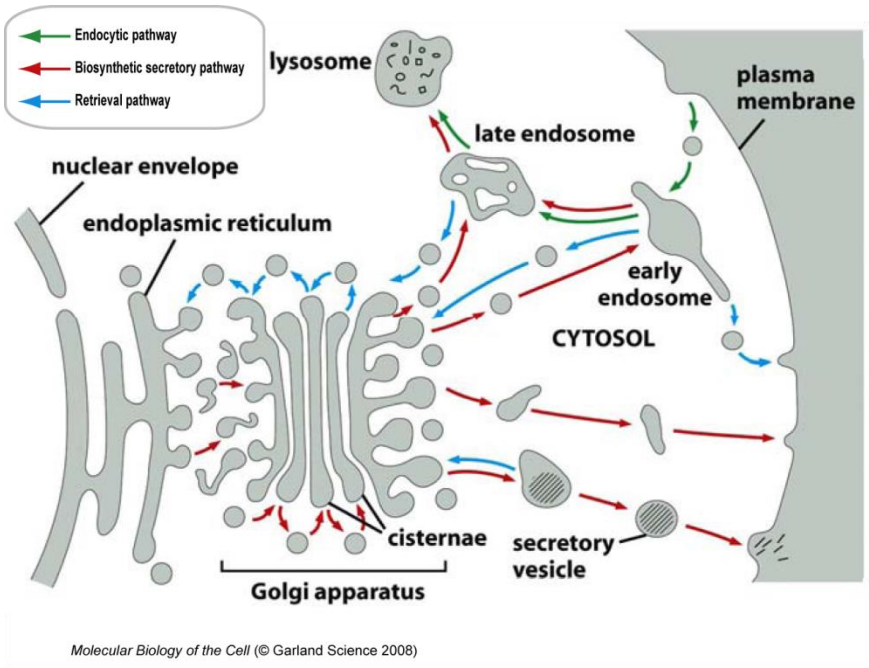

Fig. 1.1 An overview of membrane trafficking pathways in eukaryotic cells. The endocytic vesicles are budded from the plasma membrane to form nascent endosomes. The nascent endosomes follow a maturation process from early endosomes to late endosomes and finally fusion with lysosomes (Green arrow). In the biosynthetic secretory pathway, the newly synthesized proteins are transported from the ER to the plasma membrane through the Golgi complex (Red arrow). In the retrieval pathway, some proteins are recycled back from endosomes to the plasma membrane and the TGN or from the Golgi to the ER (Blue arrow). Adapted from Alberts B *et al*. 2010

Endocytic pathways

According to the characteristics of ligands, receptors or coat proteins, endocytic pathways are mainly divided into clathrin-mediated endocytosis, *caveolae*-dependent endocytosis, macropinocytosis and phagocytosis (**Fig. 1.2**).

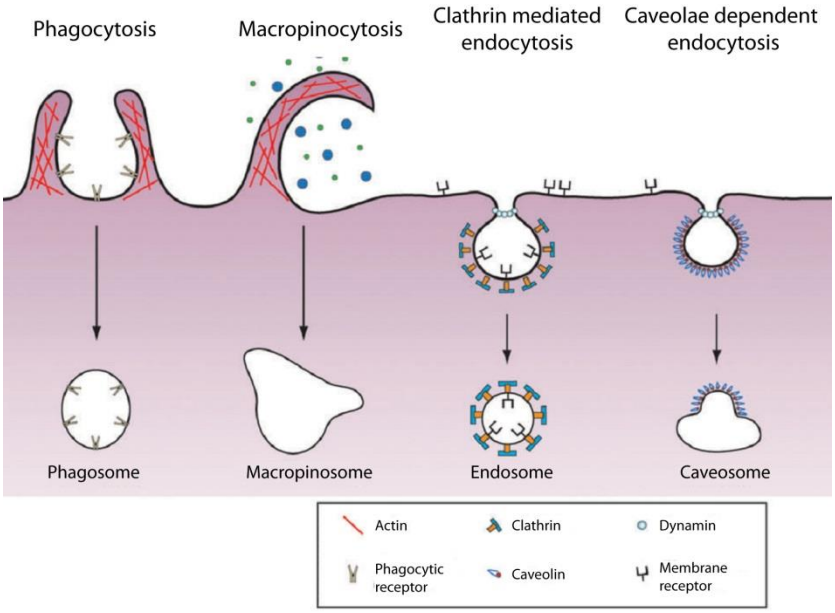

Fig. 1.2 An overview of endocytic pathways. Many membrane proteins and their ligands are internalized by clathrin-mediated endocytosis. Clathrin, as one of the coat proteins, is required for budding from the plasma membrane. Some glycosylphosphatidylinositol (GPI)-anchored proteins and glycosphingolipids are internalized by *caveolae*-dependent endocytosis. Such endosomes are coated with caveolins. For both clathrin-mediated and *caveolae*-dependent endocytosis, dynamin is required for the detachment of endosomes. Macropinocytosis is used by cells to uptake bulks of fluid and there is no

receptor involved in this process. Phagocytosis refers to the process in which macrophages, dendritic cells and neutrophils uptake pathogens or apoptotic cells. For both phagocytosis and macropinocytosis, actin rearrangement is involved. Adapted from Chou YT *et al*. 2011

Clathrin-mediated endocytosis

Many receptors on the plasma membrane and their ligands are internalized by the clathrin-mediated endocytosis (Doherty GJ and McMahon HT. 2009). The first step to initiate the clathrin-mediated endocytosis is forming a membrane invagination called a pit. This process is triggered by the recruitment of AP2 to the plasma membrane. AP2 is one of the clathrin binding adaptor proteins that are highly conserved. Phosphatidylinositol (4,5)-bisphosphate, also known as $PI(4,5)P_2$, is found on the membrane of clathrin pits and AP2 binds $PI(4,5)P_2$. This may explain how AP2 is recruited to the plasma membrane. $PI(4,5)P_2$ also facilitates budding by binding other clathrin adaptors-epsins. In this way, $PI(4,5)P_2$ defines the physiochemical features of the membrane of clathrin pits. In parallel with the membrane invaginations, cargo selection and clathrin assembly are also organized (McMahon HT and Boucrot E. 2011). For cargo selection, AP2 recognizes the tyrosine or dileucine motifs in the cytoplasmic tails of cargo proteins. In addition, some cargo specific adaptor proteins are also involved in cargo selection. When the cargos are selected, clathrin is recruited to the membrane by binding with AP2. Afterwards, clathrin is assembled and polymerized into lattice-like cages comprising both hexagons and pentagons (Fotin A *et al*. 2004). However, clathrin polymerization is not enough for the clathrin-coated pits to deform from the plasma membrane. The pinching off the plasma membrane for the clathrin-coated vesicles (CCVs) requires another protein called dynamin. Dynamin is recruited to the neck of the nascent vesicles and its association induces GTP hydrolysis and subsequent membrane scission. Once the vesicles are detached from the plasma membrane, clathrin is quickly disassembled. The formed vesicles are called endosomes and undergo a maturation process, highlighted in the text below (Rappoport JZ. 2008, Doherty GJ and McMahon HT. 2009, McMahon HT and Boucrot E. 2011).

***Caveolae*-dependent endocytosis**

Although it has been debated for long time, now it is widely accepted that the *caveolae*-dependent endocytosis does exist. Caveolae are flask-shaped plasma membrane invaginations that contain caveolin proteins with a diameter of 50-100 nm (Pelkmans L and Helenius A. 2002, Le Roy C and Wrana JL. 2005, Kiss AL and Botos E. 2009). There are three caveolin proteins, Caveolin 1, 2 and 3. It has been reported that Caveolin 1 is essential for the formation of caveolae (Drab M *et al*. 2001). Caveolin 2 is also necessary for the formation of deep plasma membrane attached caveolae. In addition, Caveolin 2 has the ability of modulating the caveolin 1-dependent caveolae assembly (Sowa G *et al*. 2003). Many

ligands, such as simian virus 40 (SV40), human immunodeficiency virus (HIV) and albumin are internalized by caveolae. However, the mechanisms of selective internalization of those ligands are still not well known. It is believed that caveolae is employed by cells to internalize membrane components rich in cholesterol, GPI-anchored proteins and glycosphingolipids (Pelkmans L and Helenius A. 2002). Hence, any ligand which can bind those components, is supposed to be internalized by caveolae. The phosphorylation of Caveolin 1 by the Src (Rous sarcoma oncogene cellular homolog) kinase is important for the caveolae formation (Li S *et al*. 1996, Pelkmans L *et al*. 2002). As in the clathrin-mediated endocytosis, dynamin also plays an important role in caveolar pinching off from the plasma membrane (Oh P *et al*. 1998, Henley JR *et al*. 1998). The detailed mechanisms of budding and pinching off from the plasma membrane for caveolae are still obscure. After detachment from the plasma membrane, caveolae vesicles transfer their cargos, e.g. SV40, to caveolin 1-positive tubular membrane structures named caveosomes. The pH of these structures is neutral, which contributes to the escape of viruses from degradation (Pelkmans L *et al*. 2001). From caveosomes, the internalized cargos can be directly transported to the ER and Golgi complex (Pelkmans L *et al*. 2001, Puri V *et al*. 2001). Moreover, the *caveolae*-dependent endocytosis also transports along the classical endosome maturation pathway (Kiss AL and Botos E. 2009).

Macropinocytosis

Macropinocytosis is one of the clathrin-independent endocytic pathways. It is used by cells to uptake bulks of fluid without any receptor involved. Unlike clathrin or caveolar vesicles, macropinocytic vesicles have no coat proteins and they are large in size with a diameter larger than 0.2 µm (Jones AT. 2007, Lim JP and Gleeson PA. 2011). Macropinocytosis is usually activated by some extracellular signals, such as macrophage colony stimulating factor (M-CSF), epidermal growth factor (EGF) among others (Haigler HT *et al*. 1979, Racoosin EL and Swanson JA. 1989). However, the constitutive macropinocytosis is also observed in dendritic cells (Sallusto F *et al*. 1995). Membrane ruffling is highly active during macropinocytosis. The closure of macropinosomes requires the back-fusion of the protruding structures with the unruffled plasma membrane. During this process, the global actin cytoskeleton reorganization is required. Hence macropinocytosis can be regulated by modulating the actin polymerization machinery. PI3-kinase inhibitors or actin polymerization inhibitors can block macropinocytosis (Jones AT. 2007, Lim JP and Gleeson PA. 2011). It has been shown that Rab5a is recruited to macropinosomes and the duration of Rab5a activation on macropinosomes is correlated to their size (Feliciano WD *et al*. 2011). Rabankyrin-5, a Rab5 effector, is involved in regulating macropinocytosis. Over-expression of

Rabankyrin-5 increases the number of macropinosomes and the fluid uptake (Schnatwinkel C *et al*. 2004). Rab34 is another Rab GTPase that is localized on macropinosomes. Over-expression of Rab34 increases the number of macropinosomes (Sun P *et al*. 2003). Sortin nexin (SNX) proteins are also involved in macropinocytosis. It has been shown that the formation of macropinocytosis is significantly increased by SNX5 expression (Lim JP *et al*. 2008). An image-based screening that analyzed the effect of SNX proteins on macropinocytosis has also shown that the expression of SNX1, SNX5, SNX9, SNX18 or SNX33 increases the macropinosome formation (Wang JT *et al*. 2010).

Phagocytosis

Phagocytosis refers to the process by which macrophages, dendritic cells and neutrophils capture large particles, e.g. bacteria, fungi and apoptotic cells, into specialized vacuoles called phagosomes (Aderem A and Underhill DM. 1999). The internalization of these particles is initiated after recognition by specific receptors on the surface of phagocytes. Then actin is polymerized at the point of attachment, forming phagocytic cups (Aderem A and Underhill DM. 1999). Once fully internalized into cells, actin is quickly dissociated from phagosomes. Afterwards, phagosomes undergo a maturation process by successively fusing with different endocytic compartments (Fairn GD and Grinstein S. 2012). There are many receptors involved in this process, such as Fcγ receptors (FcγRs), complement receptors, mannose receptors, dectin-1 among others (Flannagan RS *et al*. 2012). For FcγR-mediated phagocytosis, upon receptor clustering, the immunoreceptor tyrosine-based activation motif (ITAM) is phosphorylated by the Src family kinases and the spleen tyrosine kinase (Syk) is recruited to phosphorylate other ITAMs. Finally downstream phosphatidylinositide 3-kinases (PI-3 kinases), Rho GTPases and protein kinase C (PKC) are activated to stimulate actin polymerization and internalization. The Wiskott-Aldrich syndrome protein (WASP), actin-related protein 2/3 (Arp2/3) and cell division control protein 42 homolog (Cdc42) are also involved in actin polymerization during the FcγR-mediated phagocytosis (Greenberg S and Grinstein S. 2002, Flannagan RS *et al*. 2012).

Importance of membrane trafficking

Membrane trafficking is crucial for maintaining cell homeostasis. The defect of membrane trafficking processes results in various diseases (Howell GJ *et al*. 2006). One of the examples is the Huntington's disease. Huntingtin plays an essential role in normal nerve cell function. A mutation that causes a polyglutamine extension to Huntingtin leads to the Huntington's disease (Walling HW *et al*. 1998). It has been shown that in healthy cells, Huntingtin enhances the transport of brain-derived neurotrophic

factor (BDNF) containing vesicles that is dependent on microtubules. In the disease state, the loss of Huntingtin function in the transport of BDNF leads to the inability of neuronal cells to release BDNF, indicating that the deficiency in BDNF transport contributes to the pathogenesis of the Huntington's disease (Gauthier LR *et al*. 2004). In addition, many intracellular pathogens have evolved mechanisms to subvert the host response by manipulating membrane trafficking (Alix E *et al*. 2011). *M. tuberculosis* secretes a lipid phosphatase, SapM, which hydrolyzes phosphatidylinositol 3-phosphate (PI3P). *In vitro* assays have demonstrated that SapM is able to inhibit the PI3P-dependent phagosome-lysosome fusion (Vergne I *et al*. 2005). Moreover, *M. tuberculosis* also produces a lipid called phosphatidylinositol mannoside (PIM) which enhances the fusion of phagosomes with early endosomes (Vergne I *et al*. 2004). These reports (but not limited to) demonstrate that membrane trafficking is so important that subtle changes in membrane trafficking could lead to diseases or contribute to the pathogenesis of infectious diseases. Therefore, understanding the molecular mechanisms underlying membrane trafficking is critical for revealing the pathogenesis of different diseases.

The molecular machinery of vesicle trafficking

There are mainly four steps during vesicle trafficking (**Fig. 1.3**). The first step is vesicle budding from the donor membrane. To initiate this process, coat proteins are recruited and assembled on the membrane. Three coat proteins- clathrin, COP I and COP II are involved in this process (Kirchhausen T. 2000). Coat protein assembly leads to the formation of vesicles from the donor membrane. Coat proteins also participate in cargo selection by recognizing sorting motifs in the cytoplasmic tails of cargo proteins (McMahon HT and Mills IG. 2004). Once the vesicles are detached from the donor membrane, coat proteins are disassembled from the vesicles and recycled back for another round of budding (Bonifacino JS and Glick BS. 2004). After budding, the vesicles are transported along actin filaments or microtubules. It has been proposed that microtubules are used for the long-distance transport whereas actin filaments are for the short-distance transport (Langford GM. 1995). The actin-based motors- myosins and microtubule-based motors- kinesins and dyneins are involved in this process (Ross JL *et al*. 2008). When vesicles approach the acceptor membrane, the initial interaction with the acceptor membrane is called tethering. The last step for vesicle trafficking is vesicle fusion and it takes place by pairing t-SNAREs ((Soluble N-ethylmaleimide-sensitive fusion attachment protein receptor)) with v-SNAREs (Bonifacino JS and Glick BS. 2004, Cai H *et al*. 2007). The most important aspects in membrane trafficking are how specific cargos are selected and sorted into specific vesicles and how these vesicles are transported and

fused with the right acceptors. The answers to these questions are in the mechanisms of core machinery-Rab GTPases and SNAREs in membrane trafficking described in the following sections.

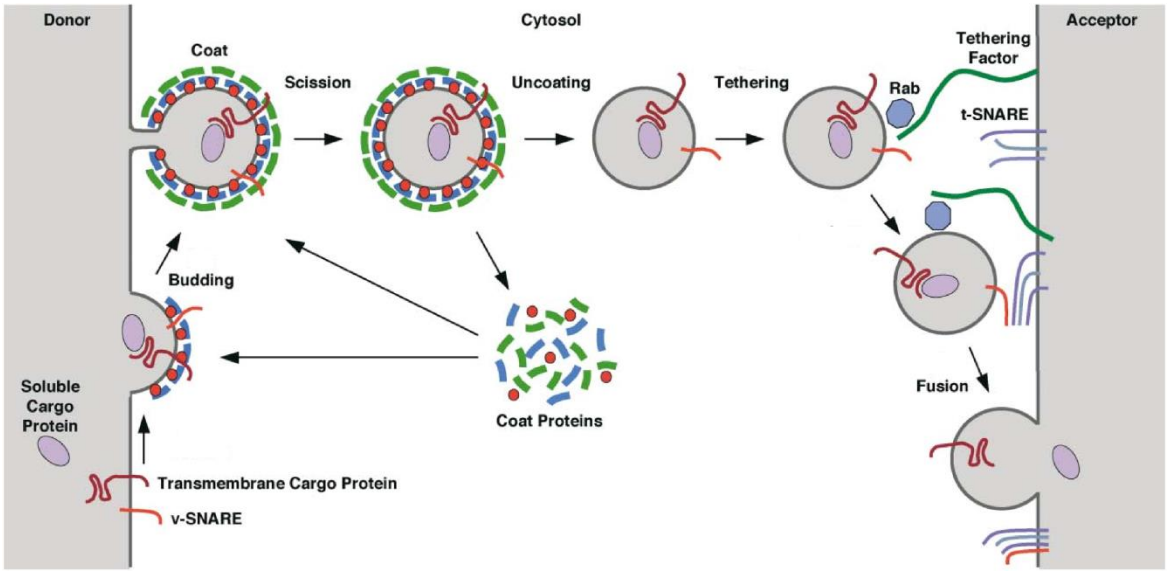

Fig. 1.3 Steps of membrane trafficking. Vesicle budding is the first step of vesicle trafficking. Coat proteins are recruited and assembled onto the donor membrane and some other proteins like dynamin are also involved in budding. The coat proteins are dissociated after vesicles are formed and recycled back for another round of budding. Then vesicles are transported along actin filaments or microtubules. With the help of tethering factors, vesicles initiate the interaction with the acceptor membrane. Finally, vesicles are fused with the acceptor membrane by forming the *trans*-SNARE complex. Adapted from Bonifacino JS and Glick BS. 2004

Coat proteins in budding

Vesicular budding is initiated when coat proteins are recruited to the donor membrane. There are two main functions for coat proteins. First, coat proteins ensure that specific cargo proteins are selected into the vesicles. Second, coat proteins shape the vesicles leading to the release of coated vesicles. There are three widely studied coat proteins: clathrin, COP I and COP II. Clathrin mediates the budding from the plasma membrane to endosomes and the TGN to endosomes. COP I-coated vesicles are derived from the Golgi complex and transport from the Golgi complex to the ER and between the Golgi cisternae, while COP II mediates the anterograde trafficking from the ER to the Golgi complex (Kirchhausen T. 2000, McMahon HT and Mills IG. 2004).

Clathrin is most abundant among all the coat proteins. Each clathrin subunit comprises of three large and three small polypeptide chains and together they form the so-called three-legged clathrin triskelion. The clathrin triskelions are finally assembled into lattice-like cages comprising hexagons and pentagons (Fotin A *et al*. 2004). The recruitment of clathrin into plasma membrane is triggered by the recruitment

of AP2 to the plasma membrane. PI(4,5)P_2 is found on the membrane of clathrin-coated pits. The initial recruitment of AP2 is through binding to PI(4,5)P_2 (Höning S *et al*. 2005). Then, clathrin is recruited to the plasma membrane by binding to the clathrin box motif of AP2 (Shih W *et al*. 1995). Cargo selection is facilitated by AP2 since AP2 recognizes the tyrosine or dileucine motifs in the cytoplasmic tails of cargo proteins in the plasma membrane. The vesicles derived from the TGN need the help of AP1 by recognizing the tyrosine or dileucine motifs of cargo proteins. In this way, the appropriate proteins are sorted into the right vesicles (Kirchhausen T. 2000, McMahon HT and Boucrot E. 2011). The recruitment of AP1 onto the Golgi membrane is dependent on ADP-ribosylation factor 1 (Arf1) and subsequently clathrin is recruited (Stamnes MA and Rothman JE. 1993).

COP I recognizes proteins with dilysine motif (KKXX or KXKXX, where X is any amino acid) in the cytoplasmic carboxy-terminal domain of cargo proteins. The initiation of COP I recruitment requires Arf1 in its GTP membrane-associated form (Donaldson JG *et al*. 1992). The GTP hydrolysis of Arf1 is stimulated by binding to COP I and the GTPase-activating protein (GAP) of Arf1. This results in the release of Arf1, which triggers the COP I uncoating (Kirchhausen T. 2000, McMahon HT and Mills IG. 2004).

COP II assembly starts with the recruitment of the small GTPase Sar1p to the ER. The GDP form of Sar1p is converted to GTP form by Sec12p that serves as a guanine exchange factor (GEF) for Sar1p (Barlowe C and Schekman R. 1993). Sec23-24 complex is then associated to the ER membrane by Sar1p and the complex is engaged in the selection of cargo. In the final step, Sec13-31 complex is also recruited, leading to the vesicles fission from the ER membrane. The recruitment of Sec13-31 complex is dependent on the presence of Sar1p and Sec23-24 complex (Kirchhausen T. 2000, Zanetti G *et al*. 2012).

Rab GTPases in vesicle trafficking

General introduction to Rab GTPases

First identified in rat brain, Rab is a subfamily of Ras (Rat sarcoma) GTPases with a high homology with Ras in the regions involved in GTP/GDP binding (Touchot N *et al*. 1987). Rab GTPases regulate membrane trafficking (Schmitt HD *et al*. 1986, Salminen A and Novick PJ. 1987) and it is widely accepted that Rab proteins are the key regulators of vesicle budding, motility, tethering and fusion during vesicle transport (Zerial M and McBride H. 2001, Stenmark H. 2009).

Rab GTPases constitute the largest Ras super-family of small GTPases. A comparative genome analysis has shown that Rab GTPases are widely distributed from yeast to humans (Bock JB *et al*. 2001). Moreover, around 8000 Rabs have been identified from genomes covering the entire eukaryotic tree (Diekmann Y *et al*. 2011). The wide distribution of Rab GTPases suggests their essential role in eukaryotic cells. In humans, there are at least 60 different members of Rab GTPases. The group of Rab GTPases present in humans is much larger than in yeast, *D. melanogaster* and *C. elegans.* The increased number of Rab GTPases present in humans is correlated with the higher degree of complexity of intracellular transport. In contrast, the number of other proteins involved in the core machinery of vesicle transport such as SNAREs and coat proteins is not significantly increased from yeast to humans, suggesting that the diversity and specificity of vesicle transport is mainly attributed to the complexity of Rab GTPases (Bock JB *et al*. 2001).

Structure of Rab GTPases

Rab GTPases consist of 6-stranded β sheets, 5 α helixes and 10 interconnecting loops (Stenmark H and Olkkonen VM. 2001). The regions that are involved in guanine and phosphate/Mg^{2+} binding are located in five of those loops. These regions are much conserved among all the members of Ras superfamily including Ras, Rho, Rab and Arf family. Hence, these regions are used to identify new GTPases by bioinformatics. Crystallographic studies have shown that similar to Ras GTPases, Rab GTPases switch between an active (GTP bound) and inactive (GDP bound) conformation (Dumas JJ *et al*. 1999, Stroupe C and Brunger AT. 2000). Two regions are involved in this conformational switch, the Switch I region and Switch II region. A threonine (T) residue localized in the phosphate-binding loop of the Switch I region, stabilizes the binding to the γ phosphate of GTP. A glutamine (Q) residue localized in the Switch II region is a critical residue required for the GTP hydrolysis. (Milburn MV *et al*. 1990, Krengel U *et al*. 1990, Dumas JJ *et al*. 1999). To distinguish from other GTPases, five Rab specific regions named as Rab family motifs (RabF) have been identified (Pereira-Leal JB and Seabra MC. 2000). RabF1 is localized in the Switch I region (loop2-β2) which is also the effector binding domain. The amino acid "G" in this motif can be used to exclude Ras and Rho from Rab GTPases. RabF2 in β3, RabF3 in loop 4, RabF4 in α2-loop 5 and RabF5 in β4-loop6 are all localized surrounding the Switch II region (**Fig. 1.4**). Because RabF regions are sensitive to the GTP/GDP state and show high identity within the overall sequence, they have been predicted to be involved in binding of general regulators such as Rab escort proteins (REPs) and Rab GDP dissociation inhibitors (GDIs) (Pereira-Leal JB and Seabra MC. 2000). Phylogenetic analysis has shown that Rab GTPases are clustered into different sub-families. 4 regions (RabSF1, RabSF2, RabSF3 and

RabSF4) have been identified to reveal the amino acids conservation within sub-families (**Fig. 1.4**). These regions show higher homology within sub-families than the overall sequence (Moore I *et al*. 1995, Pereira-Leal JB and Seabra MC. 2000). The 3D structure of the complex of Rab3A and the effector domain of Rabphilin-3A has demonstrated that two distinct interfaces of Rab3A are involved in binding to Rabphilin-3A (Ostermeier C and Brunger AT. 1999). The first interface comprises part of Switch I and Switch II regions of Rab3A. Another region, named Rab complementarity-determining region (RabCDR), consists of residues 19-22 in the loop α3-β5, and the C-terminal half of α helix α 5 (Ostermeier C and Brunger AT. 1999). RabCDRs are regions with variable sequence among the Rab family. So it has been proposed that the hypervariable RabCDRs of Rab GTPases confer the specificity of effectors. The combination of the hypervariable RabCDRs and the conserved Switch I and Switch II regions enable Rab GTPases binding to various effectors in a specific and GTP-dependent manner (Ostermeier C and Brunger AT. 1999)

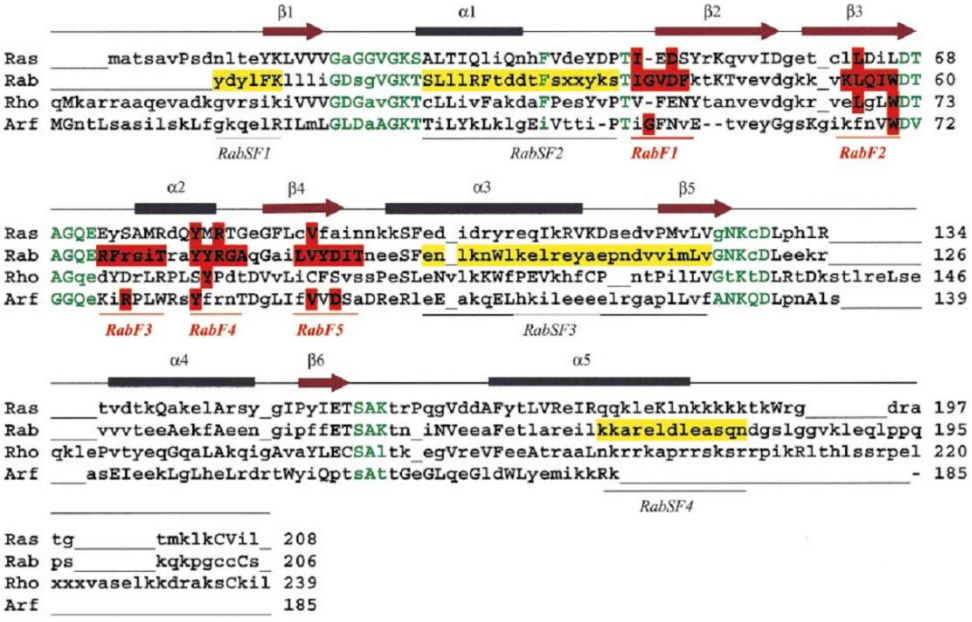

Fig. 1.4 The conserved structure of Rab GTPases. Residues which are found only conserved in the family of Rab GTPases are highlighted in red. Regions with such residues are denoted as Rab family motif (RabF). Five such motifs have been identified (RabF1, RabF2, RabF3, RabF4, RabF5). Regions with green residues are nucleotide binding motif (PM/G motif). These motifs are conserved among all the Ras superfamilies of small GTPases. Regions with yellow residues are Rab subfamily motifs (RabSFs). Four RabSFs have been identified (RabSF1, RabSF2, RabSF3, RabSF4). Adapted from Pereira-Leal JB and Seabra MC. 2000.

GTP/GDP cycling of Rab GTPases

Rab GTPases have two main states: a GTP-bound form and a GDP-bound form (**Fig. 1.5**). In the GTP-bound form, Rab GTPases are recruited to membranes from the cytosolic pool. In this state, by interacting with diverse effectors and coordinating motor proteins and SNARE proteins activity, Rab GTPases control vesicle budding, fission, mobility and fusion. The newly synthesized Rab GTPases, which

are in a GDP-bound state, are recognized by Rab escort proteins (REPs) (Alexandrov K *et al*. 1994). REPs deliver Rab GTPases to geranylgeranyl transferases (GGTs). Rab GTPases are subsequently geranylgeranylated at a cysteine residue located at the C-terminus. This post-translational modification occurs at different cysteine motifs at the C-terminus such as CXXX, CC, CXC, CCXX or CCXXX, where X here represents any amino acid (Anant JS *et al*. 1998). In the pre-existing pool of Rab GTPases, the geranylgeranylated, GDP-form Rab GTPases are recognized by GDP dissociation inhibitors (GDIs) that inhibit GDP dissociation (Ullrich O *et al*. 1993). Targeting of Rab-GDI to the specific membranes is facilitated by interacting with membrane-bound GDI displacement factors (GDFs) (Dirac-Svejstrup AB *et al*. 1997). Guanine exchange factors (GEFs) catalyze the exchange of GDP to GTP (Moya M *et al*. 1993). During vesicle fusion, GTP associated to Rab GTPases is hydrolyzed into GDP by their intrinsic GTPase and GTPase-activating proteins (GAPs) (Strom M *et al*. 1993). Hence, the GTP-bound form turns into the GDP-bound form, in which Rab GTPases dissociate from the vesicle membrane to cytosol (Stenmark H and Olkkonen VM. 2001, Stenmark H. 2009). Interestingly, Rab5A can be recruited into mitochondria by artificially directing Rabex-5 (the GEF of Rab5) to mitochondria. In the same way, the GEFs of Rab1A and Rab8A are sufficient for targeting Rab1A and Rab8A to mitochondria, respectively. Therefore, it has been proposed that the specific membrane localization of Rab GTPases is directed by RabGEFs (Blümer J *et al*. 2013).

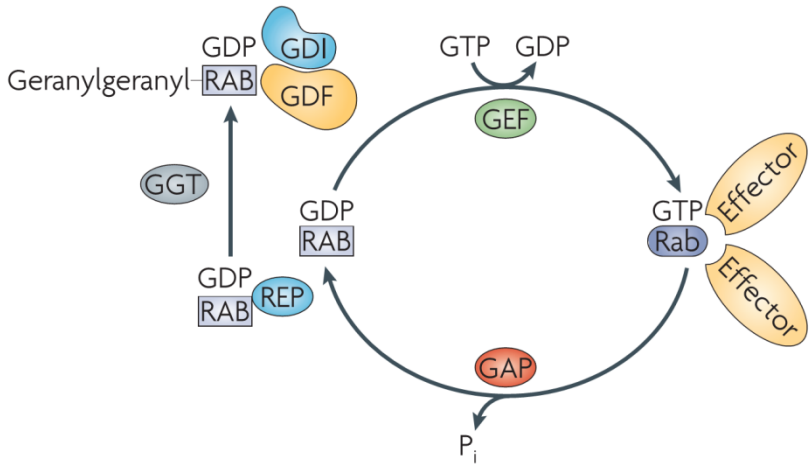

Fig. 1.5 The Rab GDP/GTP cycle. Rab GTPases switch between a GDP and GTP conformation. The newly synthesized Rab GTPases are recognized by REPs. Rab GTPases in the GDP form interact with GDFs and GDIs. The conversion from the GDP form to the GTP form requires GEFs. In the GTP form, Rab GTPases target to the specific membranes and recruit effectors. The GTP associated to Rab GTPases can be hydrolyzed to GDP with the help of GAPs. Subsequently, Rab GTPases are dissociated from membranes and ready for another round of cycle. Adapted from Stenmark H. 2009

Rab GTPases in budding and cargo selection

As mentioned before, the coat proteins COP I, COP II, clathrin and adaptins are responsible for the vesicle formation and cargo selection (Kirchhausen T. 2000, McMahon HT and Mills IG. 2004). In

addition, Rab GTPases also contribute to the budding process (**Fig. 1.6**) (Stenmark H. 2009). Rab5 is present in CCVs together with clathrin heavy chain in baby hamster kidney (BHK) cells (Bucci C *et al*. 1992). Components present in the cytosol are also required for adaptor-dependent transferrin sequestration in clathrin-coated vesicles (Smythe E *et al*. 1992). Evidence indicates that depletion of the GDI and Rab5 from the cytosol results in the inhibition of sequestration of transferrin, suggesting that both Rab5 and RabGDI are required for this process (Mclauchlan H *et al*. 1997). However, RabGDI alone has no effect on the formation of clathrin-coated pits. Altogether, evidence suggests that RabGDI may act after the recruitment of coat proteins to sequester the ligands (Mclauchlan H *et al*. 1997).

In addition to budding, Rab GTPases can participate in cargo selection. One example in which a Rab GTPase contributes to cargo selection is during the trafficking from late endosomes to the Golgi complex. Rab9 is responsible for mannose 6-phosphote receptors (MPRs) recycling from late endosomes to the TGN (Lombardi D *et al*. 1993, Riederer MA *et al*. 1994). TIP47 (MPR tail interacting protein of 47kDa) functions as a cargo selection molecule in transporting both cation-independent MPR (CI-MPR) and cation-dependent MPR (CD-MPR) from late endosomes to the TGN. TIP47 recognizes a Phe-Trp signal in the cytoplasmic domain of CD-MPR. This signal is distinct from the tyrosine and dileucine based motifs that are recognized by AP1 or AP2 (Diaz E and Pfeffer SR. 1998). TIP47 preferentially and directly binds to the GTP-form of Rab9 forming a complex with CI-MPR. Moreover, the affinity of TIP47 for CI-MPR is increased by Rab9. Hence it has been proposed that Rab9 recruits the cargo selection molecule- TIP47 to late endosomes and stimulates the binding of TIP47 with MPRs (Carroll KS *et al*. 2001).

Rab GTPases in uncoating

After vesicles closure and departure from the parental membranes, the coat proteins that interfere with membrane fusion dissociate from the vesicles (McMahon HT and Boucrot E. 2011). Clathrin uncoating from CCVs requires heat shock protein 70 (Hsc70) and auxilin (McMahon HT and Boucrot E. 2011). However, Hsc70 is not sufficient for the release of AP2 and other cytosolic factors are implicated in this process (Hannan LA *et al*. 1998) and Rab GTPases also contribute to this process (**Fig. 1.6**) (Stenmark H. 2009). Rab5 is found to be involved in AP2 uncoating *in vitro* (Semerdjieva S *et al*. 2008). The expression of the dominant negative mutant Rab5S34N decreases AP2 uncoating in cells, suggesting that Rab5 is important for AP2 uncoating. The recruitment of AP2 to the plasma membrane is dependent on the binding to $PI(4,5)P_2$. However, $PI(4,5)P_2$ turnover is compromised in cells expressing Rab5S34N. Two guanine exchange factors for Rab5, Rabex-5 and hRME-6 (mammalian ortholog of receptor-mediated endocytosis protein 6), are also involved in AP2 uncoating in cells. The recruitment of hRME-6 increases

the dephosphorylation of the AP2 component-μ2 which is necessary for efficient AP2 uncoating, arguing that Rab5/hRME-6 increases AP2 uncoating by promoting μ2 dephosphorylation and PI(4,5)P_2 turnover (Semerdjieva S *et al*. 2008).

Rab GTPases in vesicle motility

In addition to cargo selection and uncoating, Rab GTPases are also able to recruit effectors that contribute to vesicle motility along actin filaments or microtubules (**Fig. 1.6**). Myosins are a family of ATP-dependent motor proteins that promote motility along the actin cytoskeleton (Hodge T and Cope MJ. 2000). In particular, Myosin Vb interacts with Rab11a, Rab11b and Rab25 (Lapierre LA *et al*. 2001). Expression of Myosin Vb tail results in the defect of transferrin recycling (Lapierre LA *et al*. 2001). Moreover, Rab11 family interacting protein 2 (Rab11-FIP2) interacts directly with Myosin Vb, suggesting that Rab11 regulates the recycling by interacting with Myosin Vb through Rab11-FIP2 (Hales CM *et al*. 2002). In addition, Rab8a wild-type and the constitutively active mutant Rab8a-Q67L also interact with Myosin Vb (Roland JT *et al*. 2007). Rab8a is localized in clusters of perinuclear puncta instead of tubular localization in cells expressing the dominant negative Myosin, suggesting that the movement of Rab8a-positive vesicles is Myosin Vb dependent (Roland JT *et al*. 2007). The Rab27a-regulated transport of melanosomes to the plasma membrane is also Myosin Va dependent (Hume AN *et al*. 2001). Yeast two-hybrid assays have demonstrated that melanophilin interacts with Rab27a wild-type and Rab27a Q78L, but not with the dominant negative mutant Rab27a-T23N. The recruitment of melanophilin to melanosomes in turn recruits Myosin Va (Wu XS *et al*. 2002). Altogether, these examples sufficiently demonstrate that Rab GTPases regulate vesicle motility by interacting with motor proteins.

Rab GTPases in tethering and fusion

Rab GTPases also contribute to the specificity during vesicle transport by recruiting tethering factors and SNAREs to coordinate with specific membranes (**Fig. 1.6**) (Stenmark H. 2009). A well-studied example of fusion regulation is Rab5 in early endosomal fusion. Rab5 is localized on the cytoplasmic surface of the plasma membrane and early endosomes (Chavrier P *et al*. 1990). Rab5 is essential for early endosome fusion and over-expression of the constitutively active mutant Rab5Q79L results in the formation of enlarged early endosomes and the stimulated homotypic fusion of early endosomes (Gorvel J *et al*. 1991, Stenmark H *et al*. 1994). Early endosome antigen 1 (EEA1) is an effector of Rab5 and EEA1 is required for the early endosome fusion (Simonsen A *et al*. 1998). EEA1 alone significantly stimulates the early endosome fusion *in vitro*. However, the EEA1-mediated fusion is abolished when SNAREs priming is

inhibited, indicating that EEA1 is not involved in the membrane fusion. A morphological tethering assay has further suggested that EEA1 functions in early endosome membrane tethering (Christoforidis S *et al*. 1999). To coordinate the tethering and fusion, SNAREs can directly interact with EEA1. Syntaxin-6 is a SNARE protein involved in the TGN to early endosome trafficking. It has been shown that Syntaxin-6 specifically interacts with EEA1 (Simonsen A *et al*. 1999). In addition, EEA1 also binds to the SNARE protein- Syntaxin 13 which is required for the early endosome fusion (McBride HM *et al*. 1999).

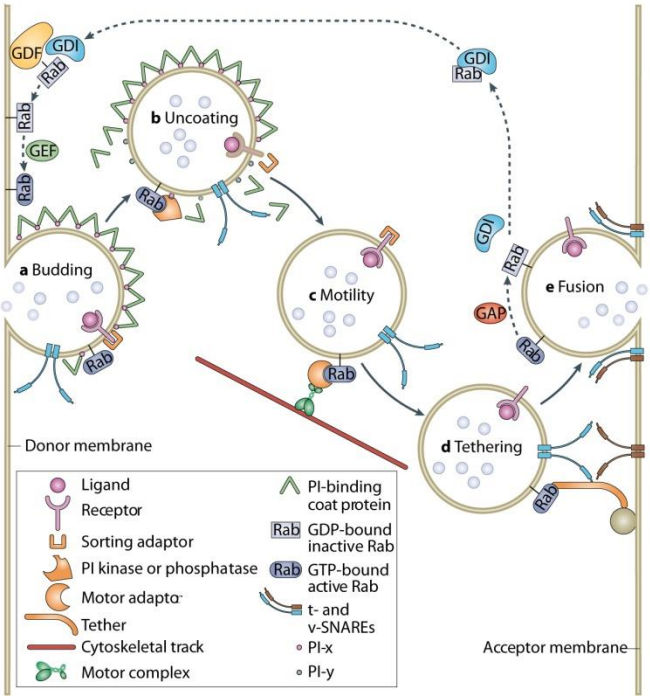

Fig. 1.6 Rab GTPases function in the process of membrane trafficking. Different steps in vesicle trafficking, such as budding, uncoating, motility, tethering and fusion, are controlled by Rab GTPases and their effectors. **a)** Rab GTPases play roles in cargo selection and sorting receptors into budding vesicles. **b)** Through recruitment of PI kinases or phosphatases, Rab GTPases alter the PI composition of vesicle membrane and causes coat proteins uncoating. **c)** Rab GTPases control vesicle transport along actin filaments or microtubules by recruiting motor proteins. **d)** Rab GTPases mediate vesicle tethering by recruiting tethering factors. Tethering factors can interact with SNAREs and their regulators to activate the formation of SNARE complex. **e)** The formation of SNARE complex leads to vesicle fusion. Meanwhile, active GTP-bound Rab GTPases are converted to inactive GDP-bound form, which is stimulated by GAPs. The GDP-bound Rab GTPases can be directed back to the donor membrane and for another round of trafficking. Adapted from Stenmark H. 2009

Role of SNAREs in fusion

As mentioned, Rab GTPases can interact with SNAREs via tethering factors to coordinate vesicle tethering and fusion. Four SNAREs including Syntaxin A, Syntaxin B, VAMP-2 and SNAP-25 were originally identified by functional affinity purification (Söllner T *et al*. 1993). All these four SNAREs are confined in synaptic vesicles in neurons. However, SNAPs are generally involved in many different fusion processes. Given this fact, the SNARE hypothesis postulates that each kind of transport vesicle or target membrane has its own v-SNAREs (vesicle-membrane SNAREs) or t-SNAREs (target- membrane SNAREs). In addition, v-SNAREs and t-SNAREs form unique complementary matches. So the unique pairs of v-SNAREs and t-

SNAREs determine the specificity of vesicle fusion (Söllner T *et al*. 1993, Rothman JE and Warren G. 1994).

SNAREs are the core regulators in vesicle fusion and constitute a family of compartment specific proteins with 25 members in *S. cerevisiae*, 36 members in humans and 54 members in *A. thaliana* (Bock JB *et al*. 2001). SNAREs have a characteristic domain-SNARE motif. At the C-terminal, a single transmembrane domain is connected to the SNARE motif. To facilitate the membrane anchorage, SNAREs are modified by palmitoylation (Jahn R and Scheller RH. 2006). Crystallography studies have revealed that v-SNAREs interact with t-SNAREs to form a stable four interwinded, parallel α-helices structure (Sutton RB *et al*. 1998, Antonin W *et al*. 2002). In this conformation, 16 stacked layers of interacting side chains are formed in the center of the bundle. Most of the layers are hydrophobic, except the central "0" layer that consists of three highly conserved glutamine (Q) residues and one highly conserved arginine (R) residue. Based on the presence of these residues, SNARE proteins were reclassified as Q- and R-SNAREs (Fasshauer D *et al*. 1998) instead of the old classification of t-SNAREs and v-SNAREs. The other layers flanking along both sides of "0" layer are composed of hydrophobic leucine, isoleucine and valine residues. These hydrophobic layers act as a watertight seal to protect the central ionic layers from the solvent. If another protein disrupts the seal, the ionic layers are exposed to the solvent resulting in a weakening of the interhelix interaction. This process may facilitate the disassembly of SNAREs (Sutton RB *et al*. 1998, Antonin W *et al*. 2002). According to the zippering hypothesis, SNARE proteins are assembled from the N-terminal SNARE motifs and then proceeded in a zipper-like fashion toward the C-terminal transmembrane domains to form the *trans*-SNARE complex. The mechanical force exerted by *trans*-SNARE complex drives the vesicle membranes fusing with each other (Jahn R and Scheller RH. 2006).

Endosome maturation and Rab GTPases

Endosome maturation

Immediately after the formation of nascent endosomes, these organelles follow a process of maturation. Early endosomes (EEs) are considered the main sorting hub in the endocytic pathway and the starting point of endosome maturation. They receive cargo proteins from other EEs and specific EEs cargo is transported to the plasma membrane, sorting endosomes and the TGN (Maxfield FR and McGraw TE. 2004). It is well established that Rab5 is the key regulator for EEs trafficking (Zerial M and McBride H. 2001). Rab5 stimulates the fusion of EEs by recruiting different effectors. One of the effectors is p150-

hVPS34, the human ortholog of yeast Vps15-Vps34 (vacuolar protein sorting 34), which belongs to the class III PI3-kinases. VPS34 is responsible for generating PI3P on the membrane of EEs (Christoforidis S *et al*. 1999). PI3P is mainly enriched in EEs and it can be recognized as one of the characteristics for EEs (Zerial M and McBride H. 2001). Other Rab proteins, such as Rab4 and Rab11 have also been identified on EEs. They are clustered in defined domains that differ in composition and function (Sönnichsen B *et al*. 2000, Zerial M and McBride H. 2001). EEs are then transformed to late endosomes (LEs) and Rab5 is gradually lost and replaced by Rab7. Rab7 is localized in LEs controlling their trafficking (Feng Y *et al*. 1995, Soldati T *et al*. 1995, Bucci *et al*. 2000). There are two models to explain how LEs are formed. The first one is called the Rab5-Rab7 conversion model (Rink J *et al*. 2005). In this model, Rab7 is recruited to endosomes right after Rab5 dissociation, resulting in the conversion from Rab5 to Rab7 (Rink J *et al*. 2005 , Poteryaev D *et al*. 2010, Kinchen JM and Ravichandran KS. 2010). The other model is called endosomal carrier vesicles (ECVs) model. It suggests that Rab7 positive vesicles are budded from Rab5 positive early endosomes (Vonderheit A and Helenius A. 2005). After the formation of LEs, they continue to undergo the maturation and finally fuse with lysosomes. This process leads to the change in morphology, the dramatic decrease of pH and acquisition of lysosomal hydrolases and proteases (Huotari J and Helenius A. 2011).

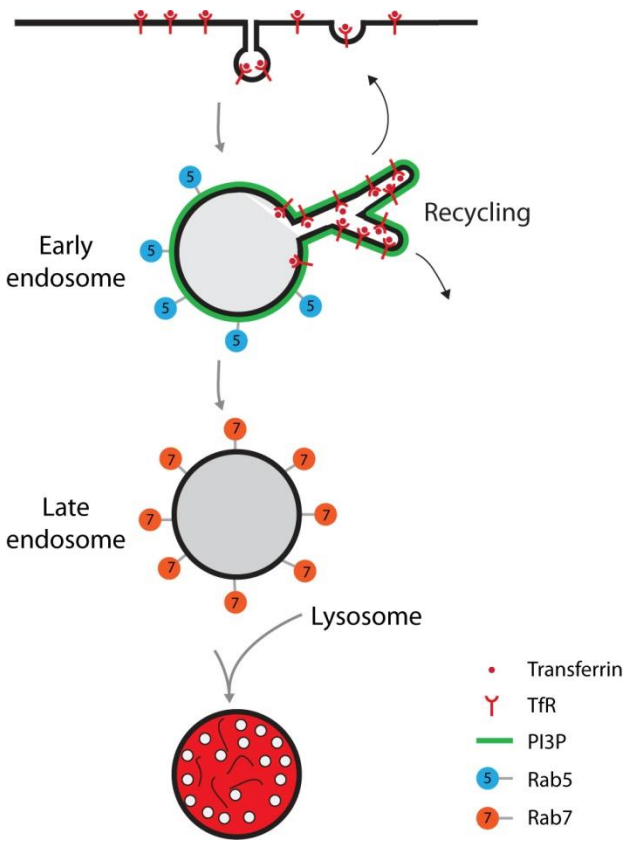

Fig. 1.7 The process of endosome maturation. Some receptors (transferrin receptor shown here) and membrane proteins are internalized by the clathrin-mediated endocytosis. Immediately after early endosomes are formed, they follow a process called endosome maturation. Early endosomes are characterized by the association of Rab5 and PI3P. They are dynamically interacting with other early endosomes. Some cargos of early endosomes can be recycled to the plasma membrane or sorted to sorting endosomes. The formation of late endosomes is preceded by the generation of a Rab7 domain. Two models have been proposed to explain how Rab7 is recruited to late endosomes, Rab5-Rab7 conversion model and ECVs model. Then late endosomes are ready to fuse with lysosomes. Finally, most of the components of late endosomes are degraded.

Mechanisms of Rab GTPases in the regulation of endosome maturation

Rab5 functions in the early endocytic pathway

In 1990 the cDNA of Rab5 was first cloned (Chavrier P *et al*. 1990). When expressed, Rab5 is localized in the cytoplasmic surface of plasma membrane and early endosomes, suggesting a role in endocytosis (Chavrier P *et al*. 1990). Subsequently, different studies have shown that Rab5 is essential for early endosome fusion *in vitro* and *in vivo* (Gorvel J *et al*. 1991, Bucci C *et al*. 1992). Over-expression of the constitutively active mutant Rab5Q79L results in the formation of enlarged early endosomes. Further, *in vitro* assays have shown that the fusion between early endosomes is strongly enhanced by Rab5Q79L. These and other experiments indicate that Rab5 plays a key role in stimulating the homotypic fusion between early endosomes (Stenmark H *et al*. 1994).

Several Rab5 effectors have been characterized giving new insights into the function of this GTPase. The first identified effector was Rabaptin-5 (Stenmark H *et al*. 1995). Rabaptin-5 is recruited to early endosomes by Rab5 in a GTP-dependent manner. Early endosomal fusion is decreased when Rabaptin-5 is depleted from the cytosol, indicating that Rabaptin-5 is required for Rab5-stimulated early endosome fusion (Stenmark H *et al*. 1995). Rabex-5 is a guanine exchange factor of Rab5 and forms a tight complex with Rabaptin-5 (Horiuchi H *et al*. 1997). Subsequently, Rabex-5 is recruited to early endosomes via Rabaptin-5. In consequence, Rabex-5 generates more active Rab5 association to early endosomes that in turn recruits more Rabaptin-5/Rabex-5 complex to early endosomes (Horiuchi H *et al*. 1997). This positive-feedback loop counteracts the GTP hydrolysis of GTP-Rab5 and creates a subcompartment rich in Rab5 and Rab5 effectors (Horiuchi H *et al*. 1997, McBride HM *et al*. 1999, Zerial M and McBride H. 2001).

EEA1 is another effector of Rab5 and it is also required for early endosome fusion (Christoforidis S *et al*. 1999). EEA1 has two important domains, one is Rab5 binding domain and the other is FYVE (named after Fab 1, YOTB, Vac 1 and EEA1) domain. FYVE domain is a cysteine-rich, Zn^{2+} binding domain which specifically binds PI3P (Stenmark H *et al*. 1996, Burd CG and Emr SD. 1998). This domain of EEA1 is required for its early endosomal localization (Stenmark H *et al*. 1996). In addition, EEA1 association to early endosomes is blocked by phosphatidylinositol-3-OH kinases (PI3Ks) inhibitors (Simonsen A *et al*. 1998). *In vitro* experiments have revealed that an excess of EEA1 significantly stimulates early endosome fusion bypassing Rab5 and PI3P functions. However, the EEA1-stimulated fusion is abolished by blocking the priming of SNAREs, indicating EEA1 itself is not involved in the process of vesicle fusion. *In vitro*

assays have suggested that EEA1 functions in early endosome membrane tethering (Christoforidis S *et al*. 1999). The fact that EEA1 forms a parallel coiled-coil dimer in cytosol indicates that EEA1 is a tethering factor, not a SNARE protein (Callaghan J *et al*. 1999). To coordinate the tethering and fusion, SNAREs directly interacts with EEA1 (Simonsen A *et al*. 1999, McBride HM *et al*. 1999). Syntaxin 6 is a SNARE involved in the trafficking from the TGN to early endosomes (Bock JB *et al*. 1997). It has been shown that Syntaxin 6 specifically interacts with EEA1 (Simonsen A *et al*. 1999). In addition, EEA1 also binds Syntaxin 13, a SNARE required for early endosome fusion (McBride HM *et al*. 1999).

Two PI3Ks have also been identified as effectors of Rab5 (Christoforidis S *et al*. 1999). The first one, p85α-P110β, is a class-I kinase which mainly produces phosphatidylinositol (3,4)-bisphosphate (PI(3,4)P_2) and phosphatidylinositol (3,4,5)-triphosphate (PI (3,4,5)P_3). The second interacting PI3K is p150-hVPS34, belonging to class-III kinases. VPS34 which is responsible for generating PI3P on the membrane of early endosomes is essential for their fusion. It has been proposed that GTP-Rab5 interacts with p150-hVPS34 to generate PI3P, facilitating the recruitment of other effectors, such as EEA1 and Rabenosyn-5 (Christoforidis S *et al*. 1999, Nielsen E *et al*. 2000). Rabenosyn-5 is another effector of Rab5 and the recruitment of this effector to early endosomes is PI3P dependent through its FYVE domain (Nielsen E *et al*. 2000). Yeast Vps45 binds to multiple SNAREs, such as Pep12p and Tlg2p (Burd CG *et al*. 1997, Abeliovich H *et al*. 1999). Rabenosyn-5 also forms a complex with hVPS45 (human ortholog of yeast Vps45) that interacts with multiple SNARE proteins, suggesting that Rabenosyn-5, similar to EEA1, functions as a linker between Rab5 and SNAREs (Nielsen E *et al*. 2000). Over-expression of Rabenosyn-5 but not EEA1 induces a delay in the processing of pro-cathepsin D to the 47-kD intermediate, suggesting that Rabenosyn-5 has a distinct role from EEA1 in early endosome trafficking (Nielsen E *et al*. 2000).

The diversity of effectors and interacting proteins of Rab5 has raised the question how these proteins cooperate to regulate membrane trafficking. It has been proposed that Rab proteins and their effectors are not distributed evenly on the membrane, but clustered in defined regions (Zerial M and McBride H. 2001). This is accordance with the study showing that EEA1, Rabaptin-5, Rabex-5, Syntaxin 13 and NSF (N-ethylmaleimide-sensitive factor) form a high molecular weight oligomer on the endosomal membrane (McBride HM *et al*. 1999). The association to early endosomes of proteins such as EEA1, Rabenosyn-5 and Syntaxin 13 directly or indirectly requires PI3P. As a result, PI3P might play a pivotal role in organizing the oligomerization of those proteins (Zerial M and McBride H. 2001).

Rab7 functions in the late endocytic pathway

Rab7 is associated to both late endosomes and lysosomes. It is well established that this small GTPase is involved in late endosomal trafficking, lysosome biogenesis and lysosome positioning (Feng Y *et al*. 1995, Soldati T *et al*. 1995, Bucci C *et al*. 2000).

According to the Rab5-Rab7 conversion model, Rab5 is simultaneously exchanged with Rab7 during endosome maturation (Rink J *et al*. 2005, Poteryaev D *et al*. 2010, Kinchen JM and Ravichandran KS. 2010). HOPS (homotypic fusion and vacuole protein sorting) complex has been implicated in the recruitment of Rab7 to late endosomes. VPS11, VPS16, VPS18, and VPS33 form the class C vacuole protein sorting (VPS-C) complex. In addition, two accessory proteins VPS39 and VPS41 associate to VPS-C complex to form the HOPS complex (Nickerson DP *et al*. 2009). The mutations of the four proteins in VPS-C complex had a defect in tethering and fusion at the stage of Golgi-to-endosome and endosome-to-vacuole transport in yeast (Peterson MR and Emr SD. 2001). The VPS-C complex interacts with a Syntaxin homolog Vam3 which binds a SNAP-25 homolog Vam7 and a vesicle-associated membrane protein (VAMP) homolog Vti 1 to form the SNARE complex. Mutations in VPS-C disrupt the assembly of SNARE complex. Thus, it is proposed that VPS-C functions in vesicle tethering and fusion by mediating the assembly of SNARE complex through Vam3 (Sato TK *et al*. 2000). VPS39 also directly binds GDP-Ypt7 (Rab7 in yeast), controling the guanine nucleotide exchange of Ypt7. This suggests that VPS39 functions as a GEF of Ypt7 (Wurmser AE *et al*. 2000). However, mVPS39 (mammalian Vps39) induces lysosomal clustering without increasing the GTP binding of Rab7 (Peralta ER *et al*. 2010). Expression of the dominant negative mutant of mVPS39 induces lysosomal fragmentation, similar with the expression of the dominant negative mutant of Rab7, indicating that mVPS39 functions in the tethering and fusion, but not as a GEF of Rab7 (Peralta ER *et al*. 2010). In addition, Mon1 (MONensin sensitivity)-Ccz1 (Calcium Caffeine Zinc sensitivity), has been identified as a GEF of Ypt7 in yeast (Nordmann M *et al*. 2010). Therefore, the HOPS complex may play a dual role as the upstream GEF and the downstream tethering and fusion effector of Rab7.

Rab-interacting lysosomal protein (RILP) is another downstream effector of Rab7 (Cantalupo G *et al*. 2001, Wang T *et al*. 2004, Colucci AM *et al*. 2005). The active, GTP-bound Rab7 recruits RILP to late endosomes/lysosomes (Cantalupo G *et al*. 2001). Over-expression of RILP causes aggregation of late endosomes and lysosomes in the perinuclear region, which is similar to the effect observed with the constitutively active mutant of Rab7 (Rab7Q67L) expression, indicating RILP may have a role in late endosomes/lysosomes organization (Cantalupo G *et al*. 2001). The RILP-C33 (a truncated mutant lacking

the N-terminal) expression results in the decreased degradation of low-density lipoprotein (LDL) and EGF, suggesting that RILP functions in the trafficking to the degradative compartments of endocytic pathways (Cantalupo G *et al*. 2001). RILP over-expression induces the recruitment of dynein-dynactin complexes to lysosome clusters (Jordens I *et al*. 2001). Disrupting the function of dynein results in the distribution of lysosomes from the perinuclear region to the peripheral area, suggesting that RILP-induced lysosome clustering is mediated by the minus-end directed transport through dynein-dynactin complex. However, there is no direct interaction between RILP and subunits of the dynein-dynactin motor complex (Jordens I *et al*. 2001). The oxysterol-binding protein homologue (ORP1L) preferentially binds to the active, GTP-bound Rab7, suggesting ORP1L is also an effector of Rab7 (Johannsson M *et al*. 2005). Over-expression of ORP1L results in the dynein-dynactin dependent clustering and enlargement of late endosomes and lysosomes (Johannsson M *et al*. 2005). Moreover, Rab7, RILP and ORP1L form a complex without direct interaction between RILP and ORP1L (Johannsson M *et al*. 2007). Interestingly, the binding ability of ORP1L with GTP-Rab7 is stimulated in the presence of RILP (Johannsson M *et al*. 2007). RILP also interacts with $p150^{Glued}$, one of the subunits of dynactin, suggesting that Rab7-RILP recruits the dynein motor through $p150^{Glued}$ (Johannsson M *et al*. 2007).

Rabring7 is a novel effector of Rab7 recruited to late endosomes/lysosomes by GTP-Rab7 (Mizuno K *et al*. 2003). Over-expression of Rabring7 induces the aggregation of lysosomes in perinuclear region and inhibits the degradation of EGF, suggesting Rabring7 has a role in vesicle trafficking to late endosomes/lysosomes (Mizuno K *et al*. 2003). Rubicon (Run domain protein as Beclin 1 interacting and cysteine-rich containing) directly and specifically interacts with GTP-Rab7, suggesting that Rubicon is also an effector of Rab7. UVRAG (UV radiation resistance-associated gene protein) binds the HOPS complex and activates its GEF activity (Sun Q *et al*. 2010). However, by interacting with UVRAG Rubicon inhibits its association to the HOPS complex and hence inhibits Rab7 activation. Epidermal growth factor receptor (EGFR) degradation is significantly reduced in cells expressing Rubicon. Altogether, Rubicon, as an effector of Rab7, plays a negative role in endosome maturation by inhibiting the GEF activity of Rab7 through interacting with UVRAG (Sun Q *et al*. 2010).

Rab4 and Rab11 function in endosomal recycling

Rab4 regulates the fast recycling pathway from early endosomes to the plasma membrane (van der Sluijs P *et al*. 1992, Sheff DR *et al*. 1999, Maxfield FR and McGraw TE. 2004). The function of Rab4 may not be limited to the early stage of recycling since Rab4 remains associated to endosomes when most of transferrin has been recycled (Sönnichsen B *et al*. 2000). Many membrane proteins, such as LDL, EGF, β_2-

Adrenergic receptor and αvβ3 integrin, can be transported in a Rab4 dependent recycling pathway (van der Sluijs P *et al*. 1992, Seachrist JL *et al*. 2000, Roberts M *et al*. 2001). The recycling function of Rab4 requires the cycles between association and dissociation from early endosomes (Mohrmann K *et al*. 2002). Rab4 is also involved in degradative pathways. Over-expression of the dominant negative mutant Rab4S22N results in a significant reduction in the degradation of EGF and LDL (McCaffrey MW *et al*. 2001).

Rabaptin-5 is an effector of Rab5 essential for early endosome fusion (Stenmark H *et al*. 1995). This Rab5 effector can also interact specifically with GTP-Rab4 through a region that is different from the region of binding to Rab5 (Vitale G *et al*. 1998). Additionally, Rabaptin-4, a homolog to Rabaptin-5, interacts with GTP-Rab4 and to a less extent with GTP-Rab5 (Nagelkerken B *et al*. 2000). The intrinsic GTPase activity of Rab4 is inhibited by its binding to Rabaptin-4 (Nagelkerken B *et al*. 2000). Rab4 forms a complex with the γ-σ subunits of AP-1 by directly binding to Rabaptin-5 (Deneka M *et al*. 2003). Rab5 also binds to Rabaptin-5 although the binding ability is less than Rab4. Over-expression of both Rabaptin-5 and γ-adaptin results in the delayed exit of transferrin from early endosomes (Deneka M *et al*. 2003) and *in vitro* formation of recycling vesicles is inhibited by adding Rabaptin-5 (Pagano A *et al*. 2004). Therefore, Rabaptin-5/Rabaptin-4 acts as a linker between Rab4 and Rab5 to coordinate endocytosis and recycling (Vitale G *et al*. 1998, Deneka M *et al*. 2003).

Rab4 also regulates endosome transport by interacting with motor proteins or other effectors. The translocation of glucose transporter type 4 (GLUT4) to the plasma membrane is Rab4 dependent in adipocytes (Vollenweider P *et al*. 1997). KIF3B, a motor protein of the kinesin II family, directly interacts with GTP-Rab4, suggesting KIF3B is an effector of Rab4 (Imamura T *et al*. 2003). It has been proposed that by interacting with KIF3, Rab4 transports the GLUT4 vesicles along microtubules to the cell surface. (Imamura T *et al*. 2003). Rabip4 is another effector of Rab4 that was originally identified in a yeast two-hybrid system. Over-expression of Rabip4 increases the overlap between the early endosomal Rab5 and the recycling endosome marker-Rab11 or Rab4. So Rabip4 may regulate the opposite transport from recycling to sorting endosomes by interacting with Rab4 (Cormont M *et al*. 2000). Rabip4' is a variant of Rabip4 with extra of 108 amino acids at the N-terminal. Rabip4' interacts with the GTP-bound Rab4 and Rab5 simultaneously, suggesting Rabip4' may function as a molecular bridge between Rab4 and Rab5 to coordinate endocytosis and recycling (Fouraux MA *et al*. 2004).

Rab11 controls the slow recycling pathway from the perinuclear recycling compartments to the plasma membrane (Ullrich O *et al*. 1996, Ren M *et al*. 1998, Maxfield FR and McGraw TE. 2004). Biochemical

analysis of Rab5 and Rab11 association with membranes has demonstrated that the distribution of Rab5 and Rab11 is segregated, suggesting that Rab11 and Rab5 regulate different steps along the endocytic pathway. It also has been shown that transferrin first enters Rab5-positive endosomes and then transit into Rab11-positive endosomes (Trischler M *et al*. 1999). Consistent with previous observations, most of transferrin-containing structures are labeled with Rab5 early after internalization. Rab11 association to transferrin-containing structures is slowly increased after 30 min (Sönnichsen B *et al*. 2000). Interestingly, Rab4, Rab5 and Rab11 are also found within the same endosomes occupying different domains. Therefore, it has been proposed that transferrin is first sorted from Rab5-domain to Rab4-domain on the same endosome via the fast recycling pathway. Once transferrin is transported into the endosomes positive for Rab4 and Rab11, the recycling is slow down (Sönnichsen B *et al*. 2000).

The first putative effector identified for Rab11 is Rab11BP. The transferrin recycling is inhibited by over-expression of Rab11BP truncated mutant lacking the functional region, suggesting that Rab11BP is involved in Rab11-dependent transferrin recycling (Zeng J *et al*. 1999). A family of Rab11 interacting proteins, including Rab11-FIP1, Rab11-FIP2, Rab11-FIP3 and pp75/Rip11, has been later identified as Rab11 effectors (Hales CM *et al*. 2001). Over-expression of a C-terminal Rab11-FIP1 mutant lacking the Rab11 binding domain inhibits the transferrin recycling, suggesting that Rab11-FIP1 is involved in Rab11-dependent transferrin recycling (Lindsay AJ and McCaffrey MW. 2002). Further studies have shown that Rab11-FIP2 interacts directly with Myosin Vb. Based on this, it is postulated that Rab11 regulates endosomal recycling by interacting with Myosin Vb through Rab11-FIP2 (Hales CM *et al*. 2002).

Rab5 to Rab7 conversion

Rab5 and Rab7 are key determinants for early and late endosomes. Rab5, Rab4 and Rab11 occupy different domains within the same early endosomes and the cargos can transfer from Rab5 domain to Rab4 domain for recycling (Sönnichsen B *et al*. 2000). Similarly, Rab7 and Rab9 are also located on the different domains within the same late endosomes (Barbero P *et al*. 2002). So it is possible that during the progression of early to late endosome, Rab7 is gradually acquired into Rab5-positive endosomes with Rab5 dissociation. Live cell imaging of cells co-expressing Rab5 and Rab7 during endocytosis of LDL has shown that LDL is accumulated in large Rab5-positive endosomes and eventually Rab5 is dissociated from these endosomes. Meanwhile, Rab7 is associated to the endosomes, resulting in the conversion from Rab5 to Rab7. It has been proposed that Rab conversion is the molecular mechanism responsible for early to late endosome maturation (Rink J *et al*. 2005).

It is known that Rab5, Rabaptin-5 and Rabex-5 constitute a positive-feedback loop which activates more Rab5 on early endosomes (Horiuchi H *et al*. 1997). According to the Rab conversion model, Rab5 dissociation occurs at the same time of Rab7 association. In this scenario, Rab5 positive feedback loop must be disrupted. Meanwhile, Rab7 is recruited to endosomes. It has been predicted that this process requires a factor to coordinate the disruption of Rab5 positive feedback and the activation of Rab7. Recently, it has been demonstrated that Mon1/SAND-1 plays a dual role in early to late endosome transition. On one hand, Mon1/SAND-1 can displace Rabex-5, the GEF of Rab5, from early endosomes, which disrupts the Rab5 positive feedback loop. Mon1/SAND-1 knockdown induces the enlargement of early endosomes which is due to the defect of Rabex-5 dissociation from early endosomes. On the other hand, Mon1/SAND-1 can sequentially recruit the HOPS complex which activates Rab7 association to late endosomes. Therefore, Mon1/SAND-1 functions as a molecular switch in early to late endosome transition by turning off Rab5 and turning on Rab7 (Poteryaev D *et al*. 2010).

Phagosome maturation and Rab GTPases

Phagosome maturation

The nascent phagosomes undergo dramatic changes in a process called phagosome maturation that ultimately generates phagolysosomes (**Fig. 1.8**). Phagosome maturation shares some features with endosome maturation (Vieira OV *et al*. 2002, Flannagan RS *et al*. 2012). Early phagosomes are mildly acidic and display poor hydrolytic activity (Flannagan RS *et al*. 2009). They behave as early endosomes by preferentially interacting with early and recycling endosomes (Vieira OV *et al*. 2002). Similar to early endosomes, Rab5 is also localized on early phagosomes (Desjardins M *et al*. 1994). *In vitro* and *in vivo* studies have demonstrated that early phagosomes preferentially fuse with early endosomes, a process that is Rab5 dependent (Mayorga LS *et al*. 1991, Desjardins M *et al*. 1997, Jahraus A *et al*. 1998). In addition, it has been shown that phagosomal proteins are recycled to endosomes (Pitt A *et al*. 1992). Expression of the dominant negative mutant Rab5S34N results in the arrest of phagosome maturation (Vieira OV *et al*. 2003). Moreover, phagosome maturation is inhibited by microinjecting antibodies against Rab5 effectors-EEA1 or VPS34 (Fratti RA *et al*. 2001). These data suggest that Rab5 function is essential for phagosome maturation. PI3P also associates to early phagosomes and retains to phagosomes for 10 min (Vieira OV *et al*. 2001). Its association to phagosomes is impaired by wortmannin, an inhibitor of PI 3-kinases. The acquisition of lysosomal-associated membrane protein 1 (LAMP-1) and LysoTracker by latex bead phagosomes decreased by reducing PI3P association, implying that PI3P is essential for phagolysosome fusion (Vieira OV *et al*. 2001, Fratti RA *et al*. 2001). *In vitro* assays have

demonstrated that SapM, a lipid phosphatase secreted by *M. tuberculosis*, is able to inhibit PI3P dependent phagosome-lysosome fusion (Vergne I *et al*. 2005).

Late phagosomes are characterized by an acidic luminal pH (5.5-6.0) (Vieira OV *et al*. 2002). LAMPs are also enriched in late phagosomes and deficiency of both LAMP-1 and LAMP-2 results in the defect of phagolysosome fusion, suggesting LAMPs are required for the fusion of phagosome with lysosomes (Huynh KK *et al*. 2007). Rab7 is associated to late phagosomes and it is required for phagosome maturation (Rabinowitz S *et al*. 1992, Desjardins M *et al*. 1994, Via LE *et al*. 1997). By recruiting RILP, Rab7 bridges phagosomes with dynein-dynactin motor complex that is required for the fusion of phagosomes with late endosomes/lysosomes (Harrison RE *et al*. 2003). Similar with Rab7, Rab34 regulates lysosome positioning by interacting with RILP (Colucci AM *et al*. 2005). Different from Rab7, Rab34 regulates a size-dependent cargo delivery during phagolysosome fusion through its effector-Munc13-2 (Kasmapour B *et al*. 2012). Phagolysosomes are the ultimate organelle for microbial killing. The pH of phagolysosomes reaches to 4.5-5.5 (Vieira OV *et al*. 2002). During phagosome maturation, phagosomes develop multiple mechanisms to eliminate pathogens, including low pH, hydrolytic enzymes, reactive oxygen species (ROS) and nitric oxide (Vieira OV *et al*. 2002, Flannagan RS *et al*. 2009).

Organelle acidification is primarily the results of the activity of the vacuolar-type H^+-ATPase (v-ATPase) (Lukacs GL *et al*. 1990, Hackam DJ *et al*. 1997). Phagosome acidification not only inhibits the growth of intracellular pathogen or even kills them, but also favors the activities of several hydrolytic enzymes (Flannagan RS *et al*. 2009). Although ROS do not play a direct role in pathogen killing (Reeves EP *et al*. 2002, Keren I *et al*. 2013), the importance of ROS in pathogen clearance is stressed by the severe infections due to loss of nicotinamide adenine dinucleotide phosphate (NADPH) oxidase (NOX2) (Babior BM. 2004). NOX2 pumps electrons across the phagosomal membrane into the lumen where molecular oxygen (O_2) is reduced to superoxide anion (O_2-), which can be converted to H_2O_2 and other ROS (Winterbourn CC. 2008). In dendritic cells, NOX2 limits antigen degradation to favor antigen presentation by increasing the phagosomal pH (Savina A *et al*. 2006). In macrophages, NOX2 also decreases the proteolysis by oxidative inactivation of cathepsins (Rybicka JM *et al*. 2010). In addition to ROS, nitric oxide plays an important role in bacterial killing (Denis M. 1991, Chan J *et al*. 1992). Inducible nitric oxide synthase (iNOS) that produces nitric oxide is recruited into phagosomes in J774 and bone marrow macrophages stimulated with IFN-γ and lipopolysaccharide (LPS) and its recruitment is dependent on the actin cytoskeleton (Miller BH *et al*. 2004). Interestingly, *M.tuberculosis* and *M.bovis* bacillus Calmette–Guérin (BCG) inhibits iNOS recruitment to their phagosomes (Miller BH *et al*. 2004).

Further studies have shown that EBP50 (Ezrin/radixin/moesin (ERM)-binding phosphoprotein 50) controls the recruitment of iNOS to phagosomes by linking iNOS to the actin cytoskeleton (Davis AS *et al*. 2007). EBP50 association to phagosomes containing live mycobacteria is shorter than phagosomes harboring dead mycobacteria, consistent with the lower iNOS recruitment. Altogether, the data suggest that the block in iNOS association with phagosomes containing live mycobacteria is dependent on the reduced EBP50 recruitment (Davis AS *et al*. 2007). Moreover, phagosomes also acquire lots of endopeptidases, exopeptidases and hydrolases to degrade different microbial components (Flannagan RS *et al*. 2009).

As mentioned, Rab proteins play the key roles in endosome and phagosome maturation by regulating vesicle budding, motility, tethering and fusion. Hereafter, I will review the molecular mechanisms of several well-characterized Rab GTPases involved in phagosome maturation.

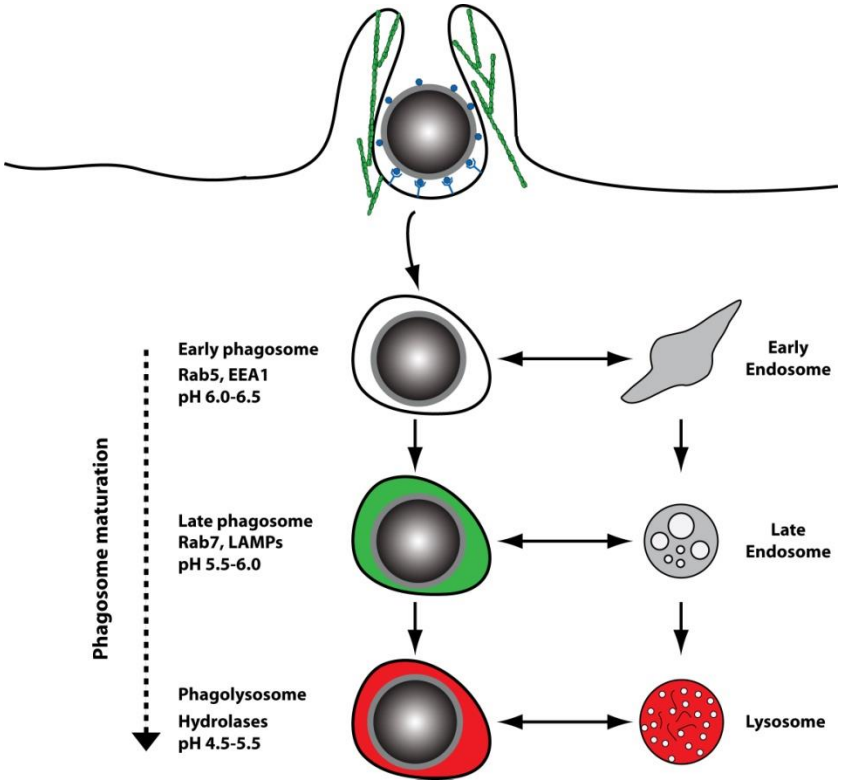

Fig. 1.8 The process of phagosome maturation. The internalization of a particle is initiated when it is recognized by specific receptors on the surface of phagocytes. Phagosome maturation starts after the particle is fully internalized and an early phagosome is formed. Early phagosomes are characterized by Rab5 association. They undergo serial fusions with early endosomes and some proteins in early phagosomes are able to recycle back to endosomes. Early phagosomes gradually mature to late phagosomes. The pH of late phagosomes is relatively acidic (5.5-6.0). Rab7 and LAMPs are associated with late phagosomes. Late phagosomes also interact with late endosomes and finally fused with lysosomes to form phagolysosomes. Phagolysosomes are very acidic (4.5-5.5). They also acquire many hydrolytic enzymes from lysosomes. Hence phagolysosomes are the ultimate compartments where many intracellular pathogens are killed.

Mechanisms of Rab GTPases in the regulation of phagosome maturation

Rab5, the best characterized endosomal GTPase, is essential for early endosome fusion (Gorvel J *et al*. 1991, Bucci C *et al*. 1992). Rab5 associates to isolated latex bead phagosomes and its association is lost

during phagosome maturation, suggesting a role of Rab5 in this process (Desjardins M *et al*. 1994). It has been suggested that the fusion of phagosomes with endosomes is important for phagosome maturation (Mayorga LS *et al*. 1991). *In vitro* fusion of phagosomes with early and late endosomes is dependent on Rab5 (Jahraus A *et al*. 1998). Expression of the dominant negative mutant Rab5S34N results in the arrest of phagosome maturation (Vieira OV *et al*. 2003). Rab5a expression enhances the *L. monocytogenes* containing phagosomes maturation into phagolysosomes. Conversely, Rab5a knockdown blocks phagolysosome fusion (Alvarez-Dominguez C and Stahl PD. 1999). Taken together, the data suggest that Rab5 is essential for phagosome maturation.

Rab7 also associates to the latex bead phagosomes after Rab5 (Rabinowitz S *et al*. 1992, Desjardins M *et al*. 1994). Its association to phagosomes requires Rab5 activation (Vieira OV *et al*. 2003). Rab7 association to *M. bovis* BCG-containing phagosomes is blocked, correlating with the phagosome maturation arrest (Via LE *et al*. 1997). In *Dictyostelium*, Rab7 is localized to early and late phagosome membranes. The delivery of α-mannosidase and lysosomal integral membrane protein (LmpA) to phagosomes is blocked in cells expressing the dominant negative mutant of Rab7, suggesting that Rab7 function is required for delivery of proteins from endosomes/lysosomes to phagosomes (Rupper A *et al*. 2001). The acquisition of LAMP-1 by *S. typhimurium*-containing vacuoles (SCVs) is blocked in HeLa cells expressing the dominant negative mutant-Rab7T22N, suggesting that Rab7 is required for the maturation of SCVs (Méresse S *et al*. 1999). Active Rab7 on the phagosomal membrane recruits the effector RILP, which in turn bridges phagosomes with a microtubule-associated motor complex, dynein-dynactin. This motor complex is required for the phagosomal tubule extension and the fusion of phagosomes with late endosomes/lysosomes (Harrison RE *et al*. 2003).

Rab10 was first cloned in 1993 (Chen YT *et al*. 1993). When expressed, Rab10 was localized to the perinuclear region, demonstrating a partial overlap with a Golgi marker β-COP, a subunit of COP I complex (Chen YT *et al*. 1993). Further studies have shown that Rab10 is localized to endosomes and the TGN and Rab10 regulates the basolateral recycling in polarized cells (Chen CC *et al*. 2006, Babbey CM *et al*. 2006). Furthermore, Rab10 transiently associates to IgG-opsonized latex bead phagosomes in RAW264.7 macrophages and A431 cells stably expressing FcγRIIA (Cardoso CM *et al*. 2010). Expression of the dominant negative mutant Rab10T23N in RAW264.7 and the engineered A431 cells results in the delayed acquisition of LAMP-2 by phagosomes. Similarly, the acquisition of LAMP-2 by phagosomes during the first 45 min of chasing is decreased by Rab10 knockdown, suggesting that Rab10 is required for the maturation of phagosomes (Cardoso CM *et al*. 2010). PI3P and EEA1 are excluded from

phagosomes harboring live mycobacteria (Fratti RA *et al*. 2001, Vergne I *et al*. 2005). However, expression of the constitutively active mutant Rab10Q68L in RAW264.7 macrophages increases PI3P and EEA1 association to phagosomes harboring live mycobacteria, suggesting that Rab10 is able to partially overcome the phagosome maturation arrest imposed by live mycobacteria. Based on these studies, it has been proposed that Rab10 promotes phagosome maturation by mediating recycling from phagosomes, a process believed to be necessary for phagolysosome biogenesis (Cardoso CM *et al*. 2010).

Rab14 is involved in the trafficking between the Golgi complex and early endosomes (Junutula JR *et al*. 2004). RabD, a Rab14 ortholog in *Dictyostelium*, regulates phagocytosis and homotypic phagosome and lysosome fusion (Harris E and Cardelli J. 2002). Live cell imaging has demonstrated that EGFP-Rab14 is recruited to phagosomes harboring live *M. bovis* BCG and remained on phagosomes for prolonged periods of time. In contrast, Rab14 only transiently associates to phagosomes harboring dead mycobacteria (Kyei GB *et al*. 2006). Because live *M. bovis* BCG arrests phagosome maturation, it is speculated that Rab14 is correlated with the impairment of phagosome maturation. Expression of the dominant negative mutant of Rab14 or knockdown of Rab14 in macrophages promotes the colocalization of live mycobacteria-containing phagosomes with late endocytic markers. Conversely, expression of the wild-type or the constitutively active mutant of Rab14 inhibits the progression of dead mycobacteria-containing phagosomes into phagolysosomes. Hence it has been proposed that Rab14 is required for the mycobacterial phagosome maturation arrest (Kyei GB *et al*. 2006). Mechanistic studies have shown that the fusion of phagosomes with early endosomes is increased by Rab14 expression. Collectively, the data suggest that Rab14 inhibits phagosome maturation into phagolysosomes by promoting the fusion of phagosomes with early endosomes (Kyei GB *et al*. 2006). Similarly, Rab14 association to phagosomes is enhanced by *S. typhimurium*, which leads to the inhibition of phagosome maturation and hence the increased survival (Kuijl C *et al*. 2007).

Rab22a was first identified in 1993 and sequence alignments suggested that Rab22a is highly homologous with Rab5 (Olkkonen VM *et al*. 1993). When expressed, Rab22a is localized to both early endosomes and late endosomes (Olkkonen VM *et al*. 1993, Mesa R *et al*. 2001). In addition, Rab22a expression leads to the formation of giant vacuole structures (Mesa R *et al*. 2001, Kauppi M *et al*. 2002). Rab22a expression inhibits EGF degradation without affecting its uptake. Yet the uptake and recycling of transferrin is not affected by Rab22a expression (Kauppi M *et al*. 2002). Altogether, the data suggest that Rab22a may play a function in endosome maturation. In addition, Rab22a also associates to phagosomes (Roberts EA *et al*. 2006). Live cell imaging has shown that EGFP-Rab22a is quickly recruited

to the *M. bovis* BCG-containing phagosomes and retained on such phagosomes even after 1 hour of internalization. In contrast, EGFP-Rab22a associates to latex-bead phagosomes at a very low level (Roberts EA *et al*. 2006). Over-expression of the constitutively active mutant of Rab22a in macrophages results in the decreased acidification and proteolytic activity of phagosomes harboring dead mycobacteria, but increased colocalization with recycling endocytic markers. Conversely, Rab22a knockdown causes the increased colocalization of live mycobacterial phagosomes with late endocytic markers-CD63 and Rab7 (Roberts EA *et al*. 2006). Therefore, Rab22 could play a negative role in the transition from early to late phagosomes (Roberts EA *et al*. 2006). A potential mechanism for these observations could be related to the ability of Rab22a to promote Rab5 activation and the fusion with early endosomes by recruiting Rabex-5, a GEF of Rab5 (Zhu H *et al*. 2009).

Rab34 is primarily associated to the Golgi complex and also localized in late endocytic compartments (Wang T and Hong W. 2002). Rab34 is proposed to mediate the lysosomal positioning from the periphery to peri-Golgi region (Wang T and Hong W. 2002). Rab34 expression is increased by NF-κB activation that is required for the fusion of mycobacterial phagosomes with late endosomes/lysosomes, arguing for a role of this GTPase in phagosome maturation (Gutierrez MG *et al*. 2008). A study in our research group has shown that Rab34 transiently associates to phagosomes (Kasmapour B *et al*. 2012). Expression of the constitutively active mutant Rab34Q111L increases the association of LAMP-1 and LAMP-2 to latex bead-containing or *M. bovis* BCG-containing phagosomes. Conversely, expression of the dominant negative mutant Rab34T66N or Rab34 knockdown decreases both LAMP-1 and LAMP-2 association. The data suggest that Rab34 regulates phagolysosome fusion (Kasmapour B *et al*. 2012).Consistent with these observations, expression of Rab34 and Rab34Q111L enhances the killing of mycobacteria and Rab34 knockdown decreases the killing (Kasmapour B *et al*. 2012). Mechanistic studies have shown that Rab34 regulates phagolysosome fusion through its effector-Munc13-2 (Kasmapour B *et al*. 2012). Interestingly, the delivery of Dextran 70kDa preload in lysosomes to phagosomes is impaired by Rab34 knockdown. The delivery of Dextran 10kDa preloaded in lysosomes is not affected, suggesting that Rab34 regulates size-selective delivery of lysosomal cargo into phagosomes (Kasmapour B *et al*. 2012).

A comprehensive analysis of 42 Rab GTPases association to *S. aureus*- and *M. tuberculosis*-containing phagosomes has shown that 22 Rab GTPases are differentially recruited to *S. aureus*- and *M. tuberculosis*-containing phagosomes. Expression of the dominant negative mutants of Rab20 or Rab39 arrests phagosome acidification, as shown by the impaired acquisition of LysoTracker. Additionally,

expression of the dominant negative mutants of Rab20, Rab22b, Rab32, Rab34, Rab38 or Rab43 blocks the delivery of Cathepsin D to latex bead phagosomes, suggesting these Rab GTPases function in phagosome maturation (Seto S *et al*. 2011). Similarly, the acquisition of LysoTracker by IgG-spsonized erythrocyte-phagosomes is delayed in RAW264.7 macrophages expressing the dominant negative mutant of Rab20 (Egami Y and Araki N. 2012).

Phagosome maturation regulated by cytokines

There is accumulating evidence showing that phagosome maturation is differentially modulated by pro-inflammatory and anti-inflammatory cytokines (Balce DR *et al*. 2011, de Keijzer S *et al*. 2011, O'Leary S *et al*. 2011, Bhattacharya M *et al*. 2006, Harris J *et al*. 2007).

IFN-γ is the key protective cytokine of macrophage that induces diverse antimicrobial activities by regulating a series of genes at the transcriptional level (Schroder K *et al*. 2004). On one hand, evidence indicates that phagosome maturation in macrophages is enhanced by IFN-γ treatment (Via LE *et al*. 1998, Schaible UE *et al*. 1998, Hostetter JM *et al*. 2002, Santic M *et al*. 2005, McCollister BD *et al*. 2005). *M. bovis* BCG-containing phagosome acidification is significantly increased by IFN-γ treatment, demonstrating that the limited acidification of *M. bovis* BCG-containing phagosome is reversed by IFN-γ (Via LE *et al*. 1998). The pH of *M. avium*-containing phagosomes drops to pH 5.2 after 3 hours of internalization in IFN-γ treated macrophages. In contrast, without IFN-γ, *M. avium* containing phagosomes showed a limited acidification and pH remains around pH 6.2. Moreover, the v-ATPase in phagosomes is increased by IFN-γ treatment for 16 h (Schaible UE *et al*. 1998). Maturation of phagosomes containing other pathogens such as *M. paratuberculosis*, *L. pneumophila* or *S. typhimurium* is also accelerated in IFN-γ activated macrophages (Hostetter JM *et al*. 2002, Santic M *et al*. 2005, McCollister BD *et al*. 2005). In addition, autophagy induced by IFN-γ contributes to the increased phagosome maturation (Gutierrez MG *et al*. 2004).

One the other hand, it also has been demonstrated that at the early steps of phagosome maturation, IFN-γ delays this process (Tsang AW *et al*. 2000, Yates RM *et al*. 2007, Jutras I *et al*. 2008, Trost M *et al*. 2009). Acquisition of the late endocytic marker LAMP-1 by IgG-opsonized erythrocytes-containing phagosomes is significantly delayed in IFN-γ activated bone marrow macrophages during the first 30 min (Tsang AW *et al*. 2000). In addition, the acidification of mannosylated bead phagosomes is slower in IFN-γ activated bone marrow macrophages than control in the first 1 hour (Yates RM *et al*. 2007). Phagolysosome fusion is also delayed during the first 2 hours by IFN-γ (Yates RM *et al*. 2007). In line with

these observations, phagosomal proteolysis, lipolysis and β-Galactosidase activity are all reduced in activated macrophages (Yates RM *et al*. 2007). Phagosome proteomic studies have shown that fusion of phagosomes with early endosomes is stimulated by IFN-γ (Jutras I *et al*. 2008). In addition, acquisition of various hydrolases and proteases by phagosomes is reduced in early phagosomes from IFN-γ treated macrophages (Trost M *et al*. 2009).

Unlike IFN-γ, IL-4 and IL-13 induce an alternative activation of macrophages, which is very important in wound repair and inflammation control (Gordon S and Martinez FO. 2010). Recent studies have shown that phagosome maturation is also affected by IL-4 and IL-13 treatment (Balce DR *et al*. 2011). Phagosomal proteolysis is enhanced by IL-4 or IL-13 (Balce DR *et al*. 2011). However, phagolysosome fusion is not stimulated by IL-4 alone (Balce DR *et al*. 2011). In this context, NOX2 mediated respiratory burst is decreased by IL-4 but not IL-13, resulting in the increased phagosomal proteolysis. This decreased respiratory burst is due to the compromised NOX2 association to phagosomes in macrophages. In addition, IL-4 increases the expression of Cathepsin S and L as well as the association of mature Cathepsin S and L to phagosomes. Overall, phagosomal proteolysis is remarkably stimulated by IL-4 due to higher expression and phagosomal association of Cathepsin S and L and lower NOX2-dependent respiratory burst in macrophages (Balce DR *et al*. 2011). Furthermore, the association of Rab5 to phagosomes is increased by IL-4 whereas Rab7 recruitment is delayed. In line with these observations, phagosome acidification is delayed by IL-4 (de Keijzer S *et al*. 2011).

Phagosome maturation is not only regulated by pro-inflammatory cytokines but also anti-inflammatory ones. IL-10 is an anti-inflammatory cytokine mainly produced by monocytes, which inhibits the synthesis of many pro-inflammatory cytokines, such as IFN-γ, TNF-α and IL-1 (Donnelly RP *et al*. 1999, Moore KW *et al*. 2001). IL-10 is involved in the regulation of phagosome maturation (Via LE *et al*. 1998, O'Leary S *et al*. 2010). The colocalization of *M. bovis* BCG with LysoTracker Red is significantly increased in macrophages from IL-10 knockout mice, indicating that phagosome maturation is suppressed by anti-inflammatory cytokine IL-10 (Via LE *et al*. 1998). After treatment with an IL-10 antibody prior *M. bovis* BCG or *M. tuberculosis* H37Rv infection, LAMP-1 acquisition by mycobacterial phagosomes is enhanced (O'Leary S *et al*. 2010). Moreover, IL-10 results in less colocalization of heat-killed *M. tuberculosis* H37Rv containing phagosomes with LAMP-1, suggesting that IL-10 may contribute to *M. tuberculosis* survival in macrophages by arresting phagosome maturation (O'Leary S *et al*. 2010).

Although it is well established that phagosome maturation is selectively regulated by pro- and anti-inflammatory cytokines, the precise mechanisms of how phagosome maturation is regulated by

cytokines remain unclear. It has been suggested that regulating the expression of Rab GTPases is one of the mechanisms (Pei G *et al*. 2012)

Regulation of Rab GTPases expression by cytokines

After IFN-γ treatment, Rab5a transcription increases in human-derived macrophages. Yet the expression of Rab5b and Rab5c is not affected. This transcriptional activation is reflected at the protein level as well (Alvarez-Dominguez C and Stahl PD. 1998). The GTP/GDP ratio of Rab5a association with phagosomal membranes after IFN-γ treatment increases 2-fold, indicating that guanine exchange, GTP hydrolysis or both are also regulated by IFN-γ (Alvarez-Dominguez C and Stahl PD. 1998). The maturation of phagosomes containing *L. monocytogenes* is accelerated by Rab5a over-expression (Alvarez-Dominguez C and Stahl PD. 1999). Moreover, IL-6 treatment specifically induces Rab5 up-regulation in a concentration dependent manner rather than other Rab proteins (Bhattacharya M *et al*. 2006). The transcription of all the isoforms of Rab5, Rab5a, b and c, is induced by IL-6 (Bhattacharya M *et al*. 2006). The promoter activity of Rab5 is activated by IL-6, suggesting IL-6 specifically activates a signal transduction pathway to increase the expression of Rab5. Moreover, the IL-6 dependent expression of Rab5 is blocked by an MEK1/2 (also known as mitogen-activated protein kinase) inhibitor, indicating that Rab5 expression is activated by IL-6 through ERK (extracellular-signal regulated kinase) signaling pathway (Bhattacharya M *et al*. 2006). Interestingly, the fusion of phagosomes with early endosomes is enhanced by IL-6, indicating that IL-6 could stimulate the fusion by up-regulating Rab5 expression (Bhattacharya M *et al*. 2006).

The expression of Rab7 increases by IL-12 treatment in a concentration dependent manner (Bhattacharya M *et al*. 2006). The expression of Rab7 induced by IL-12 is abrogated by a p38 MAPK inhibitor, indicating the expression is activated by IL-12 through p38 MAPK signaling pathway (Bhattacharya M *et al*. 2006). Phagolysosome fusion is increased by IL-12 treatment, suggesting that IL-12 could eventually stimulate phagolysosome fusion by up-regulating Rab7 expression. Remarkably, the colocalization of *Salmonella* phagosomes with late endocytic markers is increased by IL-12 (Bhattacharya M *et al*. 2006).

State of knowledge on Rab20

The small GTPase Rab20 was first cloned in 1994 and was found mainly associated to apical endocytic organelles in mouse kidney proximal tubule cells (Lütcke A *et al*.1994). In another study, Rab20 was found to label intercalated cells of the cortical collecting duct and outer medullary collecting duct in

kidney (Curtis LM and Gluck S. 2005). Subsequently, endogenous Rab20 was localized to *cis*-Golgi and medium compartment of Golgi apparatus in HeLa cells (Amillet JM *et al*. 2006). Rab20 shows a colocalization with the E subunit of v-ATPase in kidney, suggesting Rab20 may regulate the trafficking of v-ATPase (Curtis LM and Gluck S. 2005). Rab20 has also been identified as a putative regulator of Connexin 43 trafficking from the perinuclear region to the ER (Das Sarma J *et al*. 2008). A large-scale screening has identified INPP5E (72-kDa inositol polyphosphate 5-phosphatase) as an effector of Rab20 (Fukuda M *et al*. 2008). Rab20 is also transiently associated with macropinosomes positive for Rab5 and Rab21 at the early stage of macropinosome maturation (Egami Y and Araki N. 2012). After the dissociation of Rab5 and Rab21 from macropinosomes, Rab20 is then localized in Rab7 and LAMP-1 positive compartments (Egami Y and Araki N. 2012). Interestingly, endogenous or over-expressed Rab20 has been also reported to associate with mitochondria (Hackenbeck T *et al*. 2010).

There is compelling evidence indicating that the expression of Rab20 is liked to infections of intracellular pathogens. The expression of Rab20 is up-regulated by mycobacterial infection in a NF-κB dependent manner (Gutierrez MG *et al*. 2008). Rab20 expression is also enhanced against various infections in different cell types, such as *S. pyogenes*, *S. aureus*, *S. pneumoniae*, *L. monocytogenes*, *C. burnetii* and *A. fumigatus* (Cortez KJ *et al*. 2006, Goldmann O *et al*. 2007, Tchatalbachev S *et al*. 2010, Mahapatra S *et al*. 2010). Rab20 expression in peritoneal macrophages is induced by heat-killed group B *Streptococcus* in a toll-like receptor 2 (TLR2)-independent manner (Draper DW *et al*. 2006). The transcriptional regulation of Rab20 is cell-type specific since Rab20 expression is up-regulated in macrophages but not in dendritic cells after infection with *M. tuberculosis* (Tailleux L *et al*. 2008). Additionally, Rab20 expression is differentially regulated against mycobacteria infection in humans, non-human primates and zebrafish (Gonzalez-Juarrero M *et al*. 2008, van der Sar A *et al*. 2009, Mehra S *et al*. 2010). Specially, Rab20 expression and other genes involved in IFN-γ signaling are increased in early TB (tuberculosis) granulomas, correlating with highly inflammatory responses (Mehra S *et al*. 2010). Moreover, Rab20 has been identified as one of the interferon-inducible signature genes for active TB (Berry MP *et al*. 2010). Rab20 expression is also highly increased upon different TLR ligands stimulation in dendritic cells. Consequently, Rab20 has been considered as part of the inflammatory signature in dendritic cells (Torri A *et al*. 2010). Furthermore, Rab20 expression is highly increased after LPS injection in mice brain (Liang Y *et al*. 2012). Its expression is also increased by ovalbumin-induced lung inflammation in a murine model of asthma (Malik R *et al*. 2008). Altogether, it is conceivable that Rab20 may have a general role in immunity.

Several studies have demonstrated that Rab20 is associated to phagosomes although its function is still poorly characterized. Rab20 is localized to wild-type *Salmonella*-containing vacuoles (Smith AC *et al*. 2007). Besides, Rab20 is transiently associated to *S. aureus*- or *M. tuberculosis*-containing phagosomes, at early times post infection (Seto S *et al*. 2011). In addition, Rab20 is also associated to IgG-opsonized erythrocytes-containing phagosomes, after 5 min of internalization (Egami Y and Araki N. 2012). The acquisition of LysoTracker and Cathepsin D in macrophages expressing the dominant negative mutant-Rab20T19N is compromised (Seto S *et al*. 2011, Egami Y and Araki N. 2012). All the data suggest that Rab20 plays a function in phagosome maturation. However, the role and mechanisms of Rab20 in phagosome maturation need to be further investigated.

There is compelling evidence showing that IFN-γ delays phagosome maturation at early times after internalization (Tsang *et al*. 2000, Yates *et al*. 2007, Jutras *et al*. 2007, Trost *et al*. 2009). A phagosome proteomic study has demonstrated that Rab20 association to phagosomes is enhanced by IFN-γ (Trost M *et al*. 2009). Hence it is tempting to propose that Rab20 may represent the link between IFN-γ and the delayed phagosome maturation.

Aims of the study

So the aim of this study is as follows:

- Analyze the distribution of endogenous and over-expressed Rab20 in macrophages
- Study the expression of Rab20 in macrophages after IFN-γ stimulation
- Study the function of Rab20 in phagosome maturation
- Investigate the function of Rab20 in the innate immune response to mycobacteria
- Identify the effectors of Rab20 which are involved in the function of Rab20

2. Material and methods

Molecular biology

Polymerase chain reaction (PCR)

The mouse Rab20 (Gene ID: 19332) was amplified by PCR from full length cDNA obtained from RAW264.7 macrophages according to standard procedures with PrimeSTAR HS DNA polymerase (TaKaRa, Japan). All the primers in the below were synthesized by Eurofins MWG Operon, Germany. The PCR reaction system was as follows in **Table 2.1.**

Table 2.1 Standard PCR reaction system

Component	Volume	Final concentration
DNA template	100 ng	2 ng/μL
5× Buffer	10 μL	
dNTP mix (2 mM each)	5 μL	200 μM each
Primer F (10 μM)	2 μL	0.4 μM
Primer R (10 μM)	2 μL	0.4 μM
PrimeSTAR	0.4 μL	
ddH_2O	Up to 50 μL	

The primers used for subcloning Rab20 into pEGFP-C1 were:

Forward primer: 5'-GGAATTCTCGGAAGCCGGATGGGAAG-3'
Reverse primer: 5'-CGGATCCTCAGGCACAACACCCGGATCTAGTCTG- 3'

With these primers, the restriction sites for *Bam*H I and *Eco*R I were introduced and the PCR products were cloned into pEGFP-C1 vector (Clontech, USA). The plasmids of pEGFP-C1-Rab20WT and pEGFP-C1-Rab20T19N were generated by Dr. Ianina Conte. These primers were also used for cloning Rab20WT/Rab20T19N into mCherry-C1 plamsid (Clontech, USA).

The primers used for subcloning Rab20 into pGEX4T1 were:

Forward primer: 5' -CGGGATCC CGGAAGCCGGATGGGAAG- 3'
Reverse primer: 5' -CGGAATTC TCAGGCACAACACCCGGATC- 3'

With these primers, the restriction sites for *Bam*H I and *Eco*R I were introduced and the PCR products were cloned into pGEX4T1 (GE Healthcare, USA).

The primers used for HA-Rab20WT were:

Forward primer: 5' -CGGGATCC CGGAAGCCGGATGGGAAG- 3'
Reverse primer: 5' -CGGAATTC TCAGGCACAACACCCGGATC- 3'

With these primers, the restriction sites for *Bam*H I and *Eco*R I were introduced and the PCR products were cloned into FLAG-HA-pCDNA3 (Addgene, USA).

Primers used for R59L mutagenesis were:

Forward primer: 5’-GGACACCGCAGGGCTGGAGCAGTTTCATG- 3’
Reverse primer: 5’-CATGAAACTGCTCCAGCCCTGCGGTGTCC- 3’

Primers used for Q61L mutagenesis were:

Forward primer: 5’- GCAGGGCGGGAGCTGTTTCATGGTCTG- 3’
Reverse primer: 5’- CAGACCATGAAACAGCTCCCGCCCTGC- 3’

Primers used for dileucine motif deletion were:

Forward primer: 5’- CCCAAGCAGGTGCAGCCA TACAAGAAGATCCTG- 3’
Reverse primer: 5’- CTTCAGGATCTTCTTGTA TGGCTGCACCTGCTTG- 3’

Primers used for ED151 152AA were:

Forward primer: 5’-CCAAGCAGGTGCAGCCAGCCGCCGCAGTGGCCCTTTACAAG-3’

Reverse primer: 5’-CTTGTAAAGGGCCACTGCGGCGGCTGGCTGCACCTGCTTGG-3’

The cycling conditions (annealing temperature, extension time, etc.) were specifically optimized due to different primers and templates.

Restriction endonuclease digestion

Plasmid DNA or purified PCR products were digested with restriction endonucleases (10 units/1 µg DNA, New England Biolabs, USA) according to the standard protocol. After digestion, the products were

purified with QIAquick Gel extraction kit (Qiagen, Germany) and finally eluted with EB Buffer (10 mM Tris-HCl, pH 8.5). The concentration of DNA was measured with Nanodrop 1000 spectrophotometer (Thermo Scientific, USA).

Ligation

The ligation was performed according to the manufacturer's protocol. The vector and insert were mixed at a molar ratio of 1:3 and 1 µL T4 DNA ligase (NEB, USA) was added into the reaction system. All the procedures were done on ice. Then the ligation was performed at room temperature for 10 min. After the ligation reaction was finished, 5 µL of the mixture was used for transformation.

Transformation

JM109 competent cells (Promega, USA) were taken out from -80^{o}C freezer and thawed on ice. For plasmid DNA, 25 µL of competent cells were required. For ligation production, 50 µL of competent cells were needed. The mixture of DNA and competent cells were kept on ice for 5 min. Then the tube was incubated in a water bath at 42 ^{o}C for 45 seconds. After the heat shock, the tube was incubated on ice immediately for 2 min. 1 mL of LB medium (10 g/L tryptone, 5 g/L yeast extract, 10 g/L NaCl, pH 7.0) was added into the tube and incubated at 37 ^{o}C for 1 h. 500 µL of the resulting culture was plated on a LB plate with the appropriate antibiotics (Ampicillin: 50 µg/mL, Kanamycin: 50 µg/mL, Carl-Roth, Germany). Plates were incubated at 37 ^{o}C overnight to form colonies. Colonies were picked up for plasmid extraction or colony PCR to verify colonies with the right inserts.

Plasmid extraction

For preparation of large amount of plasmids at transfection grade, Qiagen midi plasmid preparation kit (Qiagen, Germany) was used according to manufacturer's protocol. For preparation of plasmids at molecular biology grade, Qiagen MiniPrep kit (Qiagen, Germany) was used according to manufacturer's protocol. The plasmids used in this study were shown in table **2.2**.

Table **2.2** plasmids used in this study

Plasmid	Backbone	Tag	Cloning sites(5', 3')	Antibiotics resistance	Reference
pEGFP-C1-Rab20WT	pEGFP-C1	EGFP	*Eco*R I, *Bam*H I	Kanamycin/Geneticin	This study
pEGFP-C1-Rab20T19N	pEGFP-C1	EGFP	*Eco*R I, *Bam*H I	Kanamycin/Geneticin	This study

pEGFP-C1-Rab20R59L	pEGFP-C1	EGFP	*Eco*R I, *Bam*H I	Kanamycin/Geneticin	This study
pEGFP-C1-Rab20Q61L	pEGFP-C1	EGFP	*Eco*R I, *Bam*H I	Kanamycin/Geneticin	This study
pEGFP-C1-ΔEDAVAL	pEGFP-C1	EGFP	*Eco*R I, *Bam*H I	Kanamycin/Geneticin	This study
pEGFP-C1-ED151 152AA	pEGFP-C1	EGFP	*Eco*R I, *Bam*H I	Kanamycin/Geneticin	This study
mCherry-C1-Rab20WT	mCherry-C1	mCherry	*Eco*R I, *Bam*H I	Kanamycin/Geneticin	This study
mCherry-C1-Rab20T19N	mCherry-C1	mCherry	*Eco*R I, *Bam*H I	Kanamycin/Geneticin	This study
pGEX-4T1	pGEX-4T1	GST	*Bam*H I, *Eco*R I	Ampicillin	
pGEX-4T1-Rab20WT	pGEX-4T1	GST	*Bam*H I, *Eco*R I	Ampicillin	This study
pGEX-4T1-Rab20T19N	pGEX-4T1	GST	*Bam*H I, *Eco*R I	Ampicillin	This study
Rab20 pSIREN shRNA1	pSIREN-RetroQ-dsRED	dsRED	*Bam*H I, *Eco*R I	Ampicillin	This study
Rab20 pSIREN shRNA2	pSIREN-RetroQ-dsRED	dsRED	*Bam*H I, *Eco*R I	Ampicillin	This study
Rab20 pSIREN shRNA3	pSIREN-RetroQ-dsRED	dsRED	*Bam*H I, *Eco*R I	Ampicillin	This study
Rab20 pSIREN shRNA4	pSIREN-RetroQ-dsRED	dsRED	*Bam*H I, *Eco*R I	Ampicillin	This study
pSIREN Scrambled shRNA	pSIREN-RetroQ-dsRED	dsRED	*Bam*H I, *Eco*R I	Ampicillin	This study
MISSION®pLKO.1-puro Control	pLKO.1-puro			Ampicillin/Puromycin	This study
MISSION® shRNA2640	pLKO.1-puro			Ampicillin/Puromycin	This study
MISSION® shRNA2641	pLKO.1-puro			Ampicillin/Puromycin	This study

MISSION® shRNA2642	pLKO.1-puro			Ampicillin/Puromycin	This study
MISSION® shRNA2643	pLKO.1-puro			Ampicillin/Puromycin	This study
MISSION® shRNA2644	pLKO.1-puro			Ampicillin/Puromycin	This study
FLAG-HA-pCDNA3	pCDNA3	FLAG-HA	*Bam*H I, *Eco*R I	Ampicillin/Geneticin	Addgene
FLAG-HA-pCDNA3-Rab20WT	pCDNA3	FLAG-HA	*Bam*H I, *Eco*R I	Ampicillin/Geneticin	This study
EGFP-Rab5A		EGFP		Kanamycin	Addgene
EGFP-Rab5S34N		EGFP		Kanamycin	Addgene
EGFP-2XFYVE		EGFP		Kanamycin	
tdTomato-LAMP-1		tdTomato		Kanamycin	
Myc-Rabex5 (1-76)	pCI-Neo	Myc	Sac II, Spe I	Ampicillin/Geneticin	Mattera R and Bonifacino JS. 2008
Myc-Rabex5 (1-399)	pCI-Neo	Myc	Sac II, Spe I	Ampicillin/Geneticin	Same as above
Myc-Rabex5 (1-460)	pCI-Neo	Myc	Sac II, Spe I	Ampicillin/Geneticin	Same as above
Myc-Rabex5WT	pCI-Neo	Myc	Sac II, Spe I	Ampicillin/Geneticin	Same as above

Site directed mutagenesis

Site directed mutagenesis was carried out with QuickChange II XL mutagenesis kit (Agilent Genomics, USA). Primers for site mutagenesis were designed with the web tool of QuickChange primer design. The PCR was carried out with 10 ng DNA as template, 125 ng each primer, 1 µL *PfuUltra* HF DNA polymerase in 50 µL system. The cycling parameters were as follows: 95 ^{o}C 60 s; 95 ^{o}C 50 s, 60 ^{o}C 50 s, 68 ^{o}C 5 min (go to step 2, 17 times); 68 ^{o}C 7 min. After amplification, 1 µL Dpn I was added into the reaction and incubated at 37 ^{o}C for 1 h. 5 µL of Dpn I treated DNA was added into 50 µL of XL1-Blue supercompetent cells for transformation. After 12-16 h incubation at 37 ^{o}C, colonies were picked to grow in LB medium with appropriate antibiotics. Plasmids were purified and verified by sequencing.

pSIREN-DsRed shRNA vector construction

The RNAi-pSIREN-RetroQ-DsRed-Express vector was purchased from Clontech, USA. Four DNA oligos targeting Rab20 were designed based on mouse Rab20 cDNA sequence using Clontech online shRNA design tool (http://bioinfo.clontech.com/rnaidesigner/oligoDesigner.do). The four pairs of complementary oligos and one scrambled control oligo were synthesized by Eurofins MWG Operon, Germany. The target sequence for each shRNA is as follows:

shRNA 1: 5'-CTGACAGAAACAGCCAACA-3'

shRNA 2: 5'-CCAACAATGACTGCCTGTT-3'

shRNA 3: 5'-CACCCAAACAGACTAGATC-3'

shRNA 4: 5'-CCGCTATCATCCTTACATA- 3'

Designed oligos based on shRNA 1 target sequence:

Top Strand (66bp):

5' -gatccGCTGACAGAAACAGCCAACATTCAAGAGATGTTGGCTGTTTCTGTCAGTTTTTTACGCGTg- 3'

Bottom Strand (66bp):

5' -aattcACGCGTAAAAAACTGACAGAAACAGCCAACATCTCTTGAATGTTGGCTGTTTCTGTCAGCg- 3'

Designed oligos based on shRNA 2 target sequence:

Top Strand (66bp)

5' -gatccGCCAACAATGACTGCCTGTTTTCAAGAGAAACAGGCAGTCATTGTTGGTTTTTTACGCGTg- 3'

Bottom Strand (66bp)

5' -aattcACGCGTAAAAAACCAACAATGACTGCCTGTTTCTCTTGAAAACAGGCAGTCATTGTTGGCg- 3'

Designed oligos based on shRNA 3 target sequence:

Top Strand (66bp)

5' -gatccGCACCCAAACAGACTAGATCTTCAAGAGAGATCTAGTCTGTTTGGGTGTTTTTTACGCGTg- 3'

Bottom Strand (66bp)

5' -aattcACGCGTAAAAAACACCCAAACAGACTAGATCTCTCTTGAAGATCTAGTCTGTTTGGGTGCg- 3'

Designed oligos based on shRNA 4 target sequence:

Top Strand (66bp)

5' -gatccGCCGCTATCATCCTTACATATTCAAGAGATATGTAAGGATGATAGCGGTTTTTTACGCGTg- 3'

Bottom Strand (66bp)

5' -aattcACGCGTAAAAAACCGCTATCATCCTTACATATCTCTTGAATATGTAAGGATGATAGCGGCg- 3'

A 5'-*Bam*H I restriction site overhangs on the top strand and a 5'-*Eco*R I restriction site overhangs on the bottom strand. The pairs of oligos were annealed and the double strand oligos were ligated into pSIREN-DsRed-Express vector according to the manufacturer's instructions. The ligation mixtures were transformed into JM109 competent *E. coli* (Promega, USA). The positive clones were verified with U6 sequencing primer (5'-ATGGACTATCATATGCTTACCGTA-3').

M. bovis BCG culture

M. bovis BCG 1173P2 expressing GFP and dsRed were kindly provided by Brigitte Gicquel (Institute Pasteur, France). Both strains were grown in 50 mL Middlebrook 7H9 liquid medium (Difco Laboratories, USA) supplemented with 10% (v/v) OADC (oleic acid, albumin, dextrose, catalase) (BD Diagnostics, USA) and 0.05 % (v/v) Tween 80 (Sigma-Aldrich, Germany). The culture was incubated at 37^{o}C in roller flasks for 4-5 days to reach OD_{600} of 0.3-0.4. An aliquot of this culture was subcultured into new medium at a ratio of 1:10. To prepare single bacteria suspension for live cell imaging, 15 mL of 4-5 days bacterial culture was centrifuged at 2500 rpm for 10min. The pellet was washed with 10 mL DMEM without phenol red once and resuspended in 5 mL D-MEM without phenol red. The suspension was passed through the 26-G needle (Ø 0.45×25mm, Sterican®, Germany) for around 40 times and the suspension was further sonicated for 10min. After sonication, it was centrifuged at 1000 rpm for 10min to eliminate remaining clumps. The supernatant was collected and diluted with D-MEM without phenol red to OD_{600} of 0.02 and used to infect macrophages.

M. bovis BCG killing experiment

Single bacteria suspension was prepared as described. The OD_{600} of the bacteria suspension is adjusted with DMEM to 0.025. $1X10^5$ cells stably transfected EGFP or EGFP-Rab20WT are seeded onto each well of 6-well plate. 1 ml of prepared bacteria suspension was added into each well for 1 h of uptake. Afterwards, medium was replaced with DMEM containing 10 µg/mL Gentamycin. Lysates were made in sterile water after 1, 6, 24 or 48 h of infection and plated on 7H10 agar plates. The colonies are counted when they are visible.

Expression and purification of GST and GST-Rab20WT

A single colony harboring GST or GST-Rab20WT was picked and grown in LB medium with Ampicillin (50 µg/mL) overnight at 37 ^{o}C with shaking (200 rpm). 1 mL of the overnight culture was transferred into 1 L fresh medium with ampicillin and grown for 3 h at 37 ^{o}C with shaking (200 rpm) and the OD_{600} should be

around 0.6-0.8. IPTG was added into the medium at the final concentration of 10 µM and incubated for 5 h at 37 ^{o}C to induce protein expression. The culture was centrifuged at 5000 rpm for 30 min and the pellet was resuspended thoroughly in 10 mL Lysis Buffer (50 mM Tris-HCl pH 7.9, 50 mM NaCl, 5 mM $MgCl_2$, 5 mM DTT with Complete protease inhibitor cocktail (Roche, Switzerland)). Lysozyme (Sigma-Aldrich, Germany) was added at a final concentration of 1 mg/mL and mixed for 30 min in the cold room. The cells then were broken with a French press for 3 times (1000 PSI). The lysate was centrifuged at 16000X g for 30 min to remove the cell debris. The glutathione-agarose columns (GST Buster QF Glutathione, Amocol, Germany) were washed twice with 11 mL of water, followed by washing with 21 mL of GST Binding Buffer (25 mM Tris-HCl, pH 7.5, 150 mM NaCl, 5 mM DTT, 10% Glycerol, 0.1% Triton X-100) three times. Then the supernatants were loaded onto the previously equilibrated glutathione-agarose columns. The columns were washed with 21 mL of GST Washing Buffer (25 mM Tris-HCl, pH 7.5, 150 mM NaCl, 5 mM DTT, 10% Glycerol, 0.1% Triton X-100) three times. Bound proteins were eluted with 5 mL GST Elution Buffer (25 mM Tris-HCl, pH 7.5, 500 mM NaCl, 5 mM DTT, 20 mM reduced Glutathione, 10% Glycerol, 0.1% Triton X-100) three times and each fraction was collected and analyzed using SDS-PAGE. PD-10 desalting column (GE Healthcare, USA) was utilized for buffer exchange and the elution was concentrated with Vivaspin® 2 centrifuge concentrator (10,000 MWCO, Vivaproducts Inc, USA). The purified protein was finally dissolved in 20 mM Tris-HCl, pH7.5. It can be kept at -20^{o}C for up to 4 weeks. The yielding of GST-Rab20WT is around 2 mg/L.

Cell Biology

Cell culture

Murine macrophage cell line RAW264.7 was purchased from American Type Culture Collection (ATCC, Cat.# TIB-71) and it was maintained in high glucose Dulbecco's Modified Eagles Medium (D-MEM) with 10% heat inactivated fetal bovin serum (FBS) and 2mM L-Glutamine (PAA, Austria) without antibiotics (referred to as full medium) and kept at 37 ^{o}C, 5% CO_2 in a humidified incubator. Every two days, RAW264.7 macrophages were washed with warm Ca^{2+}/Mg^{2+} free Dulbecco's phosphate buffered saline (abbreviated PBS, PAA, Austria) three times, scraped with a 25 cm cell scraper (Sarstedt, Germany) in 10 mL full medium and homogenized by pipetting up and down. Then the cell suspension was added into a new T-75 flask (Sarstedt, Germany) at a ratio of 1:10. For IFN-γ and LPS stimulation, RAW264.7 macrophages were grown in full medium 24 h before adding IFN-γ and LPS. Then the cells were changed with fresh medium supplemented with IFN-γ (200 U/mL, Peprotech, USA) or LPS (1 µg/mL, Sigma-Aldrich, Germany) for another 16-20 h.

Cryopreservation of the cells

When reaching to 90% confluency, cells were washed with PBS three times and scraped in 10 mL PBS for each T-75 flask (Sarstedt, Germany). Cell density was determined by using Trypan blue (Sigma-Aldrich, Germany). Cells were subsequently transferred to a 15 mL falcon tube (Sarstedt, Germany) and centrifuged at 1200 rpm (216X g) for 10 min at room temperature. The pellet was resuspended in freezing medium (40% Glutamine free medium, 50% inactivated FBS, 10% DMSO) to create a cell suspension of 1×10^6 cells/mL. The suspension was transferred to cryo-stocking vials (Thermo Scientific Nunc®, USA) and kept in -80 ^{o}C for 1 week, following by permanent storage in liquid nitrogen.

Bone marrow macrophage isolation

4 to 6 weeks-old female mice were sacrificed by cervical dislocation. The abdomen and hind legs were sterilized with 70% ethanol. The femur and tibia were obtained and trimmed at both ends. The marrow was flushed out with PBS supplemented with 100 units/mL Penicillin G, 100 µg/mL Streptomycin (PAA, Austria) using a 1-mL syringe with a 26-G needle. The cell suspension was centrifuged and the pellet was homogenized in D-MEM with 10% inactivated FBS, 20% L929 culture supernatant and 5% inactivated horse serum (Sigma-Aldrich, Germany) supplemented with 100 µg/mL Penicillin/Streptomycin. Then the cell suspension was plated into microbiological Petri dishes (Sarstedt, Germany) and incubated at 37 ^{o}C, 5% CO_2 in a humidified incubator. The medium was changed every 2 days for 10 days. For recovering the cells, the plates were washed with ice-cold PBS and placed on ice for at least for 15 min and attached macrophages cells were detached by flushing with PBS. Cells were use immediately for experiments or alternatively cryopreserved for later use.

Transfection of macrophages

(1) Lipofectamin 2000 (Invitrogen, USA) was used for immunofluorescence studies. For RAW264.7 macrophages, $0.5\text{x}10^5$cells/well were seeded in 24-well plate one day before transfection, washed twice with PBS and then incubated with 400 µL of Opti-MEM reduced serum medium (Invitrogen, USA). For each well, 0.5 µg of plasmid DNA and 1 µL of Lipofectamine 2000 were employed. 1 µL of Lipofectamine 2000 was diluted in 50 µL of Opti-MEM reduced serum medium and placed at room temperature for 5 min. Then Lipofectamine 2000 in Opti-MEM medium was added into 50 µL of Opti-MEM medium containing 0.5 µg of plasmid DNA. The mixture was incubated for 20 min at room temperature to form the transfection complexes. After that, the 100 µL mixture was added into each well gently. After 6 h of

transfection, the Opti-MEM medium was replaced with full medium. For 6-well plate, 4 µg of DNA in 250 µL of Opti-MEM and 10 µL of Lipofectamine 2000 in 250 µL of Opti-MEM were used.

(2) For experiments involving live cell imaging, jetPEI-Macrophage (Polyplus-transfection, France) was used. 1 x10^5 RAW264.7 cells in 2 mL full medium were seeded on 35mm glass bottom dishes (MatTek, USA) or CELLview^{TM} glass bottom dish with 4 compartments (Greiner bio-one, Germany). 1 µg of plasmid DNA and 3 µL of jetPEI-Macrophage were used for each dish diluted into 50 µL of 150 mM NaCl. The 50 µL jetPEI-Macrophage solution was added into 50 µL of DNA solution and the mixed solution was incubated for 30 min at room temperature. Then, the 100 µL transfection solution was directly added into the dish or 25 µL for each compartment. Transfected cells were used for further experiment after overnight incubation.

(3) In the experiment of Rab20 knockdown with pSIREN shRNA plasmids, Amaxa Nucleofector II (Lonza AG, Germany) was used for transfection. For RAW264.7 macrophages, the cell line specific kit is Amaxa cell line nucleofector Kit V. One day before transfection, RAW264.7 macrophages were subcultured at a ratio of 1:3. In the next day, the cells were scraped, homogenized and counted for cell density. 2×10^6 cells per sample were centrifuged at 90× g (775 rpm) for 10min at room temperature. The pellet was resuspended in 100 µL Nucleofector solution at room temperature. Then, 2 µg plasmid DNA was subsequently added into the suspension. The cell/DNA mixture was transferred to the provided cuvette and the Nucleofector program D-032 was used. After the program was finished, the cells were transferred to a T-25 or T-75 cell culture flasks and incubated in a humidified incubator at 37^{o}C in 5% CO_2 atmosphere.

Generation of stable cell lines

2×10^5 macrophages were seeded in each well of a 6-well plate and incubated overnight in a humidified 37^{o}C/5% CO_2 incubator. Then, cells were transfected with Lipofectamine 2000 or jetPEI-Macrophage as described with the indicated plasmids. When Lipofectamine 2000 was used, after 6-10 h transfection, the medium was replaced with full medium containing selection antibiotics. In the case of jetPEI-Macrophage transfection reagent, the medium was changed with full medium supplemented with the selection antibiotics after overnight transfection. The amount of antibiotics required for RAW264.7 macrophages was titrated in advance. The minimum concentration of the selection antibiotics should kill all the untransfected cells in 2 to 4 days. For RAW264.7 macrophages, the minimum concentration for G418 is 1 mg/mL and 3 µg/mL for Puromycin. Then, the medium was changed with medium containing

the antibiotics every 2 days. After 1-2 weeks the colonies were developed. Every colony was picked up with a 200 µL pipette and transferred into one well of 24-well plate with 1 mL selective medium. When the colonies have grown to be fairly confluent, they were examined by fluorescence or alternatively, cells were lysed and analyzed by Western blotting. The positive colonies were sequentially transferred to T-25 flasks and then T-75 flasks in selective medium for scaling up. Then the positive colonies were frozen with freezing medium in liquid nitrogen. With this method, the generated cell line culture is a polyclonal population of drug resistant cells. To generate a monoclonal cell line, limiting dilution of the resistant cells to 1 cell/well in 96-well plates were performed. After 1-2 weeks selection, the visible colonies were picked and grown for scaling up. In this study, several polyclonal stable cell lines (RAW264.7) were generated according this method, including EGFP, HA-Rab20WT, a series of MISSION® shRNA knockdown plasmids (pLKO.1-puro, shRNA2640, 2641, 2642, 2643,2644). Monoclonal EGFP-Rab20WT (RAW264.7) stable cell line was also generated in this study.

Mouse IgG coupled beads preparation

400 µL latex beads (1 µm or 3 µm in diameter, 2.5% (w/v), Polysciences, USA) or 3 µm polystyrene beads (2.5% (w/v), Krisker Biotech, Germany) were mixed with 100 µL MES buffer, pH 6.7 and 50 µg of mouse IgG (Rockland, USA) or Cy5 conjugated mouse IgG (Jackson ImmunoResearch laboratories, USA) was added and mixed with the beads solution for 15 min in a rotate wheel. Then 14 µL of EDAC (1-Ethyl-3-[3-dimethylaminopropyl] carbodiimide hydrochloride, Sigma-Aldrich, Germany) from 10 mg/mL fresh water solution was added and the whole solution was mixed at a rotate wheel for 1 h at room temperature. Then another 14 µL of EDAC was added and mixed for 1 h at room temperature. The coupling reaction was stopped by washing with Stop Buffer (1 % Triton-X 100 in 10 mM Tris (Sigma-Aldrich, Germany) pH 9.4) for three times. The beads were stored in PBS at 4^{o}C. The final concentration of the beads was 1% (w/v).

Latex-bead phagosomes isolation

RAW264.7 macrophages were grown in T-175 flasks to 90% confluency and incubated in full medium or medium containing IFN-γ (200 U/mL) or LPS (1 µg/mL) for 16-20 h at 37^{o}C, 5% CO_2 in a humidified incubator For each T-175 flask, 1 mL of 1 µm mouse IgG-coated latex beads was added into 20 mL ice-cold full medium and incubated for 1 h in a humidified 37 ^{o}C/5% CO_2 incubator (uptake). Then the cells were washed with ice-cold PBS to remove the beads outside the cells and 20 mL ice-cold full medium was added into each T-175 flask and incubated in the incubator for another 15 min, 30 min or 60 min

(chasing times). The cells were scraped off the flasks and centrifuged at 1200 rpm (216X g) for 10 min. The pellets were washed once with PBS and Homogenization Buffer (3 mM Imidazol, 250 mM sucrose, pH7.4, Sigma-Aldrich, Germany). After washing, the cells were resuspended in 3 mL Homogenization Buffer containing Complete proteases inhibitors cocktail (Roche, Switzerland) and passed through 26-G needles (Ø 0.45×25mm, Sterican®, Germany) approximately 30-40 times. The cell lysates were centrifuged at 340X g (1500 rpm) for 10 min to remove the nuclear fraction and the supernatants were mixed with same volume of 62% (w/w) sucrose in ultra-clear™ tubes (14×89 mm, Beckman, USA). The mixtures were overlay with 4 mL 25% (w/w) sucrose, 3 mL Homogenization Buffer with complete proteases inhibitors. The tubes containing the gradients were centrifuged at 100,000X g (24000 rpm, Sorvall SW40, Thermo Scientific, USA) for 1 h at 4^{o}C. The latex-bead phagosomes were moved to the interface between 25% sucrose and Homogenization Buffer. The phagosomes were collected with a pipette and processed in Sample Buffer for western blotting.

Indirect immunofluorescence

Cells were seeded on 10 mm coverslips (neolab, Germany) in a 24-well plate. Cells were fixed with 4% paraformaldehyde (PFA, Electron Microscopy Sciences, USA) in PBS pH7.4 for 10 min at room temperature, followed by incubation with pre-cooled methanol (J.T.Baker, USA) for 2 min at -20^{o}C. After fixation, the coverslips were washed with PBS twice. Then cells were incubated with 50 mM Glycin/PBS pH 7.4 for 10 min. Afterwards, they were incubated with 1% bovine serum albumin (BSA, Sigma-Aldrich, Germany) in PBS for 10 min. The primary and secondary antibodies were diluted in PBS, added onto the coverslips and incubated for 1 h at room temperature. 1 µg/mL Hoechst 33258 (Sigma-Aldrich, Germany) in PBS was added and incubated for 10 min at room temperature for nuclear staining. Images were taken by Leica SP5 (Leica Microsystems, Germany) with 63×/1.4 HCX-PLAPO oil objective (Leica Microsystems, Germany) and immersion oil Type F (Leica Microsystems, Germany). The images were acquired at 400 Hz scanning speed, 2-5× zoom, and 3 × line averaging. Image resolution was adjusted to 1024×1024 pixels. The fluorophores were excited by Diode (405 nm), multi-line Argon (488, 496, 514 nm), DPSS (561 nm) and HeNe (633 nm) lasers. 25% of argon laser power was used for excitation. Fluorescence was detected by PMT detectors. The images were exported to TIFF files with the software-LAS AF and then processed with ImageJ.

The primary and secondary antibodies used in this study are shown in the **table 2.3** below.

Table 2.3 List of primary and secondary antibodies for immunofluorescence:

(All the antibodies are diluted in PBS if it's not specifically stated)

Primary Antibodies			
Antigen	**Host**	**Dilution for IF**	**Producer** Cat. №
Rab20	Rabbit	1:50	GeneTex GTX119559
GM130	Mouse	1:250	BD Tranduction Laboratories 610822
Syntaxin6	Mouse	1:50	BD Tranduction Laboratories 610635
TGN38	Rabbit	1:100	Novus Biologicals NB110-40768
EEA1	Mouse	1:100	BD Tranduction Laboratories 610457
Rab5	Rabbit	1:100	Cell Signalling 3547
LAMP-2	Rat	1:50	DSHB ABL-93
Secondary Antibodies			
Secondary Antibodies	**Conjugate**	**Dilution for IF**	**Producer** Cat. №
Goat anti-Mouse	Alexa Fluor® 488	1:800	Invitrogen A-11001
Goat anti-Mouse	Alexa Fluor® 546	1:800	Invitrogen A-11003

Goat anti-Rabbit	Alexa Fluor® 488	1:800	Invitrogen A-11008
Donkey anti-Rabbit	Alexa Fluor® 546	1:800	Invitrogen A-10040
Donkey anti-Rabbit	Cy-3	1:500	Jackson ImmunoResearch 711-165-152
Goat anti-Rat	Alexa Fluor® 488	1:800	Invitrogen A-11006
Goat anti-Rat	Alexa Fluor® 546	1:800	Invitrogen A-11081

Blocking Rab20 immunostaining with immunizing peptide

The Rab20 antibody (GeneTex, 1 mg/mL) was diluted 1:50 in PBS pH7.4. Then the antibody solution was separated into 2 tubes. Equivalent amount of immunizing peptide was added into one of the tubes and mixed at room temperature for 30 min. The immunostaining was performed as described on the two identical samples with control antibody or antibody plus immunizing peptide mixture in parallel. Then the staining was observed with Leica SP5 Confocal microscope (Leica Microsystems, Germany). Images were acquired using the same settings.

Western blot

One T-75 flask of RAW264.7 macrophages (90% confluency) were washed with ice-cold PBS 3 times. Then the cells were scraped and centrifuged at 1200 rpm (216X g) for 10 min at 4 ^{o}C. The pellets were lysed with 400 µL of Lysis Buffer (10 mM Tris/HCl, pH7.5, 150 mM NaCl, 0.5 mM EDTA, 0.5% NP-40 (Sigma-Aldrich, Germany) supplemented with complete protease inhibitor cocktail (Roche, Switzerland) for 10 min on ice. After centrifuged at 16,000X g for 10 min, the supernatant was incubated in Sample Buffer (50mM Tris-HCl pH 6.8, 2% SDS, 10% glycerol, 1% β-mercaptoethanol, 12.5 mM EDTA, 0.02 % bromophenol blue) at 96 ^{o}C for 10 min. Then protein extracts were subjected to electrophoresis in 10% SDS-PAGE gels, transferred to a nitrocellulose membrane, and blocked with 5% low-fat milk (Carl Roth,

Germany) in PBS/0.1% Tween-20 overnight at 4°C. The nitrocellulose membrane was then incubated with primary antibody in 5% milk in PBS/0.1% Tween-20 overnight at 4 °C (only for Rab20 antibodies) or 1 h at room temperature. After 3 times washing with PBS/0.1% Tween-20 for 10 min, the membrane was incubated with HRP-conjugated secondary antibody (Jackson ImmunoResearch, 1:10000 in 5% milk in PBS/0.1% Tween-20) for 1 h at room temperature, followed by 3X 10 min washing with PBS/0.1% Tween-20. The membranes were finally developed with ECL (Enhanced chemilumescent) Detection Kit (GE Life Sciences, USA). β-Actin (1:4000 Abcam, UK) or Tubulin (1:2000 DSHB, USA) is used as the loading control. All the primary and secondary antibodies used in this study are shown in **Table 2.4**.

To re-probe the membrane, the membranes were incubated in Stripping Buffer (15 g Glycin, 1 g SDS, 10 mL Tween-20 pH 2.2, per liter). The procedure was as follows: incubate the membrane with stripping buffer two times for 10 min; wash with PBS two times for 10 min; wash with PBST two times for 5 min. After this procedure, the membrane is ready for blocking.

Table 2.4 List of primary and secondary antibodies used in Western blot
(All the antibodies are diluted in 5% milk, PBST if it's not specifically stated)

Primary Antibodies			
Antigen	**Host**	**Dilution for WB**	**Producer** Cat. №
Rab20	Rabbit	1:1000	GeneTex GTX119559
Rab20	Rabbit	1:1000	ProteinTech 11616-1-AP
Rab5	Rabbit	1:1000	Cell Signalling 3547
Rab7	Rabbit	1:1000	Cell Signalling 9367
LAMP-2	Rat	1:50 in PBST	DSHB ABL-93

Actin	Mouse	1:4000 in PBST	Abcam Ab8226
Tubulin	Mouse	1:2000	DSHB
Rabex-5	Rabbit	1:2000	Sigma R5405
EGFP	Mouse	1:3000	Clonetech 632380

Secondary Antibodies

Secondary Antibody	**Conjugate**	**Dilution for WB**	**Producer** Cat. №
Goat anti-Mouse	HRP	1:10000	Jackson ImmunoResearch 115-035-003
Goat anti-Rabbit	HRP	1:10000	Jackson ImmunoResearch 111-035-003
Goat anti-Rat	HRP	1:10000	Jackson ImmunoResearch 112-035-003

Live-cell imaging

For live cell imaging studies, 1 x10^5cells were seeded on 35mm glass bottom dishes (MatTek, USA) or 3 x10^4 cells per compartment were seeded on CELLview^{TM} glass bottom dish (Greiner Bio One, Germany). Transfections were performed with jetPEI-Macrophage transfection reagent as described. After 16h transfection, macrophages were washed with PBS and replaced with imaging medium (D-MEM without phenol Red, 10% FBS, 2 mM L-Glutamine). Afterwards, 5 µL of 3 µm mouse IgG-coated polystyrene beads solution (1%) was added into the medium. Time lapse of images were taken by Leica SP5 AOBS (Leica Microsystems, Germany) equipped with an environment control chamber (EMBLEM, Germany) which provides a 37 ^{o}C, 5% CO_2 humidified atmosphere, a 63×/1.4 HCX-PLAPO oil objective (Leica Microsystems, Germany) and temperature corrected immersion oil Type 37 (Cargille Labs, UK). The time-lapse images were taken every 30 seconds up to 4 h, at 400 Hz scanning speed and 3 × line

averaging. All the movies were taken at the same zoom factor (2.5). The image resolution was adjusted to 1024×1024 pixels. The fluorophores were excited by multi-line Argon (488, 496, 514 nm), DPSS (561 nm) or HeNe (633 nm) lasers. 25% of argon laser power was used for excitation. Fluorescence was detected by conventional photomultipliers (PMT) or Hybrid detectors (HyD). The time-lapse images were exported as uncompressed AVI-formatted movie with the software- LAS AF and then processed with ImageJ v1.43u.

Rab20 knockdown with pSIREN system

Cells were respectively transfected with control shRNA, shRNA 1, shRNA 2, shRNA 3, shRNA 4 using Amaxa Nucleuofector as described and after 30 h transfection, transfected cells were sorted for DsRed using BD Aria II sorter (BD Biosciences, USA). Sorted cells were incubated with Sample Buffer at 96 ^{o}C for 10 min. Subsequently, the cell lysates were blotted for Rab20 to check the knockdown efficiency of different shRNAs.

For live cell imaging with cells expressing the indicated shRNAs, macrophages were seeded on 35 mm glass dish and transfected with jetPEI-Macrophage transfection reagent as described. After 30h incubation, cells expressing dsRed were selected for imaging during the studies.

Rab20 knockdown with MISSION® System

MISSION® shRNA system (Sigma-Aldrich, Germany) was also used to obtain stable Rab20 knockdown cell lines. The procedures of generating stable Rab20 knockdown cell lines were described in the section of "Generation of stable cell lines". Five validated Rab20 shRNA plasmids in total were employed to generate stable knockdown cell lines, including shRNA2640, shRNA 2641, shRNA 2642, shRNA 2643 and shRNA 2644. The control shRNA plasmid is pLKO.1-puro empty vector. The sequences of the five validated shRNAs were as follows:

shRNA2640: 5'-CCGGCCTGACAGAAACAGCCAACAACTCGAGTTGTTGGCTGTTTCTGTCAGGTTTTTG-3'

shRNA2641: 5'-CCGGGCTATCATCCTTACATACGATCTCGAGATCGTATGTAAGGATGATAGCTTTTTG-3'

shRNA2642: 5'-CCGGCCTCCTCTTTGAAACCTTGTTCTCGAGAACAAGGTTTCAAAGAGGAGGTTTTTG-3'

shRNA2643: 5'-CCGGCCCTTTACAAGAAGATCCTGACTCGAGTCAGGATCTTCTTGTAAAGGGTTTTTG-3'

shRNA2644: 5'-CCGGGAAGATCCTGAAGTACAAGATCTCGAGATCTTGTACTTCAGGATCTTCTTTTTG-3'

The underlined sequences showed the target sequences for mouse Rab20.

LysoTracker labeling and phagosome maturation analysis

RAW264.7 macrophages were seeded on CELLview^{TM} glass bottom dish with 4 compartments and transfected with EGFP, EGFP-Rab20WT or EGFP-Rab20T19N by jetPEI-macrophage transfection reagent as described. After overnight incubation, cells were washed with PBS once and 0.5 mL of 50 nM LysoTracker Red DND99 (Invitrogen, USA) diluted in imaging medium was added into each compartment. For Rab20 knockdown cells with pSIREN-DsRed shRNA, the experiment was performed with 50 nM LysoTracker Green DND26 (Invitrogen, USA). The dish was transferred to the pre-warmed and temperature stabilized environmental chamber. Afterwards, 5 µL of 3 µm mouse IgG coated polystyrene beads solution (1%) was added into the medium. Then time-lapse images were acquired to monitor the dynamics of LysoTracker Red fluorescence association to phagosomes. During all these studies, all settings for image acquisition were kept constant to perform quantitative analysis.

Phosphatidylinositol 3-phosphate (PI3P) association to phagosome assay

RAW264.7 macrophages were seeded on CELLview^{TM} glass bottom dish with 4 compartments and co-transfected EGFP-2×FYVE with mCherry, mCherry-Rab20WT or mCherry-Rab20T19N by jetPEI-macrophage transfection reagent as described. After overnight incubation, cells were washed with PBS once and the medium was replaced with imaging medium. Afterwards, 5 µL of 3 µm mouse IgG-coated polystyrene beads (1%) was added into the medium. Time-lapse images were acquired to monitor the dynamics of PI3P association to phagosomes. For all the groups, the settings of microscopy were the same.

Phagolysosome fusion assay

RAW264.7 macrophages were seeded on CELLview^{TM} glass bottom dish with 4 compartments and transfected with EGFP, EGFP-Rab20WT or EGFP-Rab20T19N by jetPEI-macrophage transfection reagent as described. After 6h incubation, cells were washed with PBS once and 0.5 mL of 50 µg/mL Texas Red conjugated Dextran 70kDa (Invitrogen, USA) diluted in full medium was added and cells were incubated for 2 h at 37 ^{o}C, 5% CO_2 in a humidified incubator. Then cells were replaced with full medium and incubated for another 16-20 h. At this time, the vesicles containing Dextran 70kDa were considered as late endosomes/lysosomes. The medium was replaced with imaging medium. Afterwards, 5 µL of 3 µm mouse IgG coated polystyrene beads solution (1%) was added into the medium. Then time-lapse images

were taken to monitor the dynamics of Dextran 70 kDa fluorescence association to phagosomes. For all the groups, the settings of microscopy were the same.

Rab5A association assay

Required amount of RAW264.7 macrophages were seeded on CELLview^{TM} glass bottom dish with 4 compartments and co-transfected with EGFP-Rab5A with mCherry, mCherry-Rab20WT or mCherry-Rab20T19N by jetPEI-macrophage transfection reagent as described. After overnight transfection, cells were washed with PBS once and the medium was replaced with imaging medium. 5 µL of 3 µm mouse IgG-coated polystyrene beads were added into the medium. Time-lapse images were acquired to monitor the dynamics of Rab5A association to phagosomes. For all the groups, the settings of microscopy were the same.

EGFP-Rab20WT co-immunoprecipitation

EGFP and EGFP-Rab20WT stably transfected RAW264.7 macrophages were thawed from liquid nitrogen and grown in T-75 flasks. When reached 90% confluency, each T75 flask of EGFP stably transfected cells were scraped, collected and lysed with 200 µL of Lysis Buffer (20 mM Tris/HCl, pH 7.5, 150 mM NaCl, 0.5% NP-40, 80 mM β-GlyceroPO_4 (Sigma-Aldrich, Germany), 50 mM NaF (Carl-Roth, Germany), 5 mM EDTA, 5 mM $MgCl_2$, and Complete protease inhibitor cocktail) for 30 min on ice. For each T-75 flask of EGFP-Rab20WT stably transfected cells, they were lysed with 200 µL of Lysis Buffer supplemented with 1 mM GTPγS (EMD Chemicals, USA) or GDPβS (Merck, Germany) for 30 min on ice, followed by adding 5 mM $MgCl_2$ for another 30 min on ice. All the cell lysates were centrifuged at 16,000X g (12274 rpm) for 10 min at 4 ^{o}C. The supernatants were transferred to pre-cooled Eppendorf tubes and 200 µL of Washing Buffer (20 mM Tris/HCl, pH7.5, 150 mM NaCl, and Complete protease inhibitor cocktail) was added into each supernatant on ice. The GFP-Trap® beads (ChromoTek, Germany) were washed with 1 mL of Washing Buffer for three times and 25 µL of GFP-Trap® beads were added into each supernatant and mixed in a rotator wheel at 4 ^{o}C for 2 h. Then the beads were washed three times with Washing Buffer to remove the un-bound proteins. The beads were incubated in Sample Buffer at 96 ^{o}C for 10 min and then analyzed by western blotting to check putative proteins of interest interacting with Rab20WT.

GST-Rab20WT pull down

The glutathione-agarose beads (GST Buster QF Glutathione, Amocol, Germany) were previously equilibrated as follows: washing with 1 mL of water three times; washing with 1 mL of GST Binding

Buffer three times. 100 µg of GST or GST-Rab20WT (in 20 mM Tris-HCl, pH7.5) were added into 50 µL of equilibrated glutathione-agarose and incubated for 30 min at room temperature under rotation. The beads were centrifuged at 700X g (2500 rpm) for 1 min to remove the unbounded proteins. Then the Glutathione agarose beads containing GST or GST-Rab20 were incubated with 500 µL of Nucleotide Exchange Buffer (NE Buffer, 20 mM Tris-HCl pH7.5, 150 mM NaCl, 1 mM DTT, 5 mM EDTA, and Complete protease inhibitor cocktail) for 60 min at room temperature under rotation. The beads were centrifuged at 700X g for 1 min and for GTPγS/GDPβS loading, they were incubated with 400 µL of NE Buffer supplemented with 10 mM $MgCl_2$ and 2 mM GTPγS/GDPβS for another 30 min at room temperature under rotation. The procedures described above resulted in the production of immobilized GST-Rab20 mainly in active (GTPγS) or inactive (GDPβS) form.

For each pull down, one T-175 flasks of RAW264.7 macrophages (95% confluency) were required. For each T-175 flask, Cells were lysed with 400 µL of Lysis Buffer (20 mM Tris/HCl, pH 7.5, 150 mM NaCl, 0.5% NP-40, 80 mM β-GlyceroPO_4, 50 mM NaF, 5 mM EDTA, 5 mM $MgCl_2$, 2 mM GTP GTPγS/ GDPβS, and Complete protease inhibitor cocktail) on ice for 30 min. The cell debris was removed by centrifuging at 16000 X g (12274 rpm) at 4 ^{o}C. Each supernatant was mixed with 400 µL of Washing Buffer (20 mM Tris-HCl pH 7.5, 150 mM NaCl, and Complete protease inhibitor cocktail).

Subsequently, the beads immobilized with GST, GST-Rab20 (GTPγS) or GST-Rab20 (GDPβS) were incubated with the obtained supernatants for 2 h at 4 ^{o}C under rotation. After that, the beads were washed with Washing Buffer for three times. Then the beads were heated with Sample Buffer at 96 ^{o}C for 10 min and the samples were analyzed by western blotting for the putative direct interaction with Rab20.

Image analysis for live cell imaging

The time-lapse images were exported to uncompressed AVI-formatted movies as single channels with the software- LAS AF. The RGB-color movies were loaded into ImageJ (Version 1.43u) and transformed into 8-bit color movies (Image→ Color→ Split channels). Then the 8-bit color movies were ready for further quantification. And they also can be saved with JPEG compression.

To quantify the fluorescence association to the phagosomes, the corresponding fluorescent channel movies were loaded into ImageJ. Because all the movies among different groups were acquired at the same zoom factor, the scale of the movies was not taken into account. A circle closely adjacent to the phagosome was drawn with the “Elliptical selection” tool. In “Set Measurements”, only “Area” and

"Integrated Density" were selected. And the integrated intensity inside the circle was measured image by image (Analyze→ Measure). The position and the size of the circle was adjusted manually with the movement of the phagosome in the diferent frames. In phagosome maturation and phagolysosome fusion assay, the absolute integrated intensity was plotted. For PI3P association and Rab5A association experiments, the expression level of EGFP-2XFYVE and EGFP-Rab5A was different in different groups. To take account of this effect, the fluorescence of EGFP-FYVE was normalized to the fluorescence of same size in the nucleus. The fluorescence of EGFP-Rab5A was normalized to the fluorescence of same size in the Golgi region. The fluorescence of mCherry, mCherry-Rab20WT or mCherry-Rab20T19N was normalized to the fluorescence of same size in the cytosol. And the normalized data was plotted with GraphPad Prism v5.04.

Statistical analysis

Statistical analysis was performed with GraphPad Prism v5.04 (GraphPad software Inc., USA). P-values were calculated using student' two-tailed unpaired t-test. The confidence interval is 95%.

3. Results

Characterization of the distribution of Rab20 in macrophages

Analysis of the distribution of EGFP-Rab20 in RAW264.7 macrophages

To understand the immune role of Rab20 in membrane trafficking, the intracellular distribution of this small GTPase in macrophages was investigated. Endogenous Rab20 mainly associates to apical endocytic organelles in mouse kidney cells and in intercalated cells of the cortical and outer medullar collecting ducts (Lütcke A *et al*.1994, Curtis LM and Gluck S. 2005). Furthermore, it has been reported that endogenous Rab20 is localized to *cis* and medium stacks of the Golgi complex in HeLa cells (Amillet JM *et al*. 2006).

Several studies have shown that the Q61L mutation in Ras GTPases inhibits both the intrinsic and GAP-stimulated GTPase activity (Krengel U *et al*. 1990). It is named as the constitutively active mutant. The S17N mutant has a lower affinity for GTP than GDP (Feig LA and Cooper GM *et al*. 1988) and thus considered dominant negative mutant. For Rab GTPases, they share a similar mechanism of guanine binding and GTP/GDP switch with Ras family of GTPases. Therefore, Q61L and T/S17N mutations in Rab GTPases have the same effects with the corresponding mutations in Ras GTPases (Stenmark H *et al*. 1994). Although Glutamine and Threonine/Serine at the corresponding positions are highly conserved, there are some exceptions for Rab GTPases. In Rab20, Rab24 and Rab25, the Glutamine at the position corresponding to Ras Gln-61 is substituted by Arginine, Serine and Leucine, respectively. Several mutants at the position of the residue 61 of Ras, including Arginine substitution, display much lower GTP hydrolysis activity (Der CJ *et al*. 1986). In agreement with these observations, Rab24 that naturally possesses a Serine residue at the position corresponding to Ras Gln-61 exists predominantly in the active GTP-bound state (Erdman RA *et al*. 2000). Therefore, Rab20 that has an Arginine at the position cognate to Ras Q61 is considered to be constitutively active. Therefore, in this study Rab20 wild type and the dominant negative mutant Rab20T19N were used.

To investigate the distribution of Rab20, RAW264.7 macrophages were transfected with EGFP-Rab20WT or the dominant negative mutant EGFP-Rab20T19N. Different antibodies against organelle markers such as *cis*-Golgi network (CGN) marker- Golgi matrix protein 130 (GM130), *trans*-Golgi network (TGN) marker- *trans*-Golgi network 38 (TGN38), early endosome marker- early endosome antigen 1 (EEA1) and

Rab5, late endosome/lysosome marker- lysosome associated membrane protein 2 (LAMP-2) were further used for the indirect immunofluorescence.

In agreement with the distribution of endogenous Rab20 observed in HeLa cells (Amillet JM *et al*. 2006), EGFP-Rab20WT in RAW264.7 macrophages associated to the CGN and TGN (**Fig. 3.1 A, B**). Strikingly, RAW264.7 macrophages expressing EGFP-Rab20WT developed giant vacuoles that resembled the phenotype observed in BHK and HEp2 cells expressing the constitutively active mutant Rab5Q79L (Stenmark H *et al*. 1994, Roberts RL *et al*. 1999, Wegener CS *et al*. 2010). The formation of these enlarged vacuoles was not due to the transfection reagent since in EGFP expressing cells there were no such large vacuoles. As observed in Rab5Q79L expressing cells; the enlarged Rab20-positive vacuoles co-localized with early endosomal markers EEA1 and Rab5. In contrast, the rest of large vacuoles were positive for the late endosomal marker LAMP-2 (**Fig. 3.1 C-E**). As expected, the dominant mutant Rab20T19N showed a cytosolic distribution with almost absent membrane association (**Fig. 3.2**). Moreover, the expression of Rab20T19N did not induce the formation of enlarged vacuoles (**Fig. 3.2**).

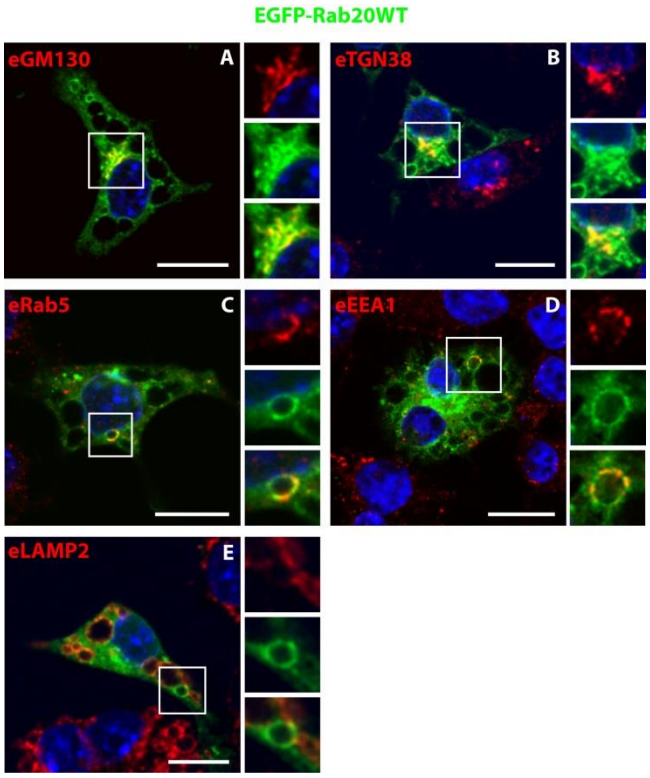

Fig. 3.1 EGFP-Rab20WT distribution in RAW264.7 macrophages. RAW264.7 macrophages were transfected with EGFP-Rab20WT for 16 hours and then fixed with 4% PFA for 10 min at room temperature (RT) followed by methanol incubation for 2 min at -20^{o}C. Immunofluorescence was performed with different antibodies to label intracellular compartments (shown in red), *cis*-Golgi network **(A)**, *trans*-Golgi network **(B),** early endosomes **(C, D)**, and late endosomes **(E)**. The nuclei were labeled by Hoechst 33258 and shown in blue. Insets show the localization of EGFP-Rab20WT in the region of interest (indicated with white squares). Scale bars are 10 µm.

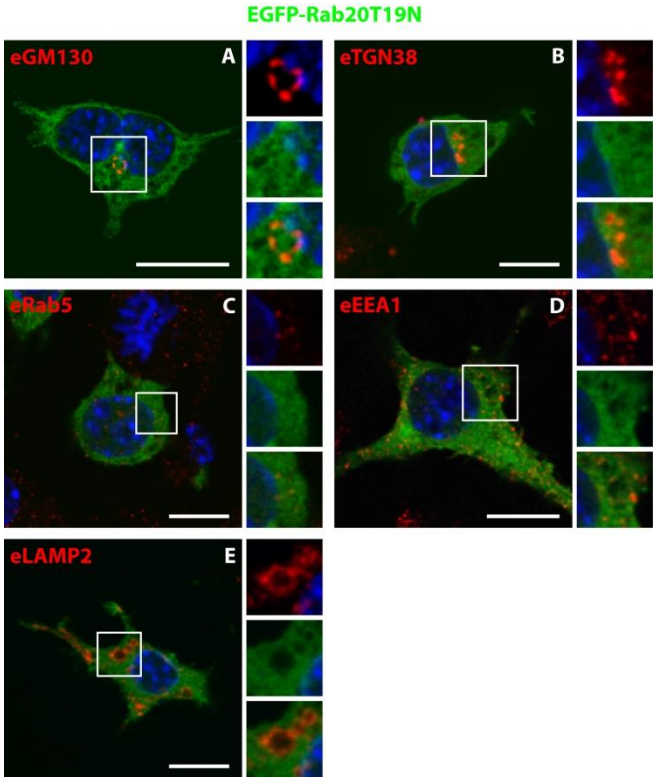

Fig. 3.2 EGFP-Rab20T19N distribution in RAW264.7 macrophages. RAW264.7 macrophages were transfected with EGFP-Rab20T19N for 16 hours and then fixed with 4% PFA for 10 min at RT followed by methanol incubation for 2 min at -20°C. Immunofluorescence was performed with different antibodies to label intracellular compartments (shown in red), *cis*-Golgi network **(A)**, *trans*-Golgi network **(B),** early endosomes **(C, D)**, and late endosomes **(E)**. The nuclei were labeled by Hoechst 33258 and shown in blue. Insets show the localization of EGFP-Rab20T19N in the region of interest (indicated with white squares). Scale bars are 10 µm.

Analysis of the distribution of endogenous Rab20 in RAW264.7 and bone marrow macrophages

To confirm the distribution of over-expressed Rab20, endogenous Rab20 distribution was also investigated. A rabbit polyclonal antibody raised against Rab20 (GeneTex, GTX119559) was employed for endogenous Rab20 immunofluorescence staining. To test the specificity of this antibody, EGFP-Rab20WT expressing RAW264.7 macrophages were fixed and immunolabeled for endogenous Rab20. The signal from this antibody highly overlapped with EGFP-Rab20WT in the Golgi region and enlarged Rab20-positive vacuoles, suggesting the antibody was specific for Rab20 (**Fig. 3.3**). To further characterize the specificity of the antibody, the immunizing peptide used for generating this antibody was incubated together with the antibody to compete for the binding. Compared with the sample stained with Rab20 antibody alone, the Rab20 signal was significantly blocked by the peptide, indicating the good sensitivity and specificity of this antibody for endogenous Rab20 labeling (**Fig. 3.4**). Hence it was used for investigating the distribution of endogenous Rab20 in the following studies.

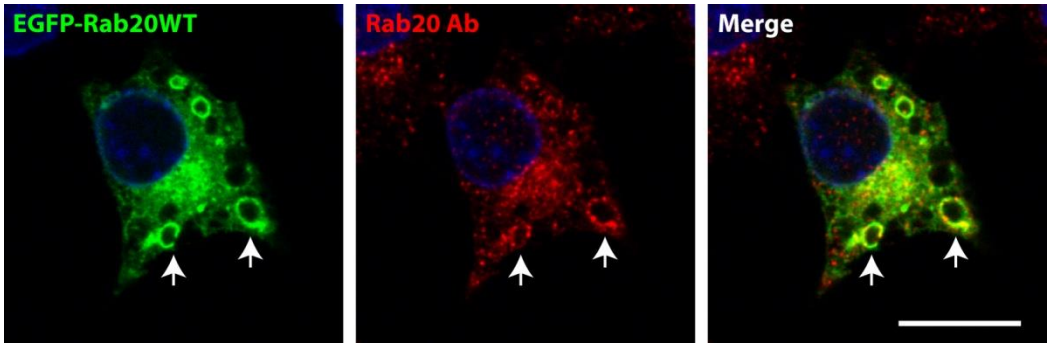

Fig. 3.3 Immunofluorescence of endogenous Rab20 in EGFP-Rab20WT expressing RAW264.7 macrophages. RAW264.7 macrophages were transfected with EGFP-Rab20WT for 16 hours and then fixed with 4% PFA for 10 min at RT followed by methanol incubation for 2 min at -20°C. Immunofluorescence was performed with Rab20 antibody from GeneTex (GTX119559, final concentration: 20 µg/mL). The signal from Rab20 antibody is shown in red. The nuclei were labeled by Hoechst 33258 and shown in blue. White arrows indicate the EGFP-Rab20WT positive vacuoles are also stained by Rab20 antibody. The scale bar is 10 µm.

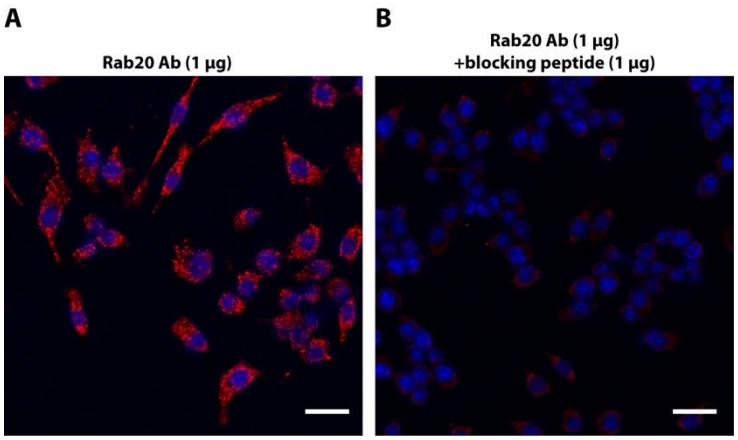

Fig. 3.4 Immunofluorescence for endogenous Rab20 in presence or absence of blocking peptide in RAW264.7 macrophages. (A) Immunostaining with Rab20 antibody only. In total 1 µg of antibody (GeneTex, GTX119559) was used. **(B)** Immunostaining with the Rab20 antibody and blocking peptide. 1 µg of antibody and same amount of blocking peptide were mixed in advance for 30 min and applied for immunofluorescence. The signal from Rab20 antibody is shown in red. The nuclei were labeled by Hoechst 33258 and shown in blue. Scale bars are 10 µm.

In RAW264.7 macrophages, endogenous Rab20 partially co-localized with the CGN marker GM130 and the TGN marker Syntaxin 6 (**Fig. 3.5 A, B**). Similarly, in bone marrow macrophages, endogenous Rab20 also localized with the CGN and TGN (**Fig. 3.6 A, B**). A low level of colocalization with the early endosome marker EEA1 was also observed in RAW264.7 and bone marrow macrophages (BMMs) (**Fig. 3.5 C; Fig. 3.6 C**). So it was concluded that endogenous Rab20 in macrophages mainly localized with the CGN and TGN and partially localized to early endosomes.

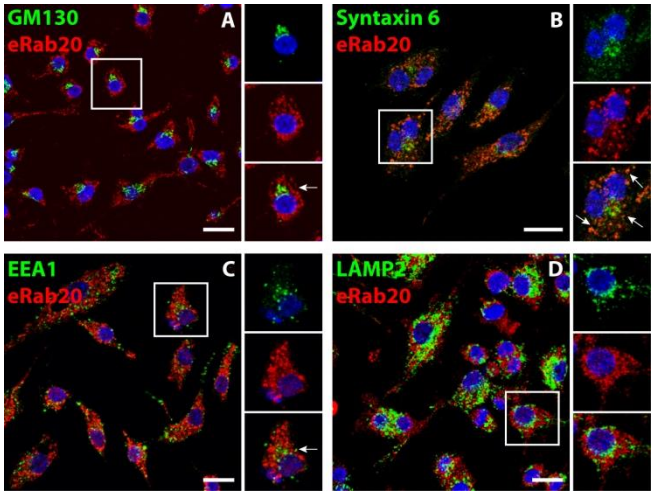

Fig. 3.5 The distribution of endogenous Rab20 in RAW264.7 macrophages. RAW264.7 macrophages were fixed with 4% PFA for 10 min at RT followed by methanol incubation for 2 min at -20°C. Immunofluorescence was performed with Rab20 antibody (shown in red) from GeneTex (GTX119559, final concentration: 20 µg/mL). Different antibodies were also used to label intracellular compartments (shown in green), *cis*-Golgi network **(A)**, *trans*-Golgi network **(B),** early endosomes **(C)**, and late endosomes **(D)**. The nuclei were labeled by Hoechst 33258 and shown in blue. Insets show the distribution of endogenous Rab20 in the region of interest (indicated with white squares). White arrows indicate endogenous Rab20 colocalization with different markers. Scale bars are 10 µm.

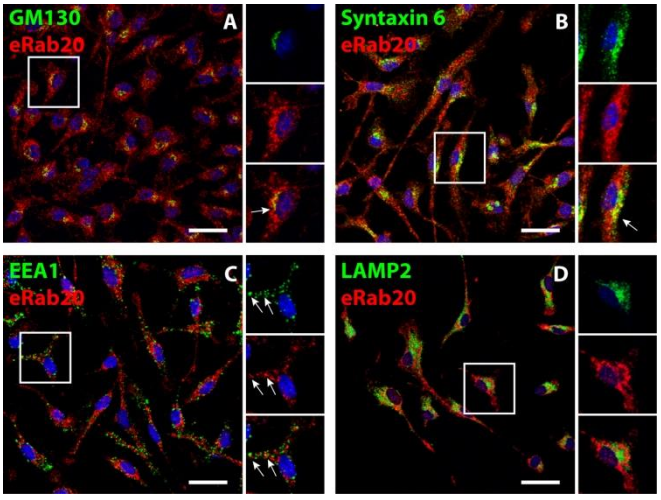

Fig. 3.6 The distribution of endogenous Rab20 in bone marrow macrophages. Bone marrow macrophages were fixed with 4% PFA for 10 min at RT followed by methanol incubation for 2 min at -20°C. Immunofluorescence was performed with Rab20 antibody (shown in red) from GeneTex (GTX119559, final concentration: 20 µg/mL). Different antibodies were also used to label intracellular compartments (shown in green), *cis*-Golgi network **(A)**, *trans*-Golgi network **(B),** early endosomes **(C)**, and late endosomes **(D)**. The nuclei were labeled by Hoechst 33258 and shown in blue. Insets show the distribution of endogenous Rab20 in the region of interest (indicated with white squares). White arrows indicate endogenous Rab20 colocalization with different markers. Scale bars are 10 µm.

Rab20 expression is up-regulated by IFN-γ in RAW264.7 and bone marrow macrophages

Natural killer (NK) and Th1 cells produce the key protective cytokine for macrophages IFN-γ, which induces diverse antimicrobial activities (Schroder K *et al*. 2004). One of the IFN-γ induced mechanisms is the vitamin D-dependent antimicrobial pathway (Fabri M *et al*. 2011). IFN-γ treatment leads to the up-regulation of vitamin D receptor and CYP27b1 (25-Hydroxyvitamin D_3 1-alpha-hydroxylase). CYP27b1 catalyzes the inactive form of vitamin D into active form, which activates the expression of antimicrobial peptides Cathelicidin and DEFB4 (defensin beta 4) (Fabri M *et al*. 2011). Interestingly, it has been found that Rab20 expression is enhanced by vitamin D treatment (Torri A *et al*. 2010). Therefore, Rab20 expression could also be modulated by IFN-γ. To investigate if Rab20 expression in RAW264.7

macrophages is regulated by IFN-γ, the expression of Rab20 was analysed in resting and activated macrophages with 200 Units/mL IFN-γ by western blot. Compared with resting macrophages, the mean expression level of Rab20 after IFN-γ treatment in RAW264.7 macrophages increased approximately 6-folds (**Fig.3.7 A, B**). BMMs were treated with 400 Units/mL IFN-γ for 48 hours to obtain an activating effect. After IFN-γ treatment, the mean expression level of Rab20 in BMMs increased approximately 4-folds (**Fig.3.7 C, D**).

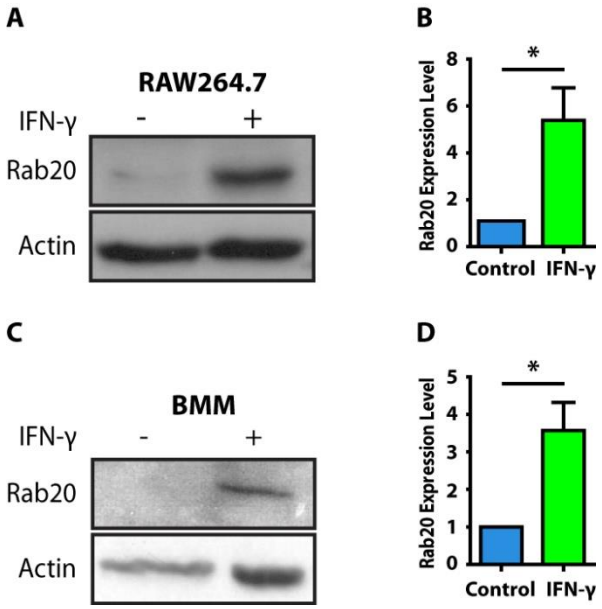

Fig. 3.7 Rab20 expression in RAW264.7 and bone marrow macrophages after IFN-γ treatment. (A, C) Western blot analysis of Rab20 expression in RAW264.7 macrophages **(A)** and bone marrow macrophages **(C)** after IFN-γ treatment. RAW264.7 macrophages **(A)** or bone marrow macrophages **(C)** were treated with 200 Units/mL IFN-γ for 16 hours or 400 Units/mL IFN-γ for 48 hours, respectively. Actin was used as the loading control. Three independent experiments were performed. Representative images are shown. **(B, D)** Statistical analysis of Rab20 expression level in RAW264.7 macrophages **(B)** and bone marrow macrophages **(D)** after IFN-γ treatment. The intensity of bands was measured using ImageJ software. The relative Rab20 intensity was calculated against the corresponding actin loading control. The relative Rab20 intensity with IFN-γ treatment was normalized against without IFN-γ treatment. The plots indicate means ± SD of three independent experiments. P values were calculated using student' two-tailed unpaired t-test. (*) $p \leq 0.05$, (**) $p \leq 0.01$.

Rab20 distribution after IFN-γ stimulation

To investigate the distribution of endogenous Rab20 after IFN-γ stimulation, RAW264.7 and bone marrow macrophages were treated with IFN-γ as mentioned in the previous experiment and then indirect immunofluorescence performed to label Rab20 and intracellular compartments. After IFN-γ treatment, the intensity of the Rab20 labeling was apparently stronger than without IFN-γ treatment (**Fig. 3.8; Fig. 3.9**). This is in agreement with the increased Rab20 expression after IFN-γ treatment observed by Western blot (**Fig. 3.7**). Endogenous Rab20 in RAW264.7 and bone marrow macrophages partially co-localized with the CGN and TGN after IFN-γ treatment (**Fig. 3.8 A, B; Fig. 3.9 A, B**). Interestingly, enlarged early and late endosomes were also observed in RAW264.7 macrophages with IFN-γ stimulation and endogenous Rab20 partially co-localized with the giant early endosomes but not with the late endosomes (**Fig. 3.8 C, D**). In contrast, the enlarged early and late endosomes observed in

RAW264.7 macrophages were not seen in bone marrow macrophages after IFN-γ stimulation (**Fig. 3.9 C, D**). Thus, after IFN-γ treatment Rab20 was localized in the CGN and TGN, and localized to enlarged early endosomes.

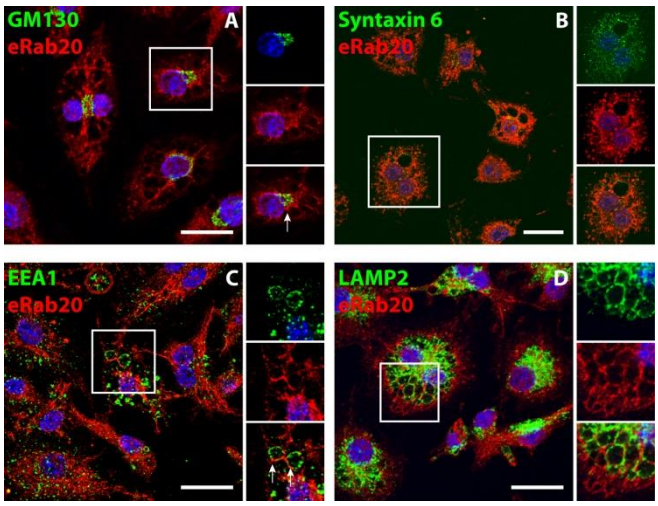

Fig. 3.8 The distribution of endogenous Rab20 in RAW264.7 macrophages after IFN-γ treatment. Cells were treated with IFN-γ (200 Units/mL) for 16 hours and then fixed with 4% PFA for 10 min at RT followed by methanol incubation for 2 min at -20°C. Immunofluorescence was performed with Rab20 antibody (shown in Red) from GeneTex (GTX119559, final concentration: 20 µg/mL). Different antibodies were also used to label intracellular compartments (shown in green), *cis*-Golgi network **(A)**, *trans*-Golgi network **(B),** early endosomes **(C)**, and late endosomes **(D)**. The nuclei were labeled by Hoechst 33258 and shown in blue. Insets show the distribution of endogenous Rab20 in the region of interest (indicated with white squares). White arrows indicate endogenous Rab20 colocalization with different markers. Scale bars are 10 µm.

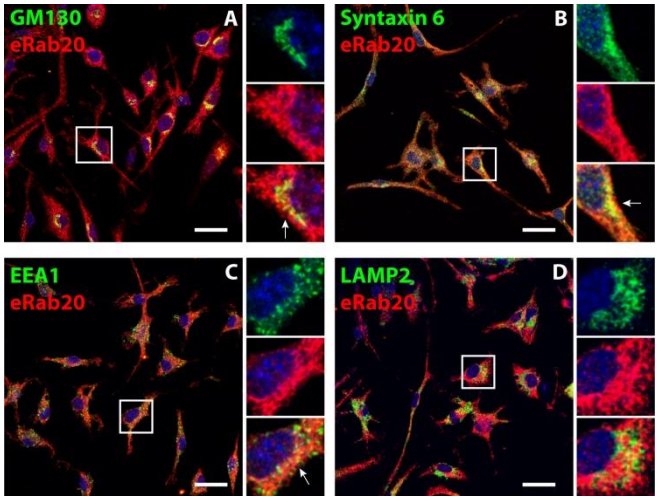

Fig. 3.9 The distribution of endogenous Rab20 in bone marrow macrophages after IFN-γ treatment. Cells were treated with IFN-γ (400 Units/mL) for 48 hours and then fixed with 4% PFA for 10 min at RT followed by methanol incubation for 2 min at -20°C. Immunofluorescence was performed with Rab20 antibody (shown in Red) from GeneTex (GTX119559, final concentration: 20 µg/mL). Different antibodies were also used to label intracellular compartments (shown in green), *cis*-Golgi network **(A)**, *trans*-Golgi network **(B),** early endosomes **(C)**, and late endosomes **(D)**. The nuclei were labeled by Hoechst 33258 and shown in blue. Insets show the distribution of endogenous Rab20 in the regions of interest (indicated with white squares). White arrows indicate endogenous Rab20 colocalization with different markers. Scale bars are 10 µm.

Rab20 expression stimulates the homotypic fusion between Rab20-positive vesicles

As shown in **Fig. 3.1** and **Fig. 3.8**, Rab20 over-expression and IFN-γ treatment induce the formation of enlarged vacuoles. To investigate the process of forming enlarged vacuoles in macrophages expressing Rab20, RAW264.7 macrophages were transfected with EGFP-Rab20WT and live cell imaging was performed to monitor this process. In macrophages expressing EGFP-Rab20WT, several fusion events between Rab20-positive vesicles were observed, suggesting that Rab20 expression induces the homotypic fusion between Rab20-positive vesicles. As shown in **Fig. 3.10**, two Rab20-positive vesicles

first moved to get close to each other. After docking, the two vesicles rapidly fused to generate a larger Rab20-positive vacuole (1'40''-2'00'' in **Fig. 3.10 B**). Afterwards, this vacuole continued to fuse with another one to become even bigger (3'40''-4'00'' in **Fig. 3.10 B**). This fusion process in macrophages expressing Rab20 resembles the "explosive" fusion in cells expressing Rab5Q79L (Roberts RL *et al*. 1999). Altogether, this data suggested that homotypic fusions between Rab20-positive vesicles induced by Rab20 expression resulted in the formation of giant vacuoles in macrophages expressing Rab20.

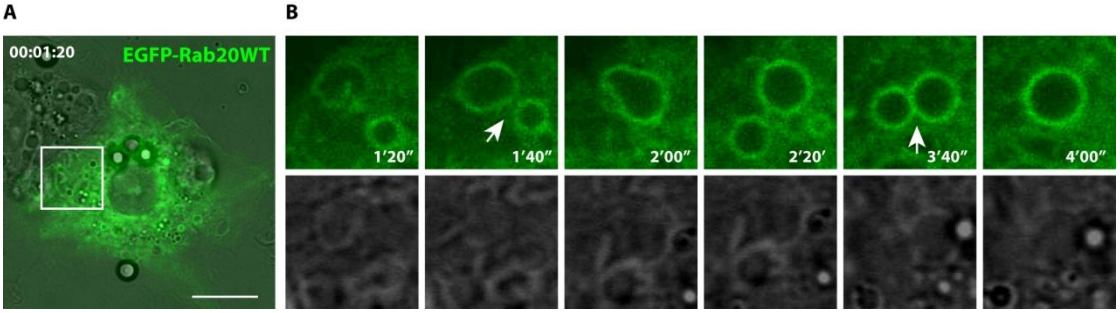

Fig. 3.10 Homotypic fusion between Rab20-positive vacuoles in RAW264.7 macrophages expressing EGFP-Rab20WT. RAW264.7 macrophages were transfected with EGFP-Rab20WT for 16 hours and subsequently live cell imaging was performed. Images were acquired every 20 seconds. **(A)** An image representing a defined time frame from a representative movie. Scale bar is 10 µm. **(B)** Time series insets (indicated with white square in A) showing the homotypic fusion between Rab20-positive vacuoles. White arrows indicate the fusion events.

Rab20 association to phagosomes

Endogenous Rab20 association to phagosomes in RAW264.7 macrophages

To investigate if endogenous Rab20 was associated to phagosomes, 3 µm IgG-coated beads were incubated with RAW264.7 macrophages for 1 hour and endogenous Rab20 detected by indirect immunofluorescence. As shown by the immunofluorescence image and plot profile, endogenous Rab20 associated to phagosomes (**Fig. 3.11 A, B**). To confirm this observation, IgG-coated latex-bead phagosomes were isolated at different time points in untreated or IFN-γ treated RAW264.7 macrophages, and Western blot was performed (**Fig. 3.11 C, D**). Rab20 associated to phagosomes during the first 30 min and dissociated from phagosomes after 1 hour of chase, which had a similar kinetics with Rab5A association. This indicates that Rab20 associated to early phagosomes. In the case of Rab7, which mainly associated to late endosomes/phagosomes, it remained longer association to phagosomes, even after 1 hour of chase **(Fig. 3.11 C)**. Compared with untreated macrophages, Rab20 association to phagosomes dramatically increased by IFN-γ treatment (**Fig. 3.11 C, D**), suggesting that not only the total amount of Rab20 increased (**Fig. 3.7 B, D**) but also the association to phagosomes. Similar with

Rab5A, Rab20 association to phagosomes was also extended to more than 1 hour by IFN-γ (**Fig. 3.11 C, D**), indicating that not only the amplitude but also the duration of Rab20 association to phagosomes increased by IFN-γ treatment.

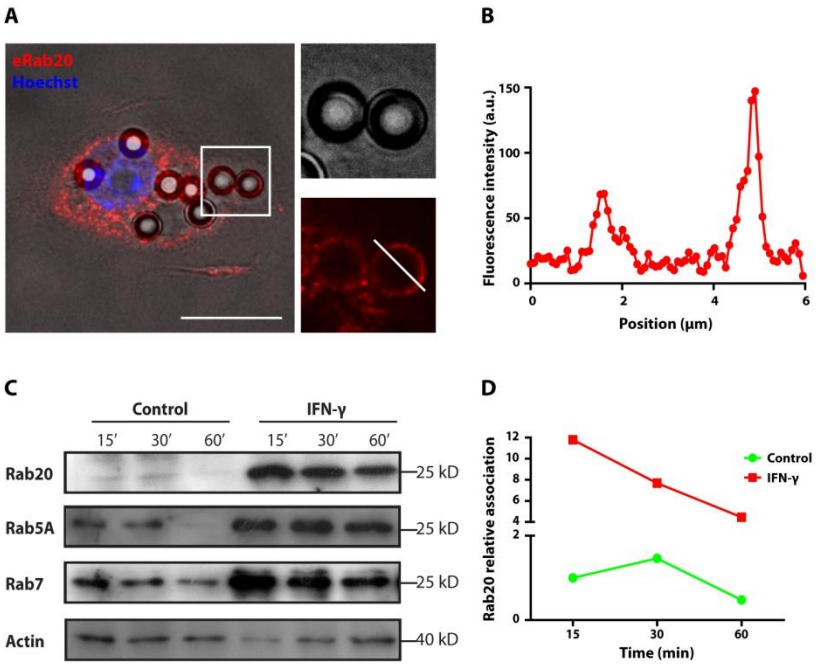

Fig. 3.11 Endogenous Rab20 association to phagosomes. (A) RAW264.7 macrophages were incubated with 3 μm IgG-coated beads for 1 hour and subsequently fixed and stained with anti-Rab20 antibody (shown in red). The nuclei were labeled by Hoechst 33258 and shown in blue. Insets on the right show bright field and Rab20 fluorescence of the phagosomes (indicated with the white square). Scale bar is 10 μm. **(B)** Plot profile of Rab20 fluorescence intensity along the phagosome (indicated with white bar in inset of A) **(C)** Western blot analysis of endogenous Rab20, Rab5A and Rab7 association to isolated phagosomes in untreated (control) or IFN-γ treated RAW264.7 macrophages. RAW264.7 macrophages were grown with or without IFN-γ (200 Units/mL) for 16 hours and phagosomes were isolated after 30 min of pulse and 15, 30 or 60 min of chase. Antibody from GeneTex was used for detecting Rab20. Actin was used as the loading control. **(D)** Quantitative analysis of endogenous Rab20 association to phagosomes in control or IFN-γ treated RAW264.7 macrophages. The intensity of bands was measured using ImageJ software. The relative Rab20 intensity of different lanes was calculated against the corresponding actin loading control. The relative Rab20 intensity at 15 min of control was set as 100% and all other relative Rab20 intensity was normalized against it.

Dynamic association of EGFP-Rab20WT to phagosomes in RAW264.7 macrophages

To better visualize the kinetics of Rab20 association to phagosomes, RAW264.7 macrophages were transiently transfected with EGFP-Rab20WT and live cell imaging experiments were performed (**Fig. 3.12 A-C**). The results showed that Rab20 was recruited to phagosomes shortly after they were internalized. The quantitative analysis showed that Rab20 association to phagosomes peaked at 5 min and dissociation started after 15 min and almost totally lost after 25 min (**Fig. 3.12 B, C**). This data suggested that both EGFP-Rab20WT and endogenous Rab20 are associated to early phagosomes. Notably, an unusual homotypic phagosome fusion between Rab20-positive phagosomes was observed, implying that Rab20 over-expression may stimulate the homotypic fusion between early phagosomes (**Fig. 3.12**

B). Additionally, the homotypic fusion between Rab20-positive vesicles and phagosomes were also observed. As shown in **Fig. 3.12 D & E**, two Rab20-positive vesicles fused to form a larger vacuole in a same manner observed in **Fig. 3.10**. Subsequently, this Rab20-positive vacuole fused with a Rab20-positive phagosome (56'00''-56'20'' in **Fig. 3.12 E**). This data indicated that homotypic fusions between Rab20 positive phagosomes and vacuoles were also stimulated by Rab20 expression.

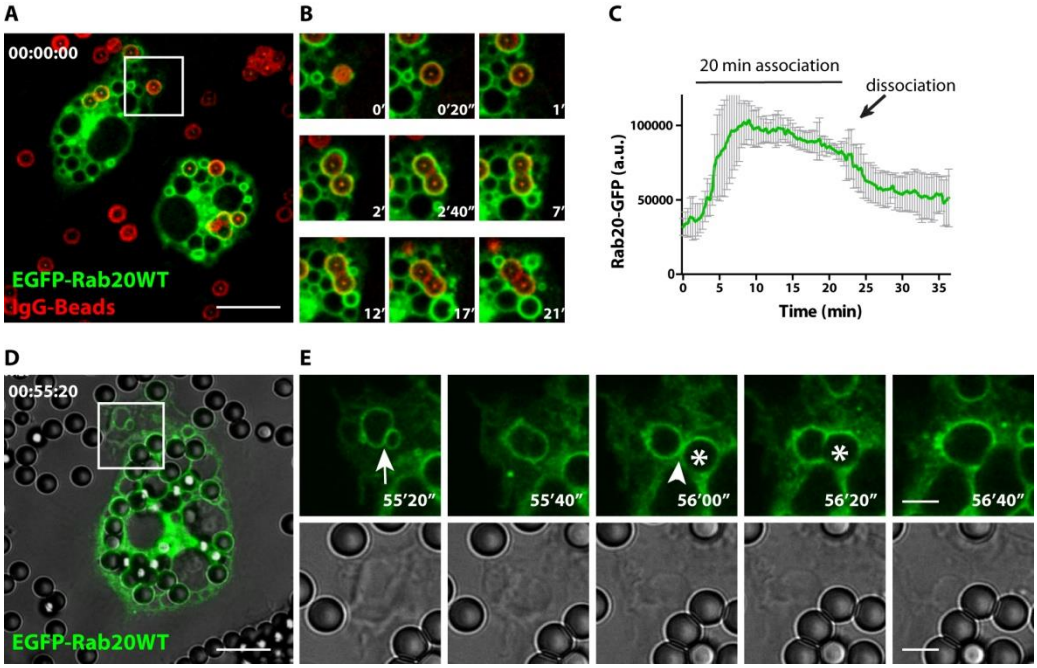

Fig. 3.12 Dynamic association of EGFP-Rab20WT to early phagosomes by live cell imaging. RAW264.7 macrophages were transfected with EGFP-Rab20WT for 16 hours and cy5-conjugated IgG-coated beads were added prior to live cell imaging. **(A)** A frame from a representative movie showing a phagosome is just formed. Scale bar is 10 µm. **(B)** Time series insets showing EGFP-Rab20WT association to the phagosome of interest (indicated with the white square in A). **(C)** Quantitative analysis of EGFP-Rab20WT association to phagosomes over 35 min post internalization. The fluorescence intensity of EGFP-Rab20WT was measured frame by frame using ImageJ software. 6 phagosomes from a representative movie are analyzed. The result shows the means ± SD of the intensity of EGFP-Rab20WT associated to phagosomes. **(D)** A defined time frame from a movie showing the fusion between Rab20-positive vacuoles and phagosomes. Scale bar is 10 µm. **(E)** Time series insets (indicated with the white square in D) showing the homotypic fusion between Rab20-positive vacuoles and phagosomes. White arrow indicates the fusion between Rab20-positive vesicles. White arrowhead indicates the fusion between a Rab20-positive vacuole and a phagosome. Asterisks represent phagosomes. Scale bar is 3 µm.

To further elucidate the interaction between actin dynamics and Rab20 association to phagosomes, RAW264.7 macrophages were co-transfected with LifeAct-RFP and EGFP-Rab20WT and live cell imaging was performed. LifeAct is a 17-amino acid peptide derived from actin binding protein 140 (Abp140) that specifically binds to F-actin (Riedl *et al*. 2008). Thus, LifeAct can be used to monitor the actin dynamics by live cell imaging. In co-transfected cells, actin assembled at the point of bead attachment without

Rab20 association during the formation of the phagocytic cup (0 min, **Fig.3.13 B**). Then, Rab20 rapidly accumulated around the phagosome after actin depolymerization and the phagocytic cup closure (1-3 min, **Fig.3.13 B**). Once fully internalized into the cells, F-actin quickly dissociated from the phagosomes, leaving Rab20 on the phagosomes (5 min, **Fig.3.13 B**). A quantitative analysis of the intensity of EGFP-Rab20WT and F-actin fluorescence associated to the phagosome confirmed that F-actin gradually dissociated from the phagosome during the first 5 min, concomitantly with an increase in Rab20 association (**Fig.3.13 C**). Taken together, this data demonstrated that Rab20 is associated to early phagosomes.

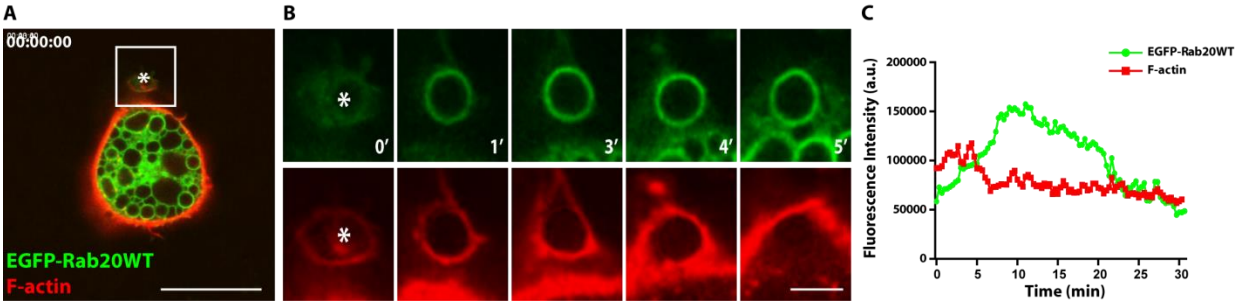

Fig. 3.13 Rab20 association to phagosomes and actin dynamics. RAW264.7 macrophages were co-transfected with LifeAct-RFP and EGFP-Rab20WT for 16 hours and IgG coated beads were added and live cell imaging was performed. **(A)** A frame from a representative movie showing a phagosome is just formed in a macrophage expressing LifeACT-RFP and EGFP-Rab20WT. The white square indicates the region containing the phagosome of interest. Scale bar is 10 µm. **(B)** Time series insets showing EGFP-Rab20WT (Green) and F-actin (Red) association to the phagosome (indicated with asterisks). Scale bar is 3 µm. **(C)** Quantitative analysis of EGFP-Rab20WT (Green) and F-actin (Red) association to the phagosome (shown in B) over 30 min post internalization. The fluorescence intensity of EGFP-Rab20WT and F-actin was measured frame by frame using ImageJ software.

The role of Rab20 during phagosome maturation

Since Rab20 was associated to early phagosomes, it was reasonable to hypothesize that Rab20 had some role during the maturation of phagosomes. To better understand the role of Rab20 on phagosome maturation, several approaches were performed to investigate different aspects of this process. First, LysoTracker was employed to label the acidic compartments in macrophages expressing EGFP, EGFP-Rab20WT or EGFP-Rab20T19N and LysoTracker acquisition by phagosomes was measured. Second, the association of phosphatidylinositol 3-phosphate (PI3P), a marker of phagosome maturation, to phagosomes was monitored in macrophages expressing mCherry, mCherry-Rab20WT or mCherry-Rab20T19N. Third, Texas Red-conjugated Dextran 70kDa was used to label the late endocytic compartments. The delivery of Texas Red-conjugated Dextran 70kDa to phagosomes was quantified in macrophages expressing EGFP, EGFP-Rab20WT or EGFP-Rab20T19N.

Rab20 association to phagosomes delays LysoTracker acquisition by phagosomes

Phagosome acidification is one of the hallmarks of phagosome maturation. LysoTracker Red/Green is an acidotropic dye that accumulates in acidic compartments upon protonation (Diwu Z *et al*. 1994). Hence, it is usually used as a tool to monitor phagosome maturation (Chow CW *et al*. 2004). RAW264.7 macrophages were transfected with EGFP, EGFP-Rab20WT or EGFP-Rab20T19N and preloaded with LysoTracker Red. Macrophages were incubated with IgG-coated beads and live cell imaging was performed to monitor the kinetics of LysoTracker acquisition by phagosomes. The time point when the beads were just internalized was denoted as 0 min hereafter.

In EGFP expressing macrophages, phagosomes started acquiring LysoTracker Red after 10 min and reached a plateau at 25 min (**Fig. 3.14**). This is comparable to the phagosomal acidification profile reported in previous studies (Yates RM *et al*. 2005, Yates RM *et al*. 2007). In contrast, phagosomes in macrophages expressing EGFP-Rab20WT, phagosomes did not acquire LysoTracker during the first 25 min (**Fig. 3.15**), correlating this delay with the presence of Rab20WT on phagosomes (**Fig. 3.12 A-C**). At longer time points, phagosomes slowly reached similar levels with control at 60 min (**Fig. 3.15**). Conversely, phagosomes in macrophages expressing EGFP-Rab20T19N acquired LysoTracker faster than in EGFP expressing macrophages. This acceleration started after 5 min and reached to a plateau after 10 min of internalization (**Fig. 3.16**). A statistical analysis of LysoTracker association to phagosomes showed that the intensity of LysoTracker associated to phagosomes in EGFP-Rab20T19N expressing macrophages was significantly higher than in cells expressing EGFP or EGFP-Rab20WT at 5 min and 15 min post internalization. In contrast, the intensity of LysoTracker associated to phagosomes in EGFP-Rab20WT expressing cells was significantly lower than EGFP and EGFP-Rab20T19N at 5 min and 15 min (**Fig. 3.17**). However, at 60 min there was no significant difference in the intensity of LysoTracker associated to phagosomes in EGFP, EGFP-Rab20WT and EGFP-Rab20T19N macrophages. Taken together, the data suggested that the starting point of LysoTracker acquisition by phagosomes was delayed by Rab20 association to the phagosomes and the desired time for reaching the plateau was also prolonged. This indicated that Rab20 may not only function in the early stage but also affect phagosome maturation at a later step.

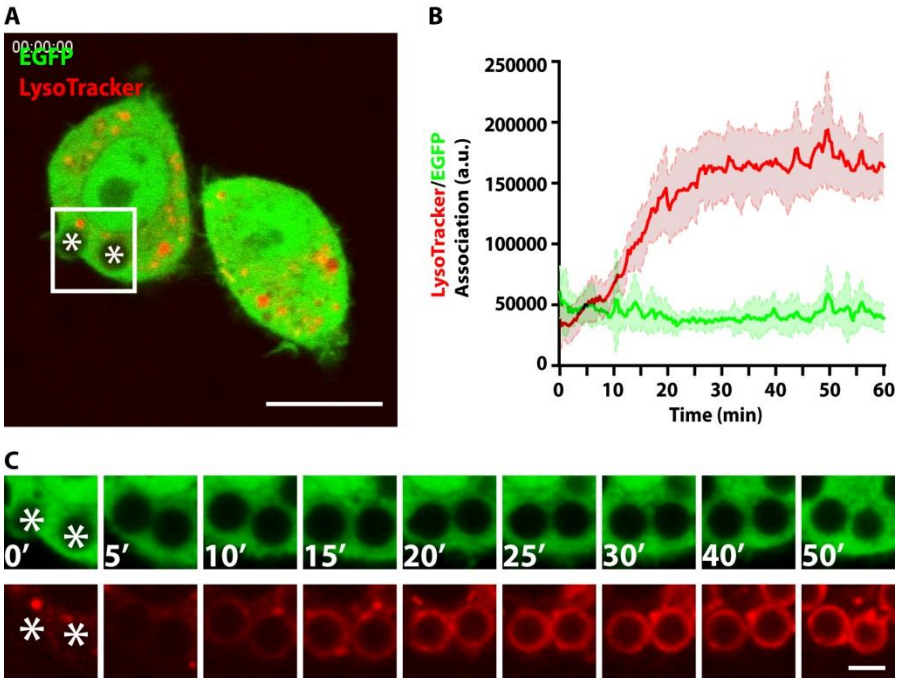

Fig. 3.14 Acquisiton of LysoTracker by phagosomes in EGFP expressing cells. RAW264.7 macrophages were transfected with EGFP for 16 hours and LysoTracker Red (50 nM) was added 30 min prior to live cell imaging. **(A)** A frame from a representative movie showing phagosomes are just formed in EGFP expressing macrophages. Asterisks indicate phagosomes of interest. Scale bar is 10 µm. **(B)** Quantitative analysis of EGFP (Green) and LysoTracker (Red) association to phagosomes over 60 min post internalization. The intensity of LysoTracker Red and EGFP was measured frame by frame using ImageJ software. 10 phagosomes from 6 cells in three independent experiments were quantified. The results show means ± SD of the intensity of EGFP and LysoTracker associated to phagosomes. **(C)** Time series insets (indicated with white square in A) showing phagosomes acquiring LysoTracker (Red) in EGFP (Green) expressing cells. Scale bar is 3 µm.

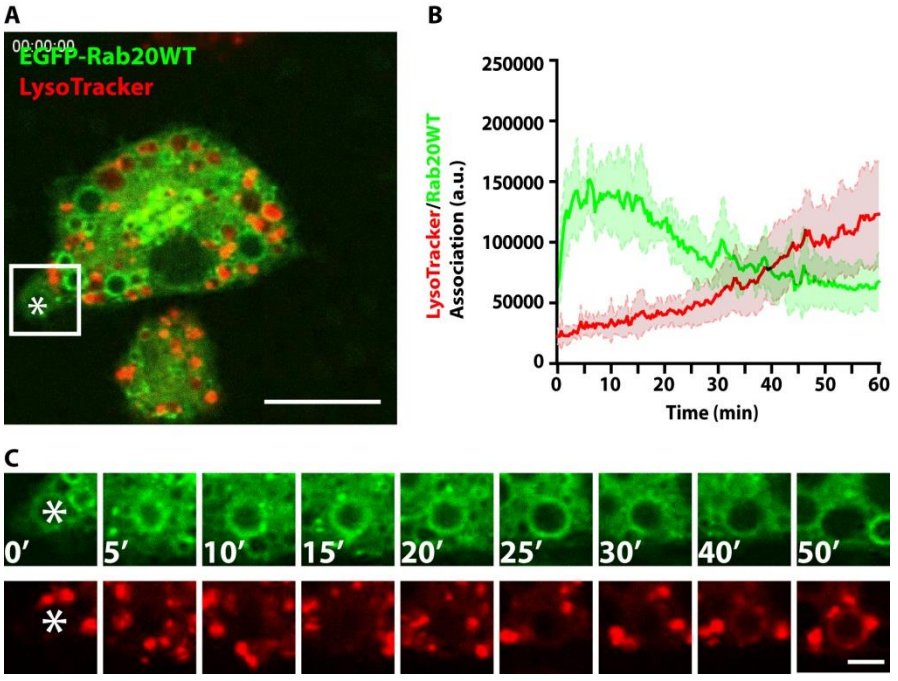

Fig. 3.15 Acquisiton of LysoTracker by phagosomes in macrophages expressing EGFP-Rab20 wild-type. RAW264.7 macrophages were transfected with EGFP-Rab20WT for 16 hours and LysoTracker Red (50 nM) was added 30 min prior to live cell imaging. **(A)** A frame from a representative movie showing a phagosome is just formed in EGFP-Rab20WT expressing macrophages. The asterisk indicates the phagosome of interest. Scale bar is 10 µm. **(B)** Quantitative analysis of EGFP-Rab20WT (Green) and LysoTracker (Red) fluorescence associated to phagosomes over 60 min post internalization. The intensity of LysoTracker Red and EGFP-Rab20WT was measured frame by frame using ImageJ software. 10 phagosomes from 4 cells in three independent experiments were quantified. The results show means ± SD of the intensity of EGFP-Rab20WT and LysoTracker associated to phagosomes. **(C)** Time series insets (indicated with white square in A) showing phagosomes acquiring LysoTracker (Red) and EGFP-Rab20WT (Green). Scale bar is 3 µm.

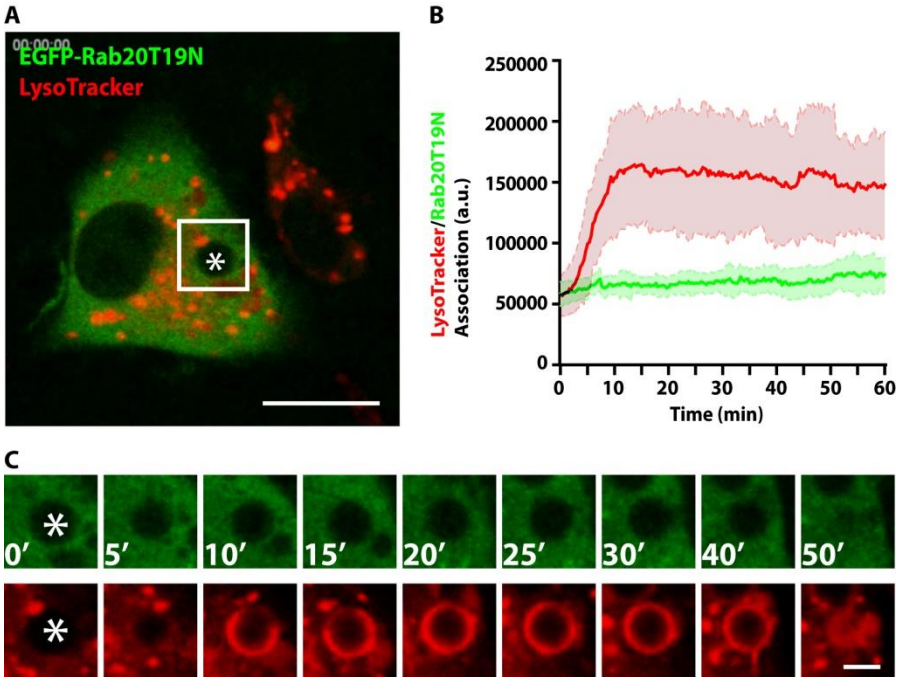

Fig. 3.16 Acquisiton of LysoTracker by phagosomes in macrophages expressing EGFP-Rab20T19N. RAW264.7 macrophages were transfected with EGFP-Rab20T19N for 16 hours and LysoTracker Red (50 nM) was added 30 min prior to live cell imaging. **(A)** A frame from a representative movie showing a phagosome is just formed in EGFP-Rab20T19N expressing macrophages. The asterisk indicates the phagosome of interest. Scale bar is 10 µm. **(B)** Quantitative analysis of EGFP-Rab20T19N (Green) and LysoTracker (Red) fluorescence associated to phagosomes over 60 min post internalization. The intensity of LysoTracker Red and EGFP-Rab20T19N was measured frame by frame using ImageJ software. 13 phagosomes from 4 cells in three independent experiments were quantified. The results show means ± SD of the intensity of EGFP-Rab20T19N and LysoTracker associated to phagosomes. **(C)** Time series insets (indicated with white square in A) showing phagosomes acquiring LysoTracker (Red) in EGFP-Rab20T19N (Green) expressing cells. Scale bar is 3 µm.

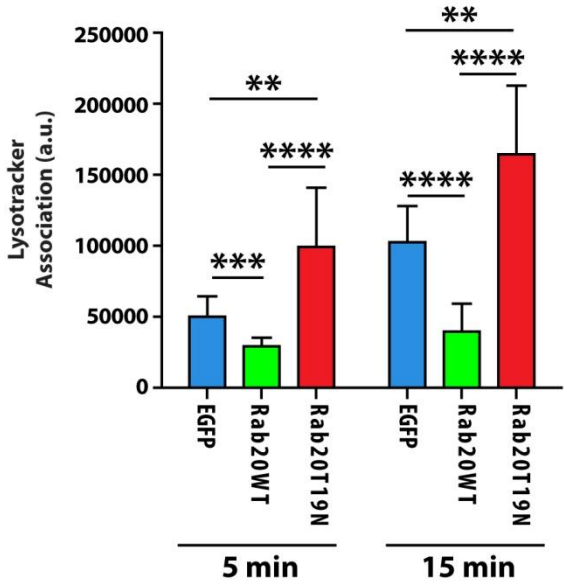

Fig. 3.17 Statistical analysis of the intensity of LysoTracker Red associated to phagosomes in EGFP, EGFP-Rab20WT or EGFP-Rab20T19N expressing macrophages at 5 min and 15 min post internalization. The LysoTracker Red intensity was measured frame by frame using ImageJ software. The results show means ± SD of the intensity of LysoTracker Red acquired by phagosomes in EGFP, EGFP-Rab20WT or EGFP-Rab20T19N expressing macrophages. 10 phagosomes for EGFP, 10 phagosomes for Rab20WT and 13 phagosomes for Rab20T19N in three independent experiments were quantified. P values were calculated using two-tailed unpaired t-test. (**) $p \leq 0.01$, (***) $p \leq 0.001$, (****) $p \leq 0.0001$.

Phosphatidylinositol 3-phosphate (PI3P) association to phagosomes is prolonged by Rab20 expression

PI3P is selectively present in early endosomes/phagosomes and is essential for phagosome maturation (RA Fratti *et al*. 2001; OV Vieira *et al*. 2001). Several Rab5 effectors, e.g. Rabenosyn-5 and EEA1, which function in early endosome progression, bind to PI3P via the PI3P binding domain-FYVE domain. FYVE domain is named after four cysteine-rich proteins: Fab1, YOTB, Vac 1 and EEA1. The affinity of FYVE domain for PI3P is increased upon dimerization. To monitor the kinetics of PI3P in the process of phagosomes maturation, a construct harboring EGFP-2XFYVE domains was co-transfected with mCherry, mCherry-Rab20WT or mCherry-Rab20T19N.

In mCherry expressing macrophages, PI3P quickly associated to phagosomes and retained on phagosomes for about 10 min as shown before (Vieira OV *et al*. 2001) (**Fig. 3.18**). In mCherry-Rab20WT expressing macrophages, PI3P associated to phagosomes in a similar kinetics with mCherry-Rab20WT. The association of PI3P to phagosomes was prolonged for about 25 min, correlating with mCherry-Rab20WT association to phagosomes (**Fig. 3.19**). Conversely, the duration of PI3P association to phagosomes in mCherry-Rab20T19N expressing macrophages was significantly diminished after 5 min (**Fig. 3.20**). A statistical analysis showed that the intensity of EGFP-2XFYVE associated to phagosomes in macrophages expressing mCherry-Rab20T19N is significantly lower than in cells expressing mCherry and Rab20WT macrophages at 7 min, suggesting that PI3P association to phagosomes was shorten by Rab20T19N expression. The intensity of EGFP-2XFYVE associated to phagosomes in macrophages expressing mCherry-Rab20WT was significantly higher than in cells expressing mCherry and Rab20T19N after 15 min of internalization (**Fig. 3.21**). Taken together, PI3P association to phagosomes was extended by Rab20 association, suggesting that the progression of early to late phagosome was transiently delayed by Rab20WT association. The kinetics of PI3P association to phagosomes in macrophages expressing mCherry, mCherry-Rab20WT or mCherry-Rab20T19N is in agreement with the kinetics of LysoTracker acquisition (EGFP, 10 min; Rab20WT, 30 min; Rab20T19N, 5 min), indicating that the phagosomes started acquiring LysoTracker after PI3P disassociation.

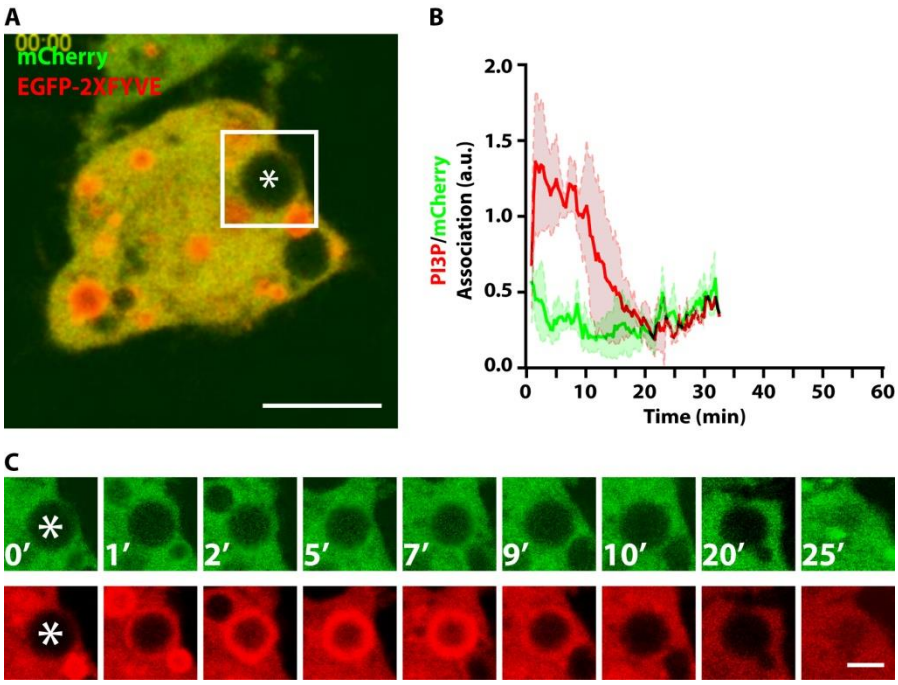

Fig. 3.18 PI3P association to phagosomes in mCherry expressing macrophages. RAW264.7 macrophages were co-transfected with EGFP-2XFYVE and mCherry for 16 hours and mouse IgG coated beads were added prior to live cell imaging. **(A)** A frame from a representative movie showing a phagosome is just formed in mCherry (Green) and EGFP-2XFYVE (Red) expressing macrophages. The asterisk indicates the phagosome of interest. Scale bar is 10 µm. **(B)** Quantitative analysis of mCherry (Green) and EGFP-2XFYVE (Red) association to phagosomes over 60 min post internalization. The intensity of EGFP-2XFYVE and mCherry was measured frame by frame using ImageJ software. Then both mCherry and EGFP-2XFYVE fluorescence were normalized to the perinuclear region with the same size. 5 phagosomes from 3 cells in three independent experiments were quantified. The results show means ± SD of the normalized intensity of mCherry and EGFP-2XFYVE fluorescence associated to phagosomes. **(C)** Time series insets (indicated with white square in A) showing phagosomes acquiring EGFP-2XFYVE (Red) in mCherry (Green) expressing cells. Scale bar is 3 µm.

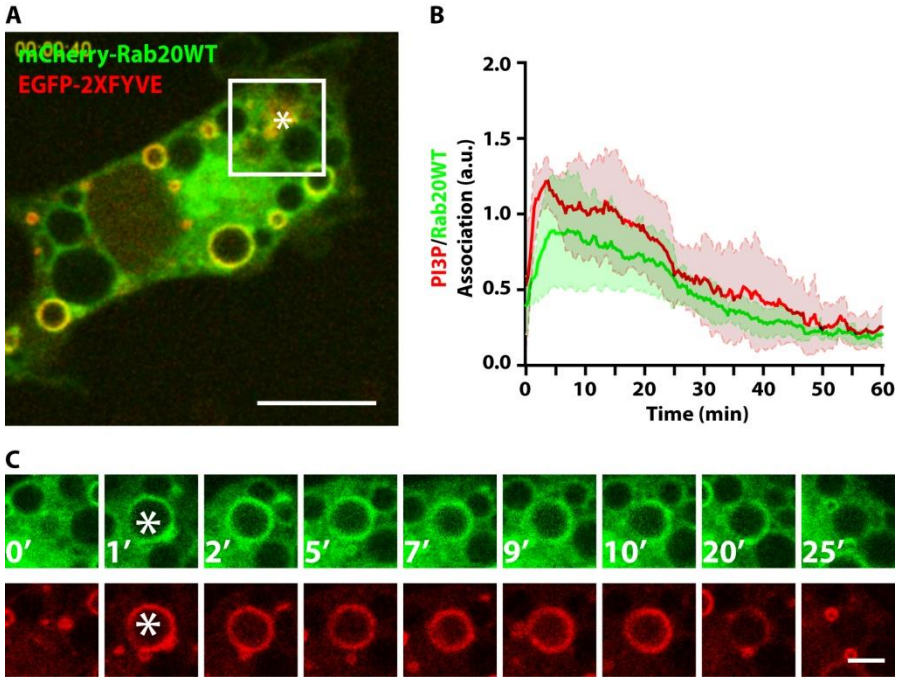

Fig. 3.19 PI3P association to phagosomes in mCherry-Rab20WT expressing macrophages. RAW264.7 macrophages were co-transfected with EGFP-2XFYVE and mCherry-Rab20WT for 16 hours and IgG coated beads were added prior to live cell imaging. **(A)** A frame from a representative movie showing a phagosome is just formed in mCherry-Rab20WT (Green) and EGFP-2XFYVE (Red) expressing macrophages. The asterisk indicates the phagosome of interest. Scale bar is 10 µm. **(B)** Quantitative analysis of mCherry-Rab20WT (Green) and EGFP-2XFYVE (Red) association to phagosomes over 60 min post internalization. The intensity of EGFP-2XFYVE and mCherry-

Rab20WT was measured frame by frame using ImageJ software. Then both mCherry-Rab20WT and EGFP-2XFYVE fluorescence were normalized to the perinuclear region with the same size. 8 phagosomes from 3 cells in three independent experiments were quantified. The results show means ± SD of the normalized intensity of mCherry-Rab20WT and EGFP-2XFYVE associated to phagosomes. **(C)** Time series insets (indicated with white square in A) showing phagosomes acquiring EGFP-2XFYVE (Red) and mCherry-Rab20WT (Green). Scale bar is 3 µm.

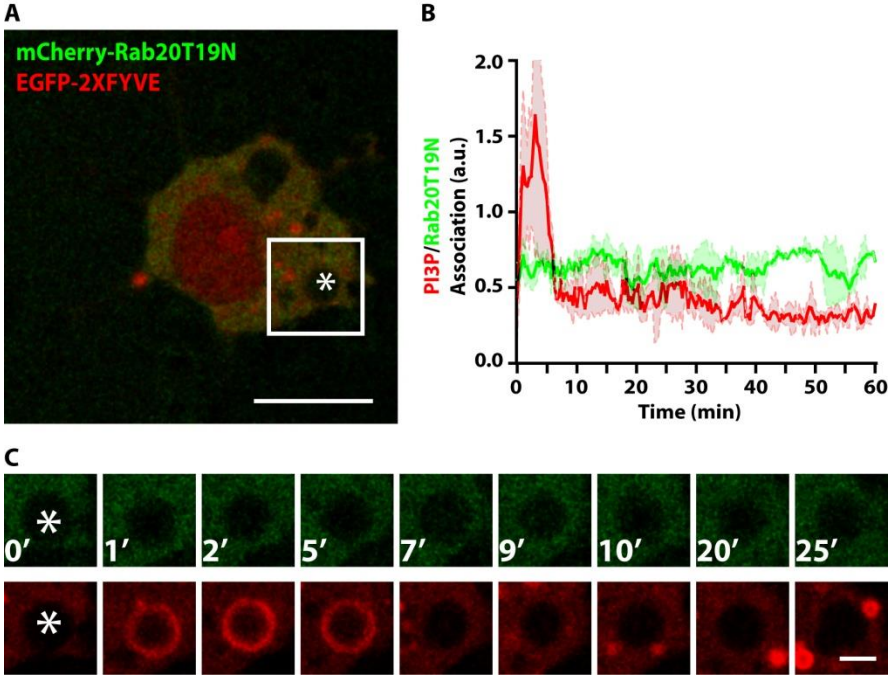

Fig. 3.20 PI3P association to phagosomes in mCherry-Rab20T19N expressing macrophages. RAW264.7 macrophages were co-transfected with EGFP-2XFYVE and mCherry-Rab20T19N for 16 hours and IgG coated beads were added prior to live cell imaging. **(A)** A frame from a representative movie showing a phagosome is just formed in mCherry-Rab20T19N (Green) and EGFP-2XFYVE (Red) expressing macrophages. The asterisk indicates the phagosome of interest. Scale bar is 10 µm. **(B)** Quantitative analysis of mCherry-Rab20T19N (Green) and EGFP-2XFYVE (Red) association to phagosomes over 60 min post internalization. The intensity of EGFP-2XFYVE and mCherry-Rab20T19N was measured frame by frame using ImageJ software. Then both mCherry-Rab20T19N and EGFP-2XFYVE fluorescence were normalized to the perinuclear region with the same size. 3 phagosomes from 3 cells in three independent experiments were quantified. The results show means ± SD of the normalized intensity of mCherry-Rab20T19N and EGFP-2XFYVE associated to phagosomes. **(C)** Time series insets (indicated with white square in A) showing phagosomes acquiring EGFP-2XFYVE (Red) in mCherry-Rab20T19N (Green) expressing cells. Scale bar is 3 µm.

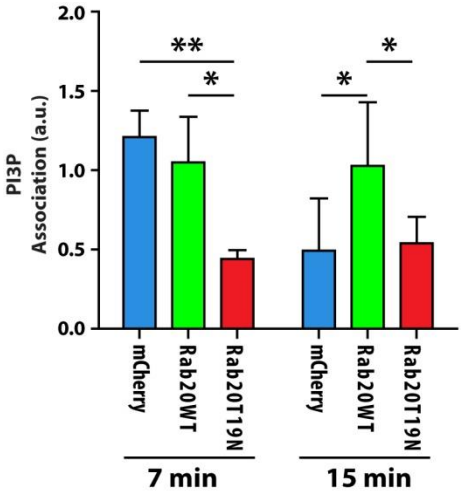

Fig. 3.21 Statistical analysis of the intensity of PI3P association to phagosomes in mCherry, mCherry-Rab20WT or mCherry-Rab20T19N expressing macrophages at 7 min and 15 min post internalization. The intensity of EGFP-2XFYVE associated to phagosomes in macrophages expressing mCherry, mCherry-Rab20WT or mCherry-Rab20T19N was measured frame by frame using ImageJ software and subsequently normalized to the perinuclear region with the same size. The results show means ± SD of the normalized intensity of EGFP-2XFYVE associated to phagosomes. 5 phagosomes for mCherry, 8 phagosomes for Rab20WT and 3 phagosomes for Rab20T19N in three independent experiments were quantified. P values were calculated using student' two-tailed unpaired t-test. (*) $p \leq 0.05$, (**) $p \leq 0.01$.

Rab5 association was prolonged by Rab20 expression

PI3P is produced by a phospatidylinositol 3-kinase (PI3K) hVPS34 which is an effector of Rab5. Since PI3P association to phagosomes is prolonged by Rab20 expression, it is reasonable to hypothesize that Rab5 association to phagosomes is also increased in this condition. To test this hypothesis, EGFP-Rab5A wild-type was co-transfected with mCherry, mCherry-Rab20WT or mCherry-Rab20T19N. Live cell imaging experiments were performed to investigate the impact of Rab20 expression on Rab5 association to phagosomes.

In mCherry expressing macrophages, Rab5A was immediately recruited to phagosomes when the phagocytic cups were just formed and retained on phagosomes for about 10 min as reported before (Roberts EA *et al*. 2006) (**Fig. 3.22**). In Rab20WT expressing macrophages, Rab5A was recruited to phagosomes earlier than Rab20, suggesting that Rab5A acts in the upstream of Rab20 during phagosome maturation. The association of EGFP-Rab5A to phagosomes was extended to 25 min, correlating with the presence of Rab20WT on phagosomes (**Fig. 3.23**). In contrast, the duration of Rab5A association to phagosomes in Rab20T19N expressing macrophages was reduced to 2 min compared to control macrophages expressing EGFP alone (**Fig. 3.24**). A statistical analysis of the normalized intensity of EGFP-Rab5A association to phagosomes indicated that the normalized intensity of Rab5A in macrophages expressing Rab20WT was significantly higher than in cells expressing Rab20T19N at 5 min and 15 min or mCherry at 15 min (**Fig. 3.25**). Altogether, these data suggested that Rab5A association to phagosomes was extended by Rab20WT association.

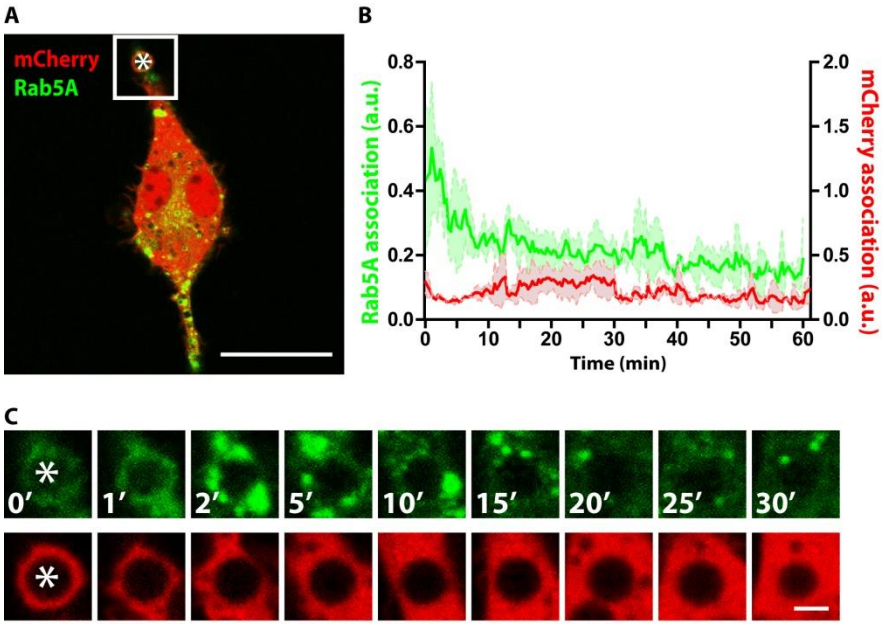

Fig. 3.22 Rab5A association to phagosomes in mCherry expressing macrophages. RAW264.7 macrophages were co-transfected with EGFP-Rab5A and mCherry for 16 hours and IgG-coated beads were added prior to live cell imaging. **(A)** A frame from a representative movie showing a phagosome (indicated with the asterisk) is just formed in mCherry (Red) and EGFP-Rab5A (Green) expressing macrophages. Scale bar is 10 µm. **(B)** Quantitative analysis of mCherry (Red) and EGFP-Rab5A (Green) association to

phagosomes over 60 min post internalization. The intensity of EGFP-Rab5A and mCherry was measured frame by frame using ImageJ software. Then both mCherry and EGFP-Rab5WT fluorescence were normalized to the perinuclear region with the same size. 7 phagosomes from 3 cells in three independent experiments were quantified. The results show means ± SD of the normalized intensity of mCherry and EGFP-Rab5A associated to phagosomes. **(C)** Time series insets (indicated with white square in A) showing phagosomes acquiring EGFP-Rab5A (Green) in mCherry (Red) expressing cells. Scale bar is 3 µm.

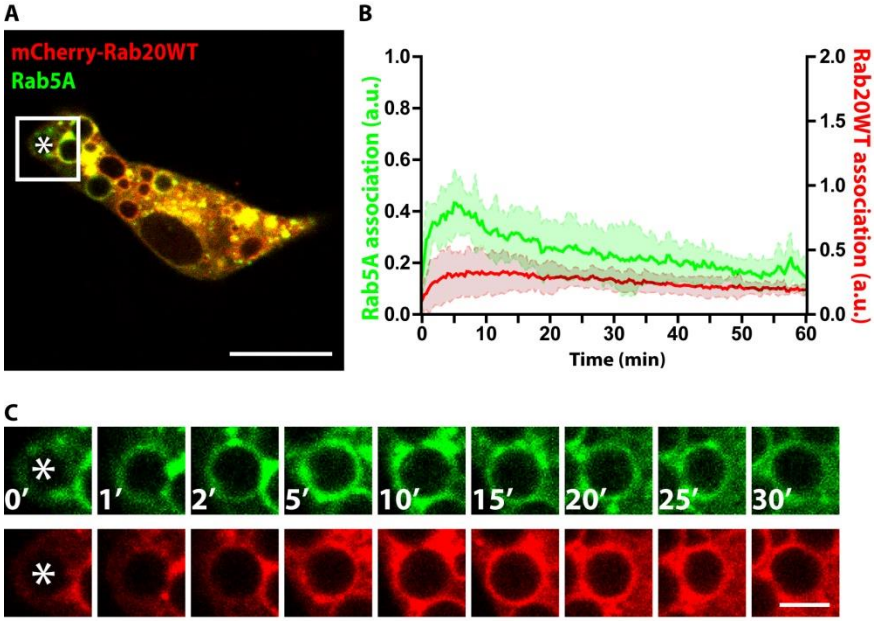

Fig. 3.23 Rab5A association to phagosomes in mCherry-Rab20WT expressing macrophages. RAW264.7 macrophages were co-transfected with EGFP-Rab5A and mCherry-Rab20WT for 16 hours and IgG-coated beads were added prior to live cell imaging. **(A)** A frame from a representative movie showing a phagosome (indicated with the asterisk) is just formed in mCherry-Rab20WT (Red) and EGFP-Rab5A (Green) expressing macrophages. Scale bar is 10 µm. **(B)** Quantitative analysis of mCherry-Rab20WT (Red) and EGFP-Rab5WT (Green) association to phagosomes over 60 min post internalization. The intensity of EGFP-Rab5A and mCherry-Rab20WT was measured frame by frame using ImageJ software. Then both mCherry-Rab20WT and EGFP-Rab5A fluorescence were normalized to the perinuclear region with the same size. 12 phagosomes from 4 cells in three independent experiments were quantified. The results show means ± SD of the normalized intensity of mCherry-Rab20WT and EGFP-Rab5A associated to phagosomes. **(C)** Time series insets (indicated with white square in A) showing phagosomes acquiring EGFP-Rab5A (Green) and mCherry-Rab20WT (Red). Scale bar is 3 µm.

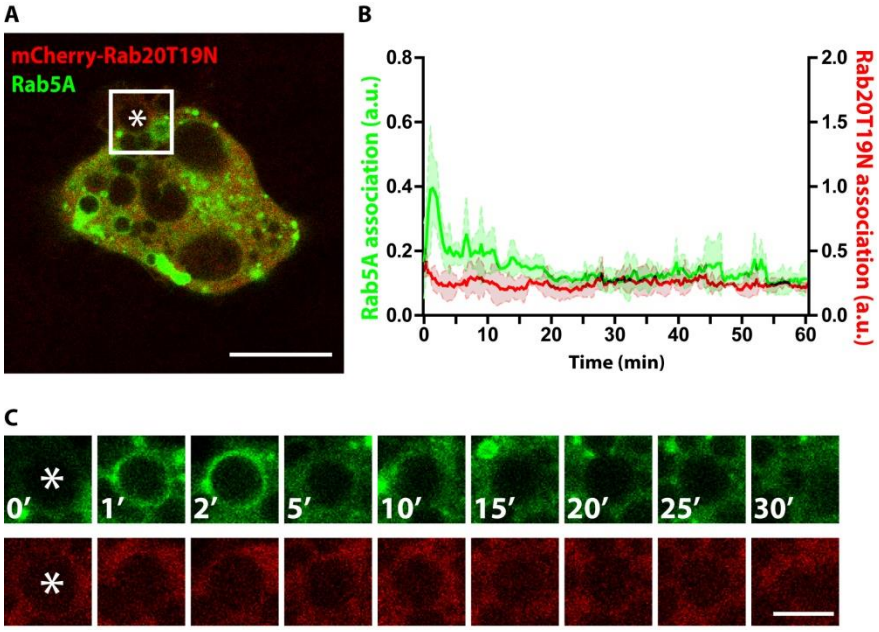

Fig. 3.24 Rab5A association to phagosomes in mCherry-Rab20T19N expressing macrophages. RAW264.7 macrophages were co-transfected with EGFP-Rab5A and mCherry-Rab20T19N for 16 hours and IgG-coated beads were added prior to live cell imaging. **(A)** A frame from a representative movie showing a phagosome (indicated with the asterisk) is just formed in mCherry-Rab20T19N (Red) and EGFP-Rab5WT (Green) expressing macrophages. Scale bar is 10 µm. **(B)** Quantitative analysis of mCherry-Rab20T19N (Red) and EGFP-Rab5WT (Green) association to phagosomes

over 60 min post internalization. The intensity of EGFP-Rab5A and mCherry-Rab20T19N was measured frame by frame using ImageJ software. Then both mCherry-Rab20T19N and EGFP-Rab5A fluorescence were normalized to the perinuclear region with the same size. 5 phagosomes from 2 cells in two independent experiments were quantified. The results show means ± SD of the normalized intensity of mCherry-Rab20T19N and EGFP-Rab5A associated to phagosomes. **(C)** Time series insets (indicated with white square in A) showing phagosomes acquiring EGFP-Rab5A (Green) in mCherry-Rab20T19N (Red) expressing cells. Scale bar is 3 µm.

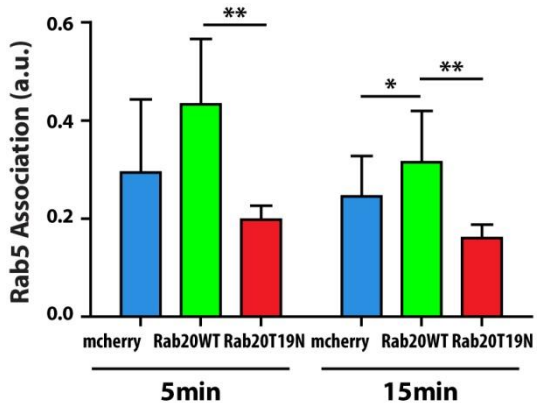

Fig. 3.25 Statistical analysis of the intensity of Rab5A association to phagosomes in mCherry, mCherry-Rab20WT or mCherry-Rab20T19N expressing macrophages at 5 min and 15 min post internalization. The intensity of EGFP-Rab5A associated to phagosomes in macrophages expressing mCherry, mCherry-Rab20WT or mCherry-Rab20T19N was measured frame by frame using ImageJ software and subsequently normalized to the perinuclear region with the same size. The results show means ± SD of the normalized intensity of EGFP-Rab5A associated to the phagosomes. For mCherry and mCherry-Rab20WT, 7 phagosomes from 3 cells and 12 phagosomes from 4 cells in three independent experiments were quantified, respectively. For mCherry-Rab20T19N, 5 phagosomes from 2 cells in two independent experiments were quantified. P values were calculated using student' two-tailed unpaired t-test. (*) $p \leq 0.05$, (**) $p \leq 0.01$.

Phagolysosome fusion was delayed by Rab20 expression

Phagolysosome fusion is the final step for phagosome maturation. During this process, many different proteases and hydrolytic enzymes are delivered to phagosomes with pH dropping dramatically (Vieira OV *et al*. 2002, Fairn GD and Grinstein S. 2012). LAMPs which are good candidate markers for lysosomes are also present on late endosomes (Höning S *et al*. 1996). A good method to label lysosomes is to incubate the cells with fluidic Dextran 70kDa for a short period of time followed by a long time of chasing (Vieira OV *et al*. 2002). To apply this approach in the context of Rab20 function in phagosome maturation, Texas Red-conjugated Dextran 70kDa (50 µg/mL) was incubated in EGFP, EGFP-Rab20WT or EGFP-Rab20T19N expressing macrophages for 2 hours, followed by 16 hours of chasing. Then the vesicles containing fluorescent Dextran 70kDa were considered as late endocytic compartments. Live cell imaging experiments were performed to probe phagosomes acquiring Texas Red-conjugated Dextran 70kDa.

In EGFP expressing macrophages, phagolysosome fusion began after 10 min and reached to a plateau after 30 min (**Fig. 3.26**). This is in agreement with the kinetics of phagolysosome fusion observed using a förster resonance energy transfer (FRET) method (Yates RM *et al*. 2005). Phagolysosome fusion was

dramatically reduced in EGFP-Rab20WT expressing macrophages even after 1 hour (**Fig. 3.27**). However, phagolysosome fusion in Rab20WT expressing macrophages was not totally inhibited. Phagosomes were fully fused with lysosomes after 170 min (**Fig. 3.27 C**). In macrophages expressing EGFP-Rab20T19N, the delivery of dextran 70kDa into phagosomes started at 5 min and reached to a plateau at approximately 20 min (**Fig. 3.28**). A statistical analysis of the intensity of Dextran 70kDa associated to phagosomes indicated that the intensity of Dextran 70kDa associated to phagosomes in EGFP-Rab20WT expressing macrophages was significantly lower than in cells expressing EGFP or EGFP-Rab20T19N at 5 min and 15 min (**Fig. 3.29**). These results are consistent with a role of Rab20 in delaying phagolysosome fusion.

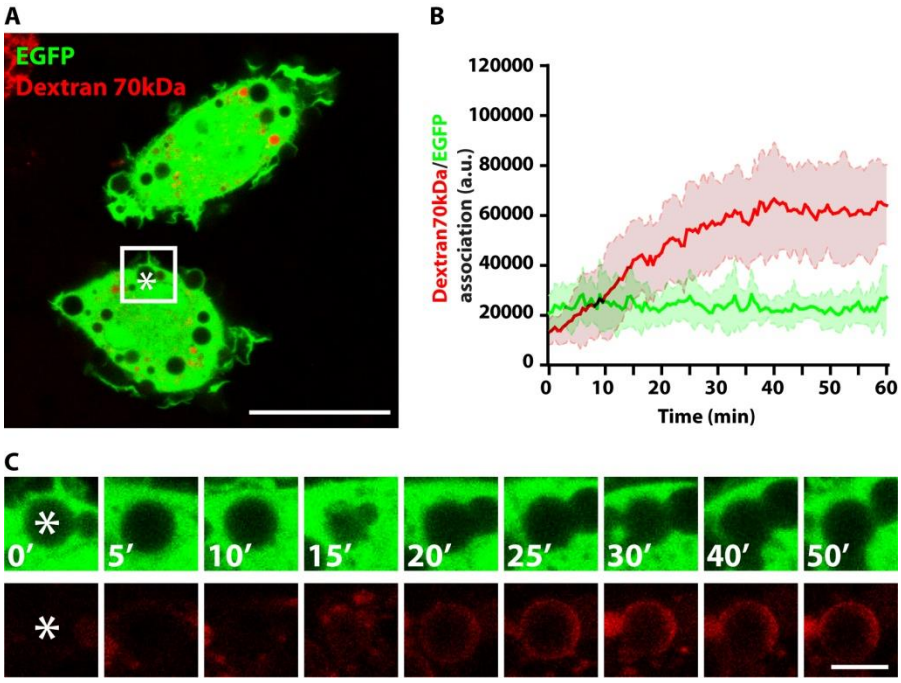

Fig. 3.26 Phagolysosome fusion in EGFP expressing macrophages. RAW264.7 macrophages were transfected with EGFP for 6 hours and Dextran 70kDa (50 µg/mL) was added for 2 hours of pulsing followed by 16 hours of chasing. Subsequently, IgG-coated beads were added and live cell imaging was performed. **(A)** A frame from a representative movie showing a phagosome (indicated with the asterisk) is just formed in EGFP expressing macrophages. Scale bar is 10 µm. **(B)** Quantitative analysis of EGFP (Green) and Dextran 70kDa (Red) association to phagosomes over 60 min post internalization. The intensity of EGFP and Dextran70kDa was measured frame by frame using ImageJ software. The results show means ± SD of the intensity of EGFP and Dextran 70kDa associated to phagosomes. 9 phagosomes from 4 cells in three independent experiments were quantified. **(C)** Time series insets (indicated with white square in A) showing phagosomes acquiring Dextran 70kDa (Red) in EGFP (Green) expressing cells. Scale bar is 3 µm.

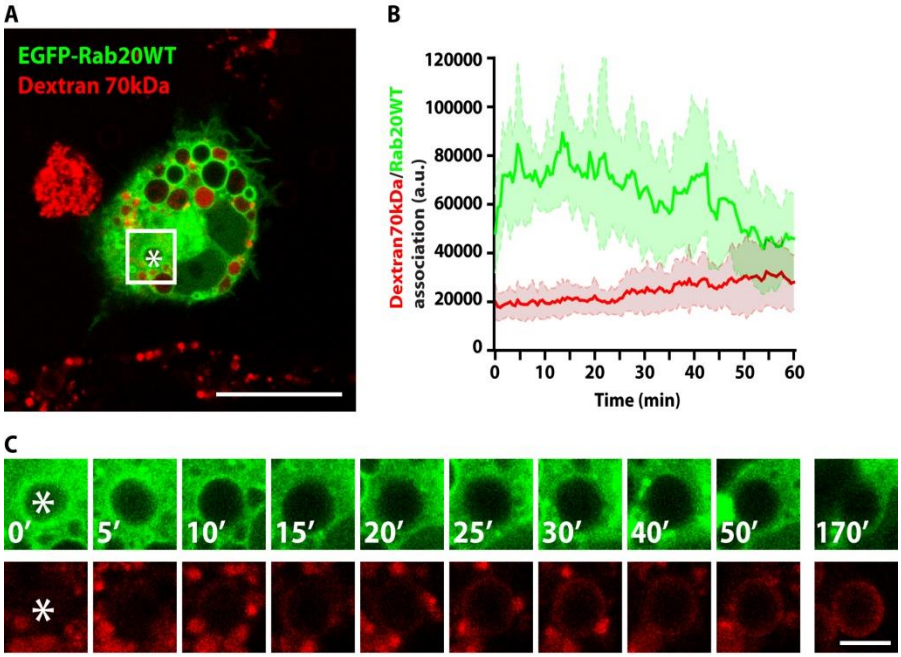

Fig. 3.27 Phagolysosome fusion in EGFP-Rab20WT expressing macrophages. RAW264.7 macrophages were transfected with EGFP-Rab20WT for 6 hours and Dextran 70kDa (50 µg/mL) was added for 2 hours of pulsing followed by 16 hours of chasing. Subsequently, IgG-coated beads were added and live cell imaging was performed. **(A)** A frame from a representative movie showing a phagosome (indicated with the asterisk) is just formed in EGFP-Rab20WT expressing macrophages. Scale bar is 10 µm. **(B)** Quantitative analysis of EGFP-Rab20WT (Green) and Dextran 70kDa (Red) association to phagosomes over 60 min post internalization. The intensity of EGFP-Rab20WT and Dextran70kDa was measured frame by frame using ImageJ software. The results show means ± SD of the intensity of EGFP-Rab20WT and Dextran 70kDa associated to phagosomes. 14 phagosomes from 3 cells in three independent experiments were quantified. **(C)** Time series insets (indicated with white square in A) showing phagosomes acquiring Dextran 70kDa (Red) in EGFP-Rab20WT (Green) expressing cells. Scale bar is 3 µm.

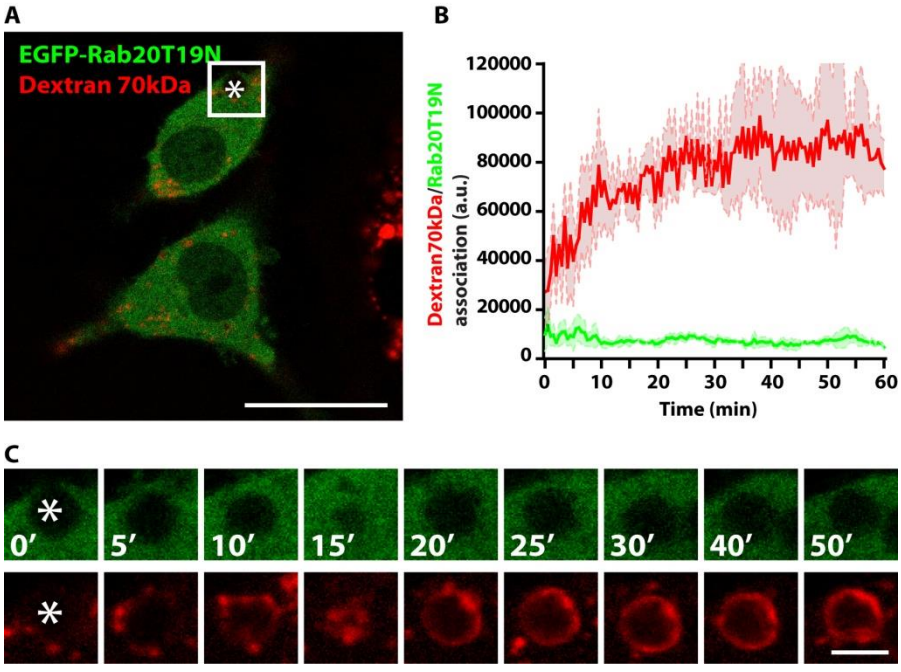

Fig. 3.28 Phagolysosome fusion in EGFP-Rab20T19N expressing macrophages. RAW264.7 macrophages were transfected with EGFP-Rab20T19N for 6 hours and Dextran 70kDa (50 µg/mL) was added for 2 hours of pulsing followed by 16 hours of chasing. Subsequently, IgG-coated beads were added and live cell imaging was performed. **(A)** A frame from a representative movie showing a phagosome (indicated with the asterisk) is just formed in EGFP-Rab20T19N expressing macrophages. Scale bar is 10 µm. **(B)** Quantitative analysis of EGFP-Rab20T19N (Green) and Dextran 70kDa (Red) fluorescence associated to phagosomes over 60 min post internalization. The intensity of EGFP-Rab20T19N and Dextran70kDa was measured frame by frame using ImageJ software. The results show means ± SD of the intensity of EGFP-Rab20T19N and Dextran 70kDa associated to phagosomes. 7 phagosomes from 5 cells in three independent experiments were quantified. **(C)** Time

series insets (indicated with white square in A) showing phagosomes acquiring Dextran 70kDa (Red) in EGFP-Rab20T19N (Green) expressing cells. Scale bar is 3 µm.

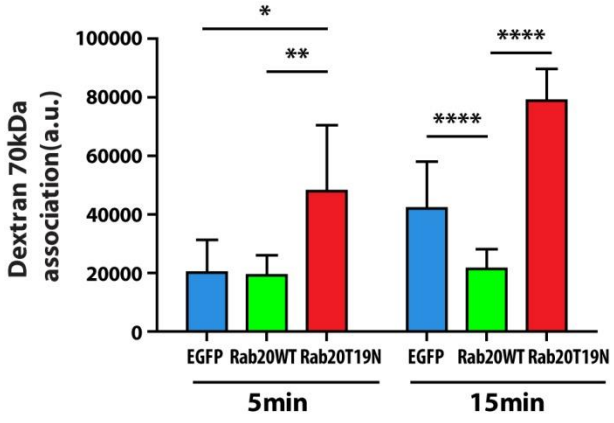

Fig. 3.29 Statistical analysis of the intensity of Dextran 70kDa association to phagosomes in EGFP, Rab20WT or Rab20T19N expressing macrophages at 5 min and 15 min post internalization. The intensity of Dextran 70kDa associated to phagosomes in macrophages expressing EGFP, EGFP-Rab20WT or EGFP-Rab20T19N was measured frame by frame using ImageJ software. The results show means ± SD of the intensity of Dextran 70kDa associated to phagosomes. 9 phagosomes from 4 cells for EGFP, 14 phagosomes from 3 cells for EGFP-Rab20WT and 7 phagosomes from 5 cells for EGFP-Rab20T19N in three independent experiments were quantified. P values were calculated using student' two-tailed unpaired t-test. (*) $p \leq 0.05$, (**) $p \leq 0.01$, (****) $p \leq 0.0001$

LAMP-1 association to phagosomes is delayed by Rab20 expression

It has been shown that in cells dificient of LAMP-1 and LAMP-2 have reduced phagolysosome fusion without loss of lysosome membrane integrity (Huynh KK *et al*. 2007). To investigate if the LAMP-1 association was also delayed by Rab20 expression, tdTomato-LAMP-1 was co-transfected with EGFP, EGFP-Rab20WT or EGFP-Rab20T19N and live cell imaging was performed to monitor the association of LAMP-1 to phagosomes. A quantitative analysis of tdTomato-LAMP-1 dynamics showed that in EGFP expressing macrophages, LAMP-1 association to phagosomes started at 5 min and reached to a plateau after 15 min (**Fig. 3.30**). In contrast, in EGFP-Rab20WT expressing macrophages LAMP-1 was not associated to phagosomes even after 1 hour of internalization (**Fig. 3.31**), correlating with the delayed phagolysosome fusion (**Fig. 3.27**). These data suggest that LAMP-1 association to phagosomes was blocked by Rab20 expression during the first hour of phagosome maturation.

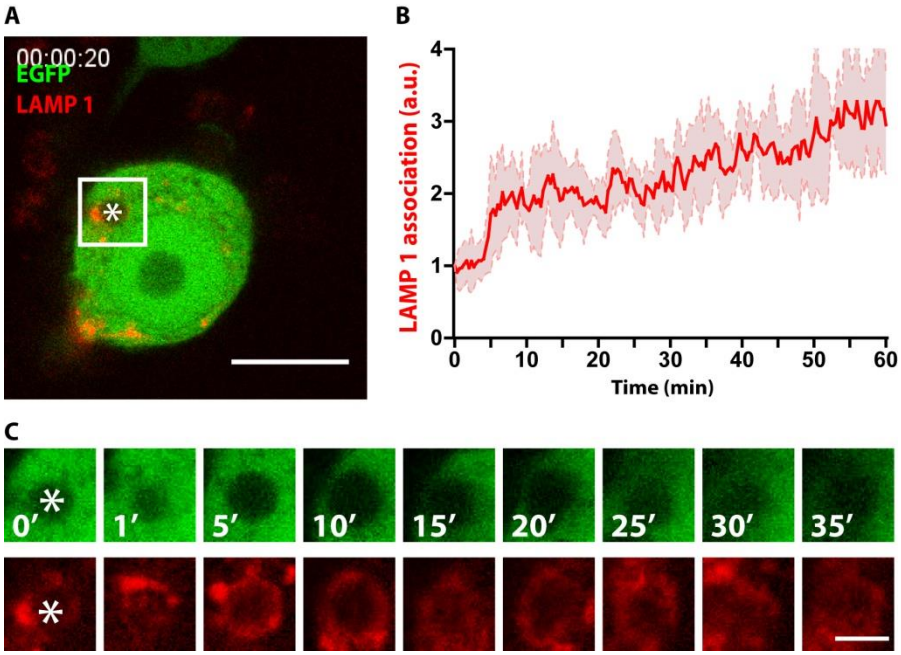

Fig. 3.30 LAMP-1 association to phagosomes in EGFP expressing macrophages. RAW264.7 macrophages were transfected with EGFP and tdTomato-LAMP-1 for 16 hours and IgG-coated beads were added prior to live cell imaging. **(A)** A frame from a representative movie showing a phagosome (indicated with the asterisk) is just formed in EGFP and LAMP-1 expressing macrophages. Scale bar is 10 µm. **(B)** Quantitative analysis of LAMP-1 (Red) association to phagosomes over 60 min post internalization. The intensity of LAMP-1 was measured frame by frame using ImageJ software. LAMP-1 fluorescence at all time points was normalized to the fluorescence at 0 min. 4 phagosomes from 2 cells in two independent experiments were quantified. The results show means ± SD of the normalized intensity of LAMP-1 associated to phagosomes. **(C)** Time series insets (indicated with white square in A) showing phagosomes acquiring LAMP-1 (Red) in EGFP (Green) expressing cells. Scale bar is 3 µm.

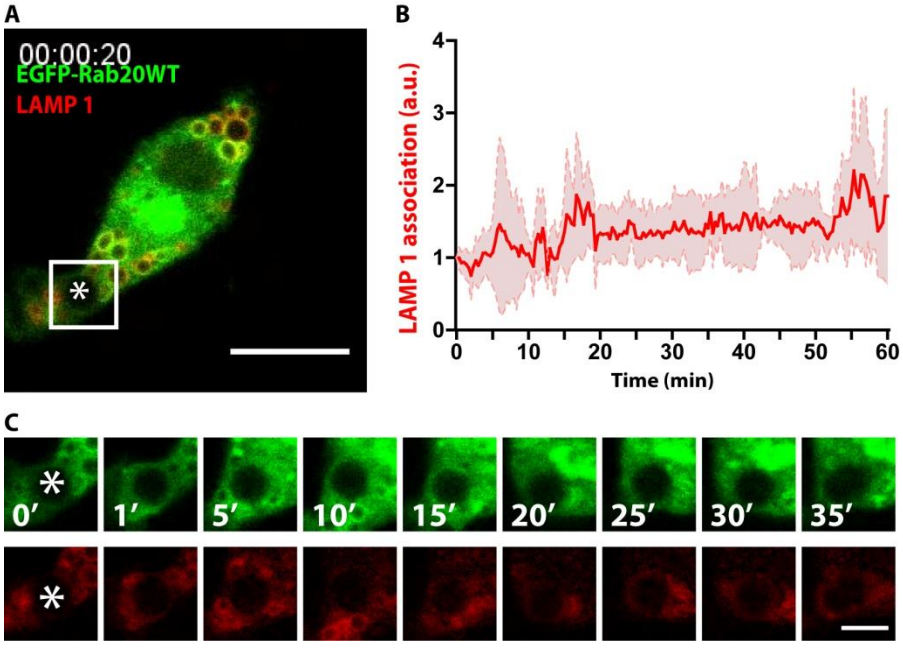

Fig. 3.31 LAMP-1 association to phagosomes in EGFP-Rab20WT expressing macrophages. RAW264.7 macrophages were transfected with EGFP-Rab20WT and tdtomato-LAMP-1 for 16 hours and IgG-coated beads were added prior to live cell imaging. **(A)** A frame from a representative movie showing a phagosome (indicated with the asterisk) is just formed in EGFP-Rab20WT and LAMP-1 expressing macrophages. Scale bar is 10 µm. **(B)** Quantitative analysis of LAMP-1 (Red) association to phagosomes over 60 min post internalization. The intensity of LAMP-1 was measured frame by frame using ImageJ software. LAMP-1 fluorescence at all time points was normalized to the fluorescence at 0 min. The results show means ± SD of the normalized intensity of LAMP-1 associated to phagosomes. 3 phagosomes from

2 cells in two independent experiments were quantified. **(C)** Time series insets (indicated with white square in A) showing a phagosome acquiring LAMP-1 (Red) in EGFP-Rab20WT (Green) expressing cells. Scale bar is 3 µm.

The role of Rab20 on phagosome maturation is distinct from Rab5

The data in previous experiments has shown that Rab20 and Rab5A are localized on early endosomes and phagosomes (**Fig. 3.1; Fig. 3.23**). To investigate if Rab5A has a function similar to Rab20 on phagosome maturation, EGFP-Rab5A was expressed in RAW264.7 macrophages and live cell imaging performed to monitor the kinetics of LysoTracker acquisition by phagosomes. In EGFP-Rab5A expressing macrophages, LysoTracker acquisition by phagosomes began after 10 min and reached to a plateau at approximately 30 min in a similar kinetics as in macrophages expressing EGFP (**Fig. 3.32**). For EGFP-Rab5A association, it stayed on phagosomes for around 5 min as reported before (Roberts EA *et al*. 2006). This data demonstrated that the phagosome maturation was not delayed by EGFP-Rab5WT over-expression, indicating Rab20 had a role on phagosome maturation distinct from Rab5A. Since Rab5A association to phagosomes is prolonged by Rab20WT expression, Rab5A might also participate in the delay of phagosome maturation induced by Rab20WT.

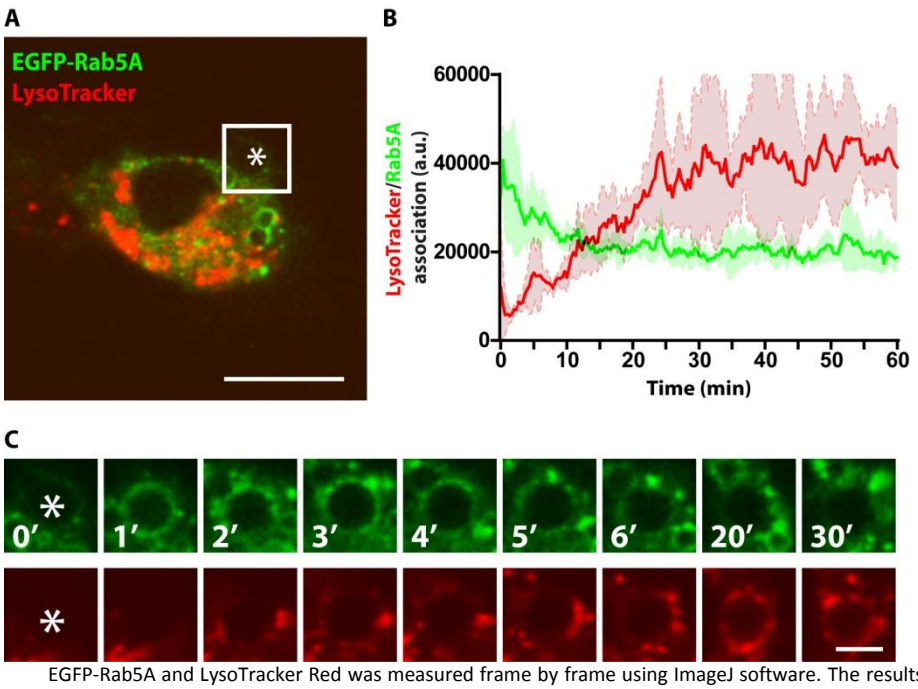

Fig. 3.32 Acquisiton of LysoTracker by phagosomes in macrophages expressing EGFP-Rab5A. RAW264.7 macrophages were transfected with EGFP-Rab5A for 16 hours and LysoTracker Red (50 nM) was added 30 min prior to live cell imaging. **(A)** A frame from a representative movie showing a phagosome (indicated with the asterisk) is just formed in EGFP-Rab5WT expressing macrophages. Scale bar is 10 µm. **(B)** Quantitative analysis of EGFP-Rab5A (Green) and LysoTracker (Red) association to phagosomes over 60 min post internalization. The intensity of EGFP-Rab5A and LysoTracker Red was measured frame by frame using ImageJ software. The results show means ± SD of the intensity of EGFP-Rab5A and LysoTracker Red associated to phagosomes. 5 phagosomes from 2 cells in two independent experiments were quantified. **(C)** Time series insets (indicated with white square in A) showing a phagosome acquiring LysoTracker (Red) and EGFP-Rab5A (Green). Scale bar is 3 µm.

Rab20 association to phagosomes is BFA-sensitive

Previous experiments have shown that Rab20 was localized in the CGN and TGN in RAW264.7 macrophages and BMMs (**Fig. 3.1; Fig. 3.5; Fig. 3.6**). To confirm that, RAW264.7 macrophages expressing EGFP-Rab20WT were treated with Brefeldin A (BFA) and indirect immunofluorescence was performed with a CGN marker GM130. BFA reversibly inhibits protein transport from the ER to the Golgi and induces retrograde transport from the Golgi to the ER (Klausner RD *et al*. 1992). Rab20 was localized in the CGN in untreated cells as showed before (**Fig. 3.33 A**). After 1 h of BFA treatment, *cis*-Golgi stacks were disrupted into dispersed dot-like structures and EGFP-Rab20 in the Golgi region was also redistributed into scattered structures which did not colocalize with the disrupted *cis*-Golgi stacks, indicating the existence of post-Golgi trafficking route for EGFP-Rab20 (**Fig. 3.33 B**). After 1 h of washing BFA out, *cis*-Golgi stacks were reformed and EGFP-Rab20 partially localized in this area (**Fig. 3.33 C**).

When the effect of BFA treatment on Rab20 association to phagosomes was investigated, Rab20 recruitment to phagosomes was dramatically reduced, suggesting that the Golgi-to-phagosome trafficking was impaired (**Fig. 3.34 A, B**). Moreover, the quantitative analysis of the intensity of LysoTracker associated to phagosomes demonstrated that the acquisition of LysoTracker by phagosomes in macrophages treated with BFA started at 10 min and reached to a plateau after 25 min, which was much faster than in cells without BFA treatment (**Fig. 3.34 C, D**). Taken together, the recruitment of Rab20 into phagosomes is Brefeldin A sensitive. In addition, these studies clearly indicated that the association of Rab20 to phagosomes is required for the observed delay of phagosome maturation.

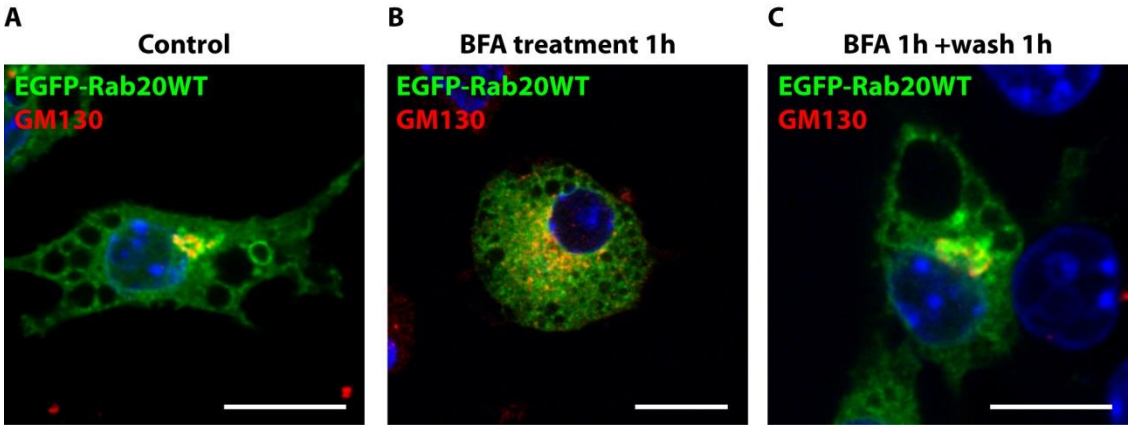

Fig. 3.33 Rab20 Golgi distribution is disrupted by Brefeldin A treatment. RAW264.7 macrophages were transfected with EGFP-Rab20WT for 16 hours and then treated with or without Brefeldin A (BFA, 1 µg/mL) for 1 hour, followed by another 1 hour recovery. Afterwards, indirect immunofluorescence was performed with antibody against the CGN marker-GM130. **(A)** The Golgi distribution of EGFP-Rab20WT in untreated macrophages **(B)** The Golgi distribution of EGFP-Rab20WT in macrophages after BFA treatment for 1 hour **(C)** The Golgi distribution of EGFP-Rab20WT in macrophages after washing BFA out for 1 hour. The nuclei were labeled by Hoechst 33258 and shown in blue. Scale bar is 10 µm.

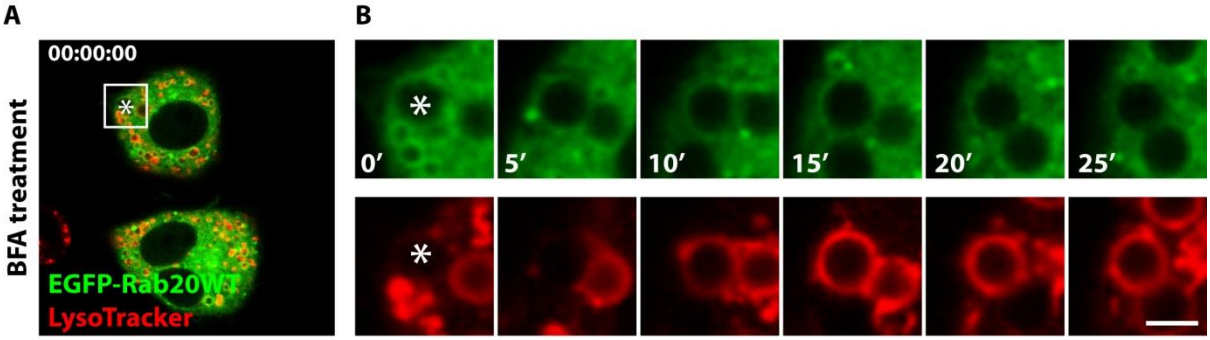

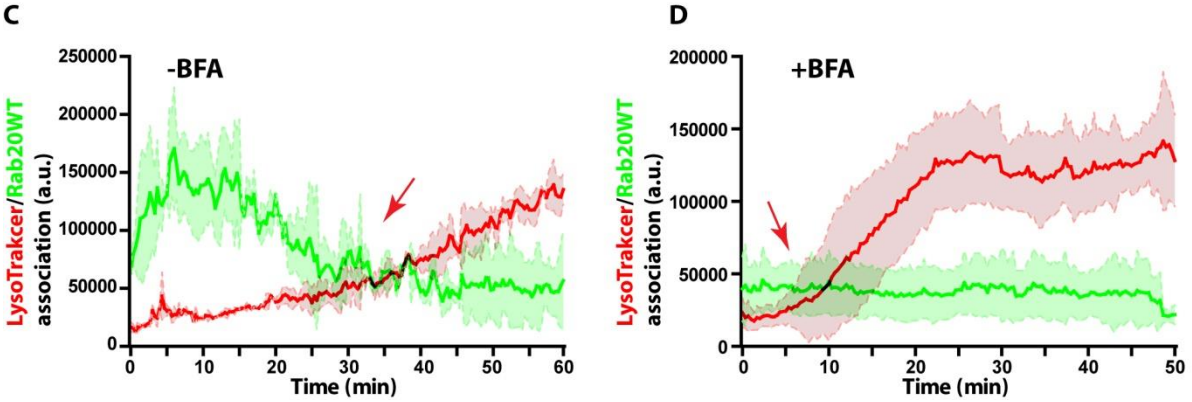

Fig. 3.34 Acquisiton of LysoTracker by phagosomes in EGFP-Rab20WT expressing macrophages after Brefeldin A treatment. RAW264.7 macrophages were transfected with EGFP-Rab20WT for 16 hours and then treated with Brefeldin A (1 µg/mL) for 1 hour. Afterwards, LysoTracker Red (50 nM) were added 30 min prior to live cell imaging. **(A)** A frame from a representative movie showing a phagosome (indicated with asterisk) is just formed in EGFP-Rab20WT expressing macrophages after BFA treatment. Scale bar is 10 µm. **(B)** Time series insets (indicated with white square in A) showing the phagosome of interest acquiring LysoTracker (Red) and EGFP-Rab20WT (Green). Scale bar is 3 µm. **(C)** Quantitative analysis of EGFP-Rab20WT (Green) and LysoTracker (Red) association to phagosomes over 60 min post internalization without BFA treatment. The intensity of EGFP-Rab20 and LysoTracker Red was measured frame by frame using ImageJ software. The results show means ± SD of the intensity of EGFP-Rab20WT and LysoTracker associated to phagosomes. 6 phagosomes from 2 cells in two independent experiments were quantified. Red arrow indicates phagosomes start acquiring LysoTracker Red. **(D)** Quantitative analysis of EGFP-Rab20WT (Green) and LysoTracker (Red) association to phagosomes over 60 min post internalization with BFA treatment. The intensity of EGFP-Rab20WT and LysoTracker Red was measured frame by frame using ImageJ software. The results show means ± SD of the intensity of EGFP-Rab20WT and LysoTracker associated to phagosomes. 12 phagosomes from 4 cells in three independent experiments were quantified. Red arrow indicates phagosomes start acquiring LysoTracker Red.

The β1, 4-galactosyltransferase 1 (GalT) is an enzyme localized in *trans*-Golgi cisterna and the TGN (Geuze HJ *et al*. 1985, Griffiths G and Simons K. 1986). To visualize the post-Golgi trafficking of Rab20 to phagosomes, RAW264.7 macrophages were co-transfected with Venus-GalT and mCherry-Rab20WT. As expected, mCherry-Rab20WT associated to the Golgi complex, as shown by colocalization with Venus-GalT (**Fig. 3.35 A**). Moreover, tubules that were positive for both Venus-GalT and mCherry-Rab20WT were observed (**Fig. 3.35 B**). They derived and separated from the Golgi complex, forming post-Golgi vesicles (as the arrowheads showed in **Fig. 3.35 B**). These data suggest the existence of post-Golgi trafficking for Rab20. Additionally, Rab20-positive vesicles budding from the Golgi complex (positive for Venus-GalT) were also observed (as the arrows showed in **Fig. 3.35 C**). Moreover, Rab20-positive vesicles and phagosomes were engaged in multiple transient contacts in a long period of time (10'00''-14'20'' in **Fig. 3.35 C**), resembling the mode of kiss and run (Desjardins M. 1995). With these events, Rab20 was delivered to phagosomes from the Golgi-derived Rab20 vesicles, as shown by the increased Rab20 on the contact sites (**Fig. 3.35 C**). Altogether, these data suggest that Rab20 traffic from the Golgi to phagosomes by a post-Golgi route as reported for other proteins (Fratti RA *et al*. 2003, Wähe A *et al*. 2010).

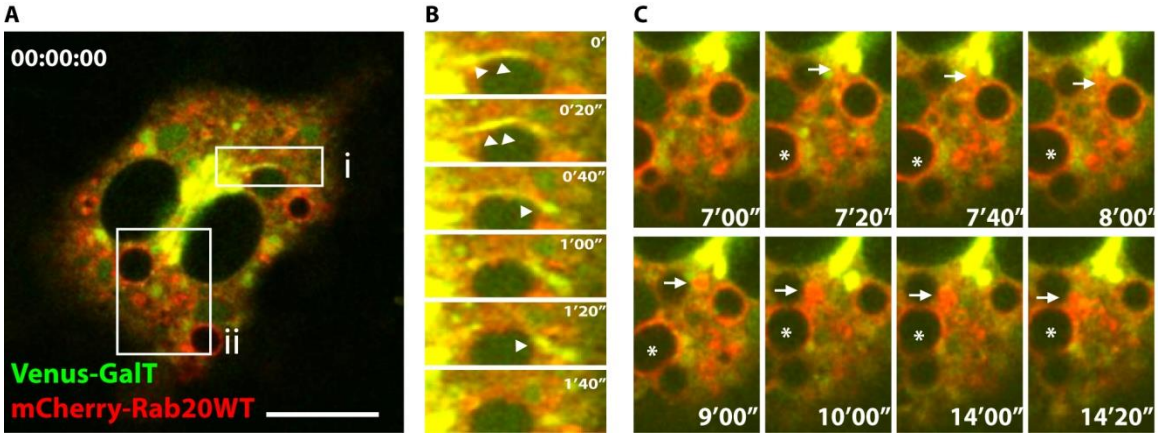

Fig. 3.35 Rab20 post-Golgi trafficking to phagosomes. RAW264.7 macrophages were transfected with Venus-GalT and mCherry-Rab20WT for 16 hours and IgG-coated beads were added prior to live cell imaging. **(A)** A frame from a representative movie showing post-Golgi trafficking of Rab20 to phagosomes. White rectangles indicate the regions of interest (region **i** and **ii**). Scale bar is 10 µm. **(B)** Time series insets of white rectangle **i** showing the tubular structure derived from the Golgi complex. The arrowheads indicate the Venus-GalT and mCherry-Rab20WT double positive Golgi tubules separated from Golgi, forming post-Golgi vesicles. **(C)** Time series insets of white rectangle **ii** showing Rab20 delivery from Golgi-derived vesicles to phagosomes via kiss and run. The arrows indicate post-Golgi vesicles transiently contact with the phagosome (indicated with asterisks).

Rab20 knockdown accelerates phagosome maturation

As shown in previous experiments, phagosome maturation was accelerated in macrophages expressing the dominant negative mutant of Rab20 (**Fig. 3.16; 3.20; 3.28**). To confirm these observations, Rab20 was knocked down in macrophages using a pSIREN plasmid system. In this system, a small hairpin RNA (shRNA) for Rab20 in cells is produced together with a DsRed fluorescent protein, enabling the monitoring of Rab20 knockdown at the single cell level by microscopy. To test the knockdown efficiency, RAW 264.7 macrophages were transfected with pSIREN expressing four different shRNAs for Rab20 and a scrambled shRNA as a control. After 48 hours, transfected cells were sorted based on DsRed fluorescence and protein levels of Rab20 analyzed by Western blot. From all the shRNAs, shRNA1 demonstrated the best knockdown efficiency for Rab20 (approximately 60%; **Fig. 3.36 A, B**).

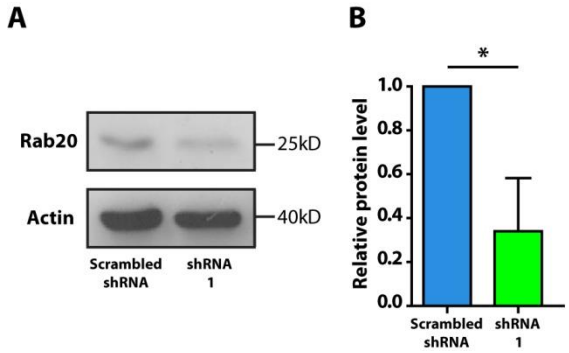

Fig. 3.36 Rab20 knockdown in RAW264.7 macrophages with pSIREN shRNAs. (A) Western blot analysis of Rab20 protein level after shRNA knockdown. Cell lysates from RAW264.7 macrophages transfected with scrambled shRNA and shRNA1 for 48 hours were analyzed with SDS-PAGE. Actin was used as the loading control. Three independent experiments were performed. Representative images are shown. **(B)** Statistical analysis of Rab20 protein level in scrambled shRNA and shRNA 1 expressing macrophages. The intensity of bands was measured using ImageJ software. The relative intensity of Rab20 was calculated against the actin loading control. Then the relative intensity of Rab20 in shRNA1 expressing macrophages was normalized to scrambled shRNA. The results show means ± SD of three independent experiments. P values were calculated using student' two-tailed unpaired t-test. (*) $p \leq 0.05$.

To investigate the dynamics of phagosome maturation in Rab20 knockdown macrophages, RAW264.7 macrophages were respectively transfected with pSIREN expressing shRNA 1 or scrambled shRNA and LysoTracker Green acquisition by phagosomes monitored by live cell imaging. In macrophages expressing scrambled shRNA, phagosomes acquired LysoTracker after 10 min and reached to a plateau at 25 min, showing a similar kinetics with EGFP expressing macrophages (**Fig. 3.37**). In macrophages expressing shRNA 1, phagosomes acquired LysoTracker faster than in scrambled shRNA expressing macrophages. The acquisition of LysoTracker started after 5 min and reached to a peak after 15 min (**Fig. 3.38**). A statistical analysis of the intensity of LysoTracker associated to phagosomes showed that the intensity of LysoTracker associated to phagosomes in shRNA 1 expressing macrophages was significantly higher than in cells expressing scrambled shRNA at 5 and 10 min post internalization (**Fig. 3.39**). These data suggested that the phagosome

maturation was significantly accelerated by Rab20 knockdown and confirmed the observed behavior of the dominant negative mutant of Rab20.

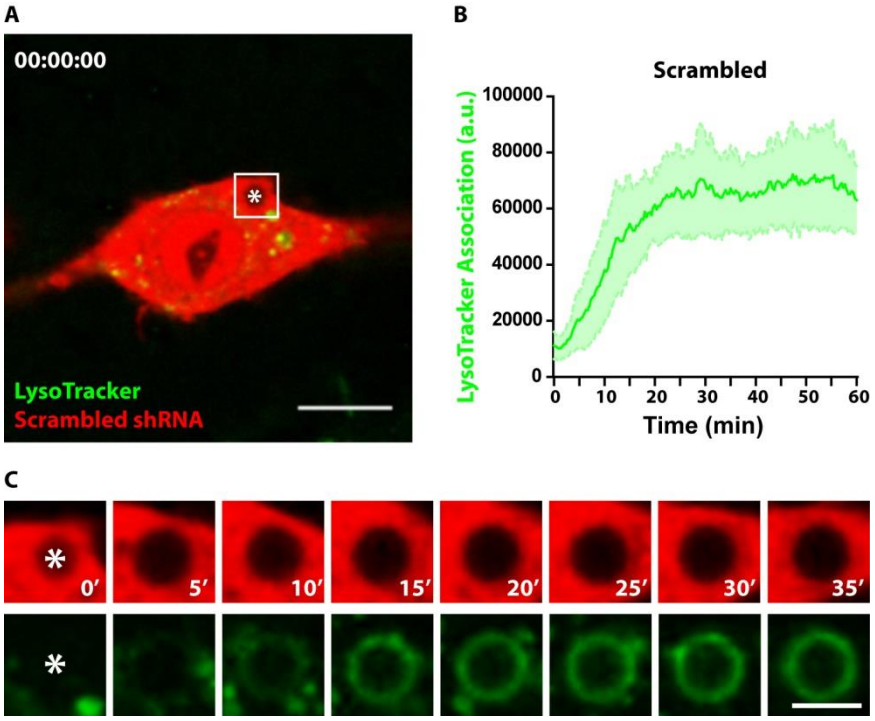

Fig. 3.37 Acquisiton of LysoTracker by phagosomes in macrophages expressing scrambled shRNA. RAW264.7 macrophages were transfected with scrambled shRNA plasmid for 30 hours and LysoTracker Green (50 nM) were added 30 min prior to live cell imaging. **(A)** A frame from a representative movie showing a phagosome (indicated with the asterisk) is just formed in macrophages expressing scrambled shRNA. Scale bar is 10 µm. **(B)** Quantitative analysis of LysoTracker (Green) association to phagosomes over 60 min post internalization. The intensity of LysoTracker Green was measured frame by frame using ImageJ software. The results show means ± SD of the intensity of LysoTracker associated to phagosomes. 20 phagosomes from 7 cells in three independent experiments were quantified. **(C)** Time-series images (indicated with the white square in A) showing the phagosome of interest acquiring LysoTracker (Green). Scale bar is 3 µm.

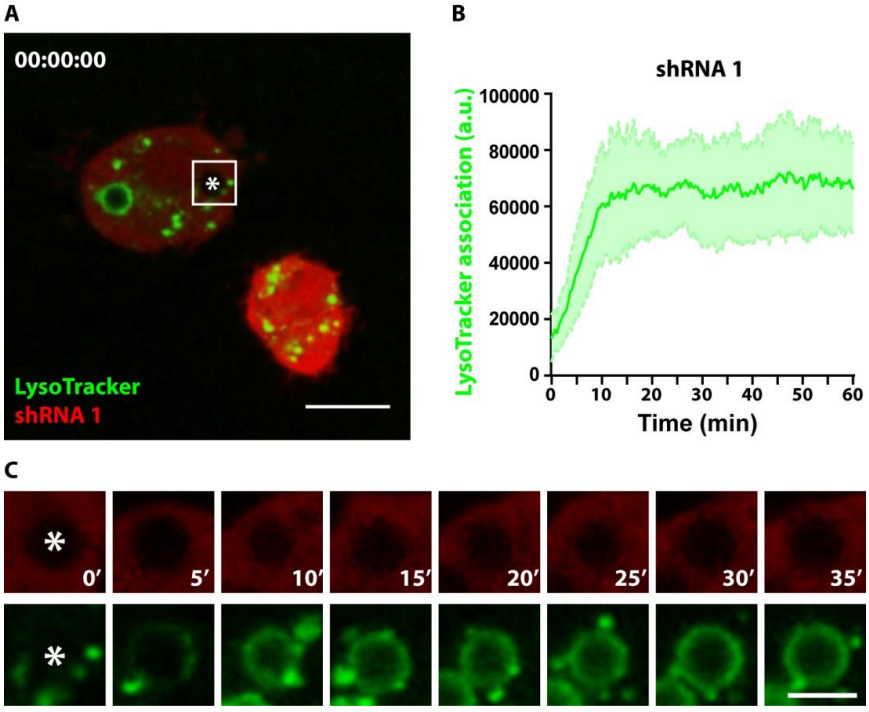

Fig. 3.38 Acquisiton of LysoTracker by phagosomes in macrophages expressing shRNA 1. RAW264.7 macrophages were transfected with shRNA 1 plasmid for 30 hours and LysoTracker Green (50 nM) were added 30 min prior to live cell imaging. **(A)** A frame from a representative movie showing a phagosome (indicated with asterisk) is just formed in shRNA 1 expressing macrophages. Scale bar is 10 µm. **(B)** Quantitative analysis of LysoTracker (Green) fluorescence association to phagosomes over 60 min post internalization. The intensity of LysoTracker Green was measured frame by frame using ImageJ software. The results show means ± SD of the intensity

of LysoTracker Green associated to phagosomes. 21 phagosomes from 6 cells in three independent experiments were quantified. **(C)** Time series insets (indicated with the white square in A) showing the phagosome of interest acquiring LysoTracker (Green). Scale bar is 3 µm.

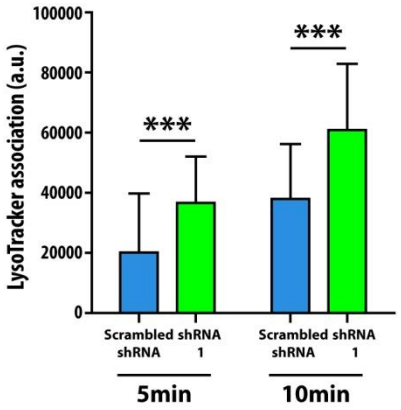

Fig. 3.39 Statistical analysis of the intensity of LysoTracker Green association to phagosomes in macrophages expressing scrambled shRNA or shRNA 1 at 5 and 10 min post internalization. The LysoTracker Green intensity was measured frame by frame using ImageJ software. The results show means ± SD of the intensity of LysoTracker Green associated to phagosomes in scrambled or shRNA 1 expressing macrophages at 5 and 10 min post internalization. 20 phagosomes for scrambled shRNA and 21 phagosomes for shRNA 1 in three independent experiments were quantified. P values were calculated using student' two-tailed unpaired t-test. (***) $p \leq 0.001$

The delay in phagosome maturation by IFN-γ is Rab20 dependent

IFN-γ delays phagosome maturation

There is accumulating evidence showing that phagosome maturation is delayed by IFN-γ treatment (Tsang AW *et al*. 2000, Yates RM *et al*. 2007, Jutras I *et al*. 2007, Trost M *et al*. 2009). However, the molecular link by which IFN-γ modulates phagosome trafficking is unknown. To investigate phagosome maturation modulated by IFN-γ, RAW264.7 macrophages were treated with IFN-γ overnight and phagosome maturation was analyzed by measuring the acquisition of LysoTracker. The kinetics of LysoTracker acquisition by phagosomes in untreated cells was consistent with previously shown experiments (**Fig. 3.40 A**). In contrast, in macrophages activated with IFN-γ, the acquisition of LysoTracker by phagosomes was delayed in the first 1 hour (**Fig. 3.40 B**). A statistical analysis of the intensity of LysoTracker associated to phagosomes showed that the intensity of LysoTracker associated to phagosomes in IFN-γ treated macrophages was significantly lower than in untreated cells at 15 min post internalization (**Fig. 3.40 C**). As shown before by other groups (Tsang AW *et al*. 2000, Yates RM *et al*. 2007, Jutras I *et al*. 2007, Trost M *et al*. 2009), this data indicated that phagosome maturation was delayed by IFN-γ.

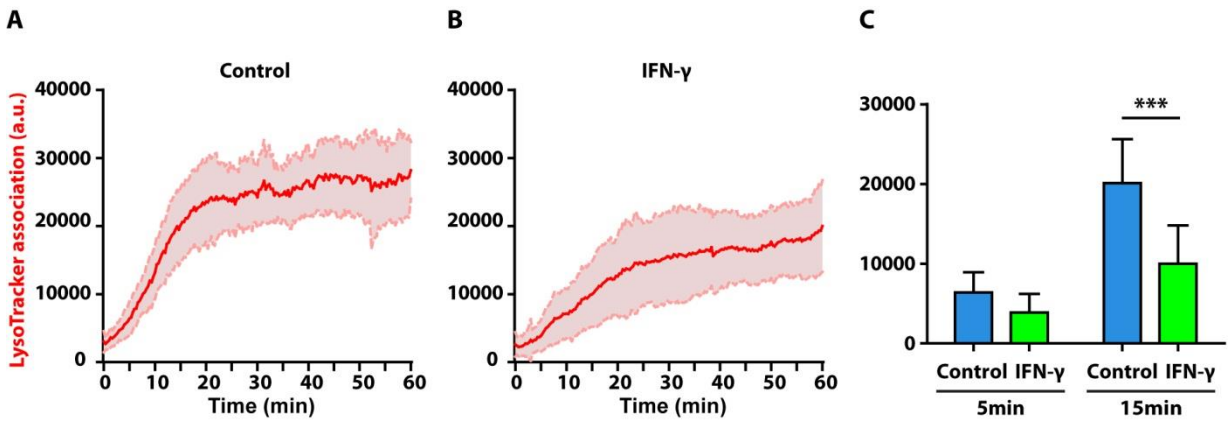

Fig. 3.40 LysoTracker acquisition by phagosomes in RAW264.7 macrophages is delayed by IFN-γ. RAW264.7 was treated without or with IFN-γ (200 Units/mL) for 16 hours and LysoTracker Red (50 nM) was added 30 min prior to live cell imaging. Quantitative analysis of LysoTracker (Red) association to phagosomes over 60 min post internalization in macrophages without **(A)** or with IFN-γ treatment **(B)**. The LysoTracker Red intensity was measured frame by frame using ImageJ software. The results show means ± SD of the intensity of LysoTracker associated to phagosomes. For **A,** 20 phagosomes from 5 cells in two independent experiments were quantified. For **B,** 28 phagosomes from 6 cells in two independent experiments were quantified. (C) Statistical analysis of the intensity of LysoTracker associated to phagosomes without or with IFN-γ treament at 5 min and 15 min post internalization. The results show means ± SD of the intensity of LysoTracker associated to phagosomes. P values were calculated using student' two-tailed unpaired t-test. (***) $p \leq 0.001$.

Phagosome maturation is not delayed by IFN-γ in cells loss of Rab20 function

In previous experiments, it was observed that phagosome maturation was delayed by Rab20WT over-expression as well as IFN-γ activation (**Fig. 3.15; Fig. 3.19; Fig. 3.27; Fig. 3.40**). In addition, endogenous Rab20 expression was significantly increased by IFN-γ (**Fig. 3.7**). Therefore, an interesting hypothesis to test was that the delayed phagosome maturation induced by IFN-γ treatment could be Rab20 dependent. To test this hypothesis, RAW264.7 macrophages were transfected with EGFP or EGFP-Rab20T19N. Afterwards, transfected macrophages were left untreated or treated with IFN-γ overnight and live cell imaging experiments were performed to monitor LysoTracker acquisition by phagosomes. As shown in **Fig. 3.41**, LysoTracker acquisition by phagosomes in EGFP expressing macrophages with IFN-γ treatment reached to the plateau at 30 min, which was slightly slower than in EGFP expressing macrophages without IFN-γ treatment. In contrast, in macrophages expressing EGFP-Rab20T19N, LysoTracker acquisition by phagosomes was not affected by IFN-γ treatment. In these cells, LysoTracker acquisition by phagosomes started at 5 min and reached a plateau after 10 min (**Fig. 3.42**).

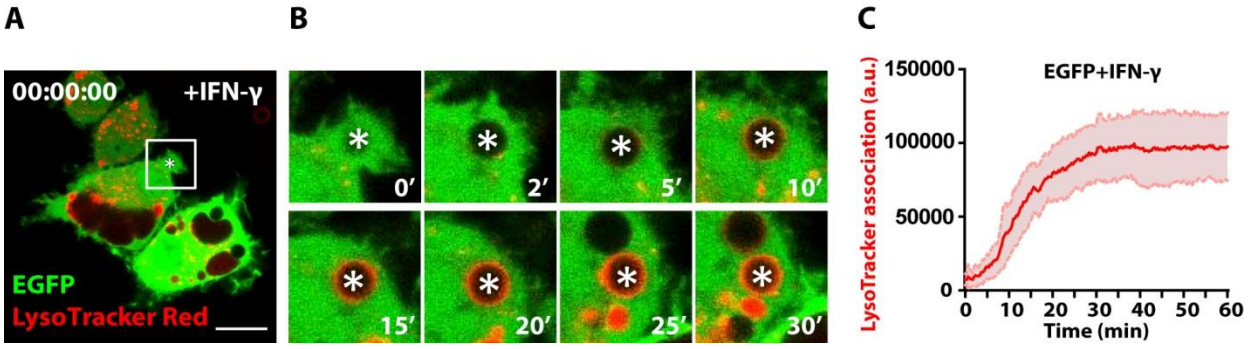

Fig. 3.41 LysoTracker acquisition by phagosomes in EGFP expressing macrophages after IFN-γ treatment. RAW264.7 macrophages were transfected with EGFP for 6 hours and IFN-γ (200 Units/mL) was added for 16 hours. Afterwards, LysoTracker Red (50 nM) was added 30 min prior to live cell imaging. **(A)** A frame from a representative movie showing a phagosome (indicated with asterisk) is just formed in EGFP expressing macrophages after IFN-γ treatment. Scale bar is 10 µm. **(B)** Time series insets (indicated with the white square in A) showing the phagosome of interest acquiring LysoTracker (Red) in EGFP (Green) expressing cells after IFN-γ treatment. Scale bar is 3 µm. **(C)** Quantitative analysis of LysoTracker (Red) association to phagosomes over 60 min post internalization after IFN-γ treatment. The intensity of LysoTracker Red was measured frame by frame using ImageJ software. The results show means ± SD of the intensity of LysoTracker fluorescence associated to the phagosomes. 12 phagosomes from 4 cells in two independent experiments were quantified.

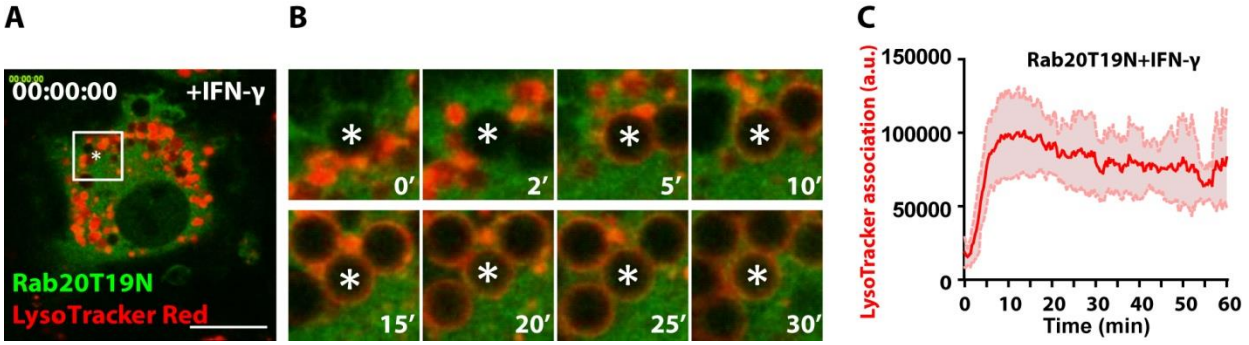

Fig. 3.42 LysoTracker acquisition by phagosomes in EGFP-Rab20T19N expressing macrophages after IFN-γ treatment. RAW264.7 macrophages were transfected with EGFP-Rab20T19N for 6 hours and IFN-γ (200 Units/mL) was added for 16 hours. Afterwards, LysoTracker Red (50 nM) was added 30 min prior to live cell imaging. **(A)** A frame from a representative movie showing a phagosome (indicated with asterisks) is just formed in EGFP-Rab20T19N expressing macrophages. Scale bar is 10 µm. **(B)** Time-series images (indicated with the white square in A) showing phagosomes acquiring LysoTracker (Red) in EGFP-Rab20T19N (Green) expressing cells after IFN-γ treatment. Scale bar is 3 µm. **(C)** Quantitative analysis of LysoTracker (Red) association to phagosomes over 60 min post internalization after IFN-γ treatment. The intensity of LysoTracker Red was measured frame by frame using ImageJ software. The results show means ± SD of the intensity of LysoTracker associated to the phagosomes. 10 phagosomes from 3 cells in three independent experiments were quantified.

To further address if the delay in phagosome maturation induced by IFN-γ is Rab20 dependent, phagosome maturation in macrophages knockdown for Rab20 was investigated. RAW264.7 macrophages were transfected with pSIREN expressing scrambled shRNA or shRNA 1. Afterwards,

macrophages were left untreated or treated with IFN-γ overnight and live cell imaging experiments were performed to monitor LysoTracker acquisition by phagosomes. As shown in **Fig. 3.43**, after IFN-γ treatment LysoTracker acquisition by phagosomes in scrambled shRNA expressing macrophages reached a plateau at approximately 25 min (**Fig. 3.43**). LysoTracker association to phagosomes in scrambled shRNA expressing macrophages with IFN-γ treatment was lower than in scrambled shRNA expressing cells without IFN-γ treatment. This was probably due to the inhibition of fusion between phagosomes and LysoTracker-containing vesicles. In macrophages expressing shRNA 1, LysoTracker acquisition by phagosomes reached to the peak at 15 min with IFN-γ treatment (**Fig. 3.44**). LysoTracker acquisition was also delayed compared with cells expressing shRNA 1 without IFN-γ treatment (reach the peak at 10 min). A statistical analysis of the intensity of LysoTracker associated to phagosomes in scrambled shRNA and shRNA 1 expressing macrophages after IFN-γ treatment showed that the LysoTracker fluorescence intensity in macrophages expressing shRNA 1 was significantly higher than in macrophages expressing scrambled shRNA at 5 and 15 min post internalization (**Fig. 3.45**). Taken together, the data of LysoTracker acquisition by phagosomes in macrophages expressing EGFP-Rab20T19N or knockdown for Rab20 clearly showed that the delay of phagosome maturation induced by IFN-γ is Rab20 dependent.

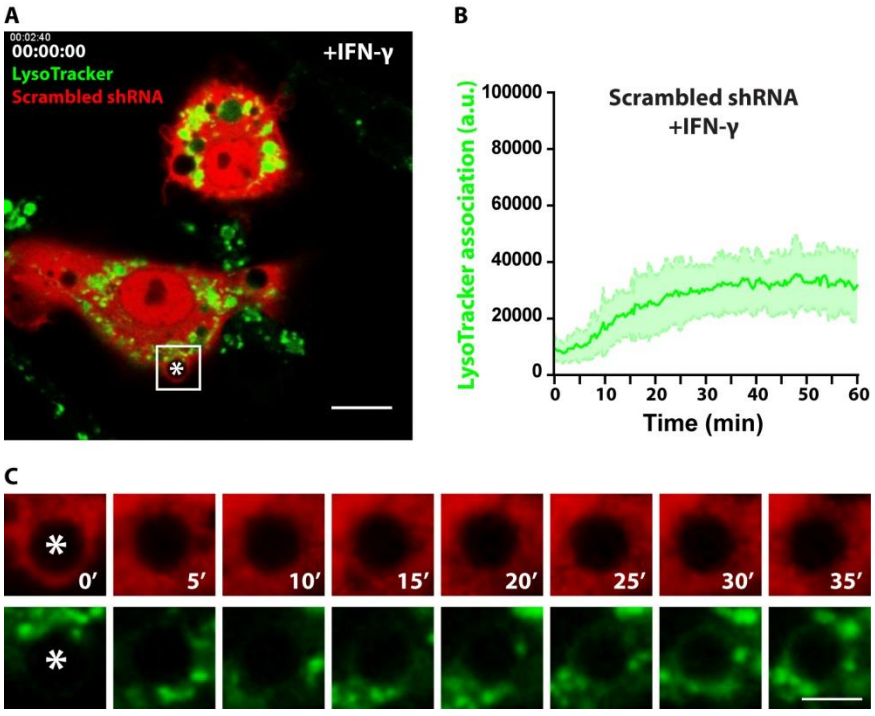

Fig. 3.43 LysoTracker acquisition by phagosomes in macrophages expressing scrambled shRNA after IFN-γ treatment. RAW264.7 macrophages were transfected with pSIREN plasmid of scrambled shRNA for 24 hours and IFN-γ (200 Units/mL) was added for 16 hours. Afterwards, LysoTracker Green (50 nM) was added 30 min prior to live cell imaging. **(A)** A frame from a representative movie showing a phagosome (indicated with an asterisk) is just formed in macrophages expressing scramble shRNA after IFN-γ treatment. Scale bar is 10 µm. **(B)** Quantitative analysis of LysoTracker (Green) association to phagosomes over 60 min post internalization. The intensity of LysoTracker was measured frame by frame using ImageJ software. The results show means ± SD of the intensity of LysoTracker associated to phagosomes. 15 phagosomes from 3 cells in two independent experiments were quantified. **(C)** Time-series images (indicated with the white square in A) showing the phagosome of interest acquiring LysoTracker (Green). Scale bar is 3 µm.

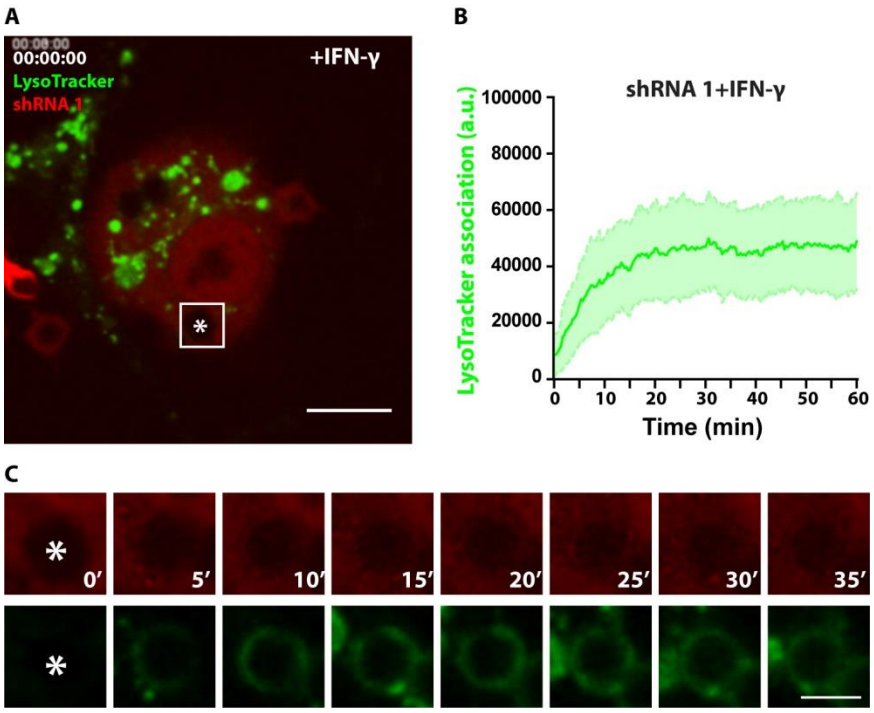

Fig. 3.44 LysoTracker acquisition by phagosomes in macrophages expressing shRNA 1 after IFN-γ treatment. RAW264.7 macrophages were transfected with pSIREN plasmid of shRNA 1 for 24 hours and IFN-γ (200 Units/mL) was added for 16 hours. Afterwards, LysoTracker Green (50 nM) was added 30 min prior to live cell imaging. **(A)** A frame from a representative movie showing a phagosome (indicated with an asterisk) is just formed in macrophages expressing shRNA 1 after IFN-γ treatment. Scale bar is 10 µm. **(B)** Quantitative analysis of LysoTracker (Green) association to phagosomes over 60 min post internalization. The intensity of LysoTracker was measured frame by frame using ImageJ software. The results show means ± SD of the intensity of LysoTracker associated to phagosomes. 18 phagosomes from 3 cells in two independent experiments were quantified. **(C)** Time-series images (indicated with the white square in A) showing the phagosome of interest acquiring LysoTracker (Green). Scale bar is 3 µm.

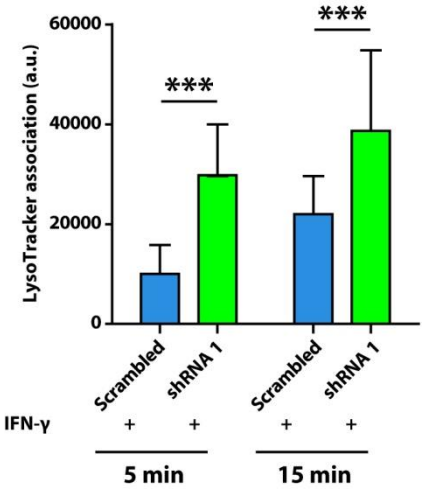

Fig. 3.45 Statistical analysis of the intensity of LysoTracker Green associated to phagosomes in macrophages expressing scrambled shRNA or shRNA 1 after IFN-γ treatment at 5 and 10 min post internalization. The intensity of LysoTracker Green was measured frame by frame using ImageJ software. The results show means ± SD of the intensity of LysoTracker Green associated to phagosomes. 15 phagosomes for scrambled shRNA and 18 phagosomes for shRNA 1 in two independent experiments were quantified. P values were calculated using student' two-tailed unpaired t-test. (***) $p \leq 0.001$.

The role of Rab20 on mycobacterial killing

Rab20 association to mycobacterial phagosomes

Previous experiments in this study have demonstrated that Rab20 is associated to IgG-coated bead phagosomes for 25 min post internalization (**Fig. 3.12**). Additionally, it has been reported that Rab20 is transiently recruited to *M. tuberculosis*-containing phagosomes, peaking at 30 min post infection (Seto S *et al*. 2011). To investigate the dynamics of Rab20 association to mycobacterial phagosomes in detail, RAW264.7 macrophages were transiently transfected with EGFP-Rab20WT and infected with *M. bovis* BCG dsRed and monitored by live cell imaging. As shown in **Fig.3.46**, the bacteria was first attached and then quickly engulfed by macrophages. After internalization, Rab20 was recruited to the mycobacteria containing phagosome (arrows showed in **Fig.3.46 B**). The quantatative analysis of EGFP-Rab20WT associated to the mycobacteria-containing phagosome showed that EGFP-Rab20WT stayed on phagosomes for around 20 min, suggesting that Rab20 is transiently associated to mycobacteria-containing phagosomes (**Fig.3.46 C**). This is in agreement with a previous report (Seto S *et al*. 2011). It was rare but noteworthy that spacious phagosomes were gradually formed after *M. bovis* BCG was uptaken (arrowheads showed in **Fig.3.46 B**). Altogether, Rab20 is also associated to mycobacteria-containing phagosomes at early time points during phagocytosis.

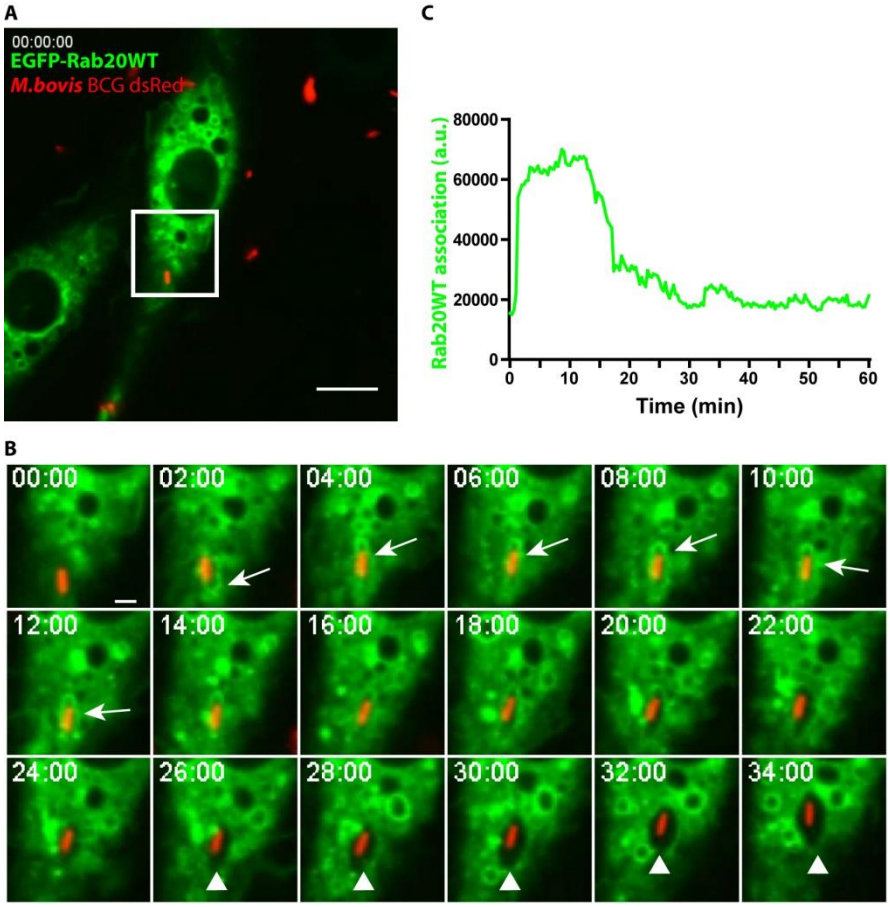

Fig. 3.46 EGFP-Rab20WT association to *M. bovis*-containing phagosomes. RAW264.7 macrophages were transfected with EGFP-Rab20WT for 16 hours and then infected with *M. bovis* BCG dsRed bacteria (final OD_{600}=0.02). Live cell imaging was performed to monitor the phagocytosis of bacteria. **(A)** A frame from a representative movie showing *M. bovis* BCG dsRed bacteria (Red) was phagocytosed by macrophages expressing EGFP-Rab20WT (Green). Scale bar is 10 µm. **(B)** Time series insets (indicated with the white square in A) showing the *M. bovis* BCG dsRed (Red) phagosome acquiring EGFP-Rab20WT (Green). The arrows indicate EGFP-Rab20WT association to the bacteria phagosome. The arrowheads indicate the formation of unusual spacious phagosome. Scale bar is 3 µm. **(C)** Quantitative analysis of EGFP-Rab20WT (Green) association to the phagosome over 60 min after internalization. The intensity of EGFP-Rab20WT associated to the bacteria in **B** was measured frame by frame using ImageJ software.

Mycobacterial killing is not affected by Rab20 over-expression

Previously, it has been shown in this research group that Rab20 is highly up-regulated by mycobacterial infection in a NF-κB dependent manner, indicating Rab20 may have a role in mycobacterial killing (Gutierrez MG *et al*. 2008). To investigate the role of Rab20 on *M. bovis* BCG survival, experiments were performed in RAW264.7 macrophages stably expressing EGFP or EGFP-Rab20WT. Cells were infected with *M. bovis* BCG for 1, 6, 24 or 48 hours. Afterwards, cells were lysed, plated and colony forming units (CFU) were counted. As shown in **Fig.3.47**, there was no significant difference for the CFU numbers between RAW264.7 untransfected macrophages or macrophages expressing EGFP or EGFP-Rab20WT (**Fig.3.47**). This data suggested that mycobacterial survival was not affected by Rab20 expression and highlighted a role for Rab20 more related to early events during phagosome maturation.

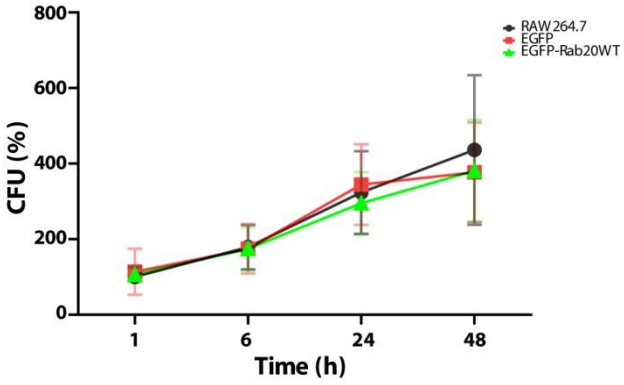

Fig. 3.47 BCG CFU in RAW264.7 stably expressing EGFP and stably expressing EGFP-Rab20WT macrophages. A suspension of BCG-dsRed in culture medium was added into macrophages for 1 hour of pulsing and 1, 6, 24 or 48 hour of chasing. Then cells were lysed and CFUs were determined. The colonies recovered at 1 hour in RAW264.7 macrophages was set as 100% and all others were normalized to it. The results indicate means ± SD of the normalized CFUs. Three independent experiments were performed.

Rabex-5 in the function of Rab20

Rabex-5 is an effector of Rab20

As shown previously in this work, enlarged early endosomes and early phagosomal homotypic fusion was observed in EGFP-Rab20WT expressing macrophages (**Fig. 3.12D, E**). Moreover, association of Rab20 to phagosomes also extended the association of Rab5 to them (**Fig. 3.23**). It is therefore tempting to hypothesize that Rab20 may interact with the Rab5 exchange factor Rabex-5. To test if Rabex-5 and Rab20 interact, EGFP immunoprecipitation (IP) was performed in macrophages stably expressing EGFP or EGFP-Rab20WT. Western blot analysis of the immunoprecipitates showed that endogenous Rabex-5 was preferentially associated to GTPγS-loaded but not to GDPβS-loaded EGFP-Rab20WT, indicating that Rabex-5 only interacts with the active form of Rab20 (**Fig.3.48 A**). To confirm that Rabex-5 binds directly with Rab20, pulldown experiments using GST-Rab20WT were performed with RAW264.7 cell lysates. Western blot analysis showed that Rabex-5 specifically binds to the active form (GTPγS-loaded) of GST-Rab20WT (**Fig.3.48 B**). Altogether, these results show that Rabex-5 interacts preferentially with GTP-Rab20 being an effector of Rab20.

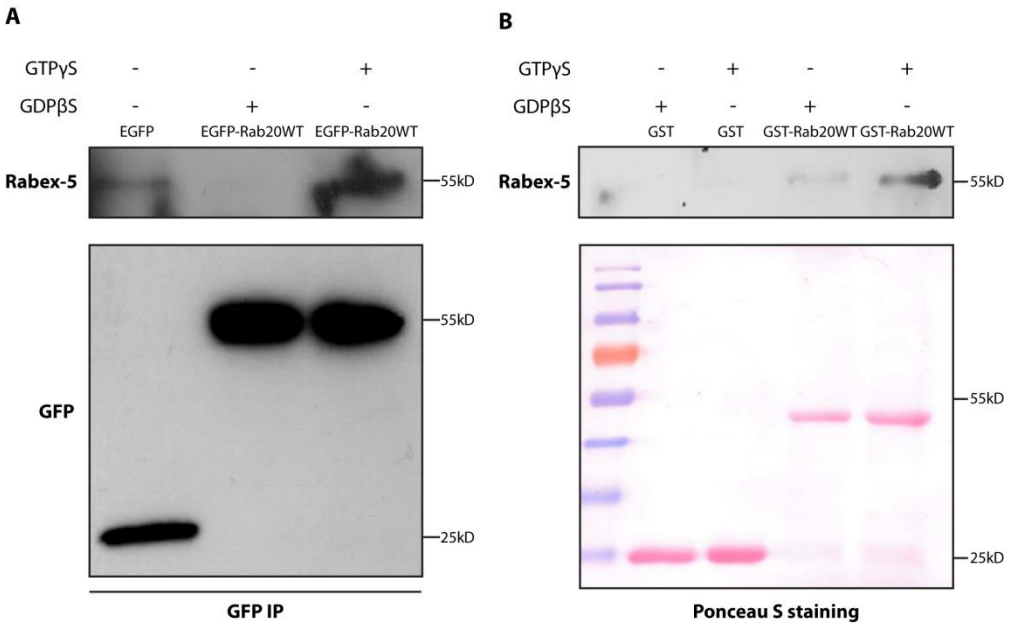

Fig. 3.48 Rabex-5 is an effector of Rab20. (A) Co-IP of Rabex-5 in stably expressing EGFP or EGFP-Rab20WT macrophages. EGFP-Rab20WT macrophages were lysed with lysis buffer supplemented with GTPγS or GDPβS. Rabex-5 was co-immunoprecipitated with GFP-Trap® beads and detected with Rabex-5 antibody. Anti-EGFP antibody was used as a control. **(B)** GST-Rab20WT pulldown with lysates of RAW264.7 macrophages. GST or GST-Rab20WT was immobilized on glutathione agarose beads and preloaded with GTPγS or GDPβS. The cell lysates were incubated with the beads for binding. After extensive washing, the proteins binding with GST-Rab20WT were collected and detected with Rabex-5 antibody. The ponceau S staining was used as a control.

Rabex-5 is recruited to phagosomes by Rab20

The finding that Rabex-5 is an effector of Rab20 raised the question whether Rabex-5 is recruited to phagosomes via Rab20. To answer this question, phagosomes were isolated from control or Rab20 stable knockdown macrophages with or without IFN-γ stimulation. To generate Rab20 stable knockdown macrophages, RAW264.7 macrophages were transfected with MISSION® shRNAs and stable transfected colonies were selected as described in material and methods. To test the knockdown efficiency, Western blot in cell lysates of different stable Rab20 knockdown macrophages was performed. From all the tested shRNAs, shRNA 2643 showed the best knockdown efficiency and hence macrophages stably expressing shRNA 2643 were used for phagosome purification (**Fig.3.49**). Western blot analysis of isolated phagosomes revealed that there was no Rab20 association to phagosomes in Rab20 knockdown

macrophages. Rabex-5 was indeed present on phagosomes in control macrophages and Rabex-5 association to phagosomes was slightly decreased in Rab20 knockdown macrophages. After IFN-γ treatment, Rabex-5 association to phagosomes significantly increased and the association was also impaired by Rab20 knockdown (**Fig.3.50**). This data clearly showed that Rabex-5 was recruited to phagosomes via Rab20. In agreement, IFN-γ stimulated Rab5 association to phagosomes was severely impaired in Rab20 knockdown macrophages, suggesting that the maintenance of Rab5 on early phagosomes depends on Rab20 recruitment. Taken together, the data presented here shows that the delay of phagosome maturation by Rab20 expression or IFN-γ treatment is mediated through Rabex-5 which in turns generates active Rab5 on phagosomes.

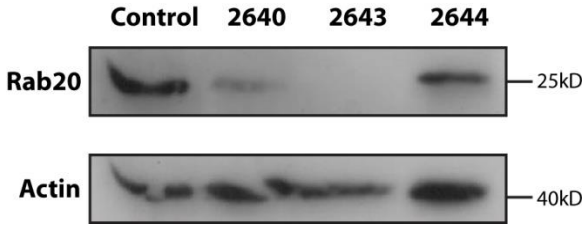

Fig. 3.49 Western blot analysis in cells knocked down with MISSION® shRNAs targeting Rab20. Macrophages stably transfected with different shRNAs were generated. Rab20 was detected in the different lysates using the antibody from Proteintech. Actin was used as the loading control.

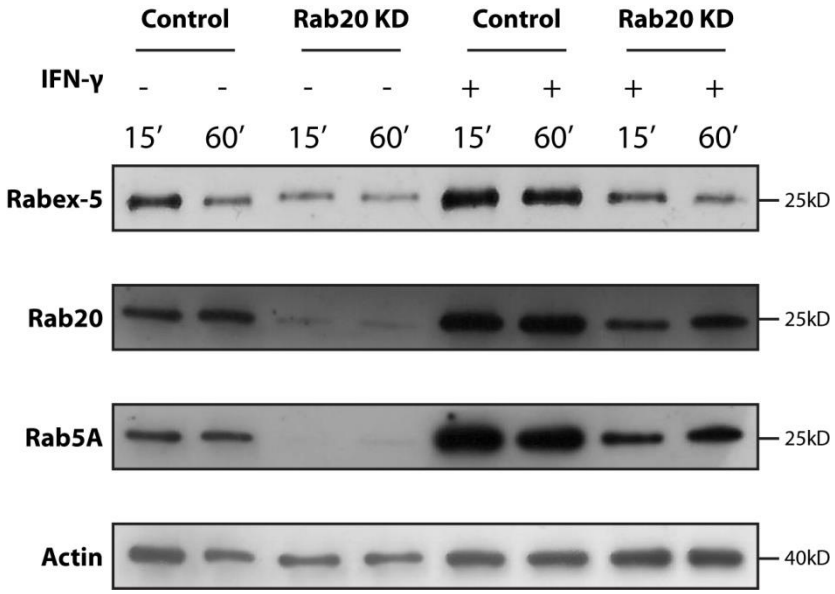

Fig. 3.50 Western blot of Rabex-5 with phagosomes in control or Rab20 knockdown macrophages with or without IFN-γ treatment. Control or Rab20 knockdown macrophages were grown without or with IFN-γ (200 Units/mL) for 16 hours and phagosomes were isolated after 60 min of pulsing and 15 or 60 min of chasing. Rabex-5 was detected with antibody from Sigma. Rab20 was detected with antibody from Proteintech. Actin was used as the loading control.

4. Discussion

Rab20 over-expression induces the enlargement of endosomes

It is known that the expression of specific active Rab GTPases induces enlargement of endocytic compartments. For example, expression of a GTPase-deficient Rab5 (Rab5Q79L) results in the formation of enlarged endosomes in baby hamster kidney (BHK) and HEp2 cells (now HeLa cells) (Stenmark H *et al*. 1994, Roberts RL *et al*. 1999). The enlarged vesicles induced by Rab5Q79L expression exhibit not only features of early endosomes but also late endosomes (Wegener CS *et al*. 2010). Rab22a expression in chinese hamster ovary (CHO) cells also induces enlarged early and late endosomal compartments (Mesa R *et al*. 2001). Here, it was found that Rab20WT was mainly localized in the CGN and TGN in RAW264.7 and bone marrow macrophages (**Fig. 3.1; Fig. 3.5; Fig. 3.6**). Enlarged vesicles were also observed in macrophages expressing the wild-type of Rab20, reminiscent to what is has been reported during the over-expression of Rab5Q79L and Rab22a wild-type. These enlarged vesicles were not observed in EGFP expressing cells, suggesting the formation of enlarged vesicles is induced by Rab20WT expression other than EGFP expression or the transfection reagent. Immunofluorescence experiments have demonstrated that EGFP-Rab20WT-positive giant vesicles co-localized with Rab5, showing characteristics of early endosomes (**Fig. 3.1**). This is further demonstrated by the colocalization of endogenous Rab20 with EEA1 (**Fig. 3.5; Fig. 3.8**). In addition, the Rab20-negative giant vesicles co-localized with the late endosome marker LAMP-2 (**Fig. 3.1**), suggesting that Rab20WT expression in RAW264.7 results in enlargement of both early endosomes and late endosomes that resembles the phenotype of Rab5Q79L expression. This result also implies that the maturation from early to late endosomes in Rab20 expressing macrophages is still proceeding and likely enhanced. Although the consequences of formation of these enlarged endosomes are not well understood, several reports have shown that the transferrin receptor recycling is impaired in Rab5Q79L expressing cells without affecting transferrin internalization (Stenmark H *et al*. 1994, Wegener CS *et al*. 2010). Therefore it is likely that Rab20WT expression may also result in delaying recycling of transferrin receptor or other receptors.

The enlarged vacuoles induced by Rab20 expression are due to the homotypic fusion

In vitro experiments with Rab5Q79L as well as live cell imaging indicated that the early endosome homotypic fusion in Rab5Q79L expressing BHK cells resulted in the formation of giant endosomes (Stenmark H *et al*. 1994, Roberts RL *et al*. 1999). Similar to Rab5Q79L, the fusion between Rab20-positive vacuoles in Rab20WT expressing macrophages was observed here by live cell imaging (**Fig. 3.10;**

Fig. 3.12). Furthermore, a striking Rab20-positive phagosome homotypic fusion was also seen in EGFP-Rab20 wild-type expressing macrophages (**Fig. 3.12**). The fusion between Rab20-positive phagosomes and Rab20-positive vacuoles was also observed (**Fig. 3.12**). Altogether, it is very likely that the enlarged vacuoles induced by Rab20 wild-type expression in macrophages are due to the homotypic fusion. Considering the comparable ability of Rab20 wild-type with the constitutively active mutant Rab5Q79L in stimulating the homotypic fusion, it could be possible that Rab20 wild-type is GTPase-deficient like Rab5Q79L. To answer this question, GTPase activity assay is required to determine the intrinsic GTPase activity of Rab20 wild-type.

Different Rab GTPases are localized on the same endosomes occupying distinct domains referred to as Rab domains (Sönnichsen B *et al*. 2000). In agreement with this model, some Rab20 “hot spots” on the membrane of the enlarged endosomes were observed, indicating Rab20 domains are also present on endosomes. Interestingly, these Rab20 “hot spots” reside in different areas with Rab5 and EEA1 on the same endosomes, suggesting that Rab20 occupies a different domain with Rab5 on early endosomes.

IFN-γ induces the enlargement of endosomes, resembling the phenotype of Rab20WT over-expression

It is well known that enlarged vacuoles are formed after IFN-γ treatment of macrophages; however the mechanism is still elusive (Montaner LJ *et al*. 1999). Enlarged vacuoles are also observed in RAW264.7 macrophages with IFN-γ stimulation compared to resting macrophages (**Fig. 3.8**). Some of the enlarged vesicles are positive for the early endosome marker EEA1 and the rest of the vesicles are labeled with the late endosomal marker LAMP-2 (**Fig. 3.8**). This is similar to the phenotype observed in macrophages expressing EGFP-Rab20 wild-type. Since Rab20 expression in macrophages is up-regulated with IFN-γ stimulation (**Fig. 3.7**), it is tempting to postulate that the increased amount of Rab20 induced by IFN-γ results in the enhanced homotypic fusion of endosomes, which finally leads to enlarged vacuoles. Although Rab5 could not be excluded from this process since its expression is also increased by IFN-γ in macrophages (Alvarez-Dominguez C and Stahl PD.1998), it may partially explain the mechanisms of how IFN-γ induces the formation of enlarged vacuoles.

Rab20 is an IFN-γ regulated Rab GTPase

It is important to understand how intracellular trafficking is coordinated with external immune stimuli. The expression of Rab GTPases, is modulated by different immune mediators and provides one potential mechanism (Pei G *et al*. 2012). Previous studies in this laboratory have shown that Rab20 expression in macrophages is up-regulated upon NF-κB activation induced by *M. smegmatis* infection (Gutierrez MG

et al. 2008). In this study, Rab20 expression significantly increased after IFN-γ stimulation in RAW264.7 and bone marrow macrophages, suggesting that Rab20 is an IFN-γ regulated Rab GTPase (**Fig. 3.7**). Similar with IFN-inducible GTPases, Rab20 lacks a glutamine (Q) at the position corresponding to residue 61 of Ras (Martens S and Howard J. 2006). It has been shown that mutations at the position of residue 61 of Ras results in much lower GTP hydrolysis (Der CJ *et al*. 1986). Therefore, it could be possible that Rab20 wild-type has a low intrinsic GTPase activity, similar with IFN-inducible GTPases. Sequence alignments with Ras and Rab GTPases have demonstrated that the helix α4 of Rab20 contains a 39 amino acid insertion in the region from residues 137 to 175 (Lütcke A *et al*. 1994, Pereira-Leal JB and Seabra MC. 2000). An insertion in Rac GTPase (residues 124-135) is implicated in its effector binding (Freeman JL *et al*. 1996). So it could be feasible that the unique insertion of Rab20 may confer it the ability to interact with some novel effectors. However, different mutation and deletion studies are required to address specifically these questions.

Macrophages activated by IFN-γ exhibit increased cell migration, enhanced ability to kill intracellular pathogens and improved antigen presentation (Mosser DM. 2003, Mosser DM and Edwards JP. 2008). It is therefore tempting to hypothesize that like IFN-inducible GTPases, Rab20 may be involved in these immune-related processes induced by IFN-γ. In agreement with this assumption, it has been reported that the transcription of Rab20 in dendritic cells is highly up-regulated upon different TLR ligands, such as LPS, poly I:C and zymosan (Torri A *et al*. 2010). Consistent with this notion, Rab20 has also been identified as one of the inflammatory signature genes (Torri A *et al*. 2010, Berry MP *et al*. 2010).

Rab20 association to early phagosomes is increased by IFN-γ

Rab20 is transiently associated to *S. aureus* and *M. tuberculosis* H37Rv containing phagosomes at 30 min of infection in macrophages (Seto S *et al*. 2011). Another study has demonstrated that Rab20 is associated to IgG-coated erythrocytes for approximately 10 min after internalization (Egami Y and Araki N 2012). In agreement with these observations, using two different approaches-Western blot and immunofluorescence, it was found that endogenous Rab20 was present on IgG-coated latex bead phagosomes and the kinetics of Rab20 association is similar to Rab5 (**Fig. 3.11**). Particularly, live cell imaging further demonstrated that EGFP-Rab20WT is only associated to phagosomes during the first 20 min of internalization (**Fig. 3.12**). In addition, Rab20 and Rab5 association to phagosomes is strongly induced by IFN-γ treatment (**Fig. 3.11**). These observations are consistent with phagosome proteomic studies showing that Rab20 association to phagosomes is increased by IFN-γ treatment (Trost M *et al*. 2009). As shown by live cell imaging, the fusion between Rab20-positive phagosomes and the fusion

between Rab20-positive phagosomes and Rab20-positive vacuoles are stimulated in EGFP-Rab20WT expressing macrophages (**Fig. 3.12**). It is therefore possible that the increased Rab20 association to phagosomes induced by IFN-γ may result from enhanced fusion.

The phagosome maturation is delayed by Rab20 association.

Previous studies suggested that Rab20 may function in phagosome maturation (Gutierrez MG *et al* 2008). Seto and co-workers have reported that LysoTracker acquisition and Cathepsin D recruitment to phagosomes decreased in cells expressing the dominant negative mutant Rab20T19N, indicating that Rab20 stimulates phagosome maturation. Another study has also shown that LysoTracker acquisition by IgG-coated erythrocyte phagosomes is delayed by Rab20T19N expression (Egami Y and Araki N 2012). In contrast, the data presented here showed that acquisition of LysoTracker Red by phagosomes was strikingly accelerated and the time required for reaching to the peak was significantly shortened by Rab20T19N expression (**Fig. 3.16**). Conversely, the starting point of LysoTracker Red acquisition by phagosomes was significantly delayed by Rab20WT association to phagosomes and the desired time for reaching to the plateau was also prolonged compared with EGFP expressing cells (**Fig. 3.15**). At least two points could explain the reasons for this discrepancy. First, observed differences might be due to the different nature of particles used for the target of phagocytosis in all these studies. The activation of different receptors during phagocytosis depends on the ligands on the surface of particles (Hoffmann E *et al*. 2010). The kinetics of phagosome maturation varies because different receptor-related signaling pathways are activated. The time of phagosomes fusing with lysosome differs from 30 min to hours (Aderem A and Underhill DM 1999). In the studies from Seto S *et al* and Egami Y, naked latex beads (0.7 μm of diameter) and rabbit IgG-opsonized erythrocytes were employed. In this study, mouse IgG-coated latex or polystyrene beads were used. Second, live cell imaging was employed in this study and the other studies used fixed cell immunofluorescence. To investigate dynamic processes such as phagosome maturation, methods with high time resolution are required. In immunofluorescence studies, it is difficult to keep the events of interest in different cells synchronized. So results from immunofluorescence actually represent events at different time points. By using live cell imaging, events of interest at single cell level in a synchronized way can be investigated. Altogether, the data presented here clearly demonstrate a role of Rab20 in delaying maturation of phagosomes.

PI3P association to phagosomes is prolonged by Rab20 association.

PI3P is associated to nascent phagosomes rapidly after phagosomes are sealed (Ellson CD *et al*. 2001). In this study, it was found that the association time of PI3P to phagosomes in macrophages is approximately 10 min which is consistent with a previous report (**Fig. 3.18**) (Vieira OV *et al*. 2001). In Rab20WT expressing macrophages, PI3P association to phagosomes is extended to 20 min by Rab20 association (**Fig. 3.19**). Conversely, its association to phagosomes in the dominant negative mutant Rab20T19N expressing macrophages is shortened to 5 min (**Fig. 3.20**). These results suggest that prolonged PI3P association by Rab20 association is correlated with the delayed phagosome maturation. It is also noteworthy that the initiation of PI3P association to phagosomes is not affected by either Rab20WT or Rab20T19N expression, suggesting that the initiation of PI3P generation is not influenced. There are two possibilities that could explain the prolonged association of PI3P to phagosomes. Firstly, the degradation of PI3P on phagosomes may be delayed by Rab20 association to phagosomes. It is in fact not clear how PI3P is cleared from the phagosomes. It has been reported that the time of PI3P association to phagosomes is increased to 20 min in FYVE finger-containing phosphoinositide kinase (PIKfyve) or phosphatase and tensin homolog (PTEN) deficient macrophages, arguing that PIKfyve and/or PTEN are involved in removing PI3P from phagosomes (Hazeki K *et al*. 2012). PIKfyve is a phosphatidylinositol metabolizing enzyme which generates PI(3,5)P from PI3P (Sbriassa D *et al*. 2002). Inhibition of PIKfyve functions by chemical inhibitors or siRNA knockdown induces the formation of enlarged vacuoles in different cells lines, resembling the phenotype reported here in cells expressing Rab20WT (Rutherford AC *et al*. 2006, Jefferies HB *et al*. 2008, de Lartigue J *et al*. 2009). Secondly, the production of PI3P on phagosomes may be prolonged by Rab20 association. PI3P is produced by class-III PI3K-hVPS34 which is an effector of Rab5 (Christoforidis S *et al*. 1999). Here it was found that Rab20 association to phagosomes also extends Rab5 association. Hence it is reasonable to propose that Rab20 association to phagosomes could also increase hVPS34 association, leading to increased duration of PI3P association to phagosomes.

It has been shown that phagosome maturation is blocked by inhibiting PI3P production (RA Fratti *et al*. 2001; OV Vieira *et al*. 2001). Several pathogens have evolved different strategies to modulate PI3P association to phagosomes and hence phagosome maturation. For example, *M. tuberculosis* secretes a lipid phosphatase, SapM, which hydrolyzes PI3P (Vergne I *et al*. 2005). This explains why PI3P is present on dead bacteria phagosomes other than live bacteria phagosomes. *In vitro,* SapM inhibits PI3P-dependent phagosome-late endosome fusion, suggesting SapM contributes to mycobacterial phagosome maturation arrest by hydrolyzing PI3P on the phagosomes (Vergne I *et al*. 2005). In addition, SopB (secreted effector protein B), a type 3 secretion system (T3SS) effector of *S. typhimurium* with

phosphoinositide phosphatase activity, is proposed to produce PI3P (Norris *et al*. 1998). Compared with wild type of *S. typhimurium*, PI3P association to *Salmonella*-containing vacuoles (SCVs) is strongly shortened by ΔSopB mutant. The intracellular survival is also impaired in the ΔSopB mutant, suggesting that the prolonged PI3P association to SCVs is import for *S. typhimurium* survival in the host (Mallo GV *et al*. 2008). These reports suggest a mechanism of modulating phagosome maturation by regulating PI3P association. In this study, it was found that PI3P association to phagosomes was enhanced by Rab20 association. Combining the data that Rab20 association delays phagosome maturation, it is conceivable that the enhanced PI3P association could serve as a mechanism for the delayed phagosome maturation.

Phagosome -early endosome fusion is increased by Rab20 expression

Recruitment of LAMP-1 into phagosomes is greatly decreased in cells expressing the dominant negative mutant of Rab5, indicating that the active form of Rab5 is required for phagosome maturation (Vieira OV *et al*. 2003). It is proposed that Rab5 association to phagosomes is required for Rab7 recruitment that in turn is required for the fusion of phagosomes with late endosomes/lysosomes (Vieira OV *et al*. 2003). However, enhanced association of Rab5 to phagosomes also induces arrest of phagosome maturation. For example, SopE that acts as a nucleotide exchange factor increases Rab5 association to *Salmonella* phagosomes, resulting in increased fusion of *Salmonella* phagosomes with early endosomes and impaired fusion with lysosomes *in vitro* (Mukherjee K *et al*. 2001, Madan R *et al*. 2008). In this study, it was found that Rab5 association to phagosomes increased by Rab20 association (**Fig. 3.23**), arguing that the increased Rab5 association contributes to the delayed maturation of phagosomes induced by Rab20 association.

Rab5 effectors, Rabaptin-5, EEA1 and hVPS34, are required for homotypic fusion of early endosomes (Stenmark H *et al*. 1995, Simonsen A *et al*. 1998, Christoforidis S *et al*. 1999). Since Rab5 association to phagosomes increased by Rab20WT association, it is predicted that the association of these Rab5 effectors also increases. So it could be possible that the fusion of phagosomes with early endosomes is enhanced by Rab20WT expression. To address this question, *in vitro* phagosome-early endosome fusion assay is needed.

In this work, it was observed that Rab5 recruitment to phagosomes proceeds earlier than Rab20, indicating that Rab5 is recruited upstream of Rab20. This is in agreement with the fact that Rab5 is localized to the plasma membrane (Bucci C *et al*. 1992). Different bioinformatics studies have shown

that Rab20 is closest relative to Rab5 (Buvelot Frei S *et al*. 2006, Schwartz SL *et al*. 2008). However, phagosome maturation is not affected by Rab5WT over-expression (**Fig. 3.32**), indicating Rab20 has a different function from Rab5 in phagosome maturation.

The delay in phagosome maturation is mediated through Rabex-5.

The recruitment of Rab5 to endosomes by Rabex-5 initiates the association of Rab5 effectors such as Rabaptin-5 and phosphoinositide kinase hVPS34, which in turn produces PI3P (Christoforidis S *et al*. 1999) and increase Rab5 on the endosomes. This forms the positive feedback loop of Rab5 activation (Zerial M and McBride H. 2001). In this study it is reported that Rabex-5 preferentially interacts with Rab20 (GTPγS) using both co-immunoprecipitation and GST pulldown assays (**Fig. 3.48**), clearly indicating Rabex-5 is an effector of Rab20. There are two pathways that promote Rabex-5 targeting to early endosomes. On one hand, Rabex-5 can directly target to early endosomes via an early endosome targeting (EET) domain or the motif interacting with ubiquitin (MIU) (Zhu H *et al*. 2007, Mattera R and Bonifacino JS. 2008). On the other hand, Rabex-5 is recruited to early endosomes by forming a complex with a Rab5 effector- Rabaptin-5 (Horiuchi H *et al*. 1997). Here as shown by western blot analysis of isolated phagosomes, Rabex-5 can be recruited to early phagosomes by directly interacting with Rab20 on the phagosomal membrane. This is the first evidence showing that Rabex-5 is associated to phagosomes. The data presented here also reveals a novel Rab20-dependent pathway for Rabex-5 targeting to early phagosomes and likely early endosomes as well. Rab5 association to phagosomes is dramatically reduced by Rab20 knockdown, suggesting Rab5 association to phagosomes requires Rabex-5 function. The induced Rab20 association to phagosomes after IFN-γ treatment brings more Rabex-5 and Rab5 to phagosomes. Because of the essential role of Rabex-5 and EEA1 in early endosome homotypic fusion, it is conceivable that the early endosome/phagosome homotypic fusion is stimulated by Rab20 expression. In fact, multiple fusion events such as homotypic fusion between Rab20-positive vacuoles/phagosomes and fusion of early phagosomes with early endosomes have been observed in macrophages expressing Rab20. As mentioned before, this also explains the formation of enlarged early endosomes induced by Rab20 over-expression or IFN-γ treatment. Therefore it is likely that Rab20 function in phagosomes operates as follow: First, when Rab20 is recruited to phagosomes via an IFN-γ induced pathway, it brings more Rabex-5 to phagosomes, which in turn converts more GDP-Rab5 into GTP-Rab5. This increases the recruitment of Rab5 effectors such as EEA1 and hVPS34, which produces more PI3P on phagosomes. In agreement with this model, Rab5 and PI3P association to phagosomes is prolonged by Rab20 association. Thus, Rab20 is involved in the positive feedback loop of Rab5 activation

and amplify this effect by recruiting Rabex-5. Altogether, the delayed maturation of phagosomes is mediated through Rabex-5 (**Figure 4.1**).

Potential routes of Rab20 trafficking to phagosomes

After Brefeldin A (BFA) treatment, there is almost no EGFP-Rab20WT recruitment to phagosomes. In addition, the delayed phagosome maturation by Rab20 expression is reversed by BFA treatment, suggesting that the delayed phagosome maturation by Rab20 expression is dependent on Rab20 association to phagosomes (**Fig. 3.33**). Then the remaining question is how Rab20 is trafficked to phagosomes. There are at least three possible routes related to Rab20 trafficking to phagosomes. First, Rab20 could be directly recruited to phagosomes from cytosol. When GTP associated to Rab GTPases is hydrolyzed to GDP, Rab GTPase is released into cytosol. The cytosolic Rab GTPases can be targeted to specific membrane with the help of GDI displacement factors (GDFs) or guanine exchange factors (GEFs) (Dirac-Svejstrup AB *et al*. 1997, Blümer J *et al*. 2013). In this study, Rab20 association to phagosomes was blocked by BFA treatment, suggesting that the direct recruitment from cytosol is not the major route for Rab20 association to phagosomes. Second, Rab20 is transported to phagosomes via post-Golgi vesicles. In this study, the formation of post-Golgi vesicles and their interaction with phagosomes were observed (**Fig. 3.34**), suggesting existence of this route. Third, Rab20 association to phagosomes could result from the fusion of phagosomes with Rab20-positive vacuoles/endosomes, as shown in **Fig. 3.12**. Because post-Golgi tubules and early endosomes are very dynamic, fusing with each other, it could be possible that both two routes contribute to Rab20 trafficking to phagosomes.

There are several adaptor proteins, for example, AP-1, GGA and sortilin, regulating trafficking from the Golgi complex to endosomes and phagosomes (Bonifacino JS and Traub LM *et al*. 2003, Puertollano R *et al*. 2001, Zhu Y *et al*. 2001, Wähe A *et al*. 2010). For the cargo proteins they are recognized by adaptor proteins with different sorting motifs. It is not known by which adaptor protein Rab20 is transported from *trans*-Golgi to phagosome. However, it is tempting to postulate that Rab20 may facilitate the post-Golgi vesicles fusing with early phagosomes by recruiting Rab5 and PI3P.

Mycobacterial killing is not affected by Rab20 expression

A previous study has suggested that Rab20 may have a function in mycobacterial killing by macrophages (Seto S *et al*. 2011). Moreover, several reports have shown that Rab20 expression is stimulated against various infections (Goldmann O *et al*. 2007, Tchatalbachev S *et al*. 2010, Mahapatra S *et al*. 2010 Cortez KJ *et al*. 2006). In this study, *M. bovis* BCG was used to investigate the role of Rab20 in mycobacterial

killing. Although Rab20 is also associated to mycobacteria-containing phagosomes, the killing is not significantly affected by Rab20 expression (**Fig. 3.46**). Considering that the delayed phagosome maturation by Rab20 occurs during first 1-2 hours, the lack of effect of Rab20 in killing could be due to the fact that mycobacterium grows very slowly, with a generation time of approximately 24 hours. Interestingly, during the infection by *M. bovis* BCG spacious phagosomes were observed. It has been shown that *S. typhimurium* persists in the spacious phagosomes, which contributes to its survival (Alpuche-Aranda CM *et al*. 1994). Similar phenotype is also shown with *L. monocytogenes* (Birmingham CL *et al*. 2008). Therefore, it is possible that Rab20 may contribute to the survival of *M. bovis* BCG by forming the spacious phagosomes. The mechanism for the formation of spacious phagosomes is not well studied. As shown by live cell imaging that the fusion between phagosomes and Rab20-positive vacuoles is stimulated by Rab20 expression, it is speculated that Rab20 contributes to the formation of spacious phagosomes by increasing the fusion of phagosomes with endosomes. Since there is no effect in killing, the physiological function regulated by Rab20 should be then related to other immune process regulated by IFN-γ, e.g. antigen presentation.

Early phagosome maturation delayed by IFN-γ and antigen presentation

It has been demonstrated that major histocompatibility complex class II (MHC II), H2M (a non-classical MHC II in mouse) and invariant chain are acquired by phagosomes in peritoneal macrophages (Ramachandra L *et al*. 1999). Moreover, the functional MHC II: immunogenic peptide complexes can be formed for stimulating T cells in macrophages (Ramachandra L *et al*. 1999). Several components of the molecular machinery required for cross presentation are present on phagosomes of J774 macrophages (Houde M *et al*. 2003). Moreover, the proliferation of OT-1 $CD8^+$ T cells (it specifically recognizes the complex of MHC I and OVA peptide) is stimulated by macrophages that have internalized OVA-beads (Houde M *et al*. 2003). These studies suggest that macrophages are capable for antigen processing and presentation although maybe they are not as efficient as dendritic cells (Hume DA. 2008). The prevailing concept is that macrophages are committed to remove pathogens or apoptotic cells. So after phagocytosis, the antigens are completely degraded in a very short time. However for efficient antigen presentation, antigen should be partially degraded (Delamarre L *et al*. 2005, Delamarre L *et al*. 2006, Savina A *et al*. 2006). Different from macrophages, the balance between antigen degradation and antigen processing is very well tuned by regulating phagosome proteolysis and acidification in dendritic cells. Delamarre *et al*. have shown that the expression of lysosomal proteases, such as Cathepsin L, S, D, B and asparagines endopeptidase, is much higher in macrophages than dendritic cells. The limited

lysosomal proteolysis in dendritic cells results in efficient antigen presentation (Delamarre L *et al*. 2005). NOX2 is responsible for the generation of ROS in phagosomes (Kotsias F *et al*. 2013). Recently, it has been reported that the phagosomal pH is remarkably decreased in gp91 (one of subunits of NOX2) knockout dendritic cells and the cross-presentation is compromised with increased antigen degradation, suggesting the alkalinization of phagosomes in dendritic cells by NOX2 is required for efficient cross-presentation (Savina A *et al*. 2006). So it has been proposed that the neutral pH and low proteolytic activity of phagosomes favor antigen presentation.

There is accumulating evidence unveiling that at early stages of phagosome maturation is delayed by IFN-γ (Tsang AW *et al*. 2000, Yates RM *et al*. 2007, Jutras I *et al*. 2008, Trost M *et al*. 2009). Tsang and coworkers have shown that the acquisition of LAMP-1 and lysosomal cargos by IgG-coated erythrocyte is significantly delayed in IFN-γ activated bone marrow macrophages during the first 30 min (Tsang AW *et al*. 2000). Yates and coworkers have employed the pH-sensitive fluorochrome carboxyflurescein to measure the pH of phagosomes and demonstrated that the acidification of mannosylated bead-containing phagosomes in the first 1 hour is slower in IFN-γ activated bone marrow macrophages (Yates RM *et al*. 2007). Phagolysosome fusion is also delayed in the first 2 hours by IFN-γ. However, phagosomes in IFN-γ activated macrophages continue to fuse with lysosomes for up to 5 hours, resulting in phagolysosomes with higher levels of lysosomal proteins (Yates RM *et al*. 2007). It is also shown that phagosomal proteolysis, lipolysis and β-glactosidase activity are significantly reduced in activated macrophages (Yates RM *et al*. 2007). However, it is also known that maturation of phagosomes containing pathogens such as *M. bovis* BCG, *M. avium, M. paratuberculosis*, *L. pneumophila* or *S. typhimurium* is accelerated in IFN-γ activated macrophages (Vie LE *et al*. 1998, Schaible UE *et al*. 1998, Hostetter JM *et al*. 2002, Santic M *et al*. 2005, McCollister BD *et al*. 2005). There are two possible reasons that could explain this discrepancy. First, in the the reports showing phagosome maturation accelerated by IFN-γ, the cells are usually infected with pathogens for several hours. So phagosomes in these reports are in general at later stages. It has been shown that phagosomes acquire more lysosomal proteins after 5 hours (Yates RM *et al*. 2007). Second, alternative signaling induced by the pathogens may contribute to the increased phagosome maturation. For example, autophagy can be induced by *M. tuberculosis* (Watson RO *et al*. 2012). This pathway can contribute to the increased phagosome maturation (Gutierrez MG *et al*. 2004). Therefore, it is reasonable to hypothesize that IFN-γ may reprogram phagosomes at early stages to favor the antigen presentation. However, this remains to be formally proved. Interestingly, phagosome proteome studies have demonstrated that many proteins involved in MHC II and MHC I antigen presentation are recruited into phagosomes by IFN-γ, suggesting

antigen presentation is regulated by IFN-γ in macrophages. The association of various hydrolases and proteases to phagosomes is decreased by IFN-γ, indicating the degradative activity of phagosomes is reduced by IFN-γ in macrophages. NOX2 negatively regulates phagosome acidification (Savina A *et al*. 2006). Its association to phagosomes is increased by IFN-γ, suggesting phagosome acidification is impaired by IFN-γ (Jutras I *et al*. 2008). In contrast, EEA1 association to the phagosomes is increased by IFN-γ, with decreased association of LAMP1, suggesting that phagosome fusion with early endosomes is stimulated by IFN-γ (Jutras I *et al*. 2008, Trost M *et al*. 2009).

In this study, it is shown that phagosome maturation is delayed by IFN-γ correlating this with an increase in Rab20 expression (**Fig. 3.15, 3.27**). In macrophages expressing the dominant negative mutant Rab20T19N, phagosome maturation was not affected by IFN-γ treatment (**Fig. 3.42**). In macrophages knocked down for Rab20, the phagosome maturation was delayed by IFN-γ (**Fig. 3.44**), which is not perfectly fit with the data of Rab20T19N. Western blot in this study has shown that Rab20 is efficiently knocked down without IFN-γ treatment. However, the protein level of Rab20 in macrophages knockdown for Rab20 after IFN-γ treatment is even higher than in resting macrophages without Rab20 knockdown. The same phenomenon also has been observed for an IFN-inducible GTPase-hGBP-1 (Tietzel I *et al*. 2009). Thus, the delay in phagosome maturation by IFN-γ in cells knockdown for Rab20 is likely due to the high protein level of Rab20. For shRNA knockdown, the shRNA is first transcribed inside cells and then processed into siRNA which induces mRNA degradation. Rab20, as an IFN-γ regulated protein, its mRNA is actively produced upon IFN-γ stimulation. Therefore, the siRNA targeted Rab20 may not be enough to cause knockdown. This may explain the high protein level of Rab20 in macrophages knockdown for Rab20 after IFN-γ treatment. These results strongly suggest that the delaying of phagosome maturation by IFN-γ treatment is Rab20 dependent. Since Rab5 expression and association to phagosomes is increased by IFN-γ treatment (Alvarez-Dominguez C and Stahl PD. 1998), it is most likely that other Rab GTPases are also involved in delaying of phagosome maturation by IFN-γ. Given that a delay in phagosome maturation by IFN-γ could eventually favor antigen presentation in macrophages (Jutras I *et al*. 2008, Trost M *et al*. 2009), it is tempting to propose that Rab20 may function in antigen presentation. Several lines of evidence support this hypothesis. First, the phagosome maturation is delayed by Rab20 expression. Second, invariant chain (Ii) is crucial for the transport of MHC II from the ER to the Golgi and to late endosomes (Sercarz EE and Maverakis E. 2003). The expression of Ii also induces enlarged endosomes and delayed endosome maturation, which increases the half-life of MHC II (Gorvel JP *et al*. 1995, Stang E and Bakke O. 1997, Landsverk OJ *et al*. 2010). Third, both Rab20 and invariant chain association to phagosomes is increased by IFN-γ (Trost M *et al*. 2009).

However, the physiological role of Rab20, especially in antigen presentation, need to be further investigated.

Conclusions

Rab20 is localized in the Golgi complex and early endosomes/phagosomes. Its expression delays phagosome maturation without affecting mycobacterial killing. Rab20 recruits its effector Rabex-5 to phagosomes in an IFN-γ dependent manner which in turn increases Rab5 and PI3P association to phagosomes, leading to stimulated homotypic fusion of early endosomes or phagosomes. The IFN-γ delayed maturation of phagosomes is dependent on Rab20 and mediated via a Rab20/Rabex-5 pathway. This is shown in the model of **Fig. 4.1**.

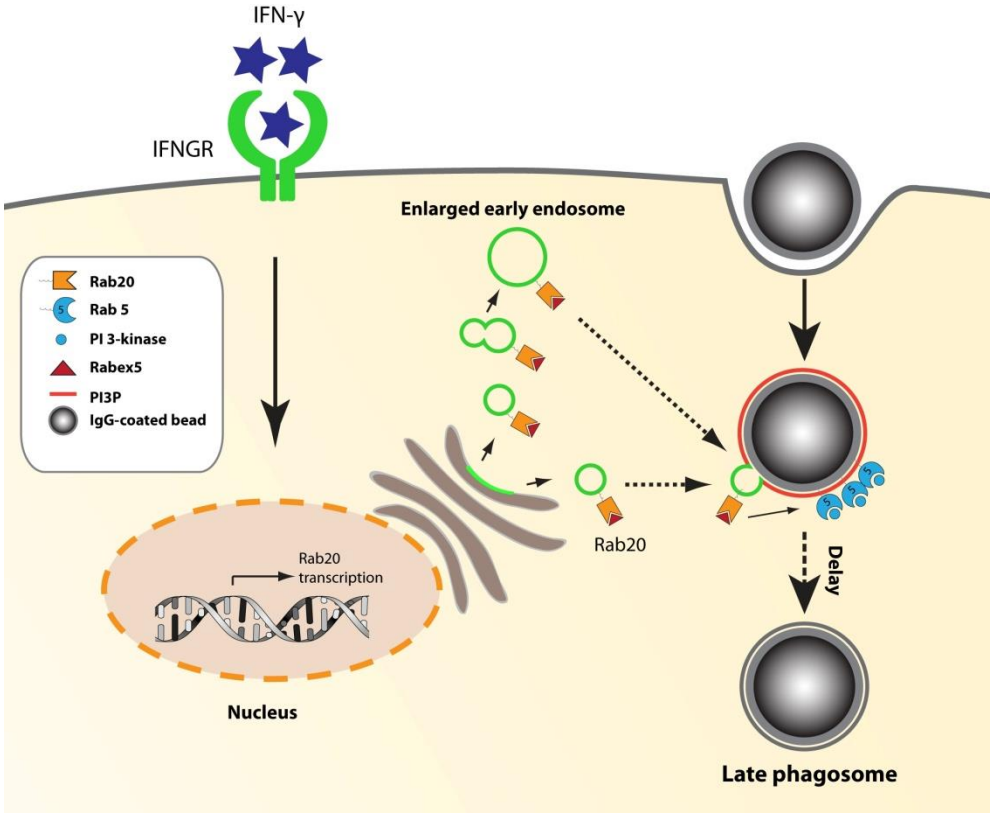

Fig. 4.1 The working model of Rab20 functions in phagosome maturation. Rab20 is mainly localized in the Golgi complex. It is also localized to early endosomes and phagosomes. After IFN-γ stimulation, Rab20 expression is highly increased. By recruiting the GEF of Rab5, Rab20 stimulates homotypic fusion of early endosomes, forming enlarged early endosomes. Rabex-5 is also recruited to phagosomes by Rab20. Rabex-5 association to phagosomes stimulates Rab5 activation on phagosomes, which also brings more Rab5 effectors, such as Rabaptin-5, PI3K and EEA1. The increased association of Rab5 and its effectors to phagosomes results in stimulated homotypic fusion of Rab20-positive phagosomes with Rab20-positive endosomes. It is also possible that Rab20 is directly transported to phagosomes via a post-Golgi route. Altogether, the delayed maturation of phagosomes by IFN-γ treatment or Rab20 expression is mediated through Rabex-5.

5. Outlook

In this study the role and mechanisms of Rab20 in phagosome maturation were investigated. It is shown here for first time that Rab20 association to phagosomes delays phagosome maturation and Rabex-5, as an effector of Rab20, functions in the Rab20-dependent delay of phagosome maturation. Based on these findings, the further investigation can continue on four aspects; 1) elucidating the mechanisms of Rab20 and Rabex-5 interaction, 2) identification of other effectors of Rab20, 3) investigating the mechanisms of Rab20 post-Golgi trafficking, 4) further investigating the physiological role of Rab20.

Rabex-5 domains include the A20-like zinc-finger (ZnF), the motif interacting with ubiquitin (MIU), the GEF catalytic core, the amphipatic helix and a C-terminal proline-rich region (PR) (Mattera R and Bonifacino JS. 2008). It has been shown that the GEF catalytic core is responsible for converting GDP-Rab5 into GTP-Rab5 (Delprato A *et al*. 2004). The amphipatic helix interacts with Rabaptin-5 (Mattera *et al*. 2006). The MIU is responsible for direct early endosome targeting by binding ubiquitinated cargos (Mattera R and Bonifacino JS. 2008). So it would be interesting to elucidate which region of Rabex-5 is involved in binding Rab20 by Co-IP using Rabex-5 mutants with different deletions. On the other hand, region(s) of Rab20 responsible for recruiting Rabex-5 are also interesting to be identified.

Sequence alignment revealed that there is a unique insertion region only in Rab20. Previous studies have demonstrated that the insertion region in Rac GTPase is responsible for the effector binding (Freeman JL *et al*. 1996). An attractive idea would be that this unique region may interact with some novel effector. Additionally, given that Rab20 stimulates the homotypic fusion of early endosomes/phagosomes, other proteins such as tethering factor and SNAREs may also interact with Rab20. By *in vitro* GST-pulldown, other effectors or binding partners of Rab20 will be identified.

The experiments using BFA in this study has revealed the existence of a putative post-Golgi route of Rab20. AP-1, GGA and sortilin, are transported from the Golgi complex to endosomes and phagosomes. They recognize different sorting motifs of cargo proteins (Bonifacino JS and Traub LM *et al*. 2003, Puertollano R *et al*. 2001, Zhu Y *et al*. 2001, Wähe A *et al*. 2010). The remaining questions here are which adaptor protein(s) are involved in Rab20 post-Golgi trafficking and how Rab20 is recognized. Several sorting motifs are implicated in Rab20. By Co-IP with mutants in these predicted motifs, these questions could be hopefully answered.

Last point but the most important one, is about the physiological role of Rab20. As shown here, Rab20 expression delays phagosome maturation. It has been speculated that Rab20 function may favor antigen presentation. The role of Rab20 in antigen presentation, if there is one for this GTPase, will be finally elucidated by performing antigen presentation assays and perhaps comparing macrophages vs. dendritic cells.

6. References

1. Tokarev A. A., Alfonso A. & Segev N. Overview of Intracellular Compartments and Trafficking Pathways, in *Trafficking Inside Cells: Pathways, Mechanisms and Regulation*. (Springer, New York; 2009).
2. Bruce A., Johnson A., Lewis J., Raff M., Roberts K. & Walter P. *Molecular Biology of the Cell*. (Garland Science, New York; 2007).
3. Palade, G. Intracellular aspects of the process of protein synthesis. *Science* **189**, 347-358 (1975).
4. Rapoport, T.A. Protein translocation across the eukaryotic endoplasmic reticulum and bacterial plasma membranes. *Nature* **450**, 663-669 (2007).
5. Swanton, E. & Bulleid, N.J. Protein folding and translocation across the endoplasmic reticulum membrane. *Mol Membr Biol* **20**, 99-104 (2003).
6. Braakman, I. & Bulleid, N.J. Protein folding and modification in the mammalian endoplasmic reticulum. *Annual review of biochemistry* **80**, 71-99 (2011).
7. Harter, C. & Wieland, F. The secretory pathway: mechanisms of protein sorting and transport. *Biochimica et biophysica acta* **1286**, 75-93 (1996).
8. Bonifacino, J.S. & Traub, L.M. Signals for sorting of transmembrane proteins to endosomes and lysosomes. *Annual review of biochemistry* **72**, 395-447 (2003).
9. Lefrancois, S., Zeng, J., Hassan, A.J., Canuel, M. & Morales, C.R. The lysosomal trafficking of sphingolipid activator proteins (SAPs) is mediated by sortilin. *EMBO J* **22**, 6430-6437 (2003).
10. Ni, X. & Morales, C.R. The lysosomal trafficking of acid sphingomyelinase is mediated by sortilin and mannose 6-phosphate receptor. *Traffic* **7**, 889-902 (2006).
11. Wähe, A. *et al.* Golgi-to-phagosome transport of acid sphingomyelinase and prosaposin is mediated by sortilin. *Journal of cell science* **123**, 2502-2511 (2010).
12. Maxfield, F.R. & McGraw, T.E. Endocytic recycling. *Nature reviews. Molecular cell biology* **5**, 121-132 (2004).
13. Lombardi, D. *et al.* Rab9 functions in transport between late endosomes and the trans Golgi network. *The EMBO journal* **12**, 677-682 (1993).
14. Kirchhausen, T. Three ways to make a vesicle. *Nature reviews. Molecular cell biology* **1**, 187-198 (2000).
15. Chou, L.Y., Ming, K. & Chan, W.C. Strategies for the intracellular delivery of nanoparticles. *Chem Soc Rev* **40**, 233-245 (2011).
16. Doherty, G.J. & McMahon, H.T. Mechanisms of endocytosis. *Annual review of biochemistry* **78**, 857-902 (2009).
17. McMahon, H.T. & Boucrot, E. Molecular mechanism and physiological functions of clathrin-mediated endocytosis. *Nature reviews. Molecular cell biology* **12**, 517-533 (2011).
18. Fotin, A. *et al.* Molecular model for a complete clathrin lattice from electron cryomicroscopy. *Nature* **432**, 573-579 (2004).
19. Rappoport, J.Z. Focusing on clathrin-mediated endocytosis. *The Biochemical journal* **412**, 415-423 (2008).
20. Pelkmans, L. & Helenius, A. Endocytosis via caveolae. *Traffic* **3**, 311-320 (2002).
21. Le Roy, C. & Wrana, J.L. Clathrin- and non-clathrin-mediated endocytic regulation of cell signalling. *Nat Rev Mol Cell Biol* **6**, 112-126 (2005).
22. Kiss, A.L. & Botos, E. Endocytosis via caveolae: alternative pathway with distinct cellular compartments to avoid lysosomal degradation? *Journal of cellular and molecular medicine* **13**, 1228-1237 (2009).

23. Drab, M. *et al.* Loss of caveolae, vascular dysfunction, and pulmonary defects in caveolin-1 gene-disrupted mice. *Science* **293**, 2449-2452 (2001).
24. Sowa, G., Pypaert, M., Fulton, D. & Sessa, W.C. The phosphorylation of caveolin-2 on serines 23 and 36 modulates caveolin-1-dependent caveolae formation. *Proceedings of the National Academy of Sciences of the United States of America* **100**, 6511-6516 (2003).
25. Li, S., Seitz, R. & Lisanti, M.P. Phosphorylation of caveolin by src tyrosine kinases. The alpha-isoform of caveolin is selectively phosphorylated by v-Src in vivo. *J Biol Chem* **271**, 3863-3868 (1996).
26. Pelkmans, L., Püntener, D. & Helenius, A. Local actin polymerization and dynamin recruitment in SV40-induced internalization of caveolae. *Science (New York, N.Y.)* **296**, 535-539 (2002).
27. Oh, P., McIntosh, D.P. & Schnitzer, J.E. Dynamin at the neck of caveolae mediates their budding to form transport vesicles by GTP-driven fission from the plasma membrane of endothelium. *J Cell Biol* **141**, 101-114 (1998).
28. Henley, J.R., Krueger, E.W., Oswald, B.J. & McNiven, M.A. Dynamin-mediated internalization of caveolae. *J Cell Biol* **141**, 85-99 (1998).
29. Pelkmans, L., Kartenbeck, J. & Helenius, A. Caveolar endocytosis of simian virus 40 reveals a new two-step vesicular-transport pathway to the ER. *Nat Cell Biol* **3**, 473-483 (2001).
30. Puri, V. *et al.* Clathrin-dependent and -independent internalization of plasma membrane sphingolipids initiates two Golgi targeting pathways. *J Cell Biol* **154**, 535-547 (2001).
31. Jones, A.T. Macropinocytosis: searching for an endocytic identity and role in the uptake of cell penetrating peptides. *Journal of cellular and molecular medicine* **11**, 670-684 (2007).
32. Lim, J.P. & Gleeson, P.A. Macropinocytosis: an endocytic pathway for internalising large gulps. *Immunol Cell Biol* **89**, 836-843 (2011).
33. Haigler, H.T., McKanna, J.A. & Cohen, S. Direct visualization of the binding and internalization of a ferritin conjugate of epidermal growth factor in human carcinoma cells A-431. *J Cell Biol* **81**, 382-395 (1979).
34. Racoosin, E.L. & Swanson, J.A. Macrophage colony-stimulating factor (rM-CSF) stimulates pinocytosis in bone marrow-derived macrophages. *J Exp Med* **170**, 1635-1648 (1989).
35. Sallusto, F., Cella, M., Danieli, C. & Lanzavecchia, A. Dendritic cells use macropinocytosis and the mannose receptor to concentrate macromolecules in the major histocompatibility complex class II compartment: downregulation by cytokines and bacterial products. *J Exp Med* **182**, 389-400 (1995).
36. Feliciano, W.D., Yoshida, S., Straight, S.W. & Swanson, J.A. Coordination of the Rab5 cycle on macropinosomes. *Traffic* **12**, 1911-1922 (2011).
37. Schnatwinkel, C. *et al.* The Rab5 effector Rabankyrin-5 regulates and coordinates different endocytic mechanisms. *PLoS biology* **2**, E261-E261 (2004).
38. Sun, P. *et al.* Small GTPase Rah/Rab34 is associated with membrane ruffles and macropinosomes and promotes macropinosome formation. *The Journal of biological chemistry* **278**, 4063-4071 (2003).
39. Lim, J.P., Wang, J.T.H., Kerr, M.C., Teasdale, R.D. & Gleeson, P.A. A role for SNX5 in the regulation of macropinocytosis. *BMC cell biology* **9**, 58-58 (2008).
40. Wang, J.T.H. *et al.* The SNX-PX-BAR family in macropinocytosis: the regulation of macropinosome formation by SNX-PX-BAR proteins. *PloS one* **5**, e13763-e13763 (2010).
41. Aderem, A. & Underhill, D.M. Mechanisms of phagocytosis in macrophages. *Annual review of immunology* **17**, 593-623 (1999).
42. Fairn, G.D. & Grinstein, S. How nascent phagosomes mature to become phagolysosomes. *Trends in immunology* **33**, 397-405 (2012).

43. Flannagan, R.S., Jaumouillé, V. & Grinstein, S. The cell biology of phagocytosis. *Annual review of pathology* **7**, 61-98 (2012).
44. Greenberg, S. & Grinstein, S. Phagocytosis and innate immunity. *Current opinion in immunology* **14**, 136-145 (2002).
45. Howell, G.J., Holloway, Z.G., Cobbold, C., Monaco, A.P. & Ponnambalam, S. Cell biology of membrane trafficking in human disease. *International review of cytology* **252**, 1-69 (2006).
46. Walling, H.W., Baldassare, J.J. & Westfall, T.C. Molecular aspects of Huntington's disease. *Journal of neuroscience research* **54**, 301-308 (1998).
47. Gauthier, L.R. *et al.* Huntingtin controls neurotrophic support and survival of neurons by enhancing BDNF vesicular transport along microtubules. *Cell* **118**, 127-138 (2004).
48. Alix, E., Mukherjee, S. & Roy, C.R. Subversion of membrane transport pathways by vacuolar pathogens. *The Journal of cell biology* **195**, 943-952 (2011).
49. Vergne, I. *et al.* Mechanism of phagolysosome biogenesis block by viable Mycobacterium tuberculosis. *Proceedings of the National Academy of Sciences of the United States of America* **102**, 4033-4038 (2005).
50. Vergne, I. *et al.* Mycobacterium tuberculosis phagosome maturation arrest: mycobacterial phosphatidylinositol analog phosphatidylinositol mannoside stimulates early endosomal fusion. *Mol Biol Cell* **15**, 751-760 (2004).
51. McMahon, H.T. & Mills, I.G. COP and clathrin-coated vesicle budding: different pathways, common approaches. *Curr Opin Cell Biol* **16**, 379-391 (2004).
52. Bonifacino, J.S. & Glick, B.S. The mechanisms of vesicle budding and fusion. *Cell* **116**, 153-166 (2004).
53. Langford, G.M. Actin- and microtubule-dependent organelle motors: interrelationships between the two motility systems. *Curr Opin Cell Biol* **7**, 82-88 (1995).
54. Ross, J.L., Ali, M.Y. & Warshaw, D.M. Cargo transport: molecular motors navigate a complex cytoskeleton. *Curr Opin Cell Biol* **20**, 41-47 (2008).
55. Cai, H., Reinisch, K. & Ferro-Novick, S. Coats, tethers, Rabs, and SNAREs work together to mediate the intracellular destination of a transport vesicle. *Developmental cell* **12**, 671-682 (2007).
56. Honing, S. *et al.* Phosphatidylinositol-(4,5)-bisphosphate regulates sorting signal recognition by the clathrin-associated adaptor complex AP2. *Molecular cell* **18**, 519-531 (2005).
57. Shih, W., Gallusser, A. & Kirchhausen, T. A clathrin-binding site in the hinge of the beta 2 chain of mammalian AP-2 complexes. *J Biol Chem* **270**, 31083-31090 (1995).
58. Stamnes, M.A. & Rothman, J.E. The binding of AP-1 clathrin adaptor particles to Golgi membranes requires ADP-ribosylation factor, a small GTP-binding protein. *Cell* **73**, 999-1005 (1993).
59. Donaldson, J.G., Cassel, D., Kahn, R.A. & Klausner, R.D. ADP-ribosylation factor, a small GTP-binding protein, is required for binding of the coatomer protein beta-COP to Golgi membranes. *Proceedings of the National Academy of Sciences of the United States of America* **89**, 6408-6412 (1992).
60. Barlowe, C. & Schekman, R. SEC12 encodes a guanine-nucleotide-exchange factor essential for transport vesicle budding from the ER. *Nature* **365**, 347-349 (1993).
61. Zanetti, G., Pahuja, K.B., Studer, S., Shim, S. & Schekman, R. COPII and the regulation of protein sorting in mammals. *Nature cell biology* **14**, 20-28 (2012).
62. Touchot, N., Chardin, P. & Tavitian, A. Four additional members of the ras gene superfamily isolated by an oligonucleotide strategy: molecular cloning of YPT-related cDNAs from a rat brain library. *Proceedings of the National Academy of Sciences of the United States of America* **84**, 8210-8214 (1987).

63. Schmitt, H.D., Wagner, P., Pfaff, E. & Gallwitz, D. The ras-related YPT1 gene product in yeast: a GTP-binding protein that might be involved in microtubule organization. *Cell* **47**, 401-412 (1986).
64. Salminen, a. & Novick, P.J. A ras-like protein is required for a post-Golgi event in yeast secretion. *Cell* **49**, 527-538 (1987).
65. Zerial, M. & McBride, H. Rab proteins as membrane organizers. *Nature reviews. Molecular cell biology* **2**, 107-117 (2001).
66. Stenmark, H. Rab GTPases as coordinators of vesicle traffic. *Nature reviews. Molecular cell biology* **10**, 513-525 (2009).
67. Bock, J.B., Matern, H.T., Peden, A.A. & Scheller, R.H. A genomic perspective on membrane compartment organization. *Nature* **409**, 839-841 (2001).
68. Diekmann, Y. *et al.* Thousands of rab GTPases for the cell biologist. *PLoS computational biology* **7**, e1002217-e1002217 (2011).
69. Stenmark, H. & Olkkonen, V.M. The Rab GTPase family. *Genome biology* **2**, REVIEWS3007 (2001).
70. Dumas, J.J., Zhu, Z., Connolly, J.L. & Lambright, D.G. Structural basis of activation and GTP hydrolysis in Rab proteins. *Structure (London, England : 1993)* **7**, 413-423 (1999).
71. Stroupe, C. & Brunger, A.T. Crystal structures of a Rab protein in its inactive and active conformations. *Journal of molecular biology* **304**, 585-598 (2000).
72. Milburn, M.V. *et al.* Molecular switch for signal transduction: structural differences between active and inactive forms of protooncogenic ras proteins. *Science* **247**, 939-945 (1990).
73. Krengel, U. *et al.* Three-dimensional structures of H-ras p21 mutants: molecular basis for their inability to function as signal switch molecules. *Cell* **62**, 539-548 (1990).
74. Pereira-Leal, J.B. & Seabra, M.C. The mammalian Rab family of small GTPases: definition of family and subfamily sequence motifs suggests a mechanism for functional specificity in the Ras superfamily. *Journal of molecular biology* **301**, 1077-1087 (2000).
75. Moore, I., Schell, J. & Palme, K. Subclass-specific sequence motifs identified in Rab GTPases. *Trends in biochemical sciences* **20**, 10-12 (1995).
76. Ostermeier, C. & Brunger, A.T. Structural basis of Rab effector specificity: crystal structure of the small G protein Rab3A complexed with the effector domain of rabphilin-3A. *Cell* **96**, 363-374 (1999).
77. Alexandrov, K., Horiuchi, H., Steele-Mortimer, O., Seabra, M.C. & Zerial, M. Rab escort protein-1 is a multifunctional protein that accompanies newly prenylated rab proteins to their target membranes. *The EMBO journal* **13**, 5262-5273 (1994).
78. Anant, J.S. *et al.* Mechanism of Rab geranylgeranylation: formation of the catalytic ternary complex. *Biochemistry* **37**, 12559-12568 (1998).
79. Ullrich, O. *et al.* Rab GDP dissociation inhibitor as a general regulator for the membrane association of rab proteins. *The Journal of biological chemistry* **268**, 18143-18150 (1993).
80. Dirac-Svejstrup, A.B., Sumizawa, T. & Pfeffer, S.R. Identification of a GDI displacement factor that releases endosomal Rab GTPases from Rab-GDI. *The EMBO journal* **16**, 465-472 (1997).
81. Moya, M., Roberts, D. & Novick, P. DSS4-1 is a dominant suppressor of sec4-8 that encodes a nucleotide exchange protein that aids Sec4p function. *Nature* **361**, 460-463 (1993).
82. Strom, M., Vollmer, P., Tan, T.J. & Gallwitz, D. A yeast GTPase-activating protein that interacts specifically with a member of the Ypt/Rab family. *Nature* **361**, 736-739 (1993).
83. Blümer, J. *et al.* RabGEFs are a major determinant for specific Rab membrane targeting. *The Journal of cell biology* **200**, 287-300 (2013).
84. Smythe, E., Carter, L.L. & Schmid, S.L. Cytosol- and clathrin-dependent stimulation of endocytosis in vitro by purified adaptors. *J Cell Biol* **119**, 1163-1171 (1992).
85. McLauchlan, H. *et al.* A novel role for Rab5-GDI in ligand sequestration into clathrin-coated pits. *Current biology : CB* **8**, 34-45 (1998).

86. Riederer, M.A., Soldati, T., Shapiro, A.D., Lin, J. & Pfeffer, S.R. Lysosome biogenesis requires Rab9 function and receptor recycling from endosomes to the trans-Golgi network. *J Cell Biol* **125**, 573-582 (1994).
87. Díaz, E. & Pfeffer, S.R. TIP47: a cargo selection device for mannose 6-phosphate receptor trafficking. *Cell* **93**, 433-443 (1998).
88. Carroll, K.S. *et al.* Role of Rab9 GTPase in facilitating receptor recruitment by TIP47. *Science (New York, N.Y.)* **292**, 1373-1376 (2001).
89. Hannan, L.A., Newmyer, S.L. & Schmid, S.L. ATP- and cytosol-dependent release of adaptor proteins from clathrin-coated vesicles: A dual role for Hsc70. *Molecular biology of the cell* **9**, 2217-2229 (1998).
90. Semerdjieva, S. *et al.* Coordinated regulation of AP2 uncoating from clathrin-coated vesicles by rab5 and hRME-6. *The Journal of cell biology* **183**, 499-511 (2008).
91. Hodge, T. & Cope, M.J. A myosin family tree. *J Cell Sci* **113 Pt 19**, 3353-3354 (2000).
92. Lapierre, L.A. *et al.* Myosin vb is associated with plasma membrane recycling systems. *Molecular biology of the cell* **12**, 1843-1857 (2001).
93. Hales, C.M., Vaerman, J.-P. & Goldenring, J.R. Rab11 family interacting protein 2 associates with Myosin Vb and regulates plasma membrane recycling. *The Journal of biological chemistry* **277**, 50415-50421 (2002).
94. Roland, J.T., Kenworthy, A.K., Peranen, J., Caplan, S. & Goldenring, J.R. Myosin Vb interacts with Rab8a on a tubular network containing EHD1 and EHD3. *Mol Biol Cell* **18**, 2828-2837 (2007).
95. Wu, X.S. *et al.* Identification of an organelle receptor for myosin-Va. *Nature cell biology* **4**, 271-278 (2002).
96. Chavrier, P., Parton, R.G., Hauri, H.P., Simons, K. & Zerial, M. Localization of low molecular weight GTP binding proteins to exocytic and endocytic compartments. *Cell* **62**, 317-329 (1990).
97. Gorvel, J.P., Chavrier, P., Zerial, M. & Gruenberg, J. rab5 controls early endosome fusion in vitro. *Cell* **64**, 915-925 (1991).
98. Stenmark, H. *et al.* Inhibition of rab5 GTPase activity stimulates membrane fusion in endocytosis. *EMBO J* **13**, 1287-1296 (1994).
99. Simonsen, A. *et al.* EEA1 links PI(3)K function to Rab5 regulation of endosome fusion. *Nature* **394**, 494-498 (1998).
100. Christoforidis, S., McBride, H.M., Burgoyne, R.D. & Zerial, M. The Rab5 effector EEA1 is a core component of endosome docking. *Nature* **397**, 621-625 (1999).
101. McBride, H.M. *et al.* Oligomeric complexes link Rab5 effectors with NSF and drive membrane fusion via interactions between EEA1 and syntaxin 13. *Cell* **98**, 377-386 (1999).
102. Sollner, T. *et al.* SNAP receptors implicated in vesicle targeting and fusion. *Nature* **362**, 318-324 (1993).
103. Rothman, J.E. & Warren, G. Implications of the SNARE hypothesis for intracellular membrane topology and dynamics. *Current biology : CB* **4**, 220-233 (1994).
104. Jahn, R. & Scheller, R.H. SNAREs--engines for membrane fusion. *Nature reviews. Molecular cell biology* **7**, 631-643 (2006).
105. Sutton, R.B., Fasshauer, D., Jahn, R. & Brunger, A.T. Crystal structure of a SNARE complex involved in synaptic exocytosis at 2.4 A resolution. *Nature* **395**, 347-353 (1998).
106. Antonin, W., Fasshauer, D., Becker, S., Jahn, R. & Schneider, T.R. Crystal structure of the endosomal SNARE complex reveals common structural principles of all SNAREs. *Nature structural biology* **9**, 107-111 (2002).
107. Fasshauer, D., Sutton, R.B., Brunger, A.T. & Jahn, R. Conserved structural features of the synaptic fusion complex: SNARE proteins reclassified as Q- and R-SNAREs. *Proceedings of the National Academy of Sciences of the United States of America* **95**, 15781-15786 (1998).

108. Christoforidis, S. *et al.* Phosphatidylinositol-3-OH kinases are Rab5 effectors. *Nature cell biology* **1**, 249-252 (1999).
109. Sönnichsen, B., De Renzis, S., Nielsen, E., Rietdorf, J. & Zerial, M. Distinct membrane domains on endosomes in the recycling pathway visualized by multicolor imaging of Rab4, Rab5, and Rab11. *The Journal of cell biology* **149**, 901-914 (2000).
110. Feng, Y., Press, B. & Wandinger-Ness, A. Rab 7: an important regulator of late endocytic membrane traffic. *The Journal of cell biology* **131**, 1435-1452 (1995).
111. Soldati, T., Rancaño, C., Geissler, H. & Pfeffer, S.R. Rab7 and Rab9 are recruited onto late endosomes by biochemically distinguishable processes. *The Journal of biological chemistry* **270**, 25541-25548 (1995).
112. Bucci, C., Thomsen, P., Nicoziani, P., McCarthy, J. & van Deurs, B. Rab7: a key to lysosome biogenesis. *Molecular biology of the cell* **11**, 467-480 (2000).
113. Rink, J., Ghigo, E., Kalaidzidis, Y. & Zerial, M. Rab conversion as a mechanism of progression from early to late endosomes. *Cell* **122**, 735-749 (2005).
114. Poteryaev, D., Datta, S., Ackema, K., Zerial, M. & Spang, A. Identification of the switch in early-to-late endosome transition. *Cell* **141**, 497-508 (2010).
115. Kinchen, J.M. & Ravichandran, K.S. Identification of two evolutionarily conserved genes regulating processing of engulfed apoptotic cells. *Nature* **464**, 778-782 (2010).
116. Vonderheit, A. & Helenius, A. Rab7 associates with early endosomes to mediate sorting and transport of Semliki forest virus to late endosomes. *PLoS biology* **3**, e233-e233 (2005).
117. Huotari, J. & Helenius, A. Endosome maturation. *EMBO J* **30**, 3481-3500 (2011).
118. Stenmark, H., Vitale, G., Ullrich, O. & Zerial, M. Rabaptin-5 is a direct effector of the small GTPase Rab5 in endocytic membrane fusion. *Cell* **83**, 423-432 (1995).
119. Horiuchi, H. *et al.* A novel Rab5 GDP/GTP exchange factor complexed to Rabaptin-5 links nucleotide exchange to effector recruitment and function. *Cell* **90**, 1149-1159 (1997).
120. Burd, C.G. & Emr, S.D. Phosphatidylinositol(3)-phosphate signaling mediated by specific binding to RING FYVE domains. *Molecular cell* **2**, 157-162 (1998).
121. Stenmark, H., Aasland, R., Toh, B.H. & D'Arrigo, A. Endosomal localization of the autoantigen EEA1 is mediated by a zinc-binding FYVE finger. *J Biol Chem* **271**, 24048-24054 (1996).
122. Callaghan, J., Simonsen, A., Gaullier, J.M., Toh, B.H. & Stenmark, H. The endosome fusion regulator early-endosomal autoantigen 1 (EEA1) is a dimer. *Biochem J* **338 (Pt 2)**, 539-543 (1999).
123. Simonsen, A., Gaullier, J.M., D'Arrigo, A. & Stenmark, H. The Rab5 effector EEA1 interacts directly with syntaxin-6. *The Journal of biological chemistry* **274**, 28857-28860 (1999).
124. Nielsen, E. *et al.* Rabenosyn-5, a novel Rab5 effector, is complexed with hVPS45 and recruited to endosomes through a FYVE finger domain. *The Journal of cell biology* **151**, 601-612 (2000).
125. Burd, C.G., Peterson, M., Cowles, C.R. & Emr, S.D. A novel Sec18p/NSF-dependent complex required for Golgi-to-endosome transport in yeast. *Mol Biol Cell* **8**, 1089-1104 (1997).
126. Abeliovich, H., Darsow, T. & Emr, S.D. Cytoplasm to vacuole trafficking of aminopeptidase I requires a t-SNARE-Sec1p complex composed of Tlg2p and Vps45p. *EMBO J* **18**, 6005-6016 (1999).
127. Nickerson, D.P., Brett, C.L. & Merz, A.J. Vps-C complexes: gatekeepers of endolysosomal traffic. *Current opinion in cell biology* **21**, 543-551 (2009).
128. Peterson, M.R. & Emr, S.D. The class C Vps complex functions at multiple stages of the vacuolar transport pathway. *Traffic* **2**, 476-486 (2001).
129. Sato, T.K., Rehling, P., Peterson, M.R. & Emr, S.D. Class C Vps protein complex regulates vacuolar SNARE pairing and is required for vesicle docking/fusion. *Molecular cell* **6**, 661-671 (2000).

130. Wurmser, A.E., Sato, T.K. & Emr, S.D. New component of the vacuolar class C-Vps complex couples nucleotide exchange on the Ypt7 GTPase to SNARE-dependent docking and fusion. *The Journal of cell biology* **151**, 551-562 (2000).
131. Peralta, E.R., Martin, B.C. & Edinger, A.L. Differential effects of TBC1D15 and mammalian Vps39 on Rab7 activation state, lysosomal morphology, and growth factor dependence. *J Biol Chem* **285**, 16814-16821 (2010).
132. Nordmann, M. *et al.* The Mon1-Ccz1 complex is the GEF of the late endosomal Rab7 homolog Ypt7. *Current biology : CB* **20**, 1654-1659 (2010).
133. Cantalupo, G., Alifano, P., Roberti, V., Bruni, C.B. & Bucci, C. Rab-interacting lysosomal protein (RILP): the Rab7 effector required for transport to lysosomes. *The EMBO journal* **20**, 683-693 (2001).
134. Wang, T., Wong, K.K. & Hong, W. A unique region of RILP distinguishes it from its related proteins in its regulation of lysosomal morphology and interaction with Rab7 and Rab34. *Mol Biol Cell* **15**, 815-826 (2004).
135. Colucci, A.M.R., Campana, M.C., Bellopede, M. & Bucci, C. The Rab-interacting lysosomal protein, a Rab7 and Rab34 effector, is capable of self-interaction. *Biochemical and biophysical research communications* **334**, 128-133 (2005).
136. Jordens, I. *et al.* The Rab7 effector protein RILP controls lysosomal transport by inducing the recruitment of dynein-dynactin motors. *Current biology : CB* **11**, 1680-1685 (2001).
137. Johansson, M., Lehto, M., Tanhuanpaa, K., Cover, T.L. & Olkkonen, V.M. The oxysterol-binding protein homologue ORP1L interacts with Rab7 and alters functional properties of late endocytic compartments. *Mol Biol Cell* **16**, 5480-5492 (2005).
138. Johansson, M. *et al.* Activation of endosomal dynein motors by stepwise assembly of Rab7-RILP-p150Glued, ORP1L, and the receptor betalll spectrin. *The Journal of cell biology* **176**, 459-471 (2007).
139. Mizuno, K., Kitamura, A. & Sasaki, T. Rabring7, a novel Rab7 target protein with a RING finger motif. *Mol Biol Cell* **14**, 3741-3752 (2003).
140. Sun, Q., Westphal, W., Wong, K.N., Tan, I. & Zhong, Q. Rubicon controls endosome maturation as a Rab7 effector. *Proceedings of the National Academy of Sciences of the United States of America* **107**, 19338-19343 (2010).
141. van der Sluijs, P. *et al.* The small GTP-binding protein rab4 controls an early sorting event on the endocytic pathway. *Cell* **70**, 729-740 (1992).
142. Sheff, D.R., Daro, E.E., Hull, M. & Mellman, I. The receptor recycling pathway contains two distinct populations of early endosomes with different sorting functions. *The Journal of cell biology* **145**, 123-139 (1999).
143. Seachrist, J.L., Anborgh, P.H. & Ferguson, S.S. beta 2-adrenergic receptor internalization, endosomal sorting, and plasma membrane recycling are regulated by rab GTPases. *The Journal of biological chemistry* **275**, 27221-27228 (2000).
144. Roberts, M., Barry, S., Woods, A., van der Sluijs, P. & Norman, J. PDGF-regulated rab4-dependent recycling of alphavbeta3 integrin from early endosomes is necessary for cell adhesion and spreading. *Current biology : CB* **11**, 1392-1402 (2001).
145. Mohrmann, K., Gerez, L., Oorschot, V., Klumperman, J. & van der Sluijs, P. Rab4 function in membrane recycling from early endosomes depends on a membrane to cytoplasm cycle. *The Journal of biological chemistry* **277**, 32029-32035 (2002).
146. McCaffrey, M.W. *et al.* Rab4 affects both recycling and degradative endosomal trafficking. *FEBS Lett* **495**, 21-30 (2001).
147. Vitale, G. *et al.* Distinct Rab-binding domains mediate the interaction of Rabaptin-5 with GTP-bound Rab4 and Rab5. *EMBO J* **17**, 1941-1951 (1998).

148. Nagelkerken, B. *et al.* Rabaptin4, a novel effector of the small GTPase rab4a, is recruited to perinuclear recycling vesicles. *Biochem J* **346 Pt 3**, 593-601 (2000).
149. Deneka, M. *et al.* Rabaptin-5alpha/rabaptin-4 serves as a linker between rab4 and gamma(1)-adaptin in membrane recycling from endosomes. *The EMBO journal* **22**, 2645-2657 (2003).
150. Pagano, A., Crottet, P., Prescianotto-Baschong, C. & Spiess, M. In vitro formation of recycling vesicles from endosomes requires adaptor protein-1/clathrin and is regulated by rab4 and the connector rabaptin-5. *Mol Biol Cell* **15**, 4990-5000 (2004).
151. Vollenweider, P. *et al.* The small guanosine triphosphate-binding protein Rab4 is involved in insulin-induced GLUT4 translocation and actin filament rearrangement in 3T3-L1 cells. *Endocrinology* **138**, 4941-4949 (1997).
152. Imamura, T. *et al.* Insulin-induced GLUT4 translocation involves protein kinase C-lambda-mediated functional coupling between Rab4 and the motor protein kinesin. *Mol Cell Biol* **23**, 4892-4900 (2003).
153. Cormont, M., Mari, M., Galmiche, A., Hofman, P. & Le Marchand-Brustel, Y. A FYVE-finger-containing protein, Rabip4, is a Rab4 effector involved in early endosomal traffic. *Proceedings of the National Academy of Sciences of the United States of America* **98**, 1637-1642 (2001).
154. Fouraux, M.A. *et al.* Rabip4' is an effector of rab5 and rab4 and regulates transport through early endosomes. *Mol Biol Cell* **15**, 611-624 (2004).
155. Ullrich, O., Reinsch, S., Urbe, S., Zerial, M. & Parton, R.G. Rab11 regulates recycling through the pericentriolar recycling endosome. *J Cell Biol* **135**, 913-924 (1996).
156. Ren, M. *et al.* Hydrolysis of GTP on rab11 is required for the direct delivery of transferrin from the pericentriolar recycling compartment to the cell surface but not from sorting endosomes. *Proceedings of the National Academy of Sciences of the United States of America* **95**, 6187-6192 (1998).
157. Trischler, M., Stoorvogel, W. & Ullrich, O. Biochemical analysis of distinct Rab5- and Rab11-positive endosomes along the transferrin pathway. *Journal of cell science* **112 (Pt 24)**, 4773-4783 (1999).
158. Zeng, J. *et al.* Identification of a putative effector protein for rab11 that participates in transferrin recycling. *Proceedings of the National Academy of Sciences of the United States of America* **96**, 2840-2845 (1999).
159. Hales, C.M. *et al.* Identification and characterization of a family of Rab11-interacting proteins. *The Journal of biological chemistry* **276**, 39067-39075 (2001).
160. Lindsay, A.J. & McCaffrey, M.W. Rab11-FIP2 functions in transferrin recycling and associates with endosomal membranes via its COOH-terminal domain. *The Journal of biological chemistry* **277**, 27193-27199 (2002).
161. Barbero, P., Bittova, L. & Pfeffer, S.R. Visualization of Rab9-mediated vesicle transport from endosomes to the trans-Golgi in living cells. *The Journal of cell biology* **156**, 511-518 (2002).
162. Vieira, O.V., Botelho, R.J. & Grinstein, S. Phagosome maturation: aging gracefully. *Biochem J* **366**, 689-704 (2002).
163. Flannagan, R.S., Cosío, G. & Grinstein, S. Antimicrobial mechanisms of phagocytes and bacterial evasion strategies. *Nature reviews. Microbiology* **7**, 355-366 (2009).
164. Desjardins, M., Huber, L.A., Parton, R.G. & Griffiths, G. Biogenesis of phagolysosomes proceeds through a sequential series of interactions with the endocytic apparatus. *The Journal of cell biology* **124**, 677-688 (1994).
165. Mayorga, L.S., Bertini, F. & Stahl, P.D. Fusion of newly formed phagosomes with endosomes in intact cells and in a cell-free system. *The Journal of biological chemistry* **266**, 6511-6517 (1991).
166. Jahraus, A. *et al.* In vitro fusion of phagosomes with different endocytic organelles from J774 macrophages. *The Journal of biological chemistry* **273**, 30379-30390 (1998).

167. Pitt, A., Mayorga, L.S., Schwartz, A.L. & Stahl, P.D. Transport of phagosomal components to an endosomal compartment. *J Biol Chem* **267**, 126-132 (1992).
168. Vieira, O.V. *et al.* Modulation of Rab5 and Rab7 recruitment to phagosomes by phosphatidylinositol 3-kinase. *Mol Cell Biol* **23**, 2501-2514 (2003).
169. Fratti, R.A., Backer, J.M., Gruenberg, J., Corvera, S. & Deretic, V. Role of phosphatidylinositol 3-kinase and Rab5 effectors in phagosomal biogenesis and mycobacterial phagosome maturation arrest. *The Journal of cell biology* **154**, 631-644 (2001).
170. Vieira, O.V. *et al.* Distinct roles of class I and class III phosphatidylinositol 3-kinases in phagosome formation and maturation. *The Journal of cell biology* **155**, 19-25 (2001).
171. Huynh, K.K. *et al.* LAMP proteins are required for fusion of lysosomes with phagosomes. *The EMBO journal* **26**, 313-324 (2007).
172. Via, L.E. *et al.* Arrest of mycobacterial phagosome maturation is caused by a block in vesicle fusion between stages controlled by rab5 and rab7. *The Journal of biological chemistry* **272**, 13326-13331 (1997).
173. Harrison, R.E., Bucci, C., Vieira, O.V., Schroer, T.A. & Grinstein, S. Phagosomes fuse with late endosomes and/or lysosomes by extension of membrane protrusions along microtubules: role of Rab7 and RILP. *Mol Cell Biol* **23**, 6494-6506 (2003).
174. Kasmapour, B., Gronow, A., Bleck, C.K.E., Hong, W. & Gutierrez, M.G. Size-dependent mechanism of cargo sorting during lysosome-phagosome fusion is controlled by Rab34. *Proceedings of the National Academy of Sciences of the United States of America* **109**, 20485-20490 (2012).
175. Lukacs, G.L., Rotstein, O.D. & Grinstein, S. Phagosomal acidification is mediated by a vacuolar-type H(+)-ATPase in murine macrophages. *J Biol Chem* **265**, 21099-21107 (1990).
176. Hackam, D.J. *et al.* Regulation of phagosomal acidification. Differential targeting of Na+/H+ exchangers, Na+/K+-ATPases, and vacuolar-type H+-atpases. *J Biol Chem* **272**, 29810-29820 (1997).
177. Reeves, E.P. *et al.* Killing activity of neutrophils is mediated through activation of proteases by K+ flux. *Nature* **416**, 291-297 (2002).
178. Keren, I., Wu, Y., Inocencio, J., Mulcahy, L.R. & Lewis, K. Killing by bactericidal antibiotics does not depend on reactive oxygen species. *Science* **339**, 1213-1216 (2013).
179. Babior, B.M. NADPH oxidase. *Current Opinion in Immunology* **16**, 42-47 (2004).
180. Winterbourn, C.C. Reconciling the chemistry and biology of reactive oxygen species. *Nature chemical biology* **4**, 278-286 (2008).
181. Savina, A. *et al.* NOX2 controls phagosomal pH to regulate antigen processing during crosspresentation by dendritic cells. *Cell* **126**, 205-218 (2006).
182. Rybicka, J.M., Balce, D.R., Khan, M.F., Krohn, R.M. & Yates, R.M. NADPH oxidase activity controls phagosomal proteolysis in macrophages through modulation of the lumenal redox environment of phagosomes. *Proc Natl Acad Sci U S A* **107**, 10496-10501 (2010).
183. Miller, B.H. *et al.* Mycobacteria inhibit nitric oxide synthase recruitment to phagosomes during macrophage infection. *Infect Immun* **72**, 2872-2878 (2004).
184. Davis, A.S. *et al.* Mechanism of inducible nitric oxide synthase exclusion from mycobacterial phagosomes. *PLoS Pathog* **3**, e186 (2007).
185. Chan, J., Xing, Y., Magliozzo, R.S. & Bloom, B.R. Killing of virulent Mycobacterium tuberculosis by reactive nitrogen intermediates produced by activated murine macrophages. *J Exp Med* **175**, 1111-1122 (1992).
186. Alvarez-Dominguez, C. & Stahl, P.D. Increased expression of Rab5a correlates directly with accelerated maturation of Listeria monocytogenes phagosomes. *The Journal of biological chemistry* **274**, 11459-11462 (1999).

187. Rabinowitz, S., Horstmann, H., Gordon, S. & Griffiths, G. Immunocytochemical characterization of the endocytic and phagolysosomal compartments in peritoneal macrophages. *The Journal of cell biology* **116**, 95-112 (1992).
188. Rupper, A., Grove, B. & Cardelli, J. Rab7 regulates phagosome maturation in Dictyostelium. *Journal of cell science* **114**, 2449-2460 (2001).
189. Méresse, S., Steele-Mortimer, O., Finlay, B.B. & Gorvel, J.P. The rab7 GTPase controls the maturation of Salmonella typhimurium-containing vacuoles in HeLa cells. *The EMBO journal* **18**, 4394-4403 (1999).
190. Chen, Y.T., Holcomb, C. & Moore, H.P. Expression and localization of two low molecular weight GTP-binding proteins, Rab8 and Rab10, by epitope tag. *Proceedings of the National Academy of Sciences of the United States of America* **90**, 6508-6512 (1993).
191. Chen, C.C. *et al.* RAB-10 is required for endocytic recycling in the Caenorhabditis elegans intestine. *Mol Biol Cell* **17**, 1286-1297 (2006).
192. Babbey, C.M. *et al.* Rab10 regulates membrane transport through early endosomes of polarized Madin-Darby canine kidney cells. *Mol Biol Cell* **17**, 3156-3175 (2006).
193. Cardoso, C.M.P., Jordao, L. & Vieira, O.V. Rab10 regulates phagosome maturation and its overexpression rescues Mycobacterium-containing phagosomes maturation. *Traffic* **11**, 221-235 (2010).
194. Junutula, J.R. *et al.* Rab14 is involved in membrane trafficking between the Golgi complex and endosomes. *Mol Biol Cell* **15**, 2218-2229 (2004).
195. Harris, E. & Cardelli, J. RabD, a Dictyostelium Rab14-related GTPase, regulates phagocytosis and homotypic phagosome and lysosome fusion. *Journal of Cell Science* **115**, 3703-3713 (2002).
196. Kyei, G.B. *et al.* Rab14 is critical for maintenance of Mycobacterium tuberculosis phagosome maturation arrest. *The EMBO journal* **25**, 5250-5259 (2006).
197. Kuijl, C. *et al.* Intracellular bacterial growth is controlled by a kinase network around PKB/AKT1. *Nature* **450**, 725-730 (2007).
198. Olkkonen, V.M. *et al.* Molecular cloning and subcellular localization of three GTP-binding proteins of the rab subfamily. *Journal of cell science* **106 (Pt 4)**, 1249-1261 (1993).
199. Mesa, R., Salomón, C., Roggero, M., Stahl, P.D. & Mayorga, L.S. Rab22a affects the morphology and function of the endocytic pathway. *Journal of cell science* **114**, 4041-4049 (2001).
200. Kauppi, M. *et al.* The small GTPase Rab22 interacts with EEA1 and controls endosomal membrane trafficking. *Journal of cell science* **115**, 899-911 (2002).
201. Roberts, E.A., Chua, J., Kyei, G.B. & Deretic, V. Higher order Rab programming in phagolysosome biogenesis. *The Journal of cell biology* **174**, 923-929 (2006).
202. Zhu, H., Liang, Z. & Li, G. Rabex-5 is a Rab22 effector and mediates a Rab22-Rab5 signaling cascade in endocytosis. *Mol Biol Cell* **20**, 4720-4729 (2009).
203. Wang, T. & Hong, W. Interorganellar Regulation of Lysosome Positioning by the Golgi Apparatus through Rab34 Interaction with Rab-interacting Lysosomal Protein. *Molecular Biology of the Cell* **13**, 4317-4332 (2002).
204. Gutierrez, M.G. *et al.* NF-kappa B activation controls phagolysosome fusion-mediated killing of mycobacteria by macrophages. *J Immunol* **181**, 2651-2663 (2008).
205. Seto, S., Tsujimura, K. & Koide, Y. Rab GTPases regulating phagosome maturation are differentially recruited to mycobacterial phagosomes. *Traffic* **12**, 407-420 (2011).
206. Egami, Y. & Araki, N. Rab20 regulates phagosome maturation in RAW264 macrophages during Fc gamma receptor-mediated phagocytosis. *PloS one* **7**, e35663-e35663 (2012).
207. Balce, D.R. *et al.* Alternative activation of macrophages by IL-4 enhances the proteolytic capacity of their phagosomes through synergistic mechanisms. *Blood* **118**, 4199-4208 (2011).

208. de Keijzer, S. *et al.* Interleukin-4 alters early phagosome phenotype by modulating class I PI3K dependent lipid remodeling and protein recruitment. *PloS one* **6**, e22328-e22328 (2011).
209. O'Leary, S., O'Sullivan, M.P. & Keane, J. IL-10 blocks phagosome maturation in mycobacterium tuberculosis-infected human macrophages. *American journal of respiratory cell and molecular biology* **45**, 172-180 (2011).
210. Bhattacharya, M. *et al.* IL-6 and IL-12 specifically regulate the expression of Rab5 and Rab7 via distinct signaling pathways. *The EMBO journal* **25**, 2878-2888 (2006).
211. Harris, J. *et al.* T helper 2 cytokines inhibit autophagic control of intracellular Mycobacterium tuberculosis. *Immunity* **27**, 505-517 (2007).
212. Schroder, K., Hertzog, P.J., Ravasi, T. & Hume, D.A. Interferon-gamma: an overview of signals, mechanisms and functions. *J Leukoc Biol* **75**, 163-189 (2004).
213. Via, L.E. *et al.* Effects of cytokines on mycobacterial phagosome maturation. *Journal of cell science* **111 (Pt 7)**, 897-905 (1998).
214. Schaible, U.E., Sturgill-Koszycki, S., Schlesinger, P.H. & Russell, D.G. Cytokine activation leads to acidification and increases maturation of Mycobacterium avium-containing phagosomes in murine macrophages. *Journal of immunology (Baltimore, Md. : 1950)* **160**, 1290-1296 (1998).
215. Hostetter, J.M., Steadham, E.M., Haynes, J.S., Bailey, T.B. & Cheville, N.F. Cytokine effects on maturation of the phagosomes containing Mycobacteria avium subspecies paratuberculosis in J774 cells. *FEMS immunology and medical microbiology* **34**, 127-134 (2002).
216. Santic, M., Molmeret, M. & Abu Kwaik, Y. Maturation of the Legionella pneumophila-containing phagosome into a phagolysosome within gamma interferon-activated macrophages. *Infect Immun* **73**, 3166-3171 (2005).
217. McCollister, B.D., Bourret, T.J., Gill, R., Jones-Carson, J. & Vázquez-Torres, A. Repression of SPI2 transcription by nitric oxide-producing, IFNgamma-activated macrophages promotes maturation of Salmonella phagosomes. *The Journal of experimental medicine* **202**, 625-635 (2005).
218. Gutierrez, M.G. *et al.* Autophagy is a defense mechanism inhibiting BCG and Mycobacterium tuberculosis survival in infected macrophages. *Cell* **119**, 753-766 (2004).
219. Tsang, A.W., Oestergaard, K., Myers, J.T. & Swanson, J.A. Altered membrane trafficking in activated bone marrow-derived macrophages. *J Leukoc Biol* **68**, 487-494 (2000).
220. Yates, R.M., Hermetter, A., Taylor, G.a. & Russell, D.G. Macrophage activation downregulates the degradative capacity of the phagosome. *Traffic (Copenhagen, Denmark)* **8**, 241-250 (2007).
221. Jutras, I. *et al.* Modulation of the phagosome proteome by interferon-gamma. *Mol Cell Proteomics* **7**, 697-715 (2008).
222. Trost, M. *et al.* The phagosomal proteome in interferon-gamma-activated macrophages. *Immunity* **30**, 143-154 (2009).
223. Gordon, S. & Martinez, F.O. Alternative activation of macrophages: mechanism and functions. *Immunity* **32**, 593-604 (2010).
224. Donnelly, R.P., Dickensheets, H. & Finbloom, D.S. The interleukin-10 signal transduction pathway and regulation of gene expression in mononuclear phagocytes. *Journal of interferon & cytokine research : the official journal of the International Society for Interferon and Cytokine Research* **19**, 563-573 (1999).
225. Moore, K.W., de Waal Malefyt, R., Coffman, R.L. & O'Garra, A. Interleukin-10 and the interleukin-10 receptor. *Annu Rev Immunol* **19**, 683-765 (2001).
226. Pei, G., Bronietzki, M. & Gutierrez, M.G. Immune regulation of Rab proteins expression and intracellular transport. *Journal of leukocyte biology* **92**, 41-50 (2012).
227. Alvarez-Dominguez, C. & Stahl, P.D. Interferon-gamma selectively induces Rab5a synthesis and processing in mononuclear cells. *The Journal of biological chemistry* **273**, 33901-33904 (1998).

228. Lütcke, A. *et al.* Cloning and subcellular localization of novel rab proteins reveals polarized and cell type-specific expression. *Journal of cell science* **107 (Pt 12)**, 3437-3448 (1994).
229. Curtis, L.M. & Gluck, S. Distribution of Rab GTPases in mouse kidney and comparison with vacuolar H+-ATPase. *Nephron. Physiology* **100**, p31-42 (2005).
230. Amillet, J.-M. *et al.* Characterization of human Rab20 overexpressed in exocrine pancreatic carcinoma. *Human Pathology* **37**, 256-263 (2006).
231. Das Sarma, J., Kaplan, B.E., Willemsen, D. & Koval, M. Identification of rab20 as a potential regulator of connexin 43 trafficking. *Cell communication & adhesion* **15**, 65-74 (2008).
232. Fukuda, M., Kanno, E., Ishibashi, K. & Itoh, T. Large scale screening for novel rab effectors reveals unexpected broad Rab binding specificity. *Molecular & cellular proteomics : MCP* **7**, 1031-1042 (2008).
233. Egami, Y. & Araki, N. Spatiotemporal Localization of Rab20 in Live RAW264 Macrophages during Macropinocytosis. *Acta histochemica et cytochemica* **45**, 317-323 (2012).
234. Hackenbeck, T. *et al.* The GTPase RAB20 is a HIF target with mitochondrial localization mediating apoptosis in hypoxia. *Biochimica et biophysica acta* **1813**, 1-13 (2011).
235. Cortez, K.J. *et al.* Functional genomics of innate host defense molecules in normal human monocytes in response to Aspergillus fumigatus. *Infect Immun* **74**, 2353-2365 (2006).
236. Goldmann, O. *et al.* Transcriptome analysis of murine macrophages in response to infection with Streptococcus pyogenes reveals an unusual activation program. *Infection and immunity* **75**, 4148-4157 (2007).
237. Tchatalbachev, S., Ghai, R., Hossain, H. & Chakraborty, T. Gram-positive pathogenic bacteria induce a common early response in human monocytes. *BMC microbiology* **10**, 275-275 (2010).
238. Mahapatra, S., Ayoubi, P. & Shaw, E.I. Coxiella burnetii Nine Mile II proteins modulate gene expression of monocytic host cells during infection. *BMC microbiology* **10**, 244-244 (2010).
239. Draper, D.W., Bethea, H.N. & He, Y.W. Toll-like receptor 2-dependent and -independent activation of macrophages by group B streptococci. *Immunology letters* **102**, 202-214 (2006).
240. Tailleux, L. *et al.* Probing host pathogen cross-talk by transcriptional profiling of both Mycobacterium tuberculosis and infected human dendritic cells and macrophages. *PloS one* **3**, e1403-e1403 (2008).
241. Gonzalez-Juarrero, M. *et al.* Immune response to Mycobacterium tuberculosis and identification of molecular markers of disease. *American journal of respiratory cell and molecular biology* **40**, 398-409 (2009).
242. van der Sar, A.M., Spaink, H.P., Zakrzewska, A., Bitter, W. & Meijer, A.H. Specificity of the zebrafish host transcriptome response to acute and chronic mycobacterial infection and the role of innate and adaptive immune components. *Molecular immunology* **46**, 2317-2332 (2009).
243. Mehra, S. *et al.* Transcriptional reprogramming in nonhuman primate (rhesus macaque) tuberculosis granulomas. *PloS one* **5**, e12266-e12266 (2010).
244. Berry, M.P.R. *et al.* An interferon-inducible neutrophil-driven blood transcriptional signature in human tuberculosis. *Nature* **466**, 973-977 (2010).
245. Torri, A. *et al.* Gene expression profiles identify inflammatory signatures in dendritic cells. *PloS one* **5**, e9404-e9404 (2010).
246. Liang, Y. *et al.* Expression profiling of Rab GTPases reveals the involvement of Rab20 and Rab32 in acute brain inflammation in mice. *Neuroscience letters* **527**, 110-114 (2012).
247. Malik, R. *et al.* Gene expression profile of ovalbumin-induced lung inflammation in a murine model of asthma. *J Investig Allergol Clin Immunol* **18**, 106-112 (2008).
248. Smith, A.C. *et al.* A network of Rab GTPases controls phagosome maturation and is modulated by Salmonella enterica serovar Typhimurium. *The Journal of cell biology* **176**, 263-268 (2007).

249. Mattera, R. & Bonifacino, J.S. Ubiquitin binding and conjugation regulate the recruitment of Rabex-5 to early endosomes. *EMBO J* **27**, 2484-2494 (2008).
250. Der, C.J., Finkel, T. & Cooper, G.M. Biological and biochemical properties of human rasH genes mutated at codon 61. *Cell* **44**, 167-176 (1986).
251. Erdman, R.A., Shellenberger, K.E., Overmeyer, J.H. & Maltese, W.A. Rab24 is an atypical member of the Rab GTPase family. Deficient GTPase activity, GDP dissociation inhibitor interaction, and prenylation of Rab24 expressed in cultured cells. *J Biol Chem* **275**, 3848-3856 (2000).
252. Roberts, R.L. *et al.* Endosome fusion in living cells overexpressing GFP-rab5. *Journal of cell science* **112 (Pt 21)**, 3667-3675 (1999).
253. Wegner, C.S. *et al.* Ultrastructural characterization of giant endosomes induced by GTPase-deficient Rab5. *Histochemistry and cell biology* **133**, 41-55 (2010).
254. Fabri, M. *et al.* Vitamin D is required for IFN-gamma-mediated antimicrobial activity of human macrophages. *Science translational medicine* **3**, 104ra102-104ra102 (2011).
255. Riedl, J. *et al.* Lifeact: a versatile marker to visualize F-actin. *Nature methods* **5**, 605-607 (2008).
256. Chow, C.-W., Downey, G.P. & Grinstein, S. Measurements of phagocytosis and phagosomal maturation. *Current protocols in cell biology / editorial board, Juan S. Bonifacino ... [et al.]* **Chapter 15**, Unit 15.17-Unit 15.17 (2004).
257. Yates, R.M., Hermetter, A. & Russell, D.G. The kinetics of phagosome maturation as a function of phagosome/lysosome fusion and acquisition of hydrolytic activity. *Traffic (Copenhagen, Denmark)* **6**, 413-420 (2005).
258. Honing, S., Griffith, J., Geuze, H.J. & Hunziker, W. The tyrosine-based lysosomal targeting signal in lamp-1 mediates sorting into Golgi-derived clathrin-coated vesicles. *EMBO J* **15**, 5230-5239 (1996).
259. Klausner, R.D., Donaldson, J.G. & Lippincott-Schwartz, J. Brefeldin A: insights into the control of membrane traffic and organelle structure. *The Journal of cell biology* **116**, 1071-1080 (1992).
260. Geuze, H.J., Slot, J.W., Strous, G.J., Hasilik, a. & von Figura, K. Possible pathways for lysosomal enzyme delivery. *The Journal of cell biology* **101**, 2253-2262 (1985).
261. Griffiths, G. & Simons, K. The trans Golgi network: sorting at the exit site of the Golgi complex. *Science* **234**, 438-443 (1986).
262. Desjardins, M. Biogenesis of phagolysosomes: the 'kiss and run' hypothesis. *Trends in cell biology* **5**, 183-186 (1995).
263. Montaner, L.J. *et al.* Type 1 and type 2 cytokine regulation of macrophage endocytosis: differential activation by IL-4/IL-13 as opposed to IFN-gamma or IL-10. *J Immunol* **162**, 4606-4613 (1999).
264. Martens, S. & Howard, J. The interferon-inducible GTPases. *Annu Rev Cell Dev Biol* **22**, 559-589 (2006).
265. Freeman, J.L., Abo, A. & Lambeth, J.D. Rac "insert region" is a novel effector region that is implicated in the activation of NADPH oxidase, but not PAK65. *J Biol Chem* **271**, 19794-19801 (1996).
266. Mosser, D.M. The many faces of macrophage activation. *Journal of Leukocyte Biology* **73**, 209-212 (2003).
267. Mosser, D.M. & Edwards, J.P. Exploring the full spectrum of macrophage activation. *Nature reviews. Immunology* **8**, 958-969 (2008).
268. Hoffmann, E. *et al.* Initial receptor-ligand interactions modulate gene expression and phagosomal properties during both early and late stages of phagocytosis. *Eur J Cell Biol* **89**, 693-704 (2010).
269. Ellson, C.D. *et al.* Phosphatidylinositol 3-phosphate is generated in phagosomal membranes. *Current biology : CB* **11**, 1631-1635 (2001).

270. Hazeki, K. *et al.* Essential roles of PIKfyve and PTEN on phagosomal phosphatidylinositol 3-phosphate dynamics. *FEBS letters* **586**, 4010-4015 (2012).
271. Sbrissa, D., Ikonomov, O.C., Deeb, R. & Shisheva, A. Phosphatidylinositol 5-phosphate biosynthesis is linked to PIKfyve and is involved in osmotic response pathway in mammalian cells. *J Biol Chem* **277**, 47276-47284 (2002).
272. Rutherford, A.C. *et al.* The mammalian phosphatidylinositol 3-phosphate 5-kinase (PIKfyve) regulates endosome-to-TGN retrograde transport. *Journal of cell science* **119**, 3944-3957 (2006).
273. Jefferies, H.B.J. *et al.* A selective PIKfyve inhibitor blocks PtdIns(3,5)P(2) production and disrupts endomembrane transport and retroviral budding. *EMBO reports* **9**, 164-170 (2008).
274. de Lartigue, J. *et al.* PIKfyve Regulation of Endosome-Linked Pathways. *Traffic* **10**, 883-893 (2009).
275. Norris, F.A., Wilson, M.P., Wallis, T.S., Galyov, E.E. & Majerus, P.W. SopB, a protein required for virulence of Salmonella dublin, is an inositol phosphate phosphatase. *Proceedings of the National Academy of Sciences of the United States of America* **95**, 14057-14059 (1998).
276. Mallo, G.V. *et al.* SopB promotes phosphatidylinositol 3-phosphate formation on Salmonella vacuoles by recruiting Rab5 and Vps34. *The Journal of cell biology* **182**, 741-752 (2008).
277. Mukherjee, K., Parashuraman, S., Raje, M. & Mukhopadhyay, A. SopE acts as an Rab5-specific nucleotide exchange factor and recruits non-prenylated Rab5 on Salmonella-containing phagosomes to promote fusion with early endosomes. *J Biol Chem* **276**, 23607-23615 (2001).
278. Madan, R., Krishnamurthy, G. & Mukhopadhyay, A. SopE-mediated recruitment of host Rab5 on phagosomes inhibits Salmonella transport to lysosomes. *Methods Mol Biol* **445**, 417-437 (2008).
279. Bucci, C. *et al.* The small GTPase rab5 functions as a regulatory factor in the early endocytic pathway. *Cell* **70**, 715-728 (1992).
280. Buvelot Frei, S. *et al.* Bioinformatic and comparative localization of Rab proteins reveals functional insights into the uncharacterized GTPases Ypt10p and Ypt11p. *Molecular and cellular biology* **26**, 7299-7317 (2006).
281. Schwartz, S.L., Cao, C., Pylypenko, O., Rak, A. & Wandinger-Ness, A. Rab GTPases at a glance. *J Cell Sci* **120**, 3905-3910 (2007).
282. Lippe, R., Miaczynska, M., Rybin, V., Runge, A. & Zerial, M. Functional synergy between Rab5 effector Rabaptin-5 and exchange factor Rabex-5 when physically associated in a complex. *Mol Biol Cell* **12**, 2219-2228 (2001).
283. Alpuche-Aranda, C.M., Racoosin, E.L., Swanson, J.A. & Miller, S.I. Salmonella stimulate macrophage macropinocytosis and persist within spacious phagosomes. *J Exp Med* **179**, 601-608 (1994).
284. Birmingham, C.L. *et al.* Listeriolysin O allows Listeria monocytogenes replication in macrophage vacuoles. *Nature* **451**, 350-354 (2008).
285. Ramachandra, L., Song, R. & Harding, C.V. Phagosomes are fully competent antigen-processing organelles that mediate the formation of peptide:class II MHC complexes. *Journal of immunology (Baltimore, Md. : 1950)* **162**, 3263-3272 (1999).
286. Houde, M. *et al.* Phagosomes are competent organelles for antigen cross-presentation. *Nature* **425**, 402-406 (2003).
287. Hume, D.a. Macrophages as APC and the dendritic cell myth. *Journal of immunology (Baltimore, Md. : 1950)* **181**, 5829-5835 (2008).
288. Delamarre, L., Pack, M., Chang, H., Mellman, I. & Trombetta, E.S. Differential lysosomal proteolysis in antigen-presenting cells determines antigen fate. *Science (New York, N.Y.)* **307**, 1630-1634 (2005).

289. Delamarre, L., Couture, R., Mellman, I. & Trombetta, E.S. Enhancing immunogenicity by limiting susceptibility to lysosomal proteolysis. *The Journal of experimental medicine* **203**, 2049-2055 (2006).
290. Kotsias, F., Hoffmann, E., Amigorena, S. & Savina, A. Reactive oxygen species production in the phagosome: impact on antigen presentation in dendritic cells. *Antioxidants & redox signaling* **18**, 714-729 (2013).
291. Watson, R.O., Manzanillo, P.S. & Cox, J.S. Extracellular M. tuberculosis DNA targets bacteria for autophagy by activating the host DNA-sensing pathway. *Cell* **150**, 803-815 (2012).
292. Tietzel, I., El-Haibi, C. & Carabeo, R.A. Human guanylate binding proteins potentiate the anti-chlamydia effects of interferon-gamma. *PloS one* **4**, e6499 (2009).
293. Sercarz, E.E. & Maverakis, E. Mhc-guided processing: binding of large antigen fragments. *Nat Rev Immunol* **3**, 621-629 (2003).
294. Gorvel, J.P., Escola, J.M., Stang, E. & Bakke, O. Invariant chain induces a delayed transport from early to late endosomes. *J Biol Chem* **270**, 2741-2746 (1995).
295. Stang, E. & Bakke, O. MHC class II-associated invariant chain-induced enlarged endosomal structures: a morphological study. *Experimental cell research* **235**, 79-92 (1997).
296. Landsverk, O.J., Barois, N., Gregers, T.F. & Bakke, O. Invariant chain increases the half-life of MHC II by delaying endosomal maturation. *Immunol Cell Biol* **89**, 619-629 (2011).
297. Delprato, A., Merithew, E. & Lambright, D.G. Structure, exchange determinants, and family-wide rab specificity of the tandem helical bundle and Vps9 domains of Rabex-5. *Cell* **118**, 607-617 (2004).
298. Mattera, R., Tsai, Y.C., Weissman, A.M. & Bonifacino, J.S. The Rab5 guanine nucleotide exchange factor Rabex-5 binds ubiquitin (Ub) and functions as a Ub ligase through an atypical Ub-interacting motif and a zinc finger domain. *J Biol Chem* **281**, 6874-6883 (2006).

7. Appendix

A compact-disc containing time-lapse movies from the results section is attached to the inner side of the back cover. The movie files are compressed with JPEG method and saved as AVI format with ImageJ1.43u. The frame rate of all movies is 15 fps. Scale bars are 10 µm.

Table 7.1: List of all the movies

File Name	Corresponding Figure	Legend
Movie 1	**Fig. 3.10**	Homotypic fusion between Rab20-positive vacuoles in RAW264.7 macrophages expressing EGFP-Rab20WT (Green)
Movie 2	**Fig. 3.12**	Dynamic association of EGFP-Rab20 (Green) with early phagosomes (Red)
Movie 3	**Fig. 3.13**	Actin dynamics and Rab20 association with phagosomes
Movie 4	**Fig. 3.14**	Lysotracker (Red) acquisition by phagosomes in macrophages expressing EGFP (Green)
Movie 5	**Fig. 3.15**	Lysotracker (Red) acquisition by phagosomes in macrophages expressing EGFP-Rab20WT (Green)
Movie 6	**Fig. 3.16**	Lysotracker (Red) acquisition by phagosomes in macrophages expressing EGFP-Rab20T19N (Green)
Movie 7	**Fig. 3.18**	PI3P (Red) association with phagosomes in macrophages expressing mCherry (Green)
Movie 8	**Fig. 3.19**	PI3P (Red) association with phagosomes in macrophages expressing mCherry-Rab20WT (Green)
Movie 9	**Fig. 3.20**	PI3P (Red) association with phagosomes in macrophages expressing mCherry-Rab20T19N (Green)
Movie 10	**Fig. 3.22**	Rab5A (Green) association with phagosomes in macrophages expressing mCherry (Red)
Movie 11	**Fig. 3.23**	Rab5A (Green) association with phagosomes in macrophages expressing mCherry-Rab20WT (Red)
Movie 12	**Fig. 3.24**	Rab5A (Green) association with phagosomes in macrophages expressing mCherry-Rab20T19N (Red)
Movie 13	**Fig. 3.26**	Dextran 70kDa (Red) delivery to phagosomes in macrophages expressing EGFP (Green)
Movie 14	**Fig. 3.27**	Dextran 70kDa (Red) delivery to phagosomes in macrophages expressing EGFP-Rab20WT (Green)
Movie 15	**Fig. 3.28**	Dextran 70kDa (Red) delivery to phagosomes in macrophages expressing EGFP-Rab20T19N (Green)
Movie 16	**Fig. 3.34**	Lysotracker (Red) acquisition by phagosomes in macrophages expressing EGFP-Rab20WT (Green) after Brefeldin A treatment
Movie 17	**Fig. 3.35**	Rab20 post-Golgi trafficking to phagosomes in macrophages expressing mCherry-Rab20WT (Red) and Venus-GalT (Green)
Movie 18	**Fig. 3.37**	Lysotracker acquisition by phagosomes in macrophages expressing scrambled shRNA
Movie 19	**Fig. 3.38**	Lysotracker (Green) acquisition by phagosomes in macrophages expressing Rab20 shRNA1 (Red)

Movie 20	**Fig. 3.43**	Lysotracker acquisition by phagosomes in macrophages expressing scrambled shRNA after IFN-γ treatment
Movie 21	**Fig. 3.44**	Lysotracker (Green) acquisition by phagosomes in macrophages expressing Rab20 shRNA1 (Red) after IFN-γ treatment
Movie 22	**Fig. 3.46**	EGFP-Rab20WT dynamic association with *M. bovis* BCG (Red)-containing phagosomes in macrophages expressing EGFP-Rab20WT (Green)